# Molecular Mechanism and Function of Endocytic Sorting of Synaptotagmin 1 at Central Synapses

Inaugural-Dissertation

to obtain the academic degree

Doctor rerum naturalium (Dr. rer. nat.)

submitted to the Department of Biology, Chemistry and Pharmacy

of the Freie Universität Berlin

by

Natalie Kaempf

from Berlin, Germany

Berlin, March 2018

Die vorliegende Arbeit wurde in der Zeit vom Oktober 2012 bis März 2018 unter Anleitung von Prof. Dr. Volker Haucke am Leibniz-Forschungsinstitut für Molekulare Pharmakologie (FMP Berlin) durchgeführt.

1st Reviewer: Prof. Volker Haucke

2nd Reviewer: Prof. Stephan Sigrist

Date of defense: 28.05.2018

# Affidavit

I declare that my PhD thesis entitled “Molecular Mechanism and Function of Endocytic Sorting of Synaptotagmin 1 at Central Synapses” has been written independently and with no other sources and aids than quoted.

*“Our greatest weakness lies in giving up. The most certain way to succeed is always to try just one more time.”*

*Thomas Alva Edison (1847-1931)*

# Acknowledgements

I would like to express my deep gratitude to **Prof. Dr. Volker Haucke**, my research supervisor, for his guidance, inspiring discussions, the multitude of scientific possibilities and the support that he provided me as well as his enthusiasm for science, which motivated me throughout the last years.

I want to thank **Dr. Natalia Kononenko** for her advice, training and great experimental support already during my undergraduate studies. Likewise, **PD Dr. Tanja Maritzen** was a constant and patient support through all the years of my Ph.D. Also her mouse managing skills were very much appreciated.

I owe special thanks to **Dr. Gaga Kochlamazashvili** for his great electrophysiological contributions to the project as well as **Dr. Dmytro Puchkov** for his insights into the ultrastructure of the synapse. I would like to thank **Prof. Dr. Michael Krauß** for his essential discussions and sharing his knowledge about PIPK1γ with me. Furthermore, I am very grateful for the capacitance measurements that supported our idea independently and for critical comments from **Dr. Takeshi Sakaba** (Doshisha University). **Dr. Martin Lehmann** was a great help for all fluorescent microscopy related issues and opened up new experimental possibilities for answering crucial questions of my project.

I am very grateful for the financial funding by the "Deutsche Forschungsgemeinschaft" Grant SFB 958 and I wish to acknowledge **Prof. Sandra Bajjalieh** (University of Washington) for providing the SV2A/B heterozygous mice, which enabled us to perform critical experiments. **Prof. Reinhard Jahn** (Max Planck Institute for Biophysical Chemistry) and **Prof. Pietro De Camili** shared with us important antibodies for the project.

I would like to express my gratefulness to the skilled and technical assistance of **Maria Mühlbauer**, who always supported me not only with numerous genotypings, but also allowed a very fast progress of experiments. **Sabine Hahn** and **Delia Löwe** supplied me beautiful neuronal cultures, while **Uwe Fink** purified with great devotion proteins and **Silke Zillmann** efficiently organized the orderings and the laboratory in general. I would also like to thank the animal facility of the FMP: **Dr. Natali Wisbrun, Eva Lojek, Sina Scholz, Jeannette Unnasch** for their help in breeding all the mouse strains of pivotal importance for my project. Moreover, I am very grateful for all the support from our great secretaries, **Alexandra Chylla** and **Heidi Petschick**.

I would like to acknowledge all past and present members of the AG Haucke, as well as from the AG Maritzen, AG Krauß and AG Schmoranzer. They created a cheerful, creative,

collaborative and supportive atmosphere inside as well as outside the laboratory. Especially, I enjoyed the scientific discussions in the office with **Dr. Tolga Soykan, Dr. Domenico Azarnia Tehran** and **Dr. Marijn Kuijpers** with excellent suggestions as well as the breaks with **Linda Sawade, Marietta Bergmann** and **Claudia Schmidt**, which made the long days in the laboratory much more enjoyable. Thanks you all for the memorable time: **Jelena Bacetic, Caroline Bruns, Gabrielle Capin, Gala Claßen Katrin Diesenberg, Michael Ebner, Marielle Eichhorn-Grünig, Fabian Feutlinske, Niclas Gimber, Marine Gil, Hannes Gonschior, Claudia Gras, Antje Gruenwald, Manuel Hessenberger, Lennart Hoffmann, Kira Gromova, Burkhard Jacob, Maria Jäpel, Lisa Jerndal, Christina Kath, Katharina Ketel, Peter Koch, Philipp Alexander Koch, Seong Joo Koo, Ludwig Krabben, André Lampe, Wen-Ting Lo, Gregor Lichtner, Guan-Ting Liu, Tania López Hernández, Fabian Lukas, Albert Mackintosh, Marta Maglione, Mouhannad Malek, Andrea Marat, Julia Mössinger, Christoph Ott, Arndt Pechstein, Jasmin Podufall, York Posor, Filiz Sila Rizalar, Christine Rückert, Giulia Russo, Paula Samso Ferre, Hannah Schachtner, Jan Schmoranzer, Irene Schütz, Kyungyeun Song, Wiebke Stahlschmidt, Susanne Thomsen, Dennis Vollweiter, Anela Vukoja, Alexander Wallroth, Alexander Walter, Ingeborg Walther, Haibin Wang, Susanne Wojtke, Haibin Wang, Anna Wawrzyniak, Mirjana Weimershaus and Marnix Wieffer.**

Finally and most importantly, I want to express my deepest gratitude to my family and friends, in particular to **Stefan Wendt**, **my mum** and **my granddad**, who constantly motivated me and gave me strength to continue. Without their support and patience it would not have been possible!

# I Table of Content

# II Summary

Communication in the central nervous system relies on fast and precise neurotransmission at synapses. The arrival of an action potential at the presynapse triggers the calcium regulated exocytic fusion of synaptic vesicles (SVs). Exocytosis and neurotransmitter release are followed by local SV membrane retrieval and reformation of functional SVs with the correct size and protein composition that can replenish the SV pool and thereby maintain neurotransmission. In spite of decades of research many aspects of SV recycling remain unclear. In particular, the precise sorting of surface-stranded SV proteins during SV endocytosis as well as the coupling of SV exo- and endocytosis are still unknown. To address these open questions, we investigated whether the endocytic sorting of synaptotagmin 1 (Syt1), the calcium sensor for SV exocytosis, is ensured by two mechanisms in mammals: by a dedicated endocytic adaptor as well as by complex formation with another SV protein. Further, we examined the functional consequences of Syt1 sorting in mammalian synapses.

I could show that endocytic sorting and maintenance of Syt1 at mammalian synapses is mediated by overlapping activities of stonin 2 (Stn2) and the SV glycoprotein SV2A/B. Deletion or knockdown of either SV2A/B or Stn2 resulted in partial Syt1 loss and missorting of Syt1 to the neuronal surface in brain slices and hippocampal neurons in culture. Combined deletion of both SV2A/B and Stn2 dramatically aggravated this phenotype. The repartitioning of Syt1 to the neuronal plasma membrane is dependent on neuronal activity and led to a partial loss of Syt1 from recycling SVs. Consequently, the defective Syt1 sorting to SVs in the absence of SV2A/B and Stn2 impaired basal neurotransmission. These results suggest that SV2A/B and Stn2 share an overlapping function in mediating endocytic sorting of Syt1 to SVs at mammalian synapses and favor a model according to which SV protein sorting is guarded by both cargo-specific endocytic adaptors as well as complex formation of SV proteins.

Interestingly, we found that deletion of the Syt1 sorting adaptors Stn2 and SV2A/B accelerated endocytic retrieval and facilitated SV exocytosis in response to repetitive electrical stimulation in hippocampal neurons. The surface-stranding of Syt1 in the absence of Stn2 and the augmented SV exo- and endocytosis correlated with elevated presynaptic levels of phosphatidylinositol-(4,5)-bisphosphate [$PI(4,5)P_2$], a membrane phospholipid essential for SV exocytic fusion and endocytic retrieval. In contrast, the levels of another plasma membrane residing phosphoinositide, PI(4)P, remained unchanged. Increased presynaptic $PI(4,5)P_2$ levels likely are caused by the direct association of Syt1 with phosphatidylinositol

4-phosphate 5-kinase type Iγ (PIPK1γ), the major PI(4,5)$P_2$-synthesizing enzyme at synapses. Indeed, superresolution nanoscopy revealed a selective relocalization of PIPK1γ towards the plasma membrane in Stn2 depleted and thus Syt1 surface-enriched neurons.

Taken together, my data suggest that Syt1 at the axonal surface triggers the recruitment of PIPK1γ to facilitate local PI(4,5)$P_2$ synthesis at or near release sites and couples thereby PI(4,5)$P_2$-dependent SV exo- and endocytosis.

# III Zusammenfassung

Die Kommunikation im zentralen Nervensystem basiert auf einer schnellen und präzisen Erregungsübertragung an Synapsen. Sobald ein Aktionspotential die Präsynapse erreicht, löst es die Kalzium-regulierte Verschmelzung synaptischer Vesikel (SV) an der aktiven Zone aus. Die Exozytose und Freisetzung von Neurotransmittern folgt die Rückgewinnung der fusionierten Membran und Bildung neuer funktionaler SV, welche wieder die richtige Größe und vor allem die korrekte Proteinzusammensetzung aufweisen müssen, um die fusionierten SV zu ersetzen. Dies ist notwendig, um lang anhaltende Neurotransmission sicher zu stellen. Trotz jahrelanger intensiver Forschung sind viele Aspekte dieses Recyclings der SV nicht geklärt. Besonders, die präzise Sortierung während der Endozytose von an der Oberfläche zurückgebliebenen SV Proteine sowie die Kopplung von Exo- und Endozytose sind noch immer unbekannt. Um diese offenen Fragen zu beantworten, haben wir untersucht, ob die Sortierung von Synaptotagmin 1 (Syt1), dem Kalzium-Sensor für die SV Fusion, in Säugetieren durch zwei Mechanismen sichergestellt wird: durch einen spezifischen, endozytotischen Adaptor sowohl als auch durch Komplexbildung mit einem weiteren SV Protein. Darüber hinaus haben wir die funktionalen Konsequenzen von der Syt1-Sortierung in Säugetiersynapsen erforscht.

In dieser Arbeit konnte ich zeigen, dass die Sortierung während der Endozytose sowie die Erhaltung von Syt1 durch überlappende Funktionen von dem spezifischen Adaptor stonin 2 (Stn2) und dem SV Protein SV2A/B in der Säugetiersynapse gewährleistet werden. Das Fehlen von SV2A/B oder Stn2 führte zu einem partiellen Verlust von Syt1, einhergehend mit der Akkumulation von Syt1 an der Zelloberfläche von Neuronen in Gehirnschnitten und in hippocampalen neuronalen Kulturen. Die Abwesenheit beider Proteine, Stn2 und SV2A/B, verstärkte diesen Phänotyp dramatisch. Zusätzlich konnte ich bestätigen, dass die Umverteilung von Syt1 zur Zelloberfäche von neuronaler Aktivität abhängig und für den Verlust von vesikulärem Syt1 verantwortlich ist. Die mangelnde Präzision der Syt1-Sortierung führte folglich zu einer stark eingeschränkten Neurotransmission. Diese Ergebnisse weisen daher auf überlappende Aktivitäten von Stn2 und SV2A/B in der Säugetiersynapse hin, um Syt1 in SV zu sortieren. Weiterhin lassen die Daten darauf schließen, dass die SV Protein Sortierung mit Hilfe zweier Mechanismen sichergestellt wird: einerseits durch spezifische Adaptoren, andererseits durch die Assoziation von SV Proteinen miteinander.

Überraschenderweise beschleunigt die Abwesenheit der Syt1-Sortierungsproteine SV2A/B und Stn2 sogar die Aufnahme der SV Proteine und verstärkt zudem die SV Exozytose, wenn hippocampale Neurone repetitiv elektrisch stimuliert werden. Die Akkumulation von Syt1 an der neuronalen Zelloberfläche korreliert nicht nur mit der gesteigerten SV Exo- und Endozytose, sondern auch mit erhöhten präsynaptischen Konzentrationen von Phosphatidylinositol-(4,5)-bisphosphat [$PI(4,5)P_2$]. $PI(4,5)P_2$ gehört zu den Phospholipiden und ist essentiell für die Fusion von SV und deren Rückgewinnung. Im Gegensatz dazu sind die Level von PI(4)P, einem weiteren Phosphoinositid, das auf der Plasmamembran lokalisiert ist, unverändert. Die erhöhten Level von $PI(4,5)P_2$ lassen sich vermutlich durch eine direkte Assoziation von Syt1 mit der Phosphatidylinositol 4-phosphat 5-kinase Typ Iγ (PIPK1γ) erklären, die hauptsächlich für die Synthese von $PI(4,5)P_2$ verantwortlich ist. Zudem bestätigt hoch-auflösende Mikroskopie eine veränderte Lokalisierung von PIPK1γ an die Plasmamembran von Neuronen, welche Stn2 defizient sind und somit an der Oberfläche angereichertes Syt1 aufweisen.

Zusammenfassend zeigen meine Daten, dass die Akkumulation von Syt1 an der Plasmamembran die Rekrutierung von PIPK1γ fördert und damit die lokale Synthese von $PI(4,5)P_2$ an oder nahe der aktiven Zone ermöglicht. Somit koppelt Syt1 die $PI(4,5)P_2$ abhängige SV Exo- und Endozytose.

# 1. Introduction

## 1.1. Neurotransmission at chemical synapses

Communication in the brain is a fundamental process that is vital for organism survival. Within the brain neurons are organized in a complex network and are able to rapidly transfer information via electrical signals, so called action potentials (APs). The AP is transmitted along the axon by depolarization of the plasma membrane. At the synapse, specialized contact sites at the interface of two neurons, this electrical signal has to be converted into a chemical signal to bridge the gap between the cells. The incoming AP leads to calcium influx into the presynapse triggering the exocytic fusion of synaptic vesicles (SVs) with the plasma membrane (Katz and Miledi, 1967b) at specialized release sites termed active zones close to voltage-gated calcium channels (Kittel et al., 2006). SVs are filled with neurotransmitters, which upon their release into the synaptic cleft bind to postsynaptic receptors and thereby elicit a new electrical signal at the postsynapse (Heuser and Reese, 1973). To sustain efficient neurotransmission the exocytic fusion of SVs has to be compensated by endocytic retrieval of SVs. The membrane expansion after the full collapse of SVs has to be immediately balanced to retain presynaptic architecture and membrane tension. In addition, the release sites have to be cleared from exocytosed SV proteins for further rounds of SV fusion and SVs have to be reformed locally within the presynpase to refill the SV pool (Neher, 2010; Soykan et al., 2016). This SV cycling is a highly regulated process that involves a plethora of proteins and signaling molecules and despite decades of research is incompletely understood. Especially, the reformation of SVs with high fidelity and the coupling of exocytic fusion and endocytic retrieval at the presynapse remain enigmatic. However, efficient neurotransmission at the synapse is crucial for brain function and its modulation is the basis of cognitive processes like memory formation. Consequently, severe alterations have been associated with neurological diseases. These include epileptic seizures or impaired information processing. To unravel neurotransmission in more mechanistic detail is therefore pivotal for understanding and treating neurological and neurodegenerative disorders.

## 1.2. SV recycling

Calcium-dependent and SNARE (soluble NSF-attachment protein receptor)-mediated fusion of SVs at the active zone is followed by presynaptic membrane retrieval adjacent to the active

zone and SV reformation. However, the exact mechanism of endocytic retrieval is controversial and recent data suggest that endocytosis is accomplished by more than one mechanism, occurs on multiple timescales and depends on the type of synapse and stimulation paradigm.

For several decades clathrin-mediated endocytosis (CME) has been proposed to be the major SV recycling mechanism after the full collapse of SVs into the plasma membrane. Ultrastructural analysis of stimulated nerve-muscle preparations revealed clathrin-coated structures lateral to the active zone either directly on the presynaptic plasma membrane (Gad et al., 2000) or on endocytic cisternae (Heuser and Reese, 1973). Given that CME is a crucial uptake pathway in all eukaryotic cells, the mechanism of CME has been extensively studied. CME includes the binding of the general endocytic adaptor protein AP-2 to phosphatidylinositide-(4,5)-bisphosphate [$PI(4,5)P_2$] enriched membrane and to cargo proteins. Clathrin triskelia are recruited by AP-2 and form a clathrin coat. With the help of accessory endocytic proteins the shallow clathrin-coated pit is bent and invaginated to be finally pinched off by the GTPase and mechano-enzyme dynamin. Subsequently, clathrin-coated vesicles are uncoated, reacidified and refilled with neurotransmitters. Therefore, CME directly links membrane retrieval and SV reformation, but at the expense of speed as CME operates on the time scale of tens of seconds. In case of high neuronal activity maintaining presynaptic integrity or clearing release sites might become rate-limiting for exocytosis (Neher, 2010) and CME would be too slow to compensate for exocytic fusion.

With “kiss and run” exo- and endocytosis (Ceccarelli et al., 1972, 1973) a fast alternative to CME has been proposed around the same time. During “kiss and run” SVs only transiently fuse with the plasma membrane to release neurotransmitter through a narrow fusion pore and are rapidly retrieved at the active zone without losing their molecular identity. Besides the observation in electron micrographs further indications for “kiss and run” endocytosis come from rapid endocytic retrieval in capacitance measurements (He et al., 2006; Wu et al., 2005) and from partial release of the fluorescent membrane dye FM1-43 from SVs through narrow fusion pores monitored by high resolution imaging (Harata et al., 2006; Richards et al., 2005). While in neuroendocrine cells there is strong evidence for “kiss and run” fusion of secretory granules (Albillos et al., 1997; Ales et al., 1999; Chiang et al., 2014), its role in neurons is highly debated. Most exocytic fusion events include the full collapse of the SV into the plasma membrane (Chen et al., 2008; Heuser, 1989; Li and Murthy, 2001; Sankaranarayanan and Ryan, 2000) and newly exocytosed SV proteins are mostly non-identical to those that are endocytosed in the same round of stimulation

(Fernandez-Alfonso et al., 2006; Gimber et al., 2015; Wienisch and Klingauf, 2006). These observations have casted doubt on the relevance of the "kiss and run" model for SV recycling and pointed towards existence of rapid modes of endocytosis that are distinct from CME and "kiss and run".

Recent evidence suggested the existence of fast clathrin-independent endocytosis mechanisms, which turn membrane retrieval and SV reformation into two separable processes and would therefore allow neurons to cope with a range of neuronal activity patterns. First, high pressure freezing electron microscopy of optogenetically stimulated neurons in *C. elegans* or mouse hippocampal cultures revealed an ultrafast endocytosis (UFE) mode (Watanabe et al., 2013a; Watanabe et al., 2013b). In a clathrin-independent manner large endocytic invaginations are formed within 50-100 ms after full collapse fusion next to the active zone. These endosomal-like vacuoles (ELVs) are subsequently consumed by a clathrin-dependent mechanism to reform SVs (Watanabe et al., 2014). Data based on monitoring SV protein retrieval showed that clathrin and AP-2 are dispensable for presynaptic membrane retrieval but are required for SV reformation from ELVs demonstrated by accumulations of ELVs in the absence of clathrin and AP-2 (Kononenko et al., 2014; Soykan et al., 2017). However, the time scale of this clathrin-independent endocytosis (CIE) in this case was shown to be broader than UFE and occurs within less than a second to several seconds. Interestingly, both ultrafast and fast endocytosis mechanisms require the actin cytoskeleton. Pharmacological perturbation of actin depolymerization inhibits UFE (Watanabe et al., 2013b), while the fast CIE is mediated by formin dependent linear actin filament assembly (Soykan et al., 2017).

Large membrane invaginations formed independently of clathrin have also been observed in response to prolonged and strong stimulation, the so called activity-dependent bulk endocytosis (ADBE) (Clayton and Cousin, 2009; Nicholson-Fish et al., 2015). How these vacuoles are consumed to reform SVs is so far unclear. Mechanisms requiring clathrin and AP-1 or AP-3 (Cheung and Cousin, 2012) as well as clathrin- and dynamin-independent SV reformation have been proposed (Wu et al., 2014b).

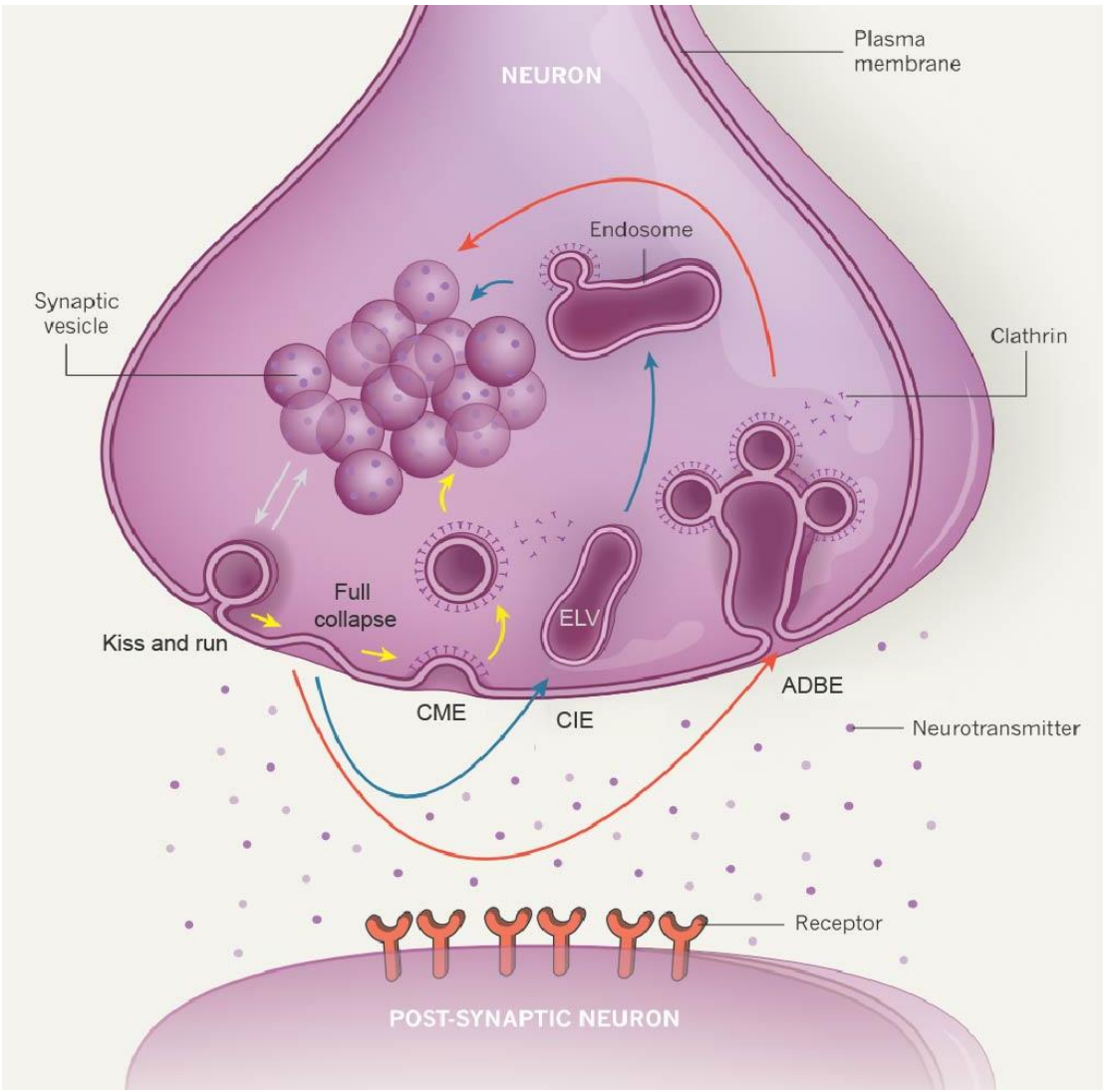


**Figure 1: Synaptic vesicle recycling in the presynapse.** Calcium triggered SV exocytosis allows the release of neurotransmitter into the synaptic cleft, which bind to post-synaptic receptors. SVs fuse either transiently and are immediately retrieved during "kiss and run" endocytosis or fully collapse into the plasma membrane that requires more elaborate endocytic retrieval mechanisms to maintain neurotransmission. Clathrin-mediated endocytosis (CME) operates at the plasma membrane or on endososmal-like vacuoles (ELVs) after fast clathrin-independent endocytosis (CIE). High frequency stimulation triggers activity-dependent bulk endocytosis (ADBE). Adapted from (Marx, 2014), license number 4279300211191.

## 1.3. The synaptic vesicle (SV)

The result of endocytic retrieval at the presynapse is a fully functional SV with the correct size and precise protein composition to maintain neurotransmission. Proteomic analysis of purified SVs revealed the presence of about 80 different integral membrane proteins with 40 known SV residents. These include SV proteins mediating neurotransmitter uptake such as

neurotransmitter transporters e.g. vGLUT1, the vacuolar ATP-dependent proton pump v-ATPase and SV proteins involved in exocytic fusion like synaptobrevin 2 (Syb2) and synaptotagmin 1 (Syt1) (Takamori et al., 2006). Syb2 is essential for SV exocytosis as it forms a tight four-helical SNARE complex with the plasma membrane localized proteins SNAP-25 and syntaxin 1 and thereby promotes SV fusion with the plasma membrane (Jahn and Fasshauer, 2012; Schoch et al., 2001). Biochemical quantification of SV protein copy numbers indicated that Syb2 is a very abundant SV protein with about 70 copies per vesicle (Takamori et al., 2006; Wilhelm et al., 2014). Synaptophysin (Syp) which has been proposed to contribute to Syb2 sorting (Gordon et al., 2011) is also found with high copy numbers on SV (about 30 molecules per SV). In contrast, other SV proteins like Syt1 and the synaptic vesicle protein 2 (SV2) are less abundant with about 15 and 12 molecules, respectively, detected via quantitative western blotting of purified SVs or whole synaptosomes (Takamori et al., 2006; Wilhelm et al., 2014). The calcium sensor Syt1 and SV2 are both crucial SV proteins as their absence severely impairs neurotransmission. Interestingly, an imaging based analysis of purified SVs revealed very little intervesicle variability for Syt1 and SV2, while the more abundant proteins Syb2 and Syp displayed more diversity (Mutch et al., 2011). These results therefore suggested that the SV copy number at least some SV proteins are tightly controlled.

## 1.4. The SV protein synaptotagmin 1

Synaptotagmins (Syt) are the major calcium sensors in cells and represent an evolutionary highly conserved protein family with 17 isoforms in the mammalian genome (Craxton, 2010). All isoforms differ in their calcium binding properties, expression and localization pattern – a diversity that has not completely been understood yet. Among all synaptotagmins Syt1 is the best characterized isoform as it is expressed in excitatory neurons and resides on SVs. Syt1 was early associated with SV exocytosis as the major $Ca^{2+}$ sensor on SVs (Perin et al., 1990) and is crucial for synchronous neurotransmitter release. Consequently, its absence leads to early postnatal death in mice (Fernandez-Chacon et al., 2001; Geppert et al., 1994).

Syt1 has a short, glycosylated luminal sequence followed by a single transmembrane domain and two characteristic cytosolic calcium binding C2 domains, termed C2A and C2B. The C2 domains can interact with the SNARE complex and the plasma membrane, especially via the phosphoinositide $PI(4,5)P_2$. Based on these interactions various models have been proposed how Syt1 can mediate calcium triggered fusion. However, the exact molecular

mechanism is debated (Jahn and Fasshauer, 2012; Koch and Holt, 2012; Koh and Bellen, 2003). While it has been shown that Syt1 can associate with the core machinery of SV fusion, the SNARE complex (Brewer et al., 2015; Chicka et al., 2008; Li et al., 1995), the interaction itself and its importance for SV exocytosis remain controversial (Jahn and Fasshauer, 2012; Park et al., 2015). Recently crystal structure analysis revealed the interaction of Syt1 with the primed pre-fusion SNARE complex at two interfaces. Calcium binding to the C2 domains is proposed to unlock the SNARE complex, allowing full SV fusion (Zhou et al., 2017). A mutagenic screen in *D. melanogaster* underlined the importance of Syt1-SNARE complex interaction for synchronous release and for the calcium cooperativity of SV exocytosis (Guan et al., 2017). Besides its association with the SNARE complex, Syt1's role during SV exocytosis has been associated with membrane remodeling. Basic residues within the C2B domain can directly bind $PI(4,5)P_2$ at the plasma membrane prior to calcium ion influx and thereby tether SVs and the plasma membrane in close proximity (Figure 2) (Bai et al., 2004; Brose et al., 1992; Park et al., 2015; Rhee et al., 2005), which could assist the SV docking and priming mediated by SNARE complex assembly (Imig et al., 2014; Walter et al., 2010; Weber et al., 2010). Moreover, the incorporation of calcium ions can shield negative charges in the C2 domains allowing them to penetrate the lipid bilayer (Bai et al., 2002; Fernandez et al., 2001). Thereby, the plasma membrane can be destabilized and SV fusion is facilitated (Hui et al., 2009; Martens et al., 2007).

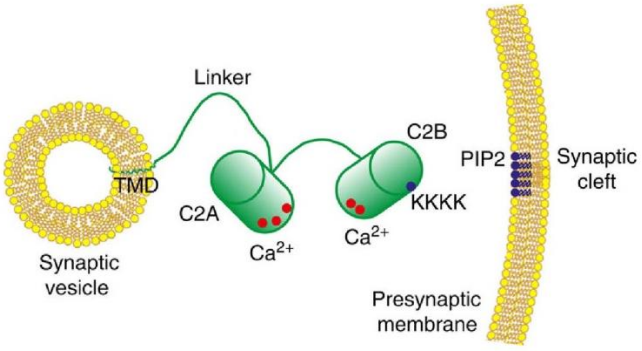


**Figure 2: Scheme of Syt1 domain structure.** The luminal N-terminus of Syt1 within the SV is followed by transmembrane domain (TMD) and a charged linker region. The two C2 domains, C2A and C2B, harbor the calcium ion binding sites marked in red. Additionally, the C2B contains a ploy-lysine patch (KKKK, blue dot) allowing to bind negatively charged $PI(4,5)P_2$ ($PIP_2$) at the presynaptic plasma membrane. Adapted from (Lin et al., 2014).

Syt1 not only has an important role in SV exocytosis, but has been shown to be involved in SV endocytosis as well. The deletion of Syt1 reduces synchronous neurotransmission, increases asynchronous release and impairs compensatory endocytosis at the same time. Despite the difficulty to discriminate between a secondary effect due to defective exocytosis and a direct effect on endocytosis, impaired endocytosis has been

observed in various model organisms after mutation, inactivation or deletion of Syt1 (Jorgensen et al., 1995; Littleton et al., 2001; Nicholson-Tomishima and Ryan, 2004; Poskanzer et al., 2003). E.g. the defective endocytic retrieval in Syt1 deficient neurons was probed by a pH-sensitive green fluorescent protein (GFP) reporter, pHluorin, and showed greatly delayed pHluorin-tagged Syp retrieval (Nicholson-Tomishima and Ryan, 2004). pHluorin allows the visualization of SV protein retrieval kinetics when it is fused to their luminal domain. Its fluorescence is quenched within acidic SVs and starts to fluoresce as soon as it is exposed to the neutral pH of the extracellular medium after SV fusion. During SV endocytosis and reacidification the fluorescent intensity is quenched and the decay is quantified to assess endocytic kinetics even though it only represents vesicular reacidification (s. section 3.4.4 and Figure 10) (Miesenbock, 2012; Miesenbock et al., 1998). The molecular mechanisms underlying Syt1's ability to regulate endocytosis at the synapse are unclear. So far, rescue experiments with calcium binding deficient Syt1 mutants have implicated a calcium sensing function of Syt1 in mediating endocytosis (Poskanzer et al., 2006; Yao et al., 2011). Moreover, based on capacitance measurements in chromaffin cells, the calcium binding ability of Syt1 has been shown to play a role in vesicle fission as well (Yao et al., 2012).

Syt1's dual roles in exocytosis and endocytosis indicate a possible function of Syt1 in coupling both processes (Koch and Holt, 2012). Together with the tightly controlled copy numbers of Syt1 this highlights the importance of correct Syt1 recycling during neurotransmission.

## 1.5. Sorting of SV proteins

To maintain neurotransmission at the synapse SVs have to be recycled locally and with high precision. During SV reformation the protein composition and the stoichiometry of SV proteins have to be preserved. In addition, the analysis of SVs has shown that for some SV proteins like Syt1 the copy numbers are tightly regulated (Mutch et al., 2011), highlighting the existence of precise sorting mechanisms.

During "kiss and run" endocytosis the SV retains its identity and thereby abrogates the need for SV protein sorting. However, the full collapse fusion of SVs requires the capture and high-fidelity sorting of SV proteins at some stage during the recycling process. Indeed, advanced imaging analysis at the presynapse has shown a rapid diffusion of SV proteins after exocytosis which is followed by a confinement and slow reclustering at the periactive zone

(Gimber et al., 2015). A general sorting adaptor like AP-2 that binds cargo proteins and orchestrates the clathrin coat assembly especially in non-neuronal cells (Wieffer et al., 2009), could be responsible for binding SV proteins and mediating their sorting. Some SV proteins like VGLUT1 have been shown to be recognized and sorted by AP-2 (Kim and Ryan, 2009; Tan et al., 1998). However, the reclustering and sorting of other SV proteins e.g. of Syb2 is in part dependent on the selective Syb2 adaptor protein AP180 (Gimber et al., 2015; Koo et al., 2015). Selective endocytic sorting is also required for Syt1 retrieval and involves the endocytic adaptor stonin 2 (Stn2). Manipulations of these selective adaptors affect the recycling of Syb2 and Syt1, respectively, leading to their partial redistribution to the presynaptic cell surface (Kononenko et al., 2013; Koo et al., 2015). Therefore, high-fidelity sorting of SV proteins is regulated by adaptors proteins and requires for some SV proteins dedicated endocytic adaptors.

Additionally SV proteins might also interact with each other and self-assemble into SV protein clusters, which allow their efficient retrieval. The interaction of SV proteins like Syb2 and Syp (Calakos and Scheller, 1994; Edelmann et al., 1995; Siddiqui et al., 2007) as well as for Syt1 and SV2 (Lazzell et al., 2004; Schivell et al., 1996; Schivell et al., 2005) has been described. Interestingly, on a functional level the interaction of Syb2 and Syp has been proposed to regulate Syb2 internalization in cultured hippocampal neurons (Gordon et al., 2011). Moreover, the vesicular glutamate transporter VGLUT1 has been proposed to control efficient retrieval of Syp and Syb2 (Pan et al., 2015).

Sorting of SV proteins has to occur at least in part at the plasma membrane as the absence of endocytic adaptors results in the accumulation of selective SV proteins at the axonal surface. However, recent data have shown that endocytic retrieval is not mediated exclusively by CME from the plasma membrane. It also relies on clathrin-independent membrane retrieval followed by clathrin- and AP-2-dependent SV reformation from ELVs (Kononenko et al., 2014; Soykan et al., 2017; Watanabe et al., 2014). This implies that SV protein sorting operates on ELVs in addition to the plasma membrane (Figure 3).

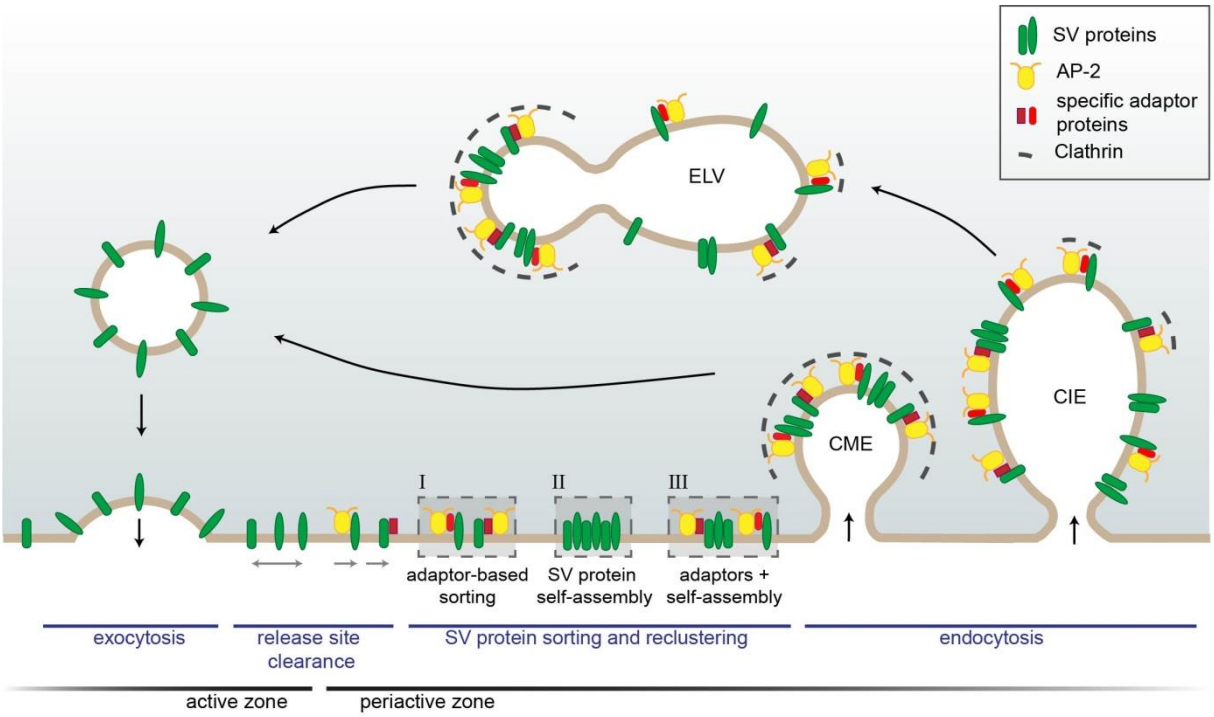


**Figure 3: Model of SV protein reclustering and sorting at the presynapse.** After full collapse fusion freely diffusing SV proteins are confined and recaptured by endocytic sorting adaptors at the periactive zone to allow for release site clearance. At the plasma membrane SV proteins might either be clustered by AP-2 and additional cargo-specific adaptor proteins (I), they might interact with each other and thereby self-assemble into clusters (II) or form mixed clusters of self-assembled SV proteins together with sorting adaptors (III). These clusters can directly be endocytosed from the plasma membrane by clathrin-mediated endocytosis (CME) to reform SVs. However, cargo-specific sorting proteins together with AP-2 and clathrin can also operate on endosomal-like vacuoles (ELVs) after clathrin-independent endocytosis (CIE) to recycle SVs with correct protein composition (Kaempf and Maritzen, 2017).

### 1.5.1. SV protein sorting by AP-2

AP-2 is an essential protein during development (Mitsunari et al., 2005) and is the main sorting adaptor of CME. It binds to cargo proteins and coordinates the clathrin coat assembly (McMahon and Boucrot, 2011; Wieffer et al., 2009). The heterotetrameric AP-2 complex displays a structure common to many endocytic adaptors. The four subunits comprising the large α and β2 subunits and the smaller σ2 and μ2 subunits are characterized by a combination of folded domains, that allow the interaction of AP-2 with cargo proteins and $PI(4,5)P_2$, and unstructured regions containing peptide motifs to recruit endocytic proteins (McPherson and Ritter, 2005; Traub and Bonifacino, 2013).

AP-2 recognizes cargo proteins via various binding motifs. While the α and σ2 subunits can bind acidic cluster di-leucine-based motifs (Doray et al., 2007) that are present

e.g. in VGLUT1 (Tan et al., 1998), the µ2 subunit can interact with tyrosine based motifs (Ohno et al., 1995) e.g. found in SV2 (Yao et al., 2010). In addition the µ2 subunit can also associate with C2 domains e.g. via a basic stretch within the C2B domain of Syt1 (Grass et al., 2004; Haucke et al., 2000). Interestingly, many of these SV proteins bind additional endocytic proteins other than AP-2. VGLUT1 has been shown to be sorted by the endocytic protein endophilin (Voglmaier et al., 2006). For Syt1 internalization the association with AP-2 is not sufficient and requires sorting via its dedicated adaptor Stn2 (Diril et al., 2006; Jarousse and Kelly, 2001). Moreover, many SV proteins like Syb2 do not harbor any canonical AP-2 binding motifs in their sequence and are integrated into the endocytic machinery with the help of cargo selective adaptor proteins. The dedicated sorting adaptors AP180 and its homolog clathrin assembly lymphoid myeloid leukaemia (CALM) both interact with AP-2 and Syb2 and thereby connect Syb2 to the clathrin-mediated endocytosis machinery (Koo et al., 2011; Maritzen et al., 2012).

### 1.5.2. Stonin2 – a specific sorting adaptor for Syt1

Ectopic expression of Syt1 in fibroblasts has demonstrated that the Syt1-AP-2 interaction is not sufficient for Syt1 internalization from the plasma membrane (Feany et al., 1993; Jarousse and Kelly, 2001). Thus, efficient Syt1 sorting requires a neuron specific and dedicated sorting adaptor.

The endocytic adaptor protein stoned B in *D. melanogaster* has been associated with SV recycling and Syt1 sorting. Genetic inactivation of stoned B leads to severely paralyzed larvae with early embryonic lethality (Andrews et al., 1996; Estes et al., 2003; Grigliatti et al., 1973). These larvae displayed impaired neurotransmission resulting from major defects in SV recycling. The SV depletion in these mutant larvae was accompanied by mislocalisation and degradation of Syt1 (Fergestad and Broadie, 2001; Fergestad et al., 1999). Interestingly, the transgenic overexpression of Syt1 rescued the severe phenotype of stoned B larvae (Fergestad and Broadie, 2001) and suggested that stoned B's main function is to sort Syt1. The localization and synaptic enrichment of stoned B and of its human homolog Stn2 further supported its proposed role as a Syt1 sorting adaptor (Diril et al., 2006; Fergestad and Broadie, 2001; Walther et al., 2001). Moreover, extensive biochemical analysis confirmed the direct and evolutionary conserved interaction of stoned B/ Stn2 with Syt1 (Diril et al., 2006; Jung et al., 2007; Martina et al., 2001; Phillips et al., 2000; Walther et al., 2001). Indeed, in

fibroblasts ectopic overexpression of Syt1 and Stn2 led to Stn2 recruitment to the plasma membrane where it enabled Syt1 internalization (Diril et al., 2006).

Stn2 belongs to the stonin protein family that is evolutionary conserved from *C.elegans* to humans. In contrast to invertebrates the mammalian genome encodes two stonin proteins, Stn2 and stonin 1 (Stn1). Structurally Stn2 and its homologs (Stn1, stonedB in *D. melanogaster* and Unc41 in *C. elegans*) resemble endocytic adaptor proteins with a folded domain allowing cargo binding and a presumably unstructured N-terminus for interaction with endocytic proteins (Maritzen et al., 2010).

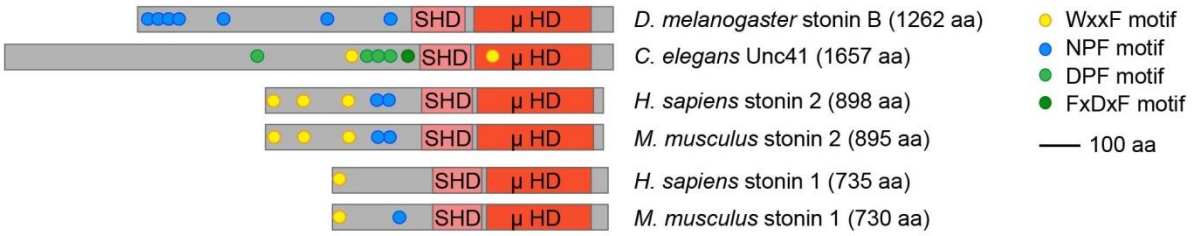


**Figure 4: Evolutionary conserved domain structure of the stonin protein family.** All stonins are characterized by a N-terminus, a central stonin homology domain (SHD) and a C-terminal µ-homology domain (µHD). The N-terminus of all stonins contains AP-2 α-appendage binding peptide motifs such as DPF and FxDxF, which are only present in *C.elegans*, as well as WxxF. The interaction with other endocytic proteins is mediated via the NPF motifs. Numbers in parentheses indicate the length of known amino acid (aa) sequences. Adapted from (Maritzen et al., 2010).

Via WxxF motifs in the N-terminus Stn2 can interact with the sandwich domain of the AP-2 α-appendage (Walther et al., 2004). Additionally, N-terminal NPF motifs allow the binding of Stn2 to EF domains which are present in endocytic proteins such as Eps15 and intersectin (Martina et al., 2001). The N-terminus is followed by a conserved stonin homology domain (SHD) which is unique to this protein family, however so far with unknown function (Maritzen et al., 2010). The C-terminus displays a structural similarity to the µ2 subunit of AP-2 and is therefore called µ-homology domain (µHD). A short tyrosine-based motif within the µHD mediates the interaction of Stn2 with a basic stretch in the C2A domain of Syt1 (Jung et al., 2007). Therefore, Stn2's structure and its various binding motifs allow Stn2 to link Syt1 to AP-2 and other proteins of the endocytic machinery and thereby facilitate Syt1 internalization (Figure 5).

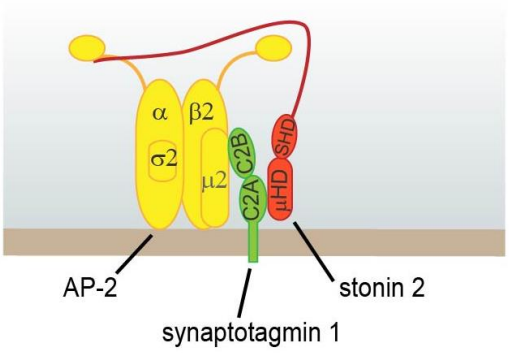


**Figure 5: Sorting of Syt1 by the dedicated adaptor protein Stn2.** Syt1 associates with AP-2µ2 via its C2B domain. However, this interaction does not suffice for efficient Syt1 retrieval. The specific adaptor protein Stn2 is required to strengthen the link between AP-2 and Syt1 by interacting simultaneously with Syt1´s C2A domain and the AP-2α ear (Kaempf and Maritzen, 2017).

Even though the deletion of stoned B in invertebrates and siRNA mediated knockdown of Stn2 in neurons resulted in severely defective SV recycling, the genomic loss of Stn2 in the mouse did not confirm Stn2's role as a general and essential endocytic protein in SV retrieval in mammalian neurotransmission. Except for increased explorative behavior the Stn2 knockout (KO) mice are viable and fertile without any overt impairment. In line with previous data, neuronal cultures as well as brain slices of Stn2 KO mice showed a partial redistribution specifically of Syt1 to the plasma membrane consistent with Stn2's function as a dedicated sorting adaptor for Syt1 retrieval during SV recycling. Surprisingly, the absence of Stn2 did not affect Syt1 internalization in general and even accelerated SV retrieval. Moreover, Stn2 loss increased the SV number and elevated short-term facilitation in mossy fiber synapses (Kononenko et al., 2013). In short, the deletion of Stn2 in the mouse resulted in mild phenotypes that are in contrast with the severe effects reported in invertebrates. A compensatory mechanism, which has evolved in the mammalian system, would be a plausible explanation. Loss of the first candidate, the closely related Stn1, however did not aggravate the Stn2 phenotype in the Stn1 and Stn2 double KO (DKO) mouse and is rather implicated in the regulation of focal adhesion dynamics (Feutlinske et al., 2015). Therefore, other mechanisms must exist for Syt1 endocytosis in mammalian synapses that functionally overlap with Stn2-mediated sorting.

### 1.5.3. Synaptic vesicle protein 2 (SV2) in SV protein complex formation

If all SV proteins required a dedicated adaptor to be captured and sorted after the full collapse fusion and their diffusional spread, SV reformation would need numerous different adaptors. However, the self-assembly of SV proteins with each other would facilitate this complex task. Such a complex formation has been shown for Syb2 and Syp (Edelmann et al., 1995; Siddiqui et al., 2007). Moreover, Gordon and colleagues proposed a Syp mediated endocytosis of

Syb2, which is abrogated in Syp KO mice and relies on a 1:2 stoichiometry of Syp and Syb2 (Gordon et al., 2016; Gordon et al., 2011). Since Syb2 also binds AP180, mixed clusters of SV protein complexes and adaptors might exist and could be incorporated into newly reforming SVs (Figure 3) (Kaempf and Maritzen, 2017).

Early biochemical data revealed that a peptide from the SV protein SV2 harboring a tryrosine-based motif facilitated Syt1 internalization by AP-2 (Haucke and De Camilli, 1999). This gave the first notion that SV2, together with the endocytic adaptor Stn2, could be implicated in Syt1 retrieval. SV2 denotes a protein family comprising three isoforms termed SV2A, SV2B and SV2C that all share a glycosylated 12-transmembrane domain structure. While the endocytic adaptor Stn2 is evolutionary conserved among invertebrates and vertebrates, the SV2 protein family appears late in evolution and is only conserved in vertebrates. Only a very distantly related protein is present in invertebrates, namely SVOP (SVtwO related protein). It shows only about 20 % homology to SV2, and no function has been assign to SVOP so far (Janz et al., 1998; Yao et al., 2013).

Among the three isoforms SV2A has a crucial role in the CNS as its deletion in mice results in impaired neurotransmission, severe epileptic seizures and premature death within 2-3 weeks after birth (Crowder et al., 1999). The additional SV2B deletion only mildly aggravates this phenotype (Janz et al., 1999). In fact, SV2B KO mice do not display any overt phenotype (Janz et al., 1999; Morgans et al., 2009). These distinct phenotypes are reflected in their different expression patterns. SV2A is expressed ubiquitously in the brain including excitatory glutamatergic as well as inhibitory GABAergic neurons (Bajjalieh et al., 1994; Buckley and Kelly, 1985). In comparison SV2B displays a restricted expression pattern in the brain. It is only present in glutamatergic neurons and absent from brain areas like dentate gyrus, globus pallidus, parts of the thalamus and substantia nigra (Bajjalieh et al., 1994). SV2C is the least studied isoform and is mostly expressed in striatum, midbrain and hindbrain (Dardou et al., 2011).

Despite the early identification of SV2 proteins (Buckley and Kelly, 1985), their function still remain unclear, even in regards to the best characterized isoform SV2A (Bartholome et al., 2017). SV2A is implicated in epilepsy as a target of the anti-epileptic drug levetiracetam (Lynch et al., 2004). In addition, its topology and homology to major facilitator superfamily (MFS) and neurotransmitter transporters suggested that SV2A functions as a transporter (Feany et al., 1992). Electrophysiological analysis of the defective neurotransmission in the absence of SV2 proteins proposed a role of SV2 in synaptic plasticity by regulating residual calcium (Chang and Sudhof, 2009; Janz et al., 1999; Wan et

al., 2010), SV release probability or the size of the readily releasable pool of SVs (Custer et al., 2006). Of note, Syt1 was shown to interact with all SV2 isoforms (Lazzell et al., 2004; Schivell et al., 1996; Schivell et al., 2005). Especially the N-terminus of SV2A has been identified to bind to the C2B domain of Syt1. This interaction is negatively regulated by calcium ions (Schivell et al., 1996) and potentiated by SV2A phosphorylation (Pyle et al., 2000; Zhang et al., 2015). Interestingly, the combined deletion of SV2A and SV2B in mice severely affected the Syt1 level and localization, providing further evidence for an important role of SV2 in Syt1 sorting. SV2A/B DKO mice display reduced Syt1 levels on SVs and an accumulation of Syt1 at the presynaptic surface. Moreover, the tyrosine-based motif within SV2A has been shown to be required for SV2A's own retrieval as well as for the correct trafficking of Syt1 (Yao et al., 2010) (Figure 6).

All in all, the cumulative evidence from biochemical interactions and *in vivo* data argue for an important role of SV2 in Syt1 trafficking. Whether SV2 is relevant for correct Syt1 sorting during neurotransmission remained unanswered so far. Together with SV2's late appearance in evolution it makes a perfect candidate to mediate Syt1 sorting and to compensate the Stn2 loss in Stn2 KO mice.

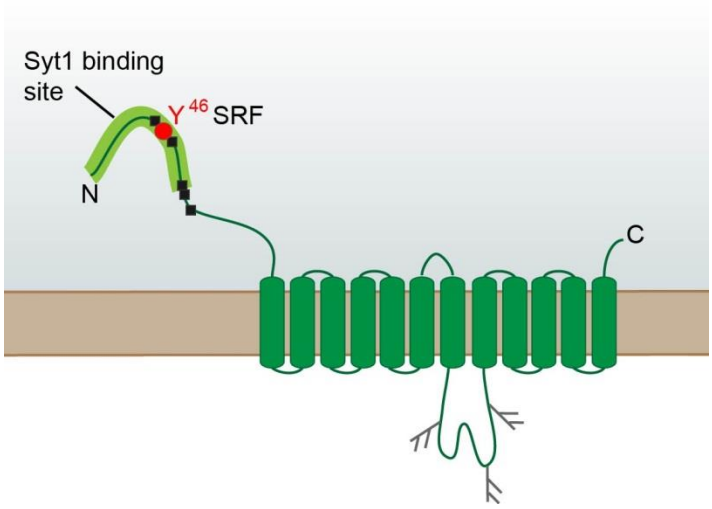


**Figure 6: Scheme of SV2A.** The intracellular N-terminus harbors the tryrosine-based motif $Y^{46}$SRF (red). In direct vicinity as well as at S80, S81 and T84 are phosphorylation sites (black)**,** that potentiate the binding to Syt1 (Syt1 binding site marked in light green). The luminal domain between transmembrane domain 7 and 8 is characterized by three N-glycosylation sites (grey).

## 1.6. Coupling of exocytosis and endocytosis

For functional neurotransmission at the synapse SV exocytosis has to be tightly coupled to compensatory endocytosis of SVs on multiple levels. In order to avoid shrinking or expansion of the presynaptic terminal, the number of released SVs has to match the amount of endocytosed material. Indeed, traces of membrane retrieval monitored by capacitance

measurements as well as SV protein retrieval visualized by pHluorin imaging both display a decay back to baseline after exocytosis (Granseth et al., 2006; Lou et al., 2008; Soykan et al., 2017; Yamashita et al., 2010). Only rarely e.g. in the case of repetitive high frequency stimulation an endocytic overshoot with membrane retrieval exceeding the amount of exocytosis was observed (Wu et al., 2014a; Wu et al., 2007). How the information of SV fusion is conveyed to or sensed by the endocytic machinery is still enigmatic. More importantly endocytic retrieval has to be tightly coupled in time to SV fusion to retain the presynaptic architecture and clear the release sites, thereby allowing responsiveness to repetitive stimulation. Indeed, subsecond endocytic kinetics have been revealed by analysis of electron micrograms of optogenetically stimulated neurons (Watanabe et al., 2013a; Watanabe et al., 2013b) as well as by pHluorin measurements of cultured hippocampal neurons stimulated with single APs (Soykan et al., 2017).

Various mechanisms have been proposed, but how endocytosis is initiated at the periactive zone adjacent to SV release sites still remains unclear (Maritzen and Haucke, 2017). The loss of membrane tension after exocytic SV fusion could affect the cytoskeleton at the presynaptic terminal. Especially the actomyosin cytoskeleton is implicated in endocytic retrieval in various model systems like yeast (Kaksonen et al., 2005), neuroendocrine cells (Gormal et al., 2015) and cultured neurons (Soykan et al., 2017; Wu et al., 2016). Furthermore, a physical link between exocytic and endocytic components could be envisioned as another coupling mechanism. A molecular association of active zone scaffold proteins like piccolo and bassoon that direct SVs to sites of calcium entry with endocytic and actin-binding proteins would allow such a connection. Such a potential link was identified for piccolo and the actin/dynamin-binding protein ABP1 (Fenster et al., 2003). Additionally, piccolo can interact with GIT1/2 at the active zone, which in turn recruits the endocytic adaptor Stn2 to endocytic sites (Podufall et al., 2014). Linking the site of SV fusion to endocytic proteins and regulators of the actin cytoskeleton is also accomplished by the large scaffold protein intersectin that interacts with the exocytic protein SNAP-25 and e.g. dynamin and AP-2 as well as Cdc42 (Pechstein et al., 2010). As the deletion of intersectin1 does not perturb endocytic membrane retrieval but does affect the replenishment of fast-releasing SVs, it was suggested that intersectin1 facilitates release site clearance to allow multiple rounds of SV fusion (Sakaba et al., 2013). Therefore, presynaptic scaffolds could coordinate release site clearance and, thereby play a role in coupling SV exo- and endocytosis (Haucke et al., 2011).

A signaling molecule that exo- and endocytosis have in common is calcium, which thereby could have a coupling role. SV fusion is triggered by a local increase of the

intracellular calcium concentration regulated by voltage-gated calcium channels at the active zone (Katz and Miledi, 1967a; Neher and Sakaba, 2008; Sabatini and Regehr, 1996). Likewise, SV endocytosis is facilitated by calcium influx (Sankaranarayanan and Ryan, 2001; Wu et al., 2009). Effector proteins that could mediate a calcium-based regulation of SV endocytosis are the calcium binding protein calmodulin and its downstream target calcineurin. Calmodulin activates calcineurin, dephosphorylating a number of endocytic proteins, called dephosphins, such as dynamin, AP180, the inositol phosphatase synaptojanin and the $PI(4,5)P_2$ synthesizing kinase phosphatidylinositol 4-phosphate 5-kinase 1γ (PIPK1γ) (Cousin and Robinson, 2001). In addition, Syt1 with its calcium binding C2 domains represents another effector that can sense calcium influx and has been suggested to play a role in SV exo- as well as endocytosis (s. section 1.4). However, calcium influx alone is not sufficient to initiate endocytic retrieval. Capacitance measurements showed that AP-triggered calcium influx was unable to induce endocytic retrieval, when SV fusion was inhibited by botulinum neurotoxin, which cleaves SNARE proteins (Wu et al., 2005; Yamashita et al., 2005). Therefore, insertion of exocytic SV material in the form of SV protein and/or membrane is additionally required to trigger endocytic uptake by a so far unresolved mechanism.

As an alternative mechanism membrane lipids could coordinate exo- and endocytosis of SVs. Phosphoinositides are important signaling molecules enriched on distinct cellular compartments and known regulators of cellular trafficking events (Behnia and Munro, 2005; De Matteis and Godi, 2004). In particular $PI(4,5)P_2$ has pivotal roles in controlling exocytosis and endocytosis during neurotransmission and will be described in detail in the next section.

## 1.7. $PI(4,5)P_2$ at the presynapse

$PI(4,5)P_2$ is one of the most abundant species among the family of phosphoinositides (PIs). PIs are membrane phospholipids derived from phosphatidylinositol that is characterized by a diacylglycerol backbone esterified to a *myo*-inositol headgroup at the 1' position. The reversible phosphorylation of hydroxylgroups at the 3', 4' and 5' position of the *myo*-inositol ring gives rise to seven different PI species. These short-lived PIs can be rapidly generated and interconverted by a complex interplay of PI metabolizing enzymes (Figure 7). PI kinases and phosphatases are stereoselective and are recruited to specific subcellular compartments allowing for the specific enrichment of PI species at distinct cellular membranes. The localization of PIs in the cytoplasmic leaflet of intracellular membranes in turn enables the binding of effector proteins and thereby defines the membrane identity of cellular

compartments. Consequently, PIs control and regulate a multitude of cell-physiological processes even though they are a rare membrane lipid species (Di Paolo and De Camilli, 2006).

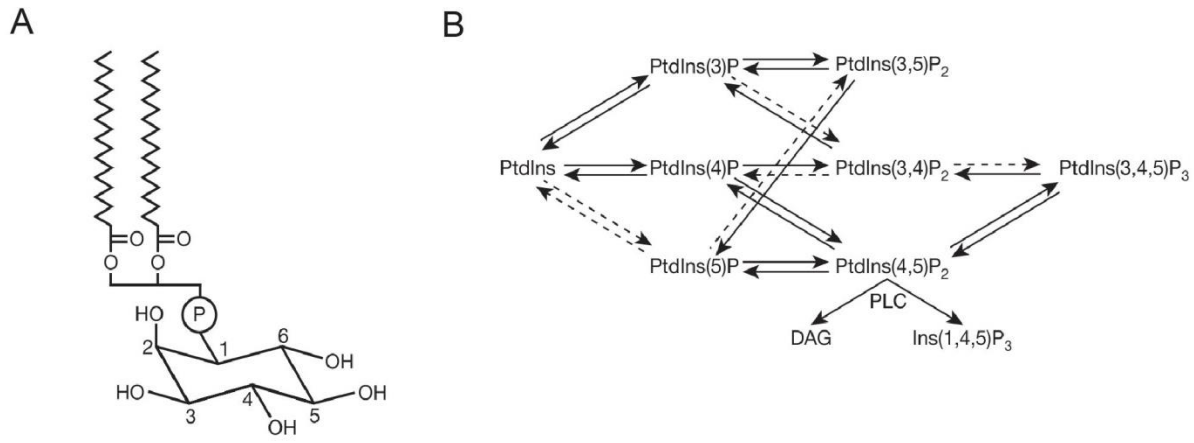


**Figure 7: Phosphoinositide metabolism. (A)** Chemical structure of phosphatidylinositol, an amphiphatic membrane phospholipid. Fatty acids are esterified to the glycerol backbone at C1 and C2, while the C3 is phosphodiesterified to a non-planar *myo*-inositol, a 6-carbon polycyclic alcohol. **(B)** The hydroxylgroups of the inositol ring at position 3', 4' and 5'can be reversibly phosphorylated to generate seven polyphosphoinositides, which can be interconverted by the concerted action of PI kinases and phosphatases. Dotted arrows represent reactions that have been demonstrated *in vitro* but whose importance *in vivo* remains unclear. PtdIns, phosphatidylinositol. Adapted from (Di Paolo and De Camilli, 2006) License number: 4287151278192.

$PI(4,5)P_2$ is the most important PI in the context of this study. It can be generated in principle from multiple precursors. The membrane residing phosphatidylinositol-4-phosphate [PI(4)P] and phosphatidylinositol-5-phosphate [PI(5)P] can serve as a substrate for additional phosphorylation at the 5' or 4' position, respectively. However, PI(5)P is only present in low concentration in cells, while PI(4)P is more abundant and localized at the plasma membrane, the Golgi complex and possibly on SVs (Guo et al., 2003). Thus, PI(4)P represents the major substrate for $PI(4,5)P_2$ synthesis by type I PI(4)P 5-kinases like PIPK1γ in the brain (Di Paolo et al., 2004). Conversely, $PI(4,5)P_2$ can be degraded by $PI(4,5)P_2$-specific phospholipases or phosphatases. The phospholipase C (PLC) consumes $PI(4,5)P_2$ to yield the second messenger molecules diacylglycerol (DAG) and inositoltrisphosphate ($IP_3$). The phosphorylation of $PI(4,5)P_2$ to phosphatidylinositol-(3,4,5)-trisphosphate [$PI(3,4,5)P_3$] represents an alternative route of $PI(4,5)P_2$ conversion and generates another important signaling molecule in the cell (Di Paolo and De Camilli, 2006).

Only less than 1 % of total brain lipids is comprised of $PI(4,5)P_2$ (Wenk et al., 2003). Nevertheless, it is an essential plasma membrane signal for vesicle trafficking, signal transduction, ion channel regulation and actin cytoskeleton remodeling (De Matteis and Godi,

2004; Di Paolo and De Camilli, 2006; Krauss and Haucke, 2007). $PI(4,5)P_2$ mediates its various tasks by recruiting effector proteins or by regulating transmembrane proteins with specific cytosolic domains. The negatively charged headgroup of $PI(4,5)P_2$ can interact with a cluster of basic residues in membrane targeting domains like the pleckstrin homology (PH) domain, the calcium-dependent C2 domain or the epsin N-terminal homology (ENTH) domain. Another level of regulation is exhibited by the spatial concentration of $PI(4,5)P_2$ at the plasma membrane. Immunocytochemistry, superresolution microscopy and live cell imaging with a GFP-tagged PH domain and $PI(4,5)P_2$ specific antibodies revealed that $PI(4,5)P_2$ is localized in nanoclusters at the plasma membrane (Milosevic et al., 2005), at exocytic release sites (van den Bogaart et al., 2011) and is present at the periactive zone of neurons (Micheva et al., 2001). Both $PI(4,5)P_2$ localization as well as the manipulation of $PI(4,5)P_2$ levels provided evidence for being an essential component in the SV exo- and endocytosis in neurons. The depletion of the major $PI(4,5)P_2$ synthesizing kinase PIPK1γ in mice reduced $PI(4,5)P_2$ levels to about 50 % severely impairing SV exocytosis, SV membrane retrieval and resulting in postnatal lethality (Di Paolo et al., 2004). These results were confirmed in neuroendocrine cells showing an increased secretion of large dense core vesicles in the presence of elevated $PI(4,5)P_2$ levels. In contrast, dense core vesicle secretion was abrogated in the absence of $PI(4,5)P_2$ (Milosevic et al., 2005). Conversely, block of $PI(4,5)P_2$ hydrolysis by depletion of the $PI(4,5)P_2$ phosphatase synaptojanin resulted in defective SV recycling accompanied by an accumulation of clathrin coated SVs (Cremona et al., 1999; Kim et al., 2002). Therefore, the regulated turnover of $PI(4,5)P_2$ is essential for synaptic homeostasis (Hammond and Schiavo, 2007).

### 1.7.1. $PI(4,5)P_2$ during SV exocytosis

The role of $PI(4,5)P_2$ in vesicle exocytosis has been addressed extensively in neuroendocrine cells as well as in neurons. Early studies in permeabilized chromaffin cells suggested a DAG and $IP_3$ independent role of phosphoinositides such as $PI(4,5)P_2$ in the exocytosis of large dense core vesicles (Eberhard et al., 1990). Later, experiments in permeabilized synaptosomes confirmed the role of $PI(4,5)P_2$ in SV release as well (Zheng et al., 2004). The shielding of $PI(4,5)P_2$ by either overexpression of an GFP-tagged PH domain in chromaffin cells or by feeding permeabilized synaptosomes with a $PI(4,5)P_2$ specific antibody inhibited the fusion of chromaffin granules and SVs, respectively (Holz et al., 2000; Zheng et al., 2004). Likewise reducing $PI(4,5)P_2$ level in mice by PIPK1γ deletion resulted in a strong exocytic phenotype

with a smaller releasable pool of SVs and defects in synaptic transmission upon high frequency stimulation (Di Paolo et al., 2004). Additionally, expressing a membrane targeted variant of synaptojanin profoundly reduced the secretion of large dense core vesicles in neuroendocrine cells (Milosevic et al., 2005). However, $PI(4,5)P_2$'s role in exocytosis could be an indirect contribution even though early studies suggested the opposite. The manipulation of $PI(4,5)P_2$ would also affect the amounts of DAG and $IP_3$ generated by the consumption of $PI(4,5)P_2$ by PLC. Especially, the stimulating effect on exocytosis of DAG has challenged $PI(4,5)P_2$'s direct role during SV exocytosis. DAG has been shown to activate two priming factors, Munc13 by direct DAG binding (Betz et al., 1998; Rhee et al., 2002) and Munc18-1 via protein kinase C (Genc et al., 2014; Nili et al., 2006) and thereby enhances secretion. Recently, an elegant study by Walter and colleagues directly dissected the role of $PI(4,5)P_2$ and DAG during exocytosis by manipulating both molecules optically with high temporal resolution. UV-uncaging of $PI(4,5)P_2$, but not of DAG, potentiated exocytosis and increased the size of the readily releasable pool monitored by capacitance measurements of adrenal chromaffin cells (Walter et al., 2017).

$PI(4,5)P_2$ presumably mediates exocytic fusion by orchestrating the recruitment and activation of exocytic proteins. Its association with proteins like Munc13, the related calcium activated protein for secretion (CAPS) and the calcium sensor Syt1 is required for their exocytic function. $PI(4,5)P_2$ at the plasma membrane binds to the C2B domain of Syt1 residing on SVs (Honigmann et al., 2013; Schiavo et al., 1996), substantially increasing the binding affinity of the C2B domain for calcium ions *in vitro* (Li et al., 2006; van den Bogaart et al., 2012). Thus, this interaction in *trans* facilitates SV fusion as it mediates Syt1's binding to the plasma membrane, its membrane penetration (Bai et al., 2004) and elevates the calcium affinity of Syt1 into a physiological range. In addition, $PI(4,5)P_2$ and its downstream product $PI(3,4,5)P_3$ act in *cis*. They interact with the juxtamembrane region of the target SNARE protein syntaxin 1A (Khuong et al., 2013), which is required for the clustering of syntaxin 1A and functional neurotransmission (Khuong et al., 2013; van den Bogaart et al., 2011). Other active zone proteins implicated in SV exocytosis like piccolo, RIM and rabphilin exhibit C2 domains and could potentially be regulated by $PI(4,5)P_2$ as well. However, the functional relevance and mechanism of their putative $PI(4,5)P_2$ interaction are so far elusive.

Interestingly, $PI(4,5)P_2$ can also affect SV exocytosis by modulating ion influx into the synapse (Rodriguez-Menchaca et al., 2012). The activity of voltage-dependent calcium channels is dependent on the $PI(4,5)P_2$ levels in the plasma membrane. The depletion of $PI(4,5)P_2$ either by PLC in response to the activation of metabotropic receptors or by targeting

5-phosphatases to the plasma membrane leads to the attenuation of calcium influx (Gamper et al., 2004; Suh et al., 2010; Wu et al., 2002). While $PI(4,5)P_2$ is required for calcium channel opening, elevated $PI(4,5)P_2$ level were reported to inhibit calcium channel activity (Wu et al., 2002) arguing for a dual regulation of voltage-gated calcium channels by $PI(4,5)P_2$.

All in all, $PI(4,5)P_2$ facilitates SV exocytosis on multiple levels. It does not only mark the sites of SV fusion but activates the fusion machinery itself and can modulate the calcium ion influx that eventually triggers the SV release.

### 1.7.2. The role of $PI(4,5)P_2$ during SV endocytosis

The action of $PI(4,5)P_2$ is not limited to the exocytic part of neurotransmission, but plays an essential role in endocytosis, which has been demonstrated by the manipulation of $PI(4,5)P_2$ metabolizing enzymes. The loss of the $PI(4,5)P_2$ synthesizing kinase PIPK1γ markedly inhibits SV endocytosis (Di Paolo et al., 2004). In contrast, the increase in $PI(4,5)P_2$ levels by blocking its hydrolysis e.g. in the absence of the $PI(4,5)P_2$ phosphatase synaptojanin or its recruitment factor endophilin initiates endocytosis but fails to reform SVs as shown by an accumulation of clathrin-coated vesicles (Bai et al., 2010; Cremona et al., 1999; Kim et al., 2002; Verstreken et al., 2003).

Similar to its role in SV exocytosis, $PI(4,5)P_2$ also serves as a recruitment hub for endocytic proteins involved in all forms of endocytosis. It is required during all stages of CME (Antonescu et al., 2011) that likely is of importance for correct SV reformation during neurotransmission. Membrane remodeling proteins of the Bin/Amphiphysin/Rvs (BAR) – domain superfamily act at different stages of endocytosis and can interact with $PI(4,5)P_2$. Fer/Cip4 homology domain only (FCHo)1/2 help to generate a shallow membrane curvature during early stages of CME (Henne et al., 2010), while amphiphysin and endophilin as well as sorting nexin 9 act at later stages by binding negatively charged lipids such as $PI(4,5)P_2$ (Ferguson et al., 2009; Rao and Haucke, 2011). Of note, adaptor proteins such as AP-2 and AP180/CALM are recruited by $PI(4,5)P_2$ either by the interaction with basic residues (Collins et al., 2002; Rohde et al., 2002) or the ANTH domain (Itoh et al., 2001), respectively. The binding of AP-2 to $PI(4,5)P_2$ initiates a conformational change within the heterotetrameric complex that is aided by the phosphorylation of the µ2 subunit and transmembrane cargo. The change from a closed to an open conformation exposes the cargo recognition sites of AP-2 and additional $PI(4,5)P_2$ binding sites within µ2 (Jackson et al., 2010). Interestingly, AP-2 has been shown to recruit and stimulate the kinase activity of PIPK1γ (Krauss et al., 2006;

Nakano-Kobayashi et al., 2007). Thereby the $PI(4,5)P_2$ pool is elevated, facilitating the nucleation of CME until the clathrin coat displaces the PIPK1γ interaction and stops the feed forward loop (Thieman et al., 2009).

The scission at the neck of endocytic membrane invaginations (Kononenko et al., 2014) is mediated by the mechanochemical GTPase dynamin (Mettlen et al., 2009). $PI(4,5)P_2$ binds to the autoinhibitory PH domain of dynamin allowing its oligomerization into a helical assembly and the fission reaction (Chappie et al., 2011; Reubold et al., 2015; Takei et al., 1995). During SV reformation $PI(4,5)P_2$ has to be degraded to enable the disassembly of the clathrin coat from SVs, while impaired $PI(4,5)P_2$ turnover results in defective SV recycling and postnatal lethality (Cremona et al., 1999). The recruitment of synaptojanin by endophilin coincides with the appearance of dynamin at late stages of clathrin-coated pit formation (Perera et al., 2006; Schuske et al., 2003). As endophilin induces or senses curved membranes, it has been suggested that synaptojanin mediates $PI(4,5)P_2$ conversion only at sites of high curvature. This spatially restricted hydrolysis of $PI(4,5)P_2$ can cooperate with dynamin to facilitate the membrane fission reaction (Chang-Ileto et al., 2011).

$PI(4,5)P_2$ can control SV endocytosis not only by recruiting endocytic proteins, but has been shown to control actin dynamics by directly regulating actin binding proteins or indirectly via small GTPases of the Rho family (Saarikangas et al., 2010). Especially during clathrin-independent endocytosis the actin cytoskeleton seems to play an essential role (Soykan et al., 2017; Watanabe et al., 2013b). While many actin binding proteins involved in multiple cellular functions associate via multivalent electrostatic interactions with $PI(4,5)P_2$ (Senju et al., 2017), it is not completely understood, which regulate SV retrieval in a $PI(4,5)P_2$-dependent manner. So far genetic manipulations as well as pharmacological inhibition of formins suggest that they are an important component of SV endocytosis (Ganguly et al., 2015; Soykan et al., 2017). Via its N-terminal basic domain the formin mDia2 can be directed to the $PI(4,5)P_2$ enriched plasma membrane and facilitate the formation of linear actin filaments (Gorelik et al., 2011; Paul and Pollard, 2009; Senju et al., 2017).

### 1.7.3. PIPK1γ as the major $PI(4,5)P_2$ synthesizing kinase in the brain

$PI(4,5)P_2$ synthesis was early associated with a type I phosphatidylinositol 4-phosphate 5-kinase that is required for calcium-dependent secretion (Hay et al., 1995). These type I kinases are conserved from yeast to human. While yeast only harbors one gene the mammalian genome has three PIPK1 isoforms, called PIPK1α, β and γ. PIPK1γ has several

splice variants (Balla, 2013; Giudici et al., 2004), but only the 661 amino acid residue isoform of murine PIPK1γ (also known as PIPK1γ-v2) is enriched in the mouse brain (Wenk et al., 2001) and therefore of special importance for PI(4,5)$P_2$ synthesis in the synapse. Even though PIPK1α and β are also present in the brain and might have compensated for the loss of PIPK1γ, PIPK1γ KO mice were found to suffer from severe neurotransmission impairments. These defects cumulated in early postnatal death (Di Paolo et al., 2004) arguing for an essential role of PIPK1γ in the synapse.

PIPK1γ is a cytoplasmic enzyme that can localize to the plasma membrane via its conserved kinase domain. Two tandem basic residues at the C-terminus of the kinase domain as well as three residues within the kinase domain confer the substrate specificity for PI(4)P and allow its association with the plasma membrane (Arioka et al., 2004; Kunz et al., 2000). The membrane targeting and the kinase activity of PIPK1γ are regulated by multiple mechanisms. In resting conditions PIPK1γ is phosphorylated at the C-terminus at serine 650 via cyclin dependent kinase 5 (CdK5). Neuronal activity and calcium influx activate the phosphatase calcineurin, which dephosphorylates PIPK1γ and thereby activates the kinase (Cousin and Robinson, 2001; Nakano-Kobayashi et al., 2007). The activated and dephosphorylated PIPK1γ is able to interact with the filamentous actin binding protein talin. Talin contains a band 4.1/ezrin/radixin/moesin-like (FERM) domain enabling interactions with various proteins implicated in focal adhesions such as integrins, actin and PI(4,5)$P_2$ (Calderwood et al., 1999). In addition, the FERM domain endows the binding and recruitment of the activated PIPK1γ to the plasma membrane (Di Paolo et al., 2002; Lee et al., 2005). This interaction of PIPK1γ and talin is implicated to play a role in the presynaptic terminal as well and argues for a coordinated mechanism of PI(4,5)$P_2$ synthesis, actin dynamics and endocytosis during SV recycling (Morgan et al., 2004). Moreover, PI(4,5)$P_2$ synthesis at the presynaptic plasma membrane is potentiated by the PIPK1γ recruitment via the small GTPase Arf6 (Krauss et al., 2003). The nucleation of clathrin-coated pits is further aided by the binding of AP-2 to PIPK1γ. The μ2 domain as well as the β2 subunit of AP-2 can interact and recruit the kinase to the plasma membrane, especially in its activated state (Kahlfeldt et al., 2010; Krauss et al., 2006; Nakano-Kobayashi et al., 2007). Therefore, PI(4,5)$P_2$ synthesis is facilitated in a spatially restricted manner to promote nucleation of clathrin-coated pits. The clathrin coat is believed to interfere with the kinase interaction and ends the feed forward loop. This is in line with biochemical data showing the absence of PIPK1γ from clathrin-coated vesicles (Wenk et al., 2001).

All in all, PIPK1γ-mediated synthesis of $PI(4,5)P_2$ is regulated and thereby spatially confined to small clusters that are essential for SV exocytosis as well as endocytosis at the presynaptic terminal. However, the exact coordination of these processes during neurotransmission remains unclear. Nevertheless, the evidence of $PI(4,5)P_2$'s role during SV recycling by governing recruitment and activation of exocytic and endocytic proteins implicated both in CME and CIE argue for an important coupling function of $PI(4,5)P_2$.

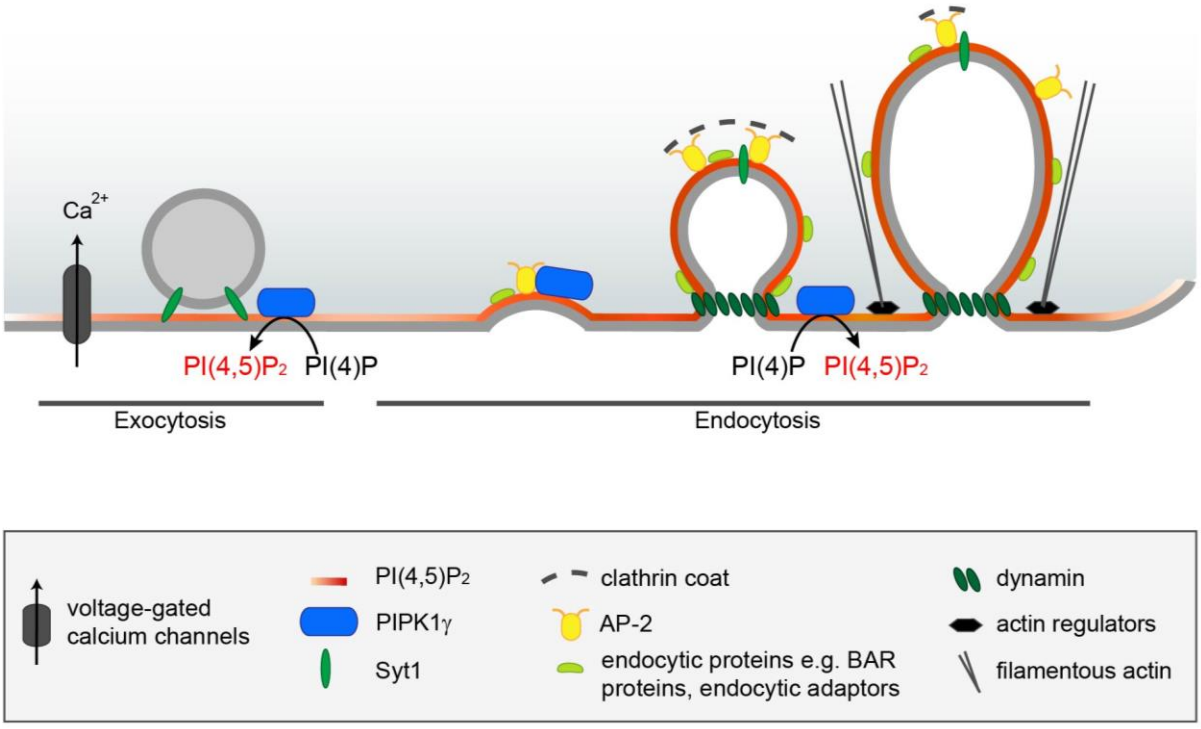


**Figure 8: $PI(4,5)P_2$ synthesized by PIPK1γ coordinates exo- and endocytosis of SVs.** $PI(4,5)P_2$ is generated from PI(4)P by PIPK1γ and is spatially concentrated at the plasma membrane, particularly at the active zone and at sites of endocytic retrieval in the periactive zone. It marks and activates the exocytic fusion machinery facilitating SV release probability after calcium influx, e.g. by the following mechanism: SV-localized Syt1 after binding $PI(4,5)P_2$ penetrates the plasma membrane thereby facilitating SV fusion. PIPK1γ is recruited to the plasma membrane i.a. by AP-2 at the periactive zone to increase the local pool of $PI(4,5)P_2$ for endocytosis. $PI(4,5)P_2$ in turn promotes the recruitment of additional endocytic adaptor proteins, of endocytic proteins controlling membrane curvature and of dynamin, which mediates the fission reaction. In addition, $PI(4,5)P_2$ activates and recruits actin regulatory proteins to the plasma membrane for remodeling the actin cytoskeleton and thus promoting SV endocytosis, especially clathrin-independent endocytosis.

# 2. Aims of this study

SV exocytosis requires temporally-coupled compensatory endocytic retrieval and precise SV reformation to maintain neurotransmission at central synapses, processes that are incompletely understood. Based on strikingly different phenotypes caused by the deletion of Syt1's dedicated endocytic adaptor Stn2 and its homologs in mice and in invertebrate model systems, we hypothesized that another sorting mechanism has evolved in mammalian synapses to ensure correct Syt1 retrieval. As the SV glycoprotein SV2A/B had been associated with Syt1 trafficking, we aimed to investigate in the first part of my thesis whether precise Syt1 sorting in mammalian synapses is accomplished not only by a cargo specific mechanism, but also by complex formation with another SV protein, specifically SV2.

Interestingly, surface-stranded Syt1 does not impair the retrieval kinetics of SVs, but facilitates SV endocytosis. This phenotype led us to the question of the second part of my thesis: What are the functional consequences of Syt1 sorting in the synapse during SV recycling? We aimed to examine whether Syt1 can mediate exo-/endocytic coupling and investigated the mechanism of how surface-stranded Syt1 in the absence of Stn2 can regulate SV exo- and endocytosis mechanistically.

# 3. Material and Methods

## 3.1. Materials

### 3.1.1. Chemicals

If not indicated otherwise chemicals were purchased from Carl Roth (Germany), Life Technologies (USA), Merck (Germany), Sigma-Aldrich (USA) and Thermo Fisher (USA). Consumables were obtained from B. Braun (Germany), Biozym (Germany), GE Healthcare (UK), Greiner (Germany), Millipore (USA), Sarstedt (Germany) and Schott (Germany).

### 3.1.2. Buffers, Media and Solutions

All buffers and solutions were prepared with ultrapure water. The pH was adjusted using NaOH or HCl unless otherwise specified. Buffers used for specific protocols are specified in the respective methods section.

**Table 1: Buffers and media used for molecular biology experiments.**

| Buffer | Composition |
|---|---|
| LB medium | 1 % (w/v) Yeast extract<br>0.5 % (w/v) NaCl<br>0.5 % (w/v) Trypton<br>pH 7.4 |
| LB plates | LB medium<br>15 g/l Agar-agar |
| 2× YT medium | 1.0 % (w/v) Yeast extract<br>1.6 % (w/v) Trypton<br>0.5 % (w/v) NaCl<br>pH 7.4 |
| Antibiotics (stock solutions) | 100 mg/ml Ampicillin, sterile filtered (1000x)<br>50 mg/ml Kanamycin, sterile filtered (1000x) |
| 50x Tris-Acetate-EDTA buffer (TAE) | 200 mM Tris<br>100 mM Glacial acetic acid<br>50 mM EDTA<br>pH 8.2 – 8.4 |

| | |
|---|---|
| 10x Tris-Borate-EDTA buffer (TBE) | 20 mM EDTA<br>890 mM Tris<br>890 mM Boric acid |
| 6x DNA loading dye | 0.03 % (w/v) Bromophenol blue<br>0.03 % (w/v) Xylene cyanol FF<br>60 % (v/v) Glycerol<br>60 mM EDTA |
| OrangeG loading dye | Spatula tip of OrangeG<br>70 % (v/v) Glycerol |
| Tail lysis buffer | 100 mM Tris, pH 8.5<br>5 mM NaEDTA<br>0.2 % (w/v) SDS<br>200 mM NaCl |

**Table 2: Buffers and solutions used for cell biological experiments and fluorescent microscopy.**

| Buffer | Composition |
|---|---|
| DMEM (Lonza)<br>(for HEK 293) | Dulbecco's modified eagles medium, 4.5 g/l glucose (Gibco)<br>Additives:<br>10 % (v/v) Fetal bovine serum (heat-inactivated, Gibco)<br>100 U/ml Penicillin<br>0.1 mg/ml Streptomycin |
| DMEM (Lonza)<br>(for Hek293 FlpIn) | Dulbecco's modified eagles medium, 4.5 g/l glucose (Gibco)<br>Additives:<br>10 % (v/v) Fetal calf serum (heat-inactivated, Gibco)<br>100 U/l Penicillin<br>0.1 mg/ml Streptomycin<br>10 µg/ml Blasticidin<br>100 µg/ml Hygromycin/ 100 µg/ml Zeocin |
| Basic medium for hippocampal neuron cultures | 1 x MEM (Minimum Essential Media; Life Technologies)<br>5 g/l Glucose<br>200 ml/l $NaHCO_3$<br>100 mg/l Transferrin (Merck) |

| | |
|---|---|
| Plating medium for hippocampal neurons | 1 x Basic medium<br>10 % (v/v) FCS (Biochrom)<br>2 mM L-glutamine (Lonza)<br>25 mg/ml Insulin<br>50 U/ml Penicillin<br>50 µg/ml Streptomycin |
| Growth medium for hippocampal neurons | 1 x Basic medium<br>5 % (v/v) FCS (Biochrom)<br>0.5 mM L-glutamine (Lonza)<br>2 % (v/v) B27-supplement (Life Technologies)<br>50 U/ml Penicillin<br>50 µg/ml Streptomycin |
| Digestion solution | 137 mM NaCl<br>5 mM KCl<br>7 mM $Na_2HPO$<br>25 mM Hepes pH 7.4 |
| Dissociation solution | Hank's balanced salt solution w/o $Ca^{2+}$ or $Mg^{2+}$<br>50 mg/l $NaHCO_3$<br>12 mM $MgSO_4$<br>1 mM Hepes pH 7.4 |
| 10x Phosphate-buffered saline (PBS) | 1.37 M NaCl<br>43 mM $Na_2HPO_4$<br>14 mM $NaH_2PO_4$<br>27 mM KCl<br>pH 7.4 |
| PBS + $MgCl_2$ | 1x PBS<br>10 mM $MgCl_2$ |
| PFA fixative | 4 % (w/v) Paraformaldehyde (PFA)<br>4 % (w/v) Sucrose<br>1x PBS<br>pH 7.4 |
| Glutaraldehyde fixative | 1 % (v/v) Glutaraldehyde (GA)<br>2 % (w/v) Paraformaldehyde (PFA)<br>2 % (w/v) Sucrose<br>1x PBS<br>pH 7.4 |

| | |
|---|---|
| 10 x Imaging stock solution | 1.2 M NaCl |
| | 35 mM KCl |
| | 40 mM $KH_2PO_4$ |
| | 200 mM TES |
| | 50 mM $NaHCO_3$ |
| | 50 mM Glucose |
| | 12 mM $Na_2SO_4$ |
| | pH 7.4 |
| Imaging buffer | 50 mM NaCl |
| | 1.2 mM $MgCl_2$ |
| | 1.3 mM $CaCl_2$ (2 mM $CaCl_2$ where indicated) |
| | 1x Imaging stock solution |
| | 50 µM APV |
| | 10 µM CNQX |
| Stimulation imaging buffer | 80 mM KCl |
| | 1.2 mM $MgCl_2$ |
| | 1.3 mM $CaCl_2$ |
| | 1x Imaging stock solution |
| Basic imaging buffer | 50 mM $NH_4Cl$ |
| | 1.2 mM $MgCl_2$ |
| | 1.3 mM $CaCl_2$ |
| | 1x Imaging stock solution |
| 10 x Acidic stock solution | 1.2 M NaCl |
| | 35 mM KCl |
| | 40 mM $KH_2PO_4$ |
| | 200 mM MES |
| | 50 mM $NaHCO_3$ |
| | 50 mM Glucose |
| | 12 mM $Na_2SO_4$ |
| | pH 5.5 |
| Acidic imaging buffer | 50 mM NaCl |
| | 1.2 mM $MgCl_2$ |
| | 1.3 mM $CaCl_2$ |
| | 1x Acidic stock solution |

**Table 3: Buffers and solutions used for biochemical experiments.**

| Buffer | Composition |
|---|---|
| Homogenization buffer I | 320 mM Sucrose |
| | 4mM Hepes |
| | pH 7.5 |
| Lysis buffer | 20 mM Hepes pH 7.4 |
| | 100 mM KCl |
| | 2 mM $MgCl_2$ |
| | 1 % (v/v) Triton X-100 |
| | 1 mM PMSF |
| | 0.3 % (v/v) Protease inhibitor cocktail |
| Brain homogenization buffer II | 50 mM Tris, pH 7.5 |
| | 150 mM NaCl |
| | 1 % (v/v) Triton X-100 |
| | 10 % (v/v) Glycerol |
| | 5 mM N-Ethylmaleimide |
| | 21 mM MG132 |
| | 1 mM PMSF |
| | 0.3 % Protease inhibitor cocktail |
| 2 × Bradford reagent | 200 ml 85 % $H_3PO_4$ |
| | 100 ml Ethanol |
| | 140 g/l Coomassie G250 |
| 6x SDS sample buffer | 18 % (w/v) SDS |
| | 30 % (v/v) β-Mercaptoethanol |
| | 60 % (v/v) Glycerol |
| | 0.25 % (w/v) Bromophenol blue |
| | 0.325 M Tris pH 6.8 |
| 4x SDS separating gel buffer | 0.4 % (w/v) SDS |
| | 1.5 M Tris pH 8.8 |
| 4x SDS stacking gel buffer | 0.4 % (w/v) SDS |
| | 0.5 M Tris pH 6.8 |
| 10x SDS running buffer | 246 mM Tris |
| | 10 % (w/v) SDS |
| | 1.92 M Glycine |
| Semi-dry blotting buffer | 1x SDS running buffer |
| | 10 % Methanol |

| | |
|---|---|
| Wet blotting buffer | 25 mM Tris<br>192 mM Glycine<br>10 % - 20% (v/v) MeOH |
| Ponceau staining | 0.4 % (w/v) Ponceau-S<br>1 % (v/v) Acetic acid |
| Ponceau destain solution | 1 % (v/v) Acetic acid |
| 10x TBS | 0.2 M Tris pH 7.6<br>1.4 M NaCl |
| Antibody dilution solution | 1 × TBS<br>2 % (w/v) Bovine serum albumin<br>0.03 % (w/v) $NaN_3$<br>sterile filtered (0.2 µm) |
| Antibody blocking solution | 1 × TBS<br>3 % (w/v) Skim milk powder |
| Coomassie stain | 1 g/l Coomassie G250<br>10 % (v/v) Acetic acid<br>25 % (v/v) Methanol |
| Coomassie destain | 10 % (v/v) Acetic acid<br>25 % (v/v) Methanol |

**Table 4: Buffers and solutions used for histological experiments.**

| Buffer | Composition |
|---|---|
| Anaesthetic | 1 × PBS<br>1.2 % (v/v) Ketamin<br>0.16 % (v/v) Rompun |
| Phosphate buffer (PB) 0.4 M | 0.4 M $NaH_2PO_4$ (Buffer A)<br>0.4 M $Na_2HPO_4$ (Buffer B)<br>(~ 85 % (v/v) buffer B and ~ 15 % (v/v) buffer A were mixed to yield pH 7.4) |
| Fixation solution | 4 % (w/v) PFA<br>in 125 mM PB pH 7.4 |
| Ringer solution | 0.85 % (w/v) NaCl<br>0.025 % (w/v) KCl<br>0.02 % (w/v) $NaHCO_3$<br>0.01 % (w/v) Heparin<br>pH 6.9 |

| | |
|---|---|
| Brain storage solution | 20 % (v/v) Glycerol |
| | 2 % (v/v) DMSO |
| | 125 mM Phosphate buffer pH 7.4 |
| Gelatin solution | 0.2 % (w/v) Porcine gelatin |
| | 50 mM Tris pH 7.6 |
| Cresyl violet solution | 0.1 % (w/v) Cresyl violet acetate |
| | 0.25 % (v/v) Glacial acetic acid |

**Table 5: Buffer for electrophysiological experiments.**

| Buffer | Composition |
|---|---|
| Artificial cerebrospinal fluid (ACSF) | 120 mM NaCl |
| | 2.5 mM KCl |
| | 1.25 mM $NaH_2PO_4$ |
| | 24 mM $NaHCO_3$ |
| | 1.5 mM $MgSO_4$ |
| | 2 mM $CaCl_2$ |
| | 25 mM Glucose |
| | pH 7.35 - 7.4 |
| Internal solution | 135 mM K-gluconate |
| | 5 mM NaCl |
| | 5 mM KCl |
| | 10 mM Hepes |
| | 0.2 mM EGTA |
| | 2 mM Mg-ATP |
| | 0.2 mM $Na_3GTP$ |
| | 5 mM QX-314 |
| | 10 mM Glucose |
| | pH 7.3 |
| | 295-305 mOsm |

| | |
|---|---|
| External solution for Calyx of Held patch clamp | 125 mM NaCl<br>2.5 mM KCl<br>25 mM Glucose<br>25 mM $NaHCO_3$<br>1.25 mM $NaH_2PO_4$<br>0.4 mM Ascorbic acid<br>3 mM Myoinositol<br>2 mM Na-pyruvate<br>2 mM $CaCl_2$<br>1 mM $MgCl_2$<br>pH 7.4 |
| Internal solution for Calyx of Held patch clamp | 135 mM Cs-gluconate<br>20 mM TEA-Cl<br>10 mM Hepes<br>5 mM $Na_2$-phosphocreatine<br>4 mM MgATP<br>0.3 mM GTP<br>0.5 or 5 mM EGTA<br>pH 7.2 |

### 3.1.3. Enzymes and kits

Phusion high fidelity DNA polymerase, restriction enzymes, calf intestinal alkaline phosphatase (CIP) and Proteinase K were purchased from New England Biolabs (NEB). T4 DNA Ligase and Dream Taq DNA Polymerase were obtained from Thermo Fisher Scientific. To genotype tail biopsies from mice either the Taq DNA Polymerase from Bio&Sell or KAPA HotStart Mouse Genotyping Kit from Sigma-Aldrich was used.

NucleoSpin Plasmid kit from Macherey-Nagel was used to prepare plasmid DNA from *Escherichia coli* (*E. coli*) overnight cultures in small scale. For large scale plasmid DNA isolation the endotoxin free plasmid DNA purification kit (NucleoBond Xtra Midi EF kit) from Macherey-Nagel was used. Purification of DNA from agarose gels and PCR reactions was performed with NucleoSpin Gel and PCR Clean-up kit from Macherey-Nagel.

For transfection of primary hippocampal cultures the calcium phosphate transfection system was purchased from promega (ProFection Mammalian Transfection system) and used according to manufacturer's instruction.

### 3.1.4. Molecular weight standards

**Table 6: Molecular weight standards**

| Marker | Marker band | Source |
|---|---|---|
| Generuler 1kbp DNA ladder | kbp marker band:<br>10, 8, 6, 5, 4, 3.5, 3, 2.5, 2, 1.5, 1, 0.75, 0.5, 0.25 | Thermo Scientific #SM311 |
| 100 Bp DNA ladder | bp marker band:<br>1500, 1000, 900, 800, 700, 600, 500, 400, 300, 200, 100 | Serva, #003931601 |
| Prestained protein standard | kDa marker bands:<br>175, 80, 58, 46, 30, 25, 17, 7 | New England Biolabs #7708 |
| PageRuler Prestained Protein Ladder | kDa marker bands:<br>180, 130, 100, 70, 55, 40, 35, 25, 15, 10 | Thermo Scientific #26616 |

### 3.1.5. Small interfering RNA and synthetic DNA oligonucleotides

Small interfering RNA (siRNA) to deplete SV2A were originally obtained from Ambion and reordered from Eurofins MWG as lyophilized powder, which was dissolved in nuclease-free siMAX buffer provided by MWG to a final concentration of 100 pmol/µl. Scrambled AP180 siRNA was used as control siRNA at the same stock concentration. All sequences are listed in Table 7.

**Table 7: Sequences of siRNAs used in this study.**

Overhang-sequences to increase siRNA stability are indicated by lower case letters.

| Targeted mRNA | siRNA | Species | Sequence 5' – 3' | Source |
|---|---|---|---|---|
| SV2A exon 6/7 | SV2A s82104 | mouse | Sense:<br>GACCCACAUUAAAACGAUUtt<br>Antisense:<br>AAUCGUUUUAAUGUGGGUCac | Ambion |
| None | AP180 scrambled | Rat | ACAACGAGCUUCCCUUCAA | MWG |
| PIPK1γ exon 11 | PIPK1γ11 | mouse | GCAGCACGGUGUUCCGGAAuu | Dharmacon |
| PIPK1γ exon 8 | PIPK1γ12 | mouse | UCGAUCAGCAGGAGCGAGAuu | Dharmacon |

All DNA oligonucleotides used as primers for polymerase chain reactions (PCRs) were purchased from BioTez as lyophilized powder and dissolved in autoclaved ultrapure water to obtain a 100 µM stock concentration. For experiments the stock was further diluted

to 10 µM. All were stored at -20 °C. Primers were either used to genotype genomic DNA from tail biopsies or ear markings of mouse strains (listed in Table 8) or for cloning and sequencing (listed in Table 9).

**Table 8: Primer sequences used for genotyping genomic DNA of mouse strains.**

WT – wildtype; KO – knockout.

| Genotype | Primer | Sequence 5' – 3' |
|---|---|---|
| Stn2 WT | p22 forward | GATCCCCGGGGCCCCCTCACCTGCCTCA |
| | p23 reverse | GATCCTCGAGCTAGGACAGCACTGGTAAATCCA |
| Stn2 KO | neo forward | GGCGCGGTCCCAGGTCCAC |
| | neo reverse | CTTCGCCCAATAGCAGCCAGTCC |
| SV2A | SV2A WT forward | GAGAATATCAGGGCATCC |
| | SV2A KO forward | CAGTCCTCACAGTCTGTT |
| | SV2A combined reverse | GCCCTCTAGATACAGCTTGC |
| SV2B | SV2B WT forward | TGAAGGCGAGTACCAAGGCA |
| | SV2B KO forward | CCTGTGTGAAATTGTTATCCGCT |
| | SV2B combined reverse | TTCGAGAAAACAAGATTTGGGAAT |

**Table 9: Primer sequences used for cloning and sequencing.**

The primer are named by the targeted coding sequence, restriction enzyme (if used) and direction of the primer either fw – forward or rev – reverse (the reverse complement is specified); mCh – mCherry; seq – sequencing; Sigpept – signal peptide; capital letters mark sequences overlapping with template sequence; low case letters indicate the restriction enzyme binding site and four additional nucleotides (cgat) at 5' end; resist – siRNA resistant; silent mutations are indicated with bold and underlined letters.

| Primer | Sequence 5' – 3' | Application |
|---|---|---|
| mch_fw_seq | GGACATCCTGTCCCCTCAGT | Sequencing of mCherry constructs. |
| mch_rev_seq | CCTCTGCTTGATCTCGCCCT | |
| pHluorin_fw_seq | AAGATGACGGGAACTACAAG | Sequencing of pHluorin constructs. |
| pHluorin_rev_seq | GCCTCCATCTTCAATGTTGTG | |
| Sigpept_AgeI_fw1 | cgat accggt ATGAAAATCCTCGTGGCGGTG | Two-step overhang PCR was used to insert a signal peptide at the N-terminus of mCherry-Syt1 for correct |
| Sigpept_mch_rev2 | CTCGCCCTTGCTCAC AAGCTTGTTGGCACCGATTT | |
| Sigpept_mch_fw3 | GGTGCCAACAAGCTT GTGAGCAAGGGCGAGGAG | |

| | | |
|---|---|---|
| mch_XhoI_rev4 | atcg ctcgag ATCTGAGTCCGGA CTTGTA | localization. |
| SV2A_resist1_fw | GCGAGTCTTCTCAGTAAC**A**CA**T**AT**C**AAAAC | Introduction of three silent mutations in siRNA binding site to obtain siRNA resistant SV2A. |
| SV2A_resist1_rev | CTGATGAATCGTTTT**G**AT**A**TG**T**GTTACTG | |
| SV2A_Sal1_fw | cgat gtcgat ATGGAAGAAGGCTTT | |
| SV2A_BamH1_rev | atcg ggatcc gc CTGCAGCACCTGTCC | |
| Syt1_Sal1_fw | cgat gtcgac ATGGTGAGTGCCAGT | Insertion of Syt1 into mCherry-C1 vector. |
| Syt1_BamH1_rev | atcg ggatcc TTACTTCTTGACAGC | |

### 3.1.6. Plasmid vectors

All bacterial and mammalian expression vectors used in this study are described in Table 10 and Table 11. They were stored at -20 °C at a concentration of 1 µg/µl.

**Table 10: Vector backbones used for cloning and protein expression.**

| Plasmid backbone | Properties | Source |
|---|---|---|
| pcDNA3.1 | Mammalian expression vector; CMV promoter; Ampicillin resistance. | Thermo Fisher Scientific |
| pcDNA3.1 modified | Mammalian expression vector; synapsin-1 promoter; Ampicillin resistance. | M. Wienisch (Wienisch and Klingauf, 2006) |
| pEGFP-N | Mammalian expression vector for fusion proteins with C-terminally tagged eGFP; CMV promoter; Neomycin/ kanamycin resistance. | Clontech (France) |
| pET28a(+) | Bacterial expression vector for His-tagged proteins; IPTG inducible T7 RNA polymerase; T7 promoter; N-terminal thrombin cleavage site; Kanamycin resistance. | Novagen |
| pFUGW | Mammalian lentiviral expression vector; human polyubiquitin promoter-C promoter; Ampicillin resistance. | David Baltimore (Lois et al., 2002) |
| pGEX-4T-1 | Bacterial expression vector with N-terminally tagged GST proteins; thrombin cleavage site; IPTG inducible Taq promoter; Ampicillin resistance. | Pharmacia |
| pmCherry-C | Mammalian expression vector for fusion proteins with N-terminally tagged mcherry; CMV promoter; Kanamycin and neomycin resistance. | Clontech (France) |
| pVitro-neo-msc | Mammalian expression vector with two multiple cloning sites for ubiquitous and constitutive co-expression of two genes of interest; two elongation factor 1 alpha (EF-1α) promoters; Kanamycin resistance | InvivoGen |

**Table 11: Plasmid DNA constructs used for recombinant protein expression.**

AA – amino acids encoded by the construct; fl – full length; C – C-terminal tag; N – N-terminal tag; siRNA resistant SV2A – 3 silent mutations were introduced in exon 7 see Table 9.

| Construct | Species | AA | Backbone | Tag | Source/Comments |
|---|---|---|---|---|---|
| eGFP | jellyfish | Fl | pFUGW | eGFP | D. Baltimore (Lois et al., 2002) |
| PH-PLCδ1-GFP | human | 1-184 | pET28a | eGFP | M. Krauss (Milosevic et al., 2005) |
| SV2A-GFP | rat | Fl | pEGFP-N | eGFP (C) | siRNA resistant SV2A |
| SV2A-GFP-Sybr2-mcherry | rat | Fl | pVitro | eGFP/ mcherry (C) | B. Jakob |
| Syb2-pHluorin | rat | 1-116 | pcDNA3.1, modified | pHluorin (C) | M. Wienisch (Wienisch and Klingauf, 2006) |
| Syt1 C2A-GST | rat | 140-265 | pGEX4T | GST (N) | N. Jung (Jung et al., 2007) |
| Syt1 C2B-GST | rat | 271-421 | pGEX4T | GST (N) | N. Jung (Jung et al., 2007) |
| Syt1-mcherry | rat | Fl | pmcherry-C | mcherry (N) | N-terminal signal peptide for correct targeting |
| Syt1-pHluorin | rat | Fl | pcDNA3.1, modified | pHluorin (N) | M. Wienisch (Wienisch and Klingauf, 2006) |
| Syt1-pHoran4 | rat | Fl | pcDNA3.1, modified | pHoran4 (N) | T. Soykan |
| Syp-pHluorin | rat | Fl | pcDNA3.1, modified | pHluorin (mid) | L. Lagnado |

## 3.1.7. Antibodies

All primary and secondary antibodies used in this study are listed in Table 12 and Table 13, respectively. All antibodies were stored at -20 °C for long-term or at 4 °C for short-term periods. They were diluted with 50 % (v/v) glycerol to protect antibodies from repetitive freeze-thawing cycles. All specified dilutions refer to the 1:1 glycerol-diluted antibody stocks.

**Table 12: Primary antibodies used in this study.**

Cat# - catalog number; WB – western blot; ICC – immunocytochemistry; IHC – immunohistochemistry. + and * indicate dilution for STED stainings and membrane stainings with GA fixation, respectively.

| Antigen | Host | Source | Clone/ Cat # | Dilution WB | Dilution ICC | Dilution IHC |
|---|---|---|---|---|---|---|
| AP-2 alpha | mouse | BD Transduction | 610502 | 1:100 | - | - |
| AP-2 alpha | mouse | abcam | AP6; ab2730 | - | 1:100+ | - |
| Bassoon | mouse | SySy | 141021 | - | 1:250+ | - |

| Antigen | Host | Source | Clone/ Cat # | Dilution WB | Dilution ICC | Dilution IHC |
|---|---|---|---|---|---|---|
| Bassoon | guinae pig | SySy | 141 004 | - | 1:100+ | - |
| Clathrin | mouse | Hybridoma cell line | CHC TD1 | 1:250 | - | - |
| Clathrin | rabbit | abcam | CHC; ab21679 | - | 1:400 | - |
| pan Dynamin | mouse | upstate | Hudy; 05-319 | 1:750 | - | - |
| GFP | rabbit | abcam | ab6556 | - | 1:1000 | - |
| HA | mouse | Babco | HA.11; 14861601 | - | 1:400 | - |
| Homer 1 | rabbit | SySy | 160003 | - | 1:200+ | - |
| Homer 1 | guinae pig | SySy | 160004 | - | 1:200+ | - |
| HSC-70 | mouse | Thermo Scientific | MA3006 | 1:1000 | - | - |
| PI(4)P | mouse | Echelon Biosciences | Z-P004 | - | 1:70 | - |
| $PI(4,5)P_2$ | mouse | Echelon Biosciences | Z-A045 | - | 1:400 | - |
| PIPK1γ | rabbit | P. De Camilli | | - | 1:750/ 1:300+ | - |
| Stonin2 | rabbit | sigma | HPA003086 | 1:800 | - | - |
| pan SV2 | mouse | P. De Camilli | C10H.4 | 1:750 | - | - |
| SV2A | mouse | SySy | 119 011 | - | 1:300 | - |
| SV2A | rabbit | S. Bajjalieh | | - | - | 1:500 |
| Synapsin1 | mouse | SySy | CL46.1; 106001 | - | - | 1:500 |
| Synaptobrevin2 | rabbit | SySy | 104202 | - | 1:100* | 1:500 |
| Synaptophysin | mouse | SySy | cl. 7.2; 101011 | 1:2000 | 1:500/ 1:150* | - |
| Synaptophysin | rabbit | R. Jahn | G96, luminal domain | - | 1:400 | - |
| Synaptotagmin1 | mouse | SySy | Cl41.1 105 011 | 1:700 | 1:100 | 1:400 |
| Synaptotagmin1 | rabbit | SySy | luminal domain 105103 | - | 1:100 | 1:400 |

**Table 13: Secondary antibodies used in this study.**

Cat# - catalog number.

| Antigen | Host | Conjugate | Source | Cat # | Dilution |
|---|---|---|---|---|---|
| Mouse IgG | goat | AlexaFluor488 | Life technologies | A-11001 | 1:400 |
| Mouse IgG | goat | AlexaFluor568 | Life technologies | A-11031 | 1:400 |
| Mouse IgG | goat | AlexaFluor594 | Life technologies | A11032 | 1:200 |
| Mouse IgG | goat | AlexaFluor647 | Life technologies | A21235 | 1:400 |
| Mouse IgG | goat | Atto 647N | Active Motif | 15038 | 1:200 |
| Mouse IgM | goat | AlexaFluor568 | Life technologies | A21043 | 1:400 |
| Rabbit IgG | goat | AlexaFluor488 | Life technologies | A-11008 | 1:400 |
| Rabbit IgG | goat | AlexaFluor488 | Life technologies | A-11034 | 1:200 |
| Rabbit IgG | goat | AlexaFluor568 | Life technologies | A-11011 | 1:400 |
| Rabbit IgG | goat | AlexaFluor647 | Life technologies | A21244 | 1:400 |
| Rabbit IgG | goat | Atto 647N | Active Motif | 15048 | 1:200 |
| Guinea pig IgG | donkey | AlexaFluor488 | Jackson | 706-545-148 | 1:200 |
| Guinea pig IgG | goat | AlexaFluor568 | Life technologies | A11075 | 1:200 |
| Mouse IgG | goat | HRP | Jackson/ Dianova | 115-035-003 | 1:10,000 |
| Rabbit IgG | goat | HRP | Jackson/ Dianova | 111-035-003 | 1:10,000 |
| Mouse IgG | goat | IRDye 800CW | LI-COR | P/N 926-32210 | 1:10,000 |
| Rabbit IgG | goat | IRDye 800CW | LI-COR | P/N 925-32211 | 1:10,000 |

### 3.1.8. Bacterial strains

The chemically competent *E. coli* TOP10 strain (Life Technologies) was used for cloning and propagation of plasmid DNA. For expression of recombinant proteins we used the *E. coli* BL21 CodonPlus (DE3)-RP strain (Stratagene). This strain is modified to contain extra copies of rare tRNA genes and its T7 RNA polymerase is under the control of the lac UV5 Promoter, which enables IPTG-inducible expression of heterologous proteins at high levels.

### 3.1.9. Eukaryotic cell lines

The human embryonic kidney cell line HEK 293T cultured in a humidified incubator at 37 °C and 5 % $CO_2$ was used for biochemical experiments. Sparsely plated cultures of HEK 293T cells stably transfected with Flag-tagged Syt1 were immunofluorescently stained for phosphoinositides. The same immunofluorescent staining was performed with HEK 293T cells that stably express HA-tagged PIPK1γ p90 wildtype or the kinase inactive (KI) mutant

K188A generated by Michael Krauss via the FlpIN system from Life Technologies. Application of 1 µM Doxycyclin (Sigma) induced the kinase expression 7 h prior to the experiment. Cultured cells were regularly tested for mycoplasma with a PCR-based Mycoplasma test kit (PromoKine).

### 3.1.10. Mouse strains

All mouse strains used in the present study were back crossed with C57BL/6J mice and are listed in Table 14. Mice were housed with food and water available ad libitum and on a 12 h light/ dark cycle. Breeding of all mouse strains as well as all experiments were reviewed and approved by the ethics committee of the "Landesamt für Gesundheit und Soziales" (LAGeSo) Berlin.

**Table 14: Mouse strains used in this study.**

WT – wildtype; KO – knockout; HET – heterozygous.

| Mouse strain | Source | Breeding |
|---|---|---|
| C57BL/6J | Charles River | C57BL/6J mice were interbred to keep a stock of wildtype mice. |
| Stn2 | (Kononenko et al., 2013) | Stn2 heterozygous mice were bred to yield Stn2 WT and KO mice. |
| SV2A/SV2B | Kind gift from S. Bajjalieh (Custer et al., 2006) ((Crowder et al., 1999) describes SV2A and (Morgans et al., 2009) describes the SV2B KO mice generation) | SV2A HET/ SV2B KO mice were interbred to obtain SV2A and SV2B double KO (DKO) mice with their corresponding SV2A WT/ SV2B KO control mice. |
| SV2A/SV2B/Stn2 | this study | SV2A HET/ SV2B KO/ Stn2 HET mice were crossed to gain SV2A KO/ SV2B KO/ Stn2 KO triple KO (TKO), SV2A KO/ SV2B KO/ Stn2 WT (DKO) mice and their control littermates SV2A WT/ SV2B KO/ Stn2 WT and SV2A WT/ SV2B KO/ Stn2 HET. |

### 3.1.11. Software and internet resources

**Table 15: Software and internet tools.**

| Program/Website | Source | Application |
|---|---|---|
| ApE (A plasmid editor) | http://biologylabs.utah.edu/jorgensen/wayned/ape/ | Cloning strategies, DNA sequence analysis |
| BLAST (Basic local alignment search tool) | www.ncbi.nlm.nih.gov/BLAST/ | Alignment of DNA and protein sequences |
| Fiji and ImageJ | http://fiji.sc/Fiji | Image analysis, quantification and editing |
| GraphPad PRISM5 | GraphPad | Statistics |
| Illustrator CS6 | Adobe Systems, USA | Illustrations and figures |
| ImageLab v5.2 | BIO-RAD | Western blot acquisition, editing and analysis |
| ImageStudioLite v4.0.21 | LI-COR | Western blot acquisition, editing and analysis |
| Micromanager v1.4.14 | https://www.micro-manager.org/ | Epifluorescent image acquisition (ImageJ-based) |
| Microsoft Office 2010 | Microsoft | Text files, quantifications and presentations |
| NCBI Homepage | www.ncbi.nlm.nih.gov/ | Database for scientific literature, DNA and protein sequences |
| PDF-XChange Viewer | Tracker Software | Editing of pdf-documents |
| PyMOL | http://www.pymol.org/ | Illustration of 3D structures of proteins |
| PyRAT (Python Based Relational Animal Tracking) | Scionics Computer Innovation | Animal facility software to organize and coordinate mouse strains, breeding and animal experiments |
| SlideBook 5.0 | Intelligent Imaging Innovation | Epifluorescent image acquisition and analysis |
| The Human Protein Atlas | http://www.proteinatlas.org/ | Information on human proteome |
| Volocity v6.2.1 | Perkin Elmer | Spinning disc confocal image acquisition |

## 3.2. Molecular biology methods

### 3.2.1. Cloning strategies

Cloning strategies were designed with the free software ApE. For specific amplification of the target sequence primers were designed to have a 15-18 bp overlap with the target sequence. To insert the target sequence into the plasmid vector of interest the corresponding restriction enzyme binding site were included together with 4 additional nucleotides (usually cgat) at the 5' end to ensure efficient cleavage by restriction enzymes. Depending on the GC content the melting temperatures lie between 50 °C and 70 °C. The complete DNA construct was controlled at the end *in silico* to guarantee the absence of unwanted frame shifts, stop codons or incompatibilities of restriction enzyme recognition sites.

### 3.2.2. Polymerase chain reaction and site directed mutagenesis

The polymerase chain reaction (PCR) developed by Kary Mullis is able to amplify a target DNA sequence exponentially. The DNA polymerase can synthesize a new strand of DNA complementary to the template DNA in the presence of nucleotides and primers. Primers are complementary to the template DNA and define the start and end point of the target sequence. Repetitive temperature cycles are essential to melt the DNA double strands, to allow primer annealing and to elongate DNA strands by the heat-stable polymerase. Newly synthesized DNA strands serve as template DNA in the following cycles. The PCR was used to amplify plasmid DNA for cloning into a new expression vector, to screen transformed bacteria clones for correct insertion of the target DNA sequence into the desired expression vector (colony-PCR), to introduce mutations into the target DNA sequence (site-directed mutagenesis) or to amplify short sequences of genomic DNA from tail biopsies to genotype mice (see section 3.2.12).

For cloning the high fidelity Phusion polymerase (New England biolabs) was used that has proofreading activity and therefore a low error rate. Plasmid DNA served as template DNA for all cloning reactions in this study.

To screen transformed bacteria clones in a colony PCR the cheaper and more error prone DreamTaq Polymerase (Fermentas) was used. Chosen primers were suitable to amplify the inserted target sequence. Transformed bacteria clones were inoculated in 100 µl of LB media supplemented with antibiotics corresponding to the resistance of the expression vector and grown for 2 h at 37 °C on a shaker. The resulting bacterial suspension and the original

template DNA as a positive control were added to the PCR mix. Typical PCR mixes for cloning and screening purposes are described in Table 16.

**Table 16: PCR mix for cloning and screening transformed bacteria clones.**
HF – high fidelity; fw – forward; rev - reverse

| Components | Cloning PCR | Colony PCR |
|---|---|---|
| Buffer | 1x HF Phusion buffer | 1x DreamTaq buffer |
| dNTPs | 100 µM of each | 100 µM of each |
| Primers | 0.5 µM of fw and rev | 0.375 µM of fw and rev |
| Template DNA | 10 ng plasmid DNA | 2 µl of bacteria suspension |
| Polymerase | 1 Unit of Phusion | 0.625 of DreamTaq |
| Sterile ultrapure water | to 50 µl | to 20 µl |

Depending on the polymerase the following PCR programs (Table 17) were run in a peqSTAR thermocycler (Peqlab).

**Table 17: PCR program for Phusion and DreamTaq Polymerase.**

| Step | Phusion polymerase | | DreamTaq polymerase | |
|---|---|---|---|---|
| 1. Initial Denaturation | 95 °C | 2 min | 95 °C | 1 min |
| 2. Denaturation | 95 °C | 20 s | 95 °C | 7 s |
| 3. Annealing | 50-70 °C | 20 s | 50-70 °C | 20 s |
| 4. Elongation | 72 °C | 15-30 s/kbp | 72 °C | 1 min/kbp |
| 5. Final elongation | 72 °C | 10 min | 72 °C | 10 min |
| 6. Storage | 8 °C | ∞ | 8 °C | ∞ |

Steps 2 to 4 were repeated for 25 cycles. The annealing temperatures were adjusted according to the melting temperatures of the individual primers.

Site-directed mutagenesis was used to insert mutations into the target DNA sequence. Four primers were designed for a two-step PCR. A forward and a reverse primer targeted the start and the end of the DNA sequence. To introduce the desired mutation at the sequence of interest a mutagenic forward and reverse primer were designed. They had an overlapping sequence of 18 bp including the mutated nucleotides and at least a melting temperature of 60°C. In the first PCR step the forward start primer was combined with the reverse mutagenic primer in one reaction resulting in a 5’ fragment. Likewise, the forward mutagenic primer was combined with the reverse end primer in another reaction yielding a 3’ fragment. Because of the overlapping mutagenic primer sequences both fragments can be fused in a second PCR step with equimolar amounts and can be amplified by the non-mutagenic forward and reverse

primers binding to the start and end sequence of the target DNA. Both PCR steps were done on the same day or in quick succession to exclude damaging of the PCR fragments or fusion PCR product.

### 3.2.3. Analytical agarose gel electrophoresis and DNA purification

DNA fragments were separated by size with agarose gel electrophoresis for analysis and purification. Depending on the size of the DNA fragments 0.7 – 2 % (w/v) agarose gels were prepared by dissolving agarose in 1x TBE or 1x TAE buffer supplemented with 100 ng/ml ethidiumbromide (Roth) to detect DNA by UV light. DNA samples with 1x loading buffer were loaded on the agarose gel. Subsequently, the gel was run in a horizontal chamber (Perfect Blue from PeqLab) filled with 1x TBE or 1x TAE buffer with 10 Volt per electrode distance in cm for 20 - 30 min. DNA fragments were visualized by UV light on a UV table (UVT-28 LV from Herolab) and documented with G:Box gel documenting system (Syngene). If the DNA fragments were used for further cloning steps, UV light exposure was minimized, bands were excised from the gel and extracted with NucleoSpin Gel and PCR clean-up kit (Macherey Nagel) according to manufacturer's instructions.

### 3.2.4. DNA restriction digests

DNA restriction digests were performed to integrate the target DNA correctly into an expression vector. DNA sequences were amplified by PCR including specific restriction enzyme binding sites at the 5' and 3' end that are compatible with the cloning site of the plasmid vector. Both the gel extracted PCR product as well as 2 µg of plasmid vector were digested in a total reaction volume of 20 µl with approximately 10 Units of FastDigest restriction enzymes (NEB) and 2 µl of 10x FastDigest Green Buffer for 1 – 2 h at 37 °C. The calf intestinal alkaline phosphatase (2 Units/ µg DNA CIP, NEB) was added to plasmid digestion reaction for 5 min at 37 °C at the end of the digestion to dephosphorylate the 5' ends of the linear DNA plasmid. Thereby, re-ligation of the linearized vector backbone can be prevented and false positive bacterial colonies can be reduced. Finally, the restriction digests were stopped by heat inactivation and purified or analyzed by agarose gel electrophoresis and extracted as described in 3.2.3.

### 3.2.5. Ligation of DNA fragments into linearized vectors

To integrate a DNA fragment into the linearized vector backbone the molar ratios were determined with the NanoDrop ND-1000 (Peqlab) first. 50 – 100 ng of linearized vector were mixed with a three to six fold molar excess of the DNA fragment. 5 Units of the T4 ligase and 4 µl of the 5x T4 ligase buffer were added to the ligation reaction with a total volume of 20 µl. The ligation reaction was either incubated at RT for 2 h or overnight at 16 °C.

### 3.2.6. Transformation of chemically competent *E. coli*

Chemically competent *E.coli* (50 µl of $CaCl_2$ competent TOP10 or BL21 CodonPlus strains) were transformed with the ligation reaction or plasmid DNA following the heat shock protocol. First, $CaCl_2$ competent *E.coli* were thawed on ice and incubated with 10 µl of the ligation reaction or 1 µg of plasmid DNA 30 min on ice. Subsequently the bacterial culture was heat shocked for 45 s at 42 °C, chilled on ice for 5 min and incubated with 500 µl LB without antibiotics at 37 °C for 30 min. For selection bacterial cultures were shortly pellet by centrifugation at 4000 x g, resuspended in approximately 50 µl LB and plated on pre-warmed LB agar plates with antibiotics corresponding to their selective resistance. Bacteria transformed with a kanamycin resistant vector were allowed to recover 1 h at 37 °C to gain kanamycin resistance before plating. The LB plates were incubated overnight at 37 °C, and colonies were picked on the next day to perform a colony PCR as described in 3.2.2. Positive colonies were grown overnight at 37 °C and 200 rpm in 5 ml LB medium with the corresponding antibiotics.

### 3.2.7. Purification of plasmid DNA from *E. coli* cultures

Plasmid DNA from small scale overnight *E. coli* cultures was purified using the NucleoSpin Plasmid kit from Macherey-Nagel according to manufacturer's instructions (Mini-prep). In principle, an alkaline and SDS containing buffer lyses the bacteria and centrifugation removes genomic DNA, proteins and cell debris, while the plasmid DNA in the supernatant can be bound to a silica column. After washing to remove contaminations, plasmid DNA is eluted.

Large scale overnight *E. coli* cultures were centrifuged at 4°C, 4000 rcf for 30 min. Plasmid DNA was isolated with NucleoBond® Xtra endotoxin free (EF) plasmid purification kit from Macherey-Nagel following the manufacturer's instructions to allow plasmid transfection of neuronal cultures. Again cells are lysed with a NaOH/ SDS containing buffer.

However, in this protocol contaminants of cell lysate are removed by a column filter and plasmid DNA binds to a silica resin, which has a high DNA binding capacity and is washed to eliminate all endotoxins. Eluted plasmid DNA is precipitated with isopropanol and reconstituted with sterile ultrapure water to 1 µg/µl.

### 3.2.8. Measurement of DNA concentrations

DNA concentrations were determined with a photometer or NanoDrop ND-1000 (Peqlab) by measuring the specific extinction E of DNA at 260 nm. The measurement is based on the Lambert-Beer law:

(I) $$c = \frac{E_{260nm}}{d * \varepsilon_{dsDNA}} \cdot dilution$$

For the photometer plastic cuvettes were used with a cross section of 1 cm defining the light path d. The light path within the NanoDrop ND-1000 was only d = 0.01 cm. With the molar extinction coefficient $\varepsilon_{dsDNA} = 50\ \frac{\text{ml}}{\text{µg}*\text{cm}}$ the DNA concentration can be calculated. To assess the quality of DNA preparations the ratio of DNA extinction at 260 nm and protein extinction at 280 nm was determined as well. Values between 1.8 and 2.1 guarantee a pure DNA preparation.

### 3.2.9. Sequencing of DNA

DNA sequences were controlled by sequencing with sequencing primers using the chain-termination method (Sanger and Coulson, 1975) performed by Source Bioscience (Germany). Sequencing results were analyzed with the free software ApE.

### 3.2.10. Cryostocks of bacterial clones

Bacterial overnight cultures in 2 ml LB medium with antibiotics were concentrated by centrifugation at 4000 x g in 750 µl and diluted 1:1 with sterile 50 % (v/v) glycerol in PBS and stored in cryotubes at -80 °C.

### 3.2.11. Isolation of genomic DNA from mouse tissue

To genotype transgenic mice first genomic DNA was isolated from mouse tissue with isopropanol precipitation. Either tail biopsies of new born pubs (p0 to p3) or ear tissue of three weeks old mice were provided by the animal facility. The mouse tissue was incubated in 300 µl tail lysis buffer (TLB) with 0.4 mg/ml of proteinase K at 55 °C for 30 min. Debris was removed by a short centrifugation for 3 min at 17,000 x g. In a new tube DNA was precipitated by adding an equal volume of isopropanol to the supernatant. The DNA precipitate was pelleted (3 min, 17,000 x g), washed shortly with 70 % (v/v) ethanol, dried at 60 °C in a heating block and resuspended in 100 µl ultrapure water.

The KAPA HotStart Mouse Genotyping Kit (Sigma-Aldrich) was used for Stn2 and SV2A/SVB/Stn2 transgenic mice to yield faster and more reliable genotyping results. Genomic DNA is extracted with the KAPA Express Extract system containing a thermostable protease. In a total reaction volume of 50 µl 1 Unit of the KAPA Express Extract enzyme and 1x KAPA Extract buffer were added to the tail biopsies. The tails are lysed 30 min at 75 °C. Finally the enzyme is heat inactivated at 95 °C for 5 min and the supernatant can directly be used for PCR amplification.

### 3.2.12. Genotyping of mouse strains

Genomic DNA purified with isopropanol precipitation was used as a template for all genotyping PCRs with the Taq Polymerase (Bio&Sell) and genotype specific primers listed in Table 8. The following PCR mix and PCR programs were used to amplify short DNA sequences that identify mice with a wildtype, heterozygous or knockout genotype (Table 18 and Table 19). Every genotyping PCR included DNA of bona fide wildtype and knockout mice as controls as well as a water control to exclude contamination of any PCR mix component.

**Table 18: PCR mix for genotyping transgenic mouse lines.**

| Components | Stn2 WT and KO | SV2A and SV2B |
|---|---|---|
| Buffer | 1x Taq buffer | 1x Taq buffer |
| $MgCl_2$ | 2.5 mM | 2.5 mM |
| Loading dye | 1x | 1x |
| dNTPs | 150 µM of each | 150 µM of each |
| Primers | 0.375 µM of fw and rev | 0.375 µM of WT_fw, KO_fw and |

| | | |
|---|---|---|
| | | combined_rev |
| Template DNA | 1 µl DNA | 1 µl DNA |
| Polymerase | 1.5 Units Taq | 2 Units Taq |
| Sterile ultrapure water | to 20 µl | to 20 µl |

**Table 19: PCR program for genotyping transgenic mouse lines.**

| Step | Stn2 | | SV2A | | SV2B | |
|---|---|---|---|---|---|---|
| 1. Initial Denaturation | 94 °C | 3 min | 94 °C | 2 min | 94 °C | 2 min |
| 2. Denaturation | 94 °C | 30 s | 94 °C | 30 s | 94 °C | 1 min |
| 3. Annealing | 55 °C | 30 s | 55 °C | 45 s | 56.5 °C | 1 min |
| 4. Elongation | 72 °C | 30s | 72 °C | 45 s | 72 °C | 1 min |
| 5. Final elongation | 72 °C | 5 min | 72 °C | 2 min | 72 °C | 5 min |
| 6. Storage | 8 °C | ∞ | 8 °C | ∞ | 8 °C | ∞ |

Steps 2 to 4 were repeated for 35 cycles for the Stn2 PCR and 30 cycles for SV2A and SV2B PCR.

For Stn2 transgenic mice two separate PCR had to be performed a Stn2 WT and a Stn2 KO PCR, as both PCRs result in a PCR product of similar size. However, the SV2A and the SV2B genotype were determined in one PCR. The expected sizes of the PCR product are listed in Table 20.

**Table 20: Band sizes of PCR products indicating the different genotypes.**

| Genotype | Stn2 | SV2A | SV2B |
|---|---|---|---|
| WT | 400 bp | 400 bp | 650 bp |
| KO | 400 bp | 300 bp | 290 bp |

In case the DNA was extracted with the KAPA HotStart Mouse Genotyping Kit the following PCR mix (Table 21) with the primers listed in Table 8 and the PCR program in Table 22 were used to genotype mutagenic mouse lines. The kit provides a 2x KAPA2G Fast (HotStart) Genotyping Mix including 1.5 mM $MgCl_2$, dNTPs, an engineered DNA polymerase and loading dye.

**Table 21: PCR mix of the KAPA HotStart Mouse Genotyping Kit**

| Components | Stn2, SV2A and SV2B |
|---|---|
| 2x KAPA2G Fast (HotStart) Genotyping Mix with dye | 1x |
| $MgCl_2$ | 1 mM |
| Primers | 0.5 µM of each |
| Template DNA | 1 µl DNA |
| Sterile ultrapure water | to 15 µl |

**Table 22: PCR program for the KAPA HotStart Mouse Genotyping Kit**

| Step | Stn2 and SV2A | | SV2B | |
|---|---|---|---|---|
| 1. Initial Denaturation | 95 °C | 3 min | 95 °C | 3 min |
| 2. Denaturation | 95 °C | 15 s | 95 °C | 15 s |
| 3. Annealing | 55 °C | 15 s | 56.5 °C | 15 s |
| 4. Elongation | 72 °C | 10 s | 72 °C | 10 s |
| 5. Final elongation | 72 °C | 2 min | 72 °C | 2 min |
| 6. Storage | 8 °C | ∞ | 8 °C | ∞ |

Steps 2 to 4 were repeated for 35 cycles for the Stn2 PCR and 30 cycles for SV2A and SV2B PCR.

## 3.3. Cell biological methods

### 3.3.1. Cell culture of HEK 293T cells

Human embryonic kidney (HEK) 293T cells were cultured in a humidified incubator at 37 °C and 5 % $CO_2$. They were grown in Dulbecco's modified Eagle's medium (DMEM) high glucose supplemented with 10 % (v/v) fetal calf serum (FCS), 1 % (v/v) penicillin/ streptomycin (Gibco) and 2 mM L-glutamine. HEK 293T cells stably transfected with Flag-tagged Syt1 were cultured with the selection antibiotic geneticin G418 (1 mg/ml, Gibco Life technologies). To select HEK 293T cells stably expressing HA-tagged PIPK1γ p90 WT and kinase dead mutant generated with the FlpIN system (Life technologies) 100 µg/ml hygromycin and 10 µg/ml blasticidin (both from Invivo Gen) were used. Control cells containing only the FlpIN system plasmids without the inserted DNA sequence of interest

were cultured with 100 µg/ml zeocin (Invivo Gen) and 10 µg/ml blasticidin. 1 µg/ml doxycyclin (Sigma) for 7 h was used to induce expression.

Cells were passaged every 2 to 7 days. Cells were briefly washed with PBS and incubated with 0.05 % (v/v) trypsin/EDTA (Gibco) for 5 min at 37 °C. To inactivate trypsin cells were resuspended in an excess of medium with FCS. Cells were then plated in 1:3 to 1:30 in a new cell culture dish. After 20 passages cells were discarded. PIPK1γ expressing cells were abandoned already after passage 10, as they lost their characteristic response to PIPK1γ expression e.g. increased $PI(4,5)P_2$ levels due to negative selection.

For biochemical experiments cells were directly plated in 6-well plates. Immunofluorescent stainings of fixed cells required the cell plating on 15 mm - glass coverslips. Coverslips were shortly covered with Matrigel (from BD Bioscience, diluted 1:20 in Opti-MEM (Gibco)) and incubated for 1 h at 37 °C to facilitate the adherence of the cells with various matrix components.

### 3.3.2. Transfection of HEK 293T cells with jetPRIME

One to two days before the experiment HEK 293T cells were transfected with plasmid DNA using jetPRIME (PolyPlus Transfection). jetPRIME is a cationic reagent that facilitates DNA uptake into cells by forming complexes with negatively charged DNA. Following manufacturer's instructions for a 6-well dish 2 µg of plasmid DNA were mixed in 200 µl jetPRIME buffer. 4 µl of jetPRIME were added. The transfection solution was thoroughly mixed and incubated for 10 min at RT before it was added to the cells. After 4 h the medium was exchanged with new pre-warmed growth medium.

### 3.3.3. Transfection of HEK 293T cells with Lipofectamin 2000

One day before transfection HEK 293T cells were plated in antibiotic-free medium. To transfect HEK cells with plasmid DNA and siRNA simultaneously Lipofectamin 2000 (Invitrogen) was used. Lipofectamin is a cationic lipid forming liposomes and complexes with negatively charged DNA, which can bind to cell membranes and thus allow DNA uptake. According to manufacturer's protocol for one well of a 6-well plate 500 ng of plasmid DNA and 50 pmol siRNA were added to 250 µl OptiMEM. 4 µl Lipofectamin 2000 were diluted in 250 µl OptiMEM as well. Both were briefly mixed and incubated for 5 min at room temperature. Subsequently, the diluted DNA and siRNA were combined with the diluted

Lipofectamin 2000 and were incubated for 20 min at room temperature. The transfection mix was then added to cells. After 4 h the growth medium was exchanged, and cells were harvested for biochemical experiments on the next day.

### 3.3.4. Preparation of primary hippocampal neurons

Glass coverslips with a diameter of 25 mm or 18 mm, were cleaned in 1 M HCl for 24 h, left in acetone overnight and in 70 % (v/v) ethanol for 24 h before being stored in 96 % (v/v) ethanol. Dry coverslips were coated with 200 µl of 100 µg/ml Poly-D-Lysin hydromide (PDL, Sigma) or 15 µg/ml Poly-L-Lysin (PLL, Biochrom). The coverslips were incubated at least for 1 h at room temperature with the coating before it was removed and the coverslips washed two times with sterile water.

Primary hippocampal neurons were prepared from p1 to p4 old mouse pups. Mice were decapitated and intact brains were dissected. Brains were collected in ice-cold sterile Hank's balanced salt solution (HBSS, Life Technologies) with 20 % fetal bovine serum (FBS) and 50 U/ ml penicillin and 50 µg/ml streptomycin (P/S). By opening the brain hemispheres the hippocampi were unfolded and isolated from the cortex. Up to 8 hippocampi from four mice in total were transferred into a new sterile dish with HBSS supplemented with FBS and P/S and cut 4 times. The pieces were collected in a 15 ml Falcon tube and after settling washed two times in 5 ml of HBSS with FCS and P/S and two times in HBSS with P/S to remove all serum. To dissociate the tissue the hippocampi were incubated with sterile filtered (syringe filter with 0.22 µm pores, Roth) 5 mg/ml Trypsin (Sigma) and 750 Units DNase (Sigma) in digestion solution for 15 min at 37 °C. Subsequently, trypsination was stopped by HBSS supplemented with 20 % FCS and P/S, and tissue was rinsed as above. To gain a dissociated cell suspension hippocampi were incubated in a sterile filtered dissociation solution with 750 Units DNase and triturated with siliconized and fire-polished Pasteur pipettes with small openings 3 to 4 times until no tissue pieces were visible anymore. HBSS with 20 % FCS was added afterwards and cells were centrifuged for 8 min at 400 x g and 4 °C. The supernatant was aspirated, and cells were resuspended in plating medium. Cells were counted in a Neubauer chamber. The plating medium volume was adjusted to yield 2200 neurons/ µl. 50 µl with 110,000 cells or 25 µl with 55,000 cells were plated as small drops on 25 mm coverslips or 18 mm coverslips, respectively. The cells were allowed to settle for 1 to 2 h at 37 °C in a humidified atmosphere of 5 % $CO_2$ before 2 ml of equilibrated plating medium per 6-well or 1 ml per 12-well was added.

On day in vitro 1 (DIV1) half of the medium was removed and the same amount of equilibrated growth medium supplemented with 2 µM Cytosine β-D-arabinofuranoside (AraC, Sigma) was added. On DIV2 only 1 ml for 6-well plates of equilibrated growth medium with 4 µM Ara-C was added. After one week in vitro 1 ml of old growth medium was removed and 1 ml of osmolarity adjusted fresh growth medium with 4 µM Ara-C was added. For 12-well plates only half the medium volumes were used for feeding. Cells were either fixed on DIV13 to 15 for immunocytochemistry or used for live-cell imaging with pHluorin from DIV13 to DIV16.

### 3.3.5. Calcium phosphate transfection of primary hippocampal neurons

Primary hippocampal neurons were transfected on DIV7 - 9 with calcium phosphate using ProFection Mammalian Transfection System from promega. This method is based on complex formation of DNA and calcium phosphate, which bind to cells and are taken up via endocytosis. The uptake is induced by starvation. Thus, starvation medium Neurobasal-A (Gibco, Life technologies) as well as calcium- and magnesium-free HBSS to remove residual precipitates at the end were adjusted with D-Mannitol to the same osmolarity as the neuronal culture medium and equilibrated at 37 °C and 5 % $CO_2$. For transfection of one coverslip with 25 mm in diameter 6 µg plasmid DNA and 6 pM siRNA (if required) were used. The plasmid DNA and 250 mM $CaCl_2$ were mixed with nuclease free water to a final volume of 100 µl. This DNA solution was added drop-wise to an equal amount of 2x Hepes buffered saline in a second tube while constantly stirring. Subsequently the mix was incubated in darkness for 20 min to allow complex formation. Neurons were starved at the same time in 1 ml of osmolarity adjusted and equilibrated Neurobasal-A medium for 20 min at 37 °C and 5 % $CO_2$. 200 µl of the DNA-calcium phosphate precipitate were added to each coverslip, and neurons were incubated with the precipitate for 30 min at 37 °C in a humidified atmosphere of 5 % $CO_2$. Finally, cells were washed two times with 2 ml of osmolarity adjusted and equilibrated HBSS and transferred back into their original medium. For 18 mm coverslips in a 12-well plate all amounts were reduced by a third.

### 3.3.6. Silencing of primary hippocampal neuron cultures

Neuronal network activity was silenced by inhibiting sodium channels with tetrodotoxin (TTX, Sigma). Hippocampal neurons were treated either with 1 µM TTX diluted in 10 mM

sodium acetate, pH 5.3, or with an equal volume of its solvent 10 mM sodium acetate (pH 5.3) as a control. TTX and sodium acetate were added directly to neuronal culture medium at DIV9 for 5 days.

### 3.3.7. Stimulation of primary hippocampal neuron cultures

To detect activity dependent changes of protein localization or membrane lipid generation neuronal cultures on DIV14 to 15 were depolarized with 80 mM potassium chloride in pre-warmed imaging buffer (stimulation imaging buffer omitting sodium chloride to avoid an osmotic shock) for 1 min at room temperature. Control neurons were incubated for 1 min at room temperature with pre-warmed imaging buffer to reveal the steady-state level. After 1 min the imaging buffer was quickly aspirated, and the fixation was immediately applied to the neuronal cultures followed by an immunofluorescent staining described in section 3.3.8. Thus, the recovery time after the strong depolarization was less than 1 s.

Electric field stimulation of neurons was used for pHluorin experiments and is described in detail in section 3.4.4.

### 3.3.8. Immunocytochemistry

Cultured primary hippocampal neurons were fixed on DIV13 to 15 with 4 % (w/v) PFA and 4 % (w/v) sucrose for 15 min on ice and washed three times with PBS. To stain for intracellular proteins fixed neurons were blocked and permeabilized for 1 h with 10 % (v/v) NGS and 0.3 % (v/v) Triton-X 100 in PBS at room temperature to avoid unspecific antibody binding. The first antibody was diluted as described in Table 12 in 0.3 % (v/v) Triton-X 100 applied in 30 - 50 µl on parafilm in a humid chamber. Coverslips were placed upside down on the drop and incubated for 1 h at room temperature. Cells were washed three times with PBS to remove unbound antibody and bound antibody was decorated with corresponding secondary antibodies (

Table **13**) for 30 min as described above. Neurons were washed again three times with PBS and mounted in Immu-Mount (Thermo Fisher) mounting solution on microscopy slides. Neuronal cultures transfected with a pHluorin construct were mounted in vectashield (Vector Laboratories), and coverslips were sealed with nail polish. As vectashield has a neutral pH, pHluorin probes stay fluorescent, whereas Immu-Mount acidifies during crystalization and quenches pHluorin molecules. Prolong Gold Antifade (Invitrogen) was used as a mounting solution for STED microscopy.

To detect surface-stranded SV proteins, the protocol was done in two consecutive rounds. In the first step, the surface SV protein fraction was labeled using non-permeabilizing conditions. Thus, Triton X-100 was omitted in the blocking and antibody incubation steps. Decorated antibodies were post-fixed with 2 % (w/v) PFA and 2 % (w/v) sucrose for 15 min and neurons were permeabilized for the subsequent immunostaining of the total pool as described above.

Immunofluoresent stainings of HEK 293T cells were performed as described for neuronal cultures except for two minor alterations. Cells were washed briefly with PBS + $MgCl_2$ to remove residual medium before fixation and Immu-Mount was supplemented with 1 µg/ml DAPI (4'-6-diamidino-2-phenylindole, Sigma) to visualize DNA containing nuclei.

Lipid stainings of neuronal cultures and HEK 293T cells required a stronger fixation protocol to preserve the membrane. Control and stimulated cells were fixed with 1 % (v/v) glutaraldehyde (GA) and 2 % (w/v) PFA and 2 % (w/v) sucrose in PBS for 20 min at room temperature. To remove residual GA and PFA and to quench free aldehyde groups, which could interfere with antibody decoration, cells were thoroughly washed three times with PBS and two times with fresh 50 mM ammoniumchloride in PBS. Subsequently, cells were permeabilized and blocked with 0.5 % (w/v) saponin (Sigma) and 1 % (w/v) BSA (Roth) in PBS for 30 min. Neurons were labeled with lipid specific antibodies together with antibodies against synaptic markers diluted in 1 % (w/v) BSA and 10 % (v/v) NGS in PBS (centrifuged for 5 min at 17,000 x g) for 2 h at room temperature. Cells were washed three times for 5 min with PBS, decorated with the corresponding secondary antibodies (centrifuged for 5 min at 17,000 x g) for 1 h at room temperature and rinsed three times for 10 min with PBS. As an alternative to antibody labeling the GFP-labeled PH domain of PLCδ1 (PH-PLCδ1-GFP) was used to specifically detect $PI(4,5)P_2$ in primary hippocampal cultures and HEK 293T cells. 0.25 µg/ml of the purified PH-PLCδ1-GFP were added during the 30 min permeabilization and blocking step. Afterwards cells were incubated in 0.25 µg/ml of PH-PLCδ1-GFP and 1 % (w/v) BSA in PBS for another 30 min to yield sufficient $PI(4,5)P_2$ labelling. Following three

washes with PBS to remove unbound PH-PLCδ1-GFP, cells were stained with an antibody against GFP to enhance the GFP signal of the domain and a synaptic marker if required for 1 h at room temperature and subsequently with corresponding secondary antibodies for 30 min at room temperature as described above.

## 3.4. Fluorescent microscopy and quantitative image analysis

Fluorescent microscopy utilizes fluorophores to detect and localize biomolecules such as proteins, DNA and membrane lipids within fixed or live cells. Light with a specific wavelength can excite the fluorophore to a higher energy state, from where it can immediately relax to the electronic ground state by emitting light with a longer wavelength. Excitation and emission wavelengths are separated in the microscope with a dichroic mirror and spectral emission filters. By choosing fluorophores with different excitation and emission wavelengths and the corresponding dichroic mirrors and filters three to four colors can be detected at the same time. Biomolecules can be visualized with fluorophores coupled to specific antibodies or with overexpressed genetically encoded fluorescent proteins. Dependent on the biological question the following microscopy methods were utilized.

Within independent experiments the same settings for microscopy and quantitative analysis were used, which allows the comparison of various conditions. If not stated otherwise raw data analyzed with ImageJ were further processed with Excel and plotted with Prism (Graphpad).

### 3.4.1. Epifluorescent microscopy

Epifluorescent microscopy illuminates the whole sample by white light and allows fast image acquisition with diffraction limited resolution. This microscopy technique was therefore mainly used for live-cell imaging to monitor changes of fluorescent intensities over time. Two epifluorescent microscopes were used in this study: Axiovert 200M from Zeiss controlled by Slidebook software (Inovision) with eGFP filter set (BP 525 – 50) and 40 x oil-immersion objective was used. Images were acquired with the Coolsnap HQ2 EM-CCD camera (Roper Scientific). Later the Nikon Eclipse Ti microscope controlled by MicroManager 4.11, eGFP filter set F36-526, TRITC filter set F36-503, 40 x oil-immersion objective and a sCMOS camera (Neo, Andor) with 200 Watt mercury lamp (Lumen 200, Prior Scientific) was

selected. Physiological live cell imaging was enabled by an incubator (Okolab) around the microscope and the PerfectFocus Autofocus system from Nikon.

### 3.4.2. Confocal microscopy

Compared to the epifluorescent microscopy confocal microscopy allows a better subcellular detection of fluorescently labeled biomolecules by focusing the illumination with a pinhole in the lightpath that enables excitation and emission of molecules in only one z-plane. For faster acquisition the spinning disc confocal microscope is equipped with two rotating pinhole discs that circumvent the point-by-point scanning of the sample.

All immunofluorescently labeled brain sections were imaged with a Leica SP5 laser confocal microscope controlled by LasX software (Leica Microsystems) and equipped with a 20 x objective, Argon/Krypton (488 nm) and Helium/Neon (546 nm) lasers and 3 PMT 400-800 nm spectral descanned detectors.

In single images of brain sections the mean fluorescent intensities of proteins of interest were analyzed with ImageJ and quantified in regions of interest (ROI). ROIs were selected in molecular dentate gyrus, stratum lucidum and oriens layer of the proximal CA3 region in the hippocampus.

If not stated otherwise all fixed and immunofluorescently stained cell cultures were imaged with a spinning disc confocal microscope Zeiss Axiovert 200M equipped with the Perkin-Elmer Ultra View ERS system and a Hamamatsu C9100 EM-CCD camera under the control of Volocity software (Perkin-Elmer).

Fluorescent intensities were quantified with ImageJ. ROIs were selected by an unbiased co-staining or by an overexpressed fluorescently tagged control protein. These ROIs were used as a mask to quantify the mean fluorescent intensities in the channel of interest. Background was subtracted, and fluorescent intensities were normalized to the control for comparison.

### 3.4.3. Stimulated emission depletion (STED) microscopy and analysis

STED superresolution microscopy is based on confocal laser scanning microscopy, but overcomes diffraction limited detection by stimulated emission. In addition to the excitation laser a second doughnut-shaped and red-shifted STED laser is superimposed. The STED laser stimulates the excited fluorophore to return from the excited to the ground energy state before

it spontaneously emits fluorescence. Because of its shape the STED laser suppresses the emission of fluorophores distant to the center of excitation and the resulting emission is effectively reduced to a narrower point-spread function.

To compare the nanoscale localization of proteins in Stn2 WT and KO neuronal cultures multicolor 3D time-gated STED was performed on a Leica SP8 TCS STED microscope (Leica Microsystems) equipped with a pulsed white-light excitation laser (WLL; ~ 80 ps pulse width, 80 MHz repetition rate; NKT Photonics) and two STED lasers for depletion at 592 nm and 775 nm. The WLL triggered the pulsed 775 nm STED laser. Alexa 488, Alexa 594/568 and ATTO647N were sequentially excited with 488 nm, 598 nm and 646 nm, respectively. Alexa 594 / 568 and ATTO647N were depleted with 775 nm STED laser and were acquired first followed by Alexa 488, which was depleted with 592 nm laser. Hybrid detectors at corresponding spectra excluding the STED laser wavelengths were used to detect the fluorescent signal. To allow enough time for stimulated emission the detection was time-gated by 0.3 - 6 ns for all dyes. A z-stack with three optical slices of 250 nm was acquired to cover 500 nm of the specimen. A HC PL APO CS2 100x/1.4 N.A. oil objective (Leica Microsystems) scanned 1,024 x 1,024 pixels with eight-bit sampling. The final image was taken with a six-fold zoom resulting in a voxel size of 18.9 x 18.9 x 166.7 nm. Martin Lehmann from the FMP imaging facility previously determined the effective lateral resolution with 54 nm for the 488 nm channel and 45 nm for the 647 nm channel using 40 nm fluorescent beads (Life technologies). An incubator (LIS Life Imaging Services) around the microscope reduced the thermal drift. For all experiments the same settings were used. Only the laser power of excitation and STED laser were adjusted for different experiment sets.

Acquired images were quantified with ImageJ. First the sum intensity of the z-stacks was projected, and only synapses with clearly distinguishable bassoon and homer1 clusters were used for further analysis. 30 synapses in total were analyzed for each condition of an independent experiment. A line was aligned perpendicular to the synapse with 1 µm length and 400 nm width to obtain the line profiles of all channels within the synapse. With the help of the ImageJ Macro from Kees Straatman (Marco_plot_lineprofile_multicolor, University of Leicester, Leicester, UK) intensities of all three channels were summed along the 400 nm wide line and plotted along 1 µm distance. All profiles were aligned to the maximum of the bassoon peak, which was set to zero. The distance of the protein of interest to bassoon within the presynapse was determined in individual synapses by measuring the distance between the maxima (Figure 9).

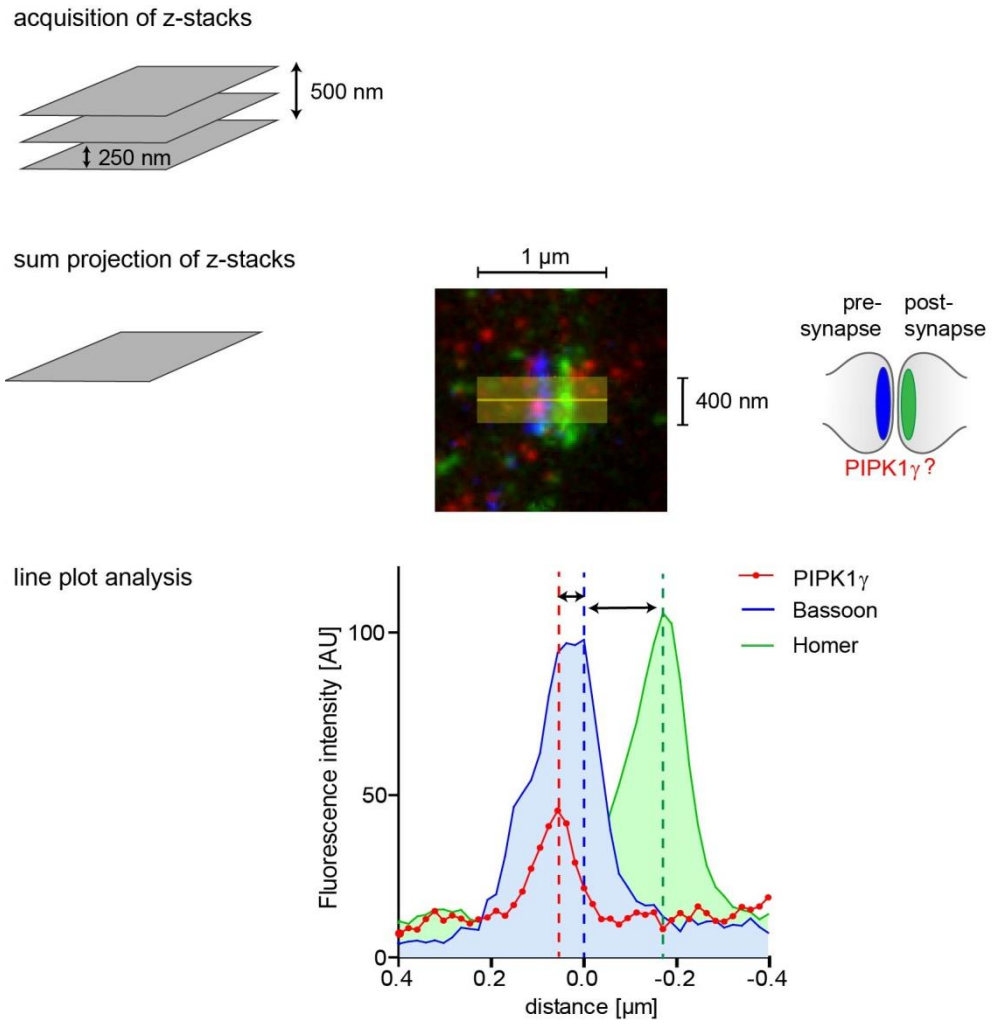


**Figure 9: Schematic illustration of nanoscale localization analysis of three-color gSTED in hippocampal synapses.** The sum intensity of Z-stacks covering 500 nm were projected and synapses with clearly separable bassoon (blue, presynapse) and homer1 (green, postsynapse) were selected for the line plot analysis. A line (yellow) was plotted perpendicular to the bassoon/homer1 coclusters with 1 µm length and 400 nm width to quantify the intensity distribution of all three channels e.g. PIPK1γ, bassoon and homer1. Multicolor line profiles were aligned to the maximum intensity of the bassoon peak and distances between the maxima of the other channels and the bassoon peak were calculated in profiles of individual synapses (dashed lines, arrows). Adapted from (Gerth et al., 2017).

### 3.4.4. pHluorin live-cell imaging

SV exo- and endocytosis was monitored with a pH-sensitive green fluorescent protein (GFP) variant called pHluorin fused to the luminal domain of synaptic vesicle proteins. pHluorin was genetically modified to have a higher pH sensitivity with a $pK_a$ of 7.1. Thus, pHluorin molecules are protonated at low pH, which quenches their fluorescence (Miesenbock et al., 1998). Within the neuron SVs are acidified by the vATPase generating a proton gradient for neurotransmitter uptake. When pHluorin tagged SV proteins are expressed in neurons all

pHluorins tagged SV proteins residing on SVs will be quenched, while surface-stranded SV proteins with a pHluorin tag will be fluorescent. Upon depolarization SVs fuse with the plasma membrane, the luminal pHluorin will be exposed to the extracellular solution with a neutral pH and will be unquenched. Consequently, the SV release can be observed by an increase of fluorescence. As soon as SVs are endocytosed and re-acidified, the fluorescent signal will be quenched again (Figure 10). Even though the fluorescent decay is dependent on SV re-acidification and requires 3 - 4 s (Atluri and Ryan, 2006), it is used as a surrogate measure of endocytosis.

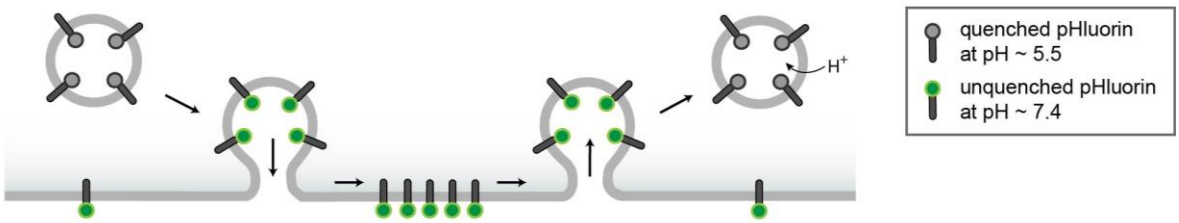


**Figure 10: SV exo- and endocytosis visualized with pHluorin.** pHluorin is fused to the luminal tail of SV proteins and while they reside on SVs, pHluorin is protonated and quenched. SV exocytosis exposes pHluorin to the neutral pH of the extracellular solution thereby resulting in unquenching. The fluorescence decays upon endocytosis and vesicle re-acidification.

Neuronal cultures were transfected on DIV7 - 9 as described in section 3.3.5 with pHluorin constructs and imaged on DIV13 - 15 in physiological imaging buffer either at room temperature or 37 °C. The coverslips were assembled in a stimulation chamber with two lateral electrodes (RC-47FSLP, Warner Instruments) connected to a stimulator (MultiStim SYSTEM-D330, Harvard Apparatus), which allowed electrical field stimulation of neurons at 100 mA and varying frequency and duration. NMDA and AMPA receptors on the postsynapse were inhibited by 50 µM APV (Abcam) and 10 µM CNQX (Sigma) to avoid action potential propagation. Images were acquired with 0.5 Hz frame rate with the epifluorescent microscopes and settings described in section 3.4.1. To avoid bleaching of fluorophores during the 2 min acquisition the neutral density filter 4 and 100 ms exposure were used for all pHluorin experiments.

30 to 50 responding boutons per recording were selected as regions of interest (ROI) and either analyzed with Slidebook software (Inovision) or with an ImageJ plugin called Time Series Analyzer. The mean fluorescent intensities of responding boutons were background corrected. To compare the apparent release of SVs the mean fluorescent intensities (F) were normalized to their initial fluorescence (F0) prior to electrical stimulation, and F/F0 traces

were plotted. The endocytic retrieval was analyzed by normalizing the fluorescent time courses subtracted by F0 (obtaining ΔF) to their maximum peak fluorescence. ΔF/F curves were plotted and the endocytic time constant τ was determined by fitting a monoexponential decay curve using Prism (Graphpad) software.

(II) $I(t) = y_0 + A*\exp(-t/\tau)$

I(t) – fluorescence intensity at time t; $y_0$ – intensity plateau at t max; A – initial intensity I(0) subtracted by $y_0$; τ – time constant.

If required, mean fluorescence intensities were corrected for bleaching. The intensity time courses of non-responding boutons or dendrites were used to obtain the fluorescent time constant τ in all datasets with monoexponential decay as described in (II). With the fluorescence time constant τ the bleach rate β was calculated:

(III) $\beta = \exp(-1/\tau)$

The mean fluorescence intensities were corrected using the bleach rate for every time point of the recording. Therefore, the difference of fluorescence intensities due to bleaching was calculated for all time points starting at time i=0 to time t, summed up and were added to the fluorescence intensity at time t (I(t)).

(IV) $I_{bc}(t) = I(t) + \sum_{i=0}^{t}(I(i) - bg) \cdot (1 - \beta)$

$I_{bc}(t)$ - bleach corrected fluorescence intensity at time t; I(t) – fluorescence intensity at time t; I(i) – fluorescence intensity at time i=0, bg – background; β - bleach rate.

To measure exocytosis the re-acidification of SVs was blocked by inhibiting the v-ATPase with folimycin (Sigma). First, pHluorin intensities of transfected neurons were recorded during stimulation to test responsiveness. Subsequently 67 nM folimycin in imaging buffer was locally applied for 20 s using a piezo-controlled perfusion Fast-Step System (VC-77SP, Warner Instruments) equipped with a three barrel glass tubing allowing fast solution exchange.

Surface levels of overexpressed Syt1-pHluorin were monitored under steady state conditions and fast exchange of extracellular solutions. To allow fast buffer substitution the perfusion Fast-Step System was used to apply solutions locally, while the Mini-Peristaltic Pump II (Harvard Apparatus) ensured a continuous flow rate and efflux of buffers. Surface-localized pHluorin molecules were quenched with an acidic imaging buffer (pH 5.5). The acidic buffer was exchanged to neutral imaging buffer before the total fluorescence of all

overexpressed Syt1-pHluorins was revealed with an ammonium chloride based basic imaging buffer. The example trace in Figure 11 illustrates the sequence of the acidic quench-unquenching protocol. Images were acquired again with a 0.5 Hz frame rate with the epifluorescent microscopes and settings described in section 3.4.1. At least 5 frames with stable fluorescence intensities were recorded before extracellular solutions were exchanged. To ensure that only healthy neurons were used for further analysis, neurons were stimulated electrically at the end. Only responding boutons were selected to determine the fraction of surface-stranded Syt1-pHluorins. The surface fraction corresponds to the fluorescence $F_{neutral}$ – $F_{acidic}$ normalized to the total pHluorin pool ($F_{basic}$ - $F_{acidic}$). Non-responding neurons were excluded from quantification.

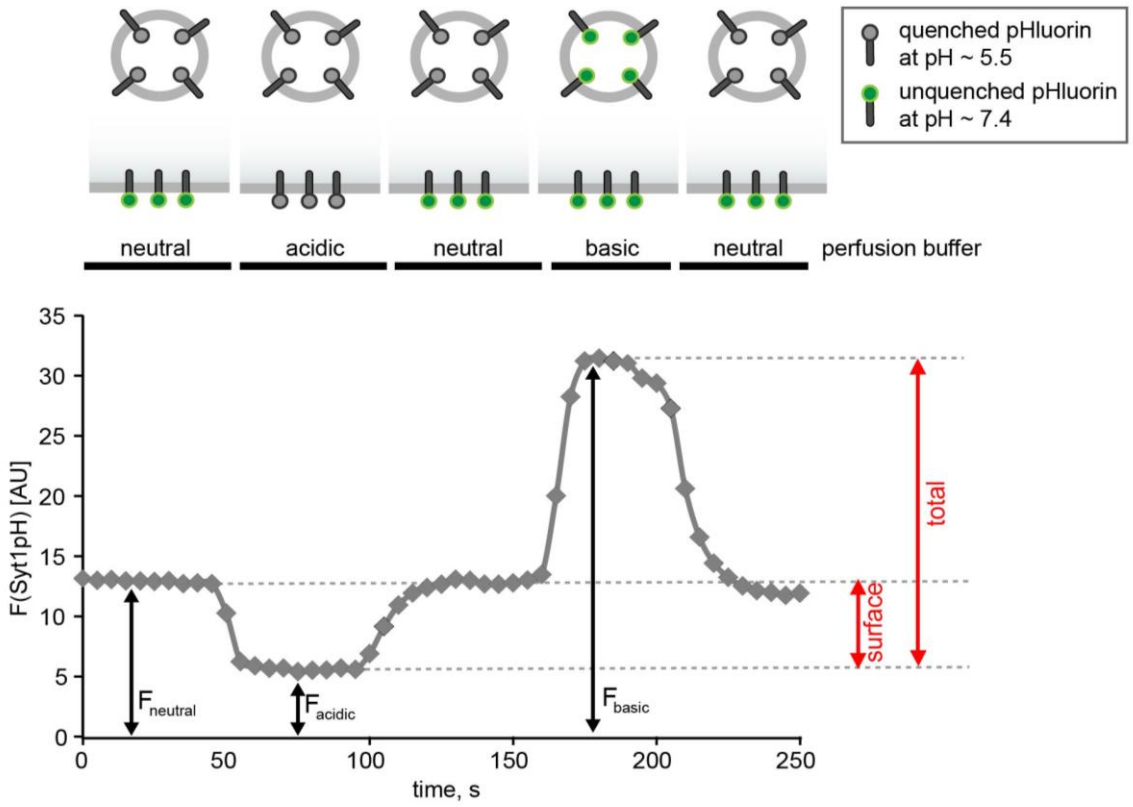


**Figure 11: Acidic quench-unquenching protocol of Syt1-pHluorin to monitor surface levels.** The surface-residing Syt1-pHluorin molecules are quenched with an acidic buffer. Physiological and neutral buffer removes the acidic buffer before the total pool of Syt1-pHluorin is unquenched with a basic buffer comprising ammonium chloride.

### 3.4.5. Calcium live-cell imaging

Calcium is an important signaling molecule during exo- and endocytosis of SVs. During electrical stimulation the cytosolic concentration of calcium can rise from 50-100 nM to concentration in the µM range (Grienberger and Konnerth, 2012), which triggers exocytic fusion of SVs. To monitor the calcium influx during neurotransmission the chemical calcium indicator Fluo-5F-AM (Thermo Fisher) was utilized. Fluo-5F is an analog of the originally developed Fluo-3 (Minta et al., 1989), which is essentially a hybrid of a calcium selective chelator and a fluorescent chromophore. These indicators increase their fluorescent intensity a 100-fold upon binding of free calcium ions without a spectral shift (excitation/emission: 494/516 nm). However, Fluo-5F is characterized by a lower binding affinity ($K_d$ = 2.3 µM) and a fast dissociation rate compared to Fluo-3. Thus, the Fluo-5F signal cannot saturate during neuronal stimulation, and calcium fluxes can be recorded in neurons. The hydrophobic acetoxymethyl (AM) ester residues of Fluo-5F ensure cell permeability, and their removal by intracellular esterases trap Fluo-5F within the cell.

Neuronal cultures of Stn2 WT and KO mice were transfected with the red-shifted pHluorin reporter Syt1pHoran4 at DIV7 - 9 as described in section 3.3.5. Syt1pHoran4 transfected boutons served as marker for the calcium imaging later. On DIV14 the neurons were incubated with 1.2 µM Fluo-5F-AM in 1 ml original culturing medium for 15 min at 37 °C and 5 % $CO_2$. Subsequently, neurons were shortly washed with the residual culturing medium, once with imaging buffer and were additionally incubated for 10 min in imaging buffer at 37 °C and 5 % $CO_2$ to remove all residual Fluo-5F-AM. Finally, Syt1pHoran transfected neurons were imaged in the stimulation chamber with imaging buffer and the Nikon Eclipse Ti microscope described in section 3.4.1. First, Syt1pHoran responses to electrical stimulation were recorded with a TRITC filterset and 0.5 Hz frame acquisition to confirm the healthiness and responsiveness of the selected neuron. The same electrical stimulation was repeated to monitor Fluo-5F intensities with the eGFP filterset and low exposure of 50 ms. However, the acquisition frame rate was adjusted to 3.33 Hz with respect to the fast calcium transients.

Syt1pHoran4 positive boutons that responded to electrical stimulation were selected as ROIs and used as a mask to quantify Fluo-5F intensity changes. Mean fluorescent intensities (F) were normalized to their initial fluorescence (F0) prior to electrical stimulation and F/F0 traces were plotted to compare calcium influx during stimulation in Stn2 WT and KO neuronal cultures. The Fluo-5F signal during time Δt of stimulation was quantified as the

area-under-the-curve (AUC) using Prism software (Graphpad) (Schauer and Leinders-Zufall, 2012).

## 3.5. Biochemical methods

### 3.5.1. Preparation of HEK 293T cell lysates

Confluent HEK 293T cells were briefly washed with PBS on ice and harvested in lysis buffer. About 200 µl per 6-well dish were used to yield a protein concentration of 0.5-1 mg/ml. Cells were collected with a cell scraper. To allow complete cell lysis by TritonX-100 the cells were incubated for 1 h at 4 °C on a rotation wheel. Subsequently, they were centrifuged at 16,200 x g for 10 min at 4 °C to remove cell debris. Soluble proteins were diluted in SDS sample buffer and stored at -20 °C.

### 3.5.2. Preparation of mouse brain extracts

Whole mouse brains of 12-days-old animals were homogenized in brain homogenization buffer II using 5 µl of lysis buffer per 1 mg brain. Cells were lysed with a manually driven homogenizer pestle (Micropestel, Eppendorf) followed by a 26G syringe on ice. The lysate was centrifuged at 241,200 x g for 15 min at 4 °C, and protein concentration of the supernatant was determined by Bradford assay.

### 3.5.3. Protein quantification using Bradford assay

Protein concentrations were measured by the Bradford assay, which is based on protein binding to Coomassie G-250 resulting in an absorbance shift from 465 nm to 610 nm and is monitored at 595 nm. Cell extracts or purified proteins were diluted 1:10 - 1:500 in 500 µl ultrapure water, and 500 µl of 2x Bradford reagent was added. The lysis buffer diluted in the same amount of water and 2x Bradford reagent was used as a reference. The solution was mixed, incubated for 5 min at room temperature, and the absorbance was measured with a photometer (BioPhotometer Plus, Eppendorf). Absorbance values of 0.1 to 0.5 were considered reliable, and protein concentrations were calculated with the help of a BSA standard curve ranging from 1 µg to 10 µg BSA.

### 3.5.4. Expression of recombinant proteins in *E.coli*

A small scale culture of 50 ml of the *E.coli* BL21 strain transformed with pET28a or pGEX4T were grown overnight at 37 °C with the respective antibiotics. The following day the overnight culture was diluted 1:10 in 2x YT protein expression medium with appropriate antibiotics and grown at 37 °C at 180 rpm until an optical density $OD_{600}$ of 0.7 - 0.8. Protein expression was induced with 0.5 mM isopropyl thiogalactoside (IPTG). Bacteria were incubated at 30 °C or 18 °C (depending on the fusion protein) for another 4 h before they were harvested at 4 °C with 4000 x g for 20 min. The bacterial pellets were resuspended in ice-cold PBS, aliquoted and stored at -20 °C.

### 3.5.5. Affinity-purification of GST- and $His_6$-fusion proteins

The recombinant proteins expressed in *E.coli* BL21 were purified via their Glutathione S-Transferase- (GST, 27 kDa) or their Hexahistidine- ($His_6$) tag. GST and $His_6$ can interact with their specific ligands, glutathione and nickel ions, which are either immobilized or coupled via nitrilotriacetic acid to beads, respectively. Therefore, all other bacterial proteins can be removed and the purified fusion protein can be eluted.

Bacterial pellets containing the GST-fusion proteins for GST pulldown assays were thawed, and 1 mM phenylmethylsulfonyl fluoride (PMSF), 125 units benzonase (DNase) and a spatula-tip of lysozyme were added to degrade bacterial cell walls and remove nucleic acids. After 15 min incubation on ice bacteria were sonicated for one min at 70 % power using Sonoplus (Bandelin) at 4 °C to physically disrupt remaining cell walls and TritonX-100 was added to a final concentration of 1 % (v/v). Cell lysis was allowed for another 15 min at 4 °C before cell debris was sedimented by centrifugation at 35,000 x g for 15 min at 4 °C. The bacterial supernatant was incubated with 0.25 ml of GST-binding resin (Novagen), which was first washed with ice-cold PBS, and the recombinant fusion protein was allowed to bind to the resin for 1 h at 4 °C while rotating. Unbound bacterial proteins were removed by three washes with ice-cold PBS, while beads were pelleted with 3000 x g for 5 min in between washes. Finally the GST-fusion proteins bound to the resin were resuspended in 1 ml PBS and stored at 4 °C.

The $His_6$-GFP-PH-PLCδ1 fusion protein was purified from a two liter bacterial culture to yield sufficient amounts of the probe for immunofluorescent stainings. The pellet was resuspended in 80 ml PBS supplemented with 500 units cyanase nuclease (Serva) and 1 mM PMSF. The bacteria were directly sonicated for 2 min at 30 % power with the Branson digital

sonifier at 4 °C. 350 mM NaCl was added to yield a final NaCl concentration of 500 mM. The bacterial cells were allowed to lyse for 10 min on ice before cell debris was pelleted by centrifugation with 35,000 x g for 20 min. The supernatant comprising the $His_6$-fusion protein was added to a GE Healthcare nickel-nitrilotriacetic acid-agarose (Ni-NTA) column and eluted with an imidazole gradient. First PBS with 500 mM NaCl and 20 % (w/v) glycerol was applied, followed by the same buffer supplemented with 500 mM imidazole. With size exclusion chromatography using a GE Heathcare Superdex 75 column the eluted $His_6$-GFP-PH-PLCδ1 fusion protein was concentrated, and imidazole was removed with 20 % (w/v) glycerol in PBS.

The protein concentration was determined by Bradford assay or measuring absorption at 280 nm, and the protein was stored at 4 °C.

### 3.5.6. GST-pulldown from rat brain extract

The GST-pulldown of GST-Syt1 C2A and C2B domain with rat brain extracts was performed by Dr. Michael Krauss from the Leibniz Research Institute for Molecular Pharmacology (FMP, Berlin). 1.5 rat brains were homogenized in homogenization buffer I with 10 strokes of a glass-teflon-homogenizer at 900 rpm. 100 mM PMSF and the mammalian protease inhibitor cocktail (Sigma) were added and cell debris was centrifuged at 1000 x g at 4 °C for 15 min. The supernatant was supplemented to a final concentration of 100 mM KCl, 20 mM HEPES pH 7.4, 2 mM MgCl2, 1 % TritonX-100 (lysis buffer), incubated for 15 min on ice and centrifuged for 15 min at 10,000 x g at 4 °C to enrich synaptosomal membranes. The pellet (P2) was resuspended in lysis buffer and protein aggregates were removed with 241,200 x g for 15 min at 4 °C centrifugation. 8 mg of rat brain extracts were applied to the corresponding beads washed in lysis buffer and incubated for 2 h at 4 °C on a rotation wheel. To remove unspecific protein interactions the beads were washed four times with lysis buffer and once with lysis buffer omitting TritonX-100. Bound proteins were eluted by adding twice 40 µl of 1x SDS sample buffer at 95 °C for 5 min.

### 3.5.7. Co-Immunoprecipitation of synaptosomal extracts

The interaction of Syt1 with PIPK1γ was investigated with co-immunoprecipitation from TritonX-100 extracted synaptosomes of rat brains by Dr. Michael Krauss (FMP, Berlin). In brief, two rat brains were homogenized in homogenization buffer I with 10 strokes of a glass-

teflon-homogenizer at 900 rpm and centrifuged for 15 min at 900 x g. The supernatant was centrifuged again for 15 min at 15,000 x g, and the pellet P2 containing crude synaptosomal membranes was resuspended in homogenization buffer I. To separate the supernatant from the membrane fraction the crude synaptosomal membranes were centrifuged for 15 min at 16,000 x g, and the pellet was resuspended and lysed in lysis buffer followed by two additional centrifugations for 15 min at 81,000 x g and at 241,200 x g. The 6 mg of supernatant were added to protein A/G beads (Santa Cruz Biotechnology), which had been incubated with the respective antibodies overnight at 4 °C and washed three times with lysis buffer. The synaptosomal extracts were additionally either supplemented with 5 mM EGTA or 200 µM $CaCl_2$ with calpain/cathepsin D inhibitors to prevent proteolysis. After 4.5 h incubation at 4 °C on a rotation wheel the beads were washed four times with lysis buffer and once with lysis buffer omitting TritonX-100. Bound proteins were extracted from the beads twice with 30 µl of 1x SDS sample buffer at 95 °C for 5 min.

### 3.5.8. SDS polyacrylamide gel electrophoresis (SDS-PAGE)

To separate proteins according to their molecular weight, a sodium dodecylsulfate polyacrylamide gel electrophoresis (SDS-PAGE) was performed. SDS is an anionic detergent that disrupts non-covalent protein interactions and thereby the three-dimensional structure of native proteins. Together with β-mercaptoethanol, which reduces disulfide bonds, proteins are denatured. The negatively charged SDS binds to the unfolded polypeptide-chains according to their molecular mass, masks their native charge with a uniform negative charge and creates a constant molecular mass to charge ratio. Thus, proteins can be separated in an electrical field according to their molecular weight.

Discontinuous polyacrylamide gels are used as a gel matrix according to Laemmli (Laemmli 1970) with Tris-glycine based buffers. First the stacking gel (3 %) with wide pores and low pH 6.8 concentrates the protein samples between fast running chloride ions and slowly migrating glycine that is only partially ionized due to the low pH. The separation gel with pH 8.8 charges the glycine ions, and proteins can migrate according to their mass in the electric field. Depending on the acrylamide concentration the gel pore sizes can be varied. The acrylamide (A/A) can polymerize and is crosslinked with N, N’-methylenebisacrylamide (BA) with the help of free radicals generated by ammonium peroxodisulfate (APS) and N,N,N',N'-tetramethylethylenediamine (TEMED). The compositions of separation and stacking gel are summarized in Table 23. Gels were run at a constant current of 10 – 20 mA

per gel and were either directly used for immunoblotting or proteins were visualized in the gel by Coomassie staining.

**Table 23: Composition of SDS polyacrylamide gels**

| Components | Separation gel | | | Stacking gel |
|---|---|---|---|---|
| | 12 % | 10 % | 8 % | 3 % |
| 30 % AA/BA mix | 3 ml | 2.5 ml | 2 ml | 0.33 ml |
| Ultrapure water | 2.5 ml | 3 ml | 3.5 ml | 1.625 ml |
| 4x stacking or separation buffer | 1.875 ml | 1.875 ml | 1.875 ml | 0.625 ml |
| 10 % (w/v) APS | 75 µl | 75 µl | 75 µl | 37.5 µl |
| TEMED | 7.5 µl | 7.5 µl | 7.5 µl | 3.75 µl |

## 3.5.9. Immunoblotting

Immunoblotting or also called western blotting is a very sensitive method to detect specific proteins after their separation by SDS-PAGE. The still negatively charged proteins are transferred from the polyacrylamide gel to a nitrocellulose membrane (GE Healthcare, Amersham Protran 0.2 NC) using an electric field. Either the semi-dry blotting chamber (Biometra FastBlot B44) or tank blotting chambers (BioRad) were used. For both systems blotting paper, the nitrocellulose membrane, the gel and blotting paper all soaked in blotting buffer were stacked. For the wet blotting two sponges were placed additionally on both sides. Air bubbles were removed thoroughly during the assembly. Proteins were transferred with 60 mA/ gel for 3 h using the semi-dry blotting or with 110 V for 65 min at 4 °C using the wet blotting system.

Subsequently, membranes were stained reversibly with ponceau stain for 10 min at room temperature followed by short washes with ponceau destain solution to assess the protein transfer and equal protein loading. The ponceau staining was removed thoroughly with TBS washes, and the membrane was blocked with antibody blocking solution for 1 h at room temperature. Before the primary antibodies diluted in antibody dilution solution were applied overnight at 4 °C, the residual blocking solution was removed by rinsing the membrane four times with 0.05 % (v/v) Tween-20 in TBS for 5 min at room temperature. The primary antibody solution was recycled and unbound antibody was eliminated by four washes in 0.05 % (v/v) Tween-20 in TBS for 5 min at room temperature. The corresponding secondary antibodies were incubated for 1 h at room temperature. Before detection the

membrane was washed again carefully as described before. For chemiluminescence detection of weak signals and qualitative analysis HRP-conjugated secondary antibodies, ECL substrate (Amersham Bioscience) and light sensitive x-ray films were used.

For quantitative analysis of protein amounts by western blot the nitrocellulose membranes were washed with PBS or 0.05 % (v/v) Tween-20 in PBS and blocked with Odyssey blocking buffer (Blotto, LI-COR) diluted 1:1 in PBS. Primary antibodies were diluted in Odyssey blocking buffer with PBS and finally detected with fluorescently conjugated secondary antibodies (IRDye 800CW, LI-COR) and the LI-COR Odyssey Fc Imaging system.

### 3.5.10. Coomassie staining of SDS-polyacrylamide gels

If polyacrylamide gels were not subjected to immunoblotting they were shortly stained with Coomassie stain at 60 °C and incubated at room temperature for 20 min. Unspecific background staining was removed with repeated coomassie destain washes at 60 °C and room temperature.

## 3.6. Histological Methods

### 3.6.1. Perfusion of mice

12-days-old mice were anaesthetized intraperitoneally with 100 µl of 10 % Ketamine and 2 % Rompun in PBS per 10 g of body weight. The onset of deep anesthesia was verified by testing the pedal withdrawal reflex. Subsequently, mice were fixed on a styropor board and the thorax was opened starting with the abdominal wall beneath the rib cage. The diaphragm was cut, and the rib cage was opened and removed. The left ventricle was penetrated with a perfusion needle connected by tubes to a perfusion pump PeriStarPRO (WPI). The needle was quickly fixed, and the right atrial chamber was lacerated to allow the efflux of blood and perfusion solutions. The mice were first perfused with about 15 ml of ice-cold Ringer solution supplemented with 0.01 % heparin at a constant flow rate of 1.0 ml/min. Blanching of the liver was taken as a quality control for efficient blood removal before the solution was exchanged for freshly prepared, ice-cold 4 % PFA in PB. The brains of the perfused mice were dissected and incubated overnight at 4 °C in fixation solution. Finally, they were transferred to brain storage solution until they were sectioned.

### 3.6.2. Cryosectioning of mouse brains

Within a week after the perfusion brains were sectioned with a Microm HM 430 (Thermo Scientific). Brains were glued to the platform with Tissue-Tek (Sakura Finetek Europe) and were cooled down to -40 °C. Additionally, the glued brains were shortly covered with dry ice to freeze them entirely. 40 µm thick sagittal sections were cut with a sliding blade. The sections were collected in 6 series and stored in cryotubes with brain storage solution. For long-term storage the sections were transferred to -80 °C.

### 3.6.3. Nissl staining

The Nissl staining is based on a cresyl-violet acetate solution that reacts with nucleic acids of DNA and RNA. Therefore, mainly cell bodies are stained in blue and visualize the overall morphology of tissue e.g. of the brain in brain slices.

Brain slices of one series were thawed, sorted from lateral to medial in gelatin solution at 41 °C and mounted on SuperFrost Plus slides (Thermo Scientific). Sections were dried overnight on a stretching table (OTS 40, Medite) and stained on the next day. The slides were shortly rinsed with ultrapure water for 1 min and stained for 8 min in the dark with 0.1 % (w/v) cresyl violet in ultrapure water. The slides were immersed three times in ultrapure water for 2 min to remove excess stain before the sections were slowly dehydrated with increasing ethanol concentrations starting from 50 %, 70 %, 80 % to 90 % (v/v) for 2 min each. The staining was differentiated with 0.5 % (v/v) glacial acetic acid in 96 % (v/v) ethanol for 1-3 min. Finally, slides were incubated two times in absolute ethanol for 2 min, in xylene for 2 min and sealed with coverslips mounted in Entellan (Millipore).

### 3.6.4. Immunohistochemistry

Free floating brain sections of control and KO mice were simultaneously immunofluorescently stained. They were selected from the same cutting series to correspond to the same position within the brain. The whole protocol was performed with two sections of each genotype in embryo dishes on a standard 1000 orbital shaker (VWR) at 100 rpm. To remove residual cryo-protecting solution the sections were washed three times in 125 mM PB for 20 min, followed by permeabilization with freshly prepared 0.3 % (v/v) TritonX-100 in 125 mM PB. During permeabilization the solution was exchanged 9 times in 20 min intervals. Afterwards the sections were blocked with 5 % (v/v) NGS and 0.3 % (v/v) TritonX-100 in

125 mM PB for 1 h and incubated with the primary antibody (Table 12) in 0.3 % (v/v) TritonX-100 in 125 mM PB for 48 h at 4 °C. Unbound antibodies were removed by 9 washes a 20 min each with 0.3 % (v/v) TritonX-100 in 125 mM PB, and bound antibodies were decorated with the corresponding Alexa-conjugated secondary antibodies (Table 13) in 0.3 % (v/v) TritonX-100 in 125 mM PB for 12 h at 4 °C. Finally, the sections were rinsed three times for 15 min in 125 mM PB to remove excess antibody and mounted in gelatin solution at 41 °C on microscope slides. As soon as the brain sections were dry (after 20 min at 41 °C) coverslips were mounted on top using Immu-Mount (Thermo Fisher).

Surface-stranded Syt1 was detected by omitting TritonX-100 from all incubations. Selected section were washed in 125 mM PB for 3.5 h at room temperature exchanging the solution every 20 min. Sections were blocked with 5 % (v/v) NGS in 125 mM PB for 1 h before they were incubated with the primary antibody directed against the luminal domain of Syt1 in 5 % (v/v) NGS in 125 mM PB for 12 h at room temperature. Unbound antibodies were removed by rinsing the sections with 125 mM PB 8 times for 15 min each. Corresponding secondary antibodies were diluted in 125 mM PB and incubated for 1.5 h. Sections were washed three times for 15 min with 125 mM PB before they were post-fixed with 2 % (w/v) PFA in 125 mM PB for 50 min. The PFA was removed by three washes for 15 min with 125 mM PB. Subsequently, sections were permeabilized with TritonX-100 and stained as described above to detect the total pool of Syt1. To do so the sections were labeled with a primary antibody against the cytosolic domain of Syt1 and a corresponding Alexa-conjugated secondary antibody.

## 3.7. Electron microscopy

Electron microscopy was performed in collaboration with Dr. Dmytro Puchkov from the EM facility at Leibniz Research Institute for Molecular Pharmacology (FMP, Berlin). Three pairs of 12-days-old DKO or TKO animals and their control littermates were perfused with 4 % (w/v) PFA in 125 mM PB as described in section 3.6.1. Brains were isolated and post-fixed in 2.5 % glutaraldehyde in 125 mM PB overnight at 4 °C. After washing in PBS, the brains were embedded in 5 % (w/v) agar and cut coronally in 200 µm thick sections on the vibratome (Leica). Sections comprising the dorsal hippocampus were post-fixed with 1 % (w/v) $OsO_4$, 1.5 % (w/v) potassium hexacyanoferrate in ultrapure water and stained with 1 % (w/v) uranyl acetate. Subsequently, the sections were dehydrated in methanol and propylenoxide and embedded in Epoxy resin. CA1 pyramidal cell layer and proximal stratum radiatum were

trimmed and ultrathin sectioned after Epoxy resin polymerisation. Digital images of excitatory synapses (> 70 per genotype) were acquired with a Zeiss 900 TEM for subsequent morphometric analysis.

## 3.8. Electrophysiology

### 3.8.1. Input-output recordings, short term plasticity and high frequency stimulation train recordings

All electrophysiological analyses were performed by Dr. Gaga Kochlamazashvili (Leibniz Research Institute for Molecular Pharmacology, FMP, Berlin). 12-days-old DKO and TKO mice with their corresponding littermates were quickly decapitated after cervical dislocation, and brains were extracted into the ice-cold dissection artificial cerebrospinal fluid (ACSF). Hippocampal sagittal sections (400 μm) were prepared from both hemispheres using a vibratome (VT 1200S, Leica) and were allowed to recover before recordings for at least 1.5 h at room temperature in ACSF in which sucrose was exchanged for 120 mM NaCl. Recordings were performed in a submerged chamber (RC-27L, Warner Instruments) perfused with ACSF ( ~ 3 mL/min) similar to the resting solution and continuously bubbled with 95 % $O_2$ and 5 % $CO_2$, pH 7.35 – 7.4. Stimulating (1 – 1.5 MΩ) and recording (1.5 – 2.5 MΩ) electrodes (filled with ACSF) were placed in CA1 stratum radiatum and slowly advanced until the maximal field excitatory postsynaptic potentials (fEPSPs) were obtained. 10 min of stable baseline recordings were followed by monitoring input-output stimulus response curves with increasing stimulation intensity (0 – 200 μA). Presynaptic input, fiber volley, postsynaptic output, and fEPSP amplitudes were plotted as a measure of basal excitatory synaptic transmission.

Short-term synaptic plasticity was measured by paired-pulse facilitation (PPF). The ratio of the second and first fEPSP amplitudes was determined and normalized to the control. To induce significant facilitation, only one-third of the maximal fEPSP amplitude was chosen to evoke PPF responses. Each value measured was an average of three consecutive stimulations repeated every 20 s for stimulus response measurements and every 30 s for PPF measurements. For short time intervals (10 and 20 ms), the first fEPSP was digitally subtracted before measurement of the second fEPSP.

To test the refilling of the releasable SV pool, the acute slices were challenged with a high frequency stimulation train. 500 pulses at 20 Hz were applied with a stimulation

intensity similar to PPF measurements, which initially facilitated and subsequently depressed fEPSP amplitudes. Thereby, the readily releasable SV pool can be depleted.

The data were recorded at a sampling rate of 10 kHz, low-pass filtered at 3 kHz, and analyzed using PatchMaster software and EPC9 amplifier (Heka Elektronics). SigmaPlot (Systat), and IGOR Pro (WaveMetrics) software were used for data analyses and presentation.

For data presentation, two different littermate control genotypes (WT/KO/WT and WT/KO/HET) were pooled together as controls, as no differences for any electrophysiological parameters were observed.

### 3.8.2. mEPSC recordings

Whole-cell voltage-clamp recordings were performed by Dr. Gaga Kochlamazashvili (Leibniz Research Institute for Molecular Pharmacology, FMP, Berlin) in acute hippocampal slices from visually identified CA1 pyramidal neurons. The patch electrodes (2.5 – 3.5 MΩ) were filled with an internal solution. After whole-cell configuration, cells were voltage-clamped at – 60 mV holding potential for at least 10 min before recordings were started. Series resistance less than 20 MΩ (compensated to 70 %) and leak currents less than 200 pA were included for analyses. To isolate the miniature EPSCs the acute slices were treated with a $GABA_A$ antagonist (100 µM Picrotoxin), a NMDA receptor antagonist (50 µM APV) and an inhibitor of sodium channels (1µM TTX). At the end of each experiment, AMPA/kainate receptor antagonist CNQX (20 µM) was applied for 10 min to verify mEPSCs. For each experiment, mEPSCs were recorded for 5 min and subsequently analyzed with MiniAnalysis Program (Synaptosoft).

### 3.8.3. Membrane capacitance measurements at the calyx of Held

Endocytic retrieval can be monitored by the membrane capacitance as it is proportional to the cell surface area. During depolarization SVs fuse with the plasma membrane and thereby increase the cell surface area. This is directly reflected by an increase in capacitance (capacitance jump). Endocytic retrieval results subsequently in a capacitance decay.

Capacitance responses of the calyx of Held were measured by our collaborator Dr. Takeshi Sakaba (Doshisha University, Japan). In brief, calyx of Held terminals of 8- to 12-days-old Stn2 WT and KO mice were patch-clamped at room temperature. Capacitance measurements (sine wave amplitude of 30 mV with frequency of 1000 Hz) were performed

using EPC10/2 patch clamp amplifier (HEKA, Germany). Acute brainstem slices were prepared as previously described (Schneggenburger et al., 1999). The extracellular solution was gassed with 95 % $O_2$ and 5 % $CO_2$ and the patch pipettes (~10 MΩ) were filled with intracellular solution. The terminal was depolarized from -80 mV to 0 mV for varied durations (50 ms or longer) or repetitively depolarized to +40 mV for 1 ms (100 Hz for 20 or 50 times. The half decay of capacitance in response to depolarization was analyzed and plotted against the capacitance jump which represents the amount of exocytosis.

## 3.9. Statistical analysis

All quantifications are based on at least three independent experiments. If not indicated differently a two-tailed Student t test was used to assess statistical significance for all pHluorin experiments. Cell culture data of each independent experiment represent the individual neurons (with at least 30 – 50 boutons analyzed per neuron), taken from the hippocampi of several genotypically identical pups. Data from several independent experiments were pooled to calculate the mean and SEM and to assess statistical significance. Normal distribution was assessed within individual experiments to allow statistical analysis with the two-tailed Student t test as the number of individual experiments was too low. If data of more than two groups were compared with each other the One-way ANOVA with repeated measures and Tukey's posttest was calculated. Significant differences were accepted at * $P < 0.05$. Statistical significance for electrophysiology was detected using two-way ANOVA with repeated measures; significant differences were accepted at *** $P < 0.001$ and ** $P < 0.01$.

# 4. Results

## 4.1. Sorting of synaptotagmin 1 during SV recycling

The calcium sensor Syt1 is a crucial protein for the exocytic fusion of SV and copy numbers of Syt1 on SVs are tightly regulated (Mutch et al., 2011). Thus, a molecular mechanism has to exist to ensure sorting of Syt1 with high fidelity especially in the case of full collapse of SVs into the plasma membrane. AP-2, the major adaptor protein for clathrin-mediated endocytosis, can directly interact with Syt1. However, this binding is not sufficient to retrieve Syt1 from the plasma membrane as shown by ectopically expressed Syt1 in fibroblasts (Feany and Buckley, 1993; Jarousse and Kelly, 2001). Therefore, in neurons specific sorting mechanisms have to safeguard correct Syt1 sorting from the plasma membrane into SV. Earlier data have implicated the orthologs of Stn2, stoned B and Unc41, as the major sorting adaptors of Syt1 in invertebrates (Fergestad and Broadie, 2001; Fergestad et al., 1999; Mullen et al., 2012). SiRNA mediated knockdown of Stn2 in neurons confirmed these results (Willox and Royle, 2012). In contrast to the Stn2 deletion in invertebrates, the Stn2 loss in mice surprisingly did not cause increased lethality and severely impaired neurotransmission. The mice were viable and able to internalize Syt1 albeit with reduced fidelity resulting in Syt1 surface accumulation and slightly reduced Syt1 levels in brain slices (Kononenko et al., 2013). This led us to the hypothesis that mammals have evolved another additional sorting mechanism ensuring correct Syt1 retrieval possibly via complex formation with another SV protein. The SV2 family of transmembrane proteins seemed to be a likely candidate to facilitate Syt1 sorting due to multiple reasons. First of all SV2 was shown to directly interact with Syt1 (Schivell et al., 1996). Secondly, a tyrosine-based motif within the N-terminus of SV2 facilitates complex formation with Syt1 (Haucke and De Camilli, 1999). Furthermore, SVs isolated from SV2A/B double knockout brains showed reduced Syt1 level implicating SV2A/B in Syt1 trafficking (Yao et al., 2010). We therefore addressed the question whether Stn2 and SV2 have overlapping functions in Syt1 sorting and maintenance in the mammalian brain and thereby affect the efficacy of basal neurotransmission.

### 4.1.1. Generation and characterisation of SV2A/B x Stn2 triple knockout mice

In order to analyse whether Stn2 and SV2 are both required in the mammalian synapse to sort and maintain Syt1 we generated mice with a combined deletion of Stn2 and SV2A/B. We

crossed SV2A heterozygous and SV2B KO mice (a kind gift from Sandra Bajjelieh) with Stn2 KO mice to obtain the first generation of mice with SV2A HET/ SV2B HET/ Stn2 HET (HET/HET/HET) genotype. Breeding those mice with each other resulted in the final parental generation of mice, which were heterozygous for SV2A, knockout for SV2B and heterozygous for Stn2 (HET/KO/HET). Their crossing eventually generated double knockout (DKO) mice lacking SV2A and SV2B (KO/KO/WT) or triple knockouts (TKO) harbouring the deletion of all three proteins (KO/KO/KO). As SV2B KO mice as well as Stn2 heterozygotes have been shown to be phenotypically indistinguishable from WT mice (Janz et al., 1999; Kononenko et al., 2013), the genotypes (WT/KO/WT) and (WT/KO/HET) were used as controls (Figure 12A). Control mice were born close to Mendelian ratios. In contrast, DKO and TKO mice displayed only about half of the expected birth rate (Figure 12B). At birth both DKO and TKO mice appeared normal, however, both genotypes showed decreased postnatal viability. The new born TKO mice showed more severe lethality within the first 3 days of their postnatal lives as 70 % of them died in contrast to 50 % of the DKO mice. Most of the remaining mice survived up to 13 days postnatally but lagged behind their control littermates in postnatal development and weight gain (Figure 12D, E). They displayed major neurological defects with spontaneous epileptic seizures and poor motor coordination.

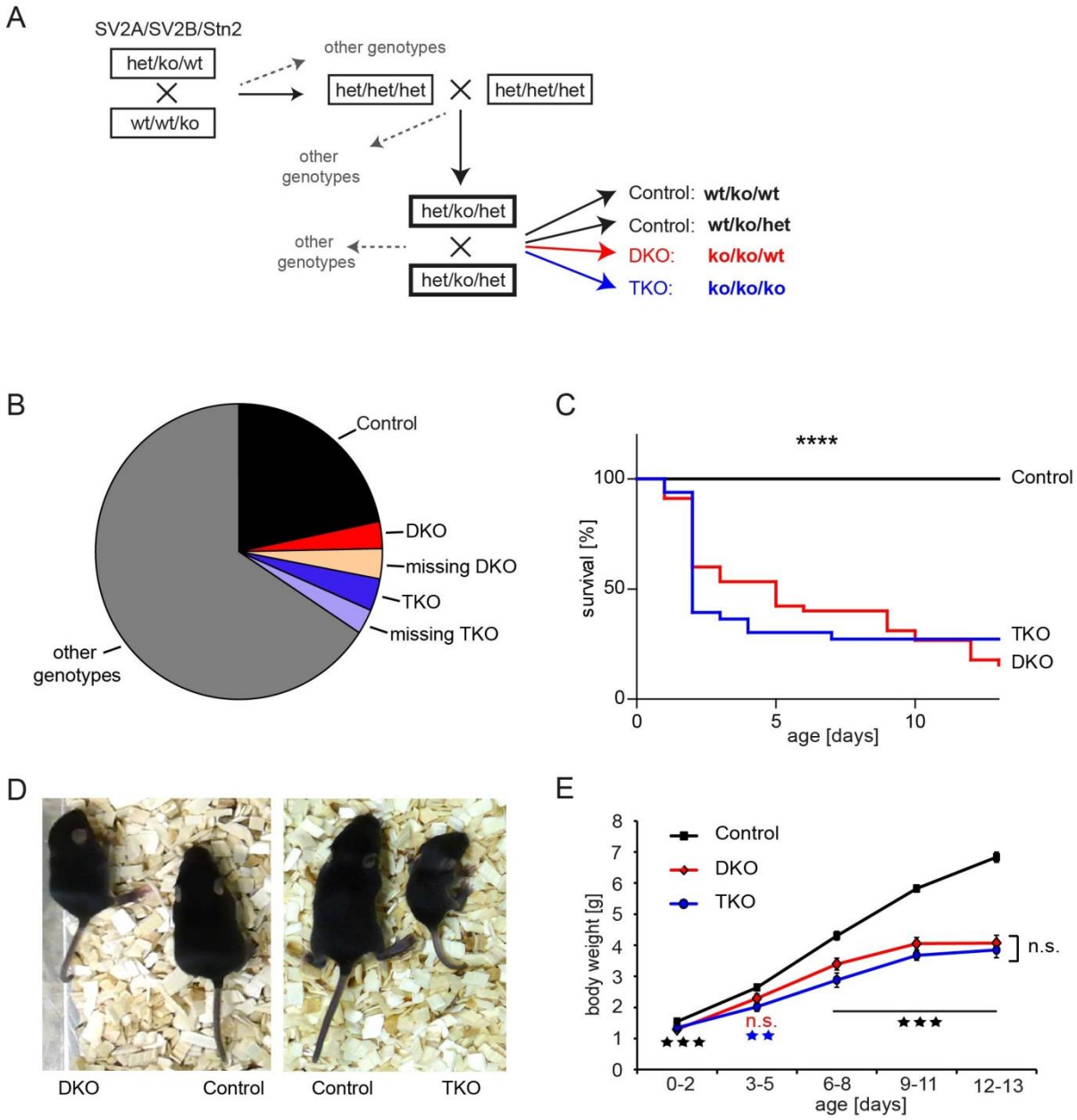


**Figure 12: Generation and characterization of SV2A/B DKO and SV2A/B/Stn2 TKO mice. (A)** Scheme illustrating the generation of DKO and TKO animals as well as their corresponding controls. SV2A HET/ SV2B KO mice (HET/KO/WT) were bred with Stn2 KO mice (WT/WT/KO) to generate triple heterozygous mice (HET/HET/HET), which were subsequently crossed to obtain mice lacking SV2B but heterozygous for SV2A and Stn2 (HET/KO/HET). These were crossed to generate DKO (KO/KO/WT), TKO (KO/KO/KO), as well as control mice (WT/KO/HET and WT/KO/WT) used in the current study. **(B)** Genotype distribution of 2919 offspring from SV2A/B x Stn2 breeding. Control animals were born close to Mendelian ratio with 21.7 % (expected 18.75%) while only 3 % DKO and 3.5 % TKO were born instead of the expected 6.25 %. **(C)** Kaplan Meier Survival Curves of control (n = 52), DKO (n = 45) and TKO (n = 33) animals show increased lethality especially within the first 3 days after birth for TKO (36.4 % survival) and for DKO (53.3 % survival) compared to control littermates. Statistical analysis by log-rank (Mantel–Cox) test (****P < 0.001). **(D)** Representative images of DKO and TKO animals and their corresponding littermates at p12. **(E)** Growth charts of DKO and TKO mice. Body weights of DKO and TKO mice do not differ significantly at any time

point, whereas they are significantly reduced compared to controls (n control = 63, n DKO = 21, n TKO = 25; **P < 0.01, ***P < 0.001). All data represent mean ± SEM.

These severe phenotypes comprising reduced postnatal viability, reduced weight gain and neurological defects in DKO and even more so in the TKO mice are in great contrast to the mild phenotype of Stn2 KO mice. This suggests that SV2A/B and Stn2 fulfil together an important physiological function in vivo.

Developmental changes in the brain can be the cause for seizures and early lethality. DKO mice were already extensively investigated and did not show any defects in their brain morphology or on an ultrastructural level (Custer et al., 2006; Janz et al., 1999). To test whether the additional deletion of Stn2 in the TKO animals affects brain morphology we used Nissl staining of sagittal brain sections from 12-days-old control and TKO mice. We could not observe any abnormalities such as morphological changes or differences in the formation of brain areas. As shown in Figure 13A, the hippocampus of SV2A/B and Stn2 deficient mice showed no anatomical alterations. The cortex of the TKO mice also showed the characteristic cell layers and no defects in cell body localization. Furthermore, we analysed the ultrastructure of Schaffer collateral synapses in the CA1 region of the hippocampus by electron microscopy (EM). As shown previously (Janz et al., 1999) synapses of DKO mice are indistinguishable from control mice and the combined deletion of Stn2 and SV2A/B does not affect synapse morphology, SV number and presynaptic organization (Figure 13 and Table 24). Hence, postnatal mortality and neurological defects in mice with combined deletion of SV2A/B and Stn2 cannot be explained by alterations in brain morphology or synapse structure.

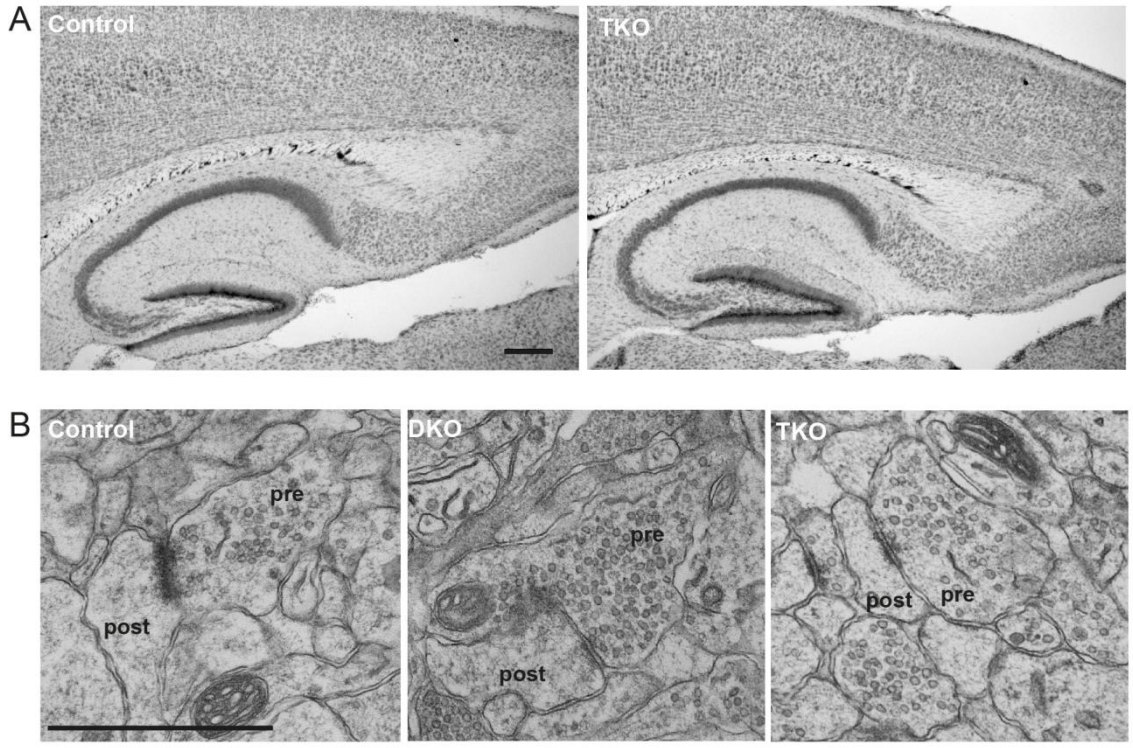


**Figure 13: Normal brain morphology and synapse ultrastructure in TKO mice. (A)** Example images of sagittal sections from 12-days-old control and TKO mice stained with cresyl violet (Nissl) show no developmental defects in hippocampus and cortex anatomy (scale bar, 100 µm). **(B)** Electron micrographs of synapses from the proximal CA1 stratum radiatum. Control, DKO and TKO mice show normal synapse formation, SV number, localization and morphology (>70 synapses per genotype; scale bar, 1 µm). Electron microscopy was performed by Dr. Dmytro Puchkov (FMP Berlin, Germany).

**Table 24: Normal gross morphology of synapses and number of SVs in absence of SV2 and Stn2.**

| | # of SVs/ µm² | Active zone length [nm] |
|---|---|---|
| **Control** | 108.70 ± 5.28 | 268.49 ± 8.34 |
| **DKO** | 114.24 ± 7.32 | 286.46 ± 11.43 |
| **TKO** | 119.79 ± 6.23 | 285.86 ± 14.42 |

## 4.1.2. Combined deletion of SV2A/B and Stn2 aggravates Syt1 loss in vivo

To determine whether Stn2 and SV2 are both required for high-fidelity sorting of Syt1 in mammals, we analysed brain extracts from 12-days-old control, DKO and TKO mice. We verified that SV2A and B were both depleted in DKO and TKO mice compared to control mice by using an antibody directed against all SV2 isoforms (pan SV2). The remaining band in both genotypes corresponds to the SV2C isoform (Figure 14A). We then investigated the expression levels of endocytic proteins in brains of SV2A/B deficient mice. While the levels

of AP-2, clathrin and dynamin1-3 did not change (Figure 14A, D), Stn2 expression was significantly increased to 131.8 ± 7.2 % in the brain lysates of DKO mice compared to control mice (Figure 14A, B). Thus, loss of SV2A/B results in a compensatory increase in the steady-state levels of Stn2 in vivo. In line with previous work (Yao et al., 2010) the Syt1 expression levels were reduced to 42.3 ± 3.2 % in SV2A/B deficient brains, whereas Syp levels were unaffected (Figure 14A, C). Interestingly, the combined deletion of SV2A/B and Stn2 (Figure 14A, B) decreased the steady-state level of Syt1 significantly further to 29.9 ± 2.6 % compared to DKO. In contrast, Syp levels were not different compared to control or DKO (Figure 14A, C), which is consistent with the selective association of Stn2 with Syt1 but not with other SV proteins.

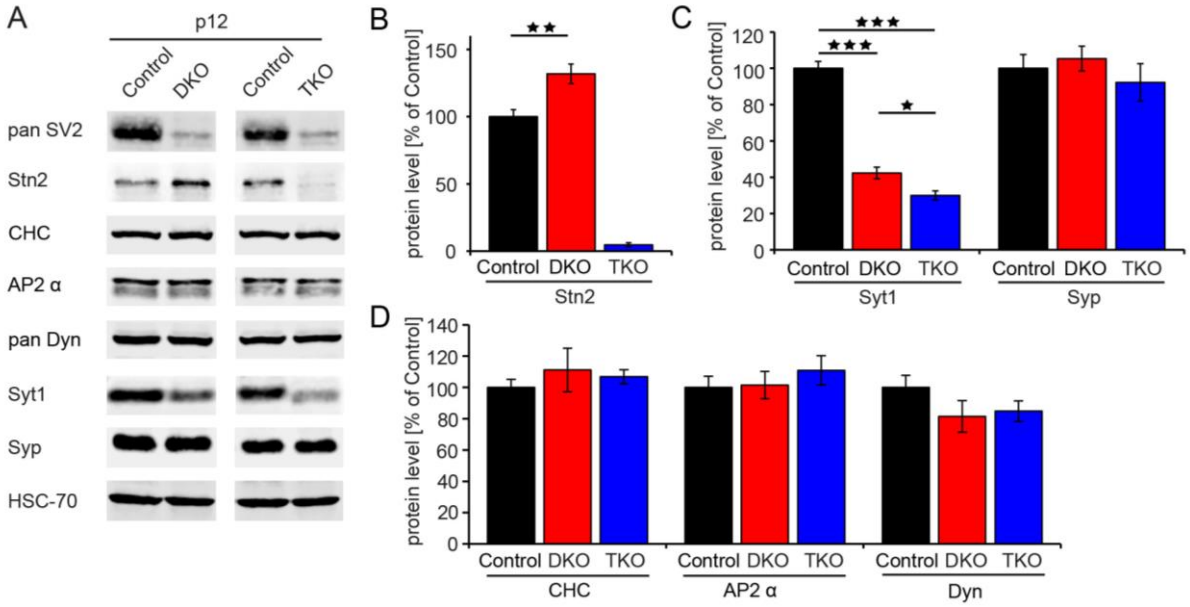


**Figure 14: Exacerbated loss of Syt1 upon combined deletion of Stn2 and SV2A/B. (A)** Levels of synaptic and endocytic proteins in total brain lysates from p12 control, SV2A/B DKO, and SV2A/B/Stn2 TKO mice probed by immunoblotting with specific antibodies. AP-2 α, adaptor protein 2α; CHC, clathrin heavy chain; Hsc70, heat shock cognate protein of 70 kDa; pan-Dyn, dynamin 1–3; Syp, synaptophysin; Syt1, synaptotagmin 1. The band remaining in DKO and TKO lysates decorated with pan-SV2 antibodies corresponds to the SV2C isoform. **(B)** Stn2 is up-regulated in the absence of SV2A/B (control, 100.0 ± 6.9 %; DKO, 131.8 ± 7.2 %; TKO, 4.7 ± 1.5 %; n control/DKO = 6; n control/TKO = 5; **P < 0.01). **(C)** Syt1 levels are significantly reduced in DKO (42.3 ± 3.2 %) and in TKO (29.9 ± 2.6 %) compared to control (100.0 ± 6.0 %; n control/DKO = 6; n control/TKO = 5; *P < 0.05, **P < 0.01, ***P < 0.001), and Syp levels are unaffected (control, 100.0 ± 7.6 %; DKO, 105.3 ± 6.8 %; TKO, 92.3 ± 10.2 %; n control/DKO = 6; n control/TKO = 5). **(D)** Levels of clathrin (CHC), AP-2α, and dynamin 1–3 (Dyn) in total brain lysates derived from p12 control, DKO, and TKO mice were unaltered (CHC: control, 100.0 ± 5.2 %; DKO, 111.2 ± 14.0 %; TKO, 106.9 ± 4.4 %; AP-2: control, 100.0 ± 7.1 %; DKO, 101.5 ± 8.7 %; TKO, 110.9 ± 9.3 %; Dyn: control, 100.0 ± 7.7 %; DKO, 81.5 ± 10.1 %; TKO, 84.9 ± 6.5 %; n control/DKO = 6; n control/TKO = 5). All data represent mean ± SEM.

To investigate SV protein levels specifically in the hippocampus we stained sagittal brain sections of control, DKO and TKO mice with specific antibodies and analysed samples by immunofluorescence confocal microscopy. As expected, brain slices displayed reduced Syt1 levels in the hippocampus of DKO mice, which was further aggravated in TKO tissue (Figure 15A, B). The protein levels of other presynaptic proteins like the SV associated protein synapsin 1 or the SV protein Syb2 were not significantly changed in the absence of SV2A/B or upon combined deletion of SV2A/B and Stn2 (Figure 15C-F). Given the normal brain morphology and synapse formation in TKO mice (Figure 13A, B), these results suggest that SV2A/B and Stn2 fulfil a specific and overlapping function in Syt1 maintenance in the brain and play no role in general synapse organisation.

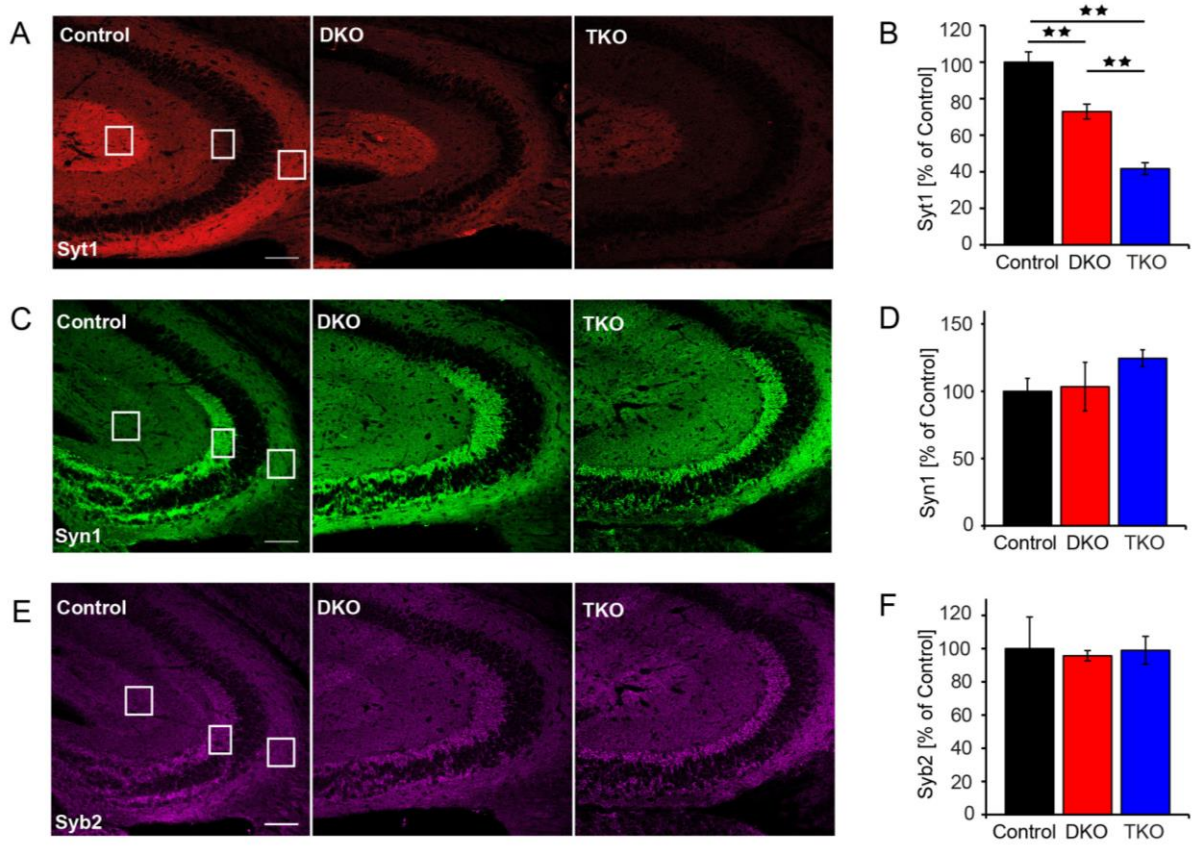


**Figure 15: Aggravated Syt1 loss in the hippocampus of SV2A/B and Stn2 deficient mice. (A, C, E)** Representative confocal images of perfused sagittal brain sections immunostained for Syt1, Syn1 and Syb2. Total levels of Syt1 **(A** and **B)**, Syn1 **(C** and **D)**, and Syb2 **(E** and **F)** were analyzed in the hippocampus of control, DKO, and TKO mice. (Scale bar, 100 µm.) **(B)** Syt1 intensity levels are reduced in DKO and even further decreased in TKO mice compared to controls (control, 100.0 ±5.6 %; DKO, 71.4 ± 3.5 %; TKO, 41.7 ± 3.0 %; n control/DKO = 4; n control/TKO =3, *P < 0.05, **P < 0.01). **(D** and **F)** Syn1 and Syb2 protein levels are not significantly different in DKO and TKO mice compared to controls (control Syn1, 100.0 ± 9.6 %; DKO Syn1, 103.4 ± 18.1 %; TKO Syn1, 124.5 ± 6.3 %; control Syb2, 100,0 ± 19.0 %; DKO Syb2, 95.7 ± 3.1 %; TKO Syb2, 99.0 ± 8.4 %; n WT/DKO = 4; n WT/TKO = 3). Regions of interest (ROI) in A, C, and E indicate areas taken for quantification. All data represent mean ± SEM.

### 4.1.3. Knockdown of SV2A in hippocampal neuron culture causes partial Syt1 loss

The data so far suggest that SV2A/B and Stn2 are both involved in Syt1 maintenance at mammalian synapses. To investigate the role of Stn2 and SV2A/B further we circumvented the high mortality of DKO and TKO mice and by using siRNA mediated knockdown. We first validated the knockdown efficiency in HEK 293T fibroblasts overexpressing eGFP-SV2A. Immunoblotting of HEK cell lysates showed efficient suppression of eGFP-SV2A expression in HEK cells that were treated with SV2A siRNA compared to scramble siRNA (Figure 16A). Subsequently, we tested the SV2A knockdown efficacy in hippocampal cultures. We co-transfected neuronal cultures with Syt1-pHluorin, a Syt1 chimera carrying the pH sensitive green fluorescent protein pHluorin to identify synaptic boutons, together with control siRNA or SV2A siRNA. 5 days post-transfection staining for endogenous SV2A in hippocampal cultures showed that the levels of endogenous SV2A were significantly reduced in Syt1pHluorin positive and SV2A siRNA treated neurons (Figure 16B). Quantification revealed a knockdown efficiency > 65 % (Figure 16C).

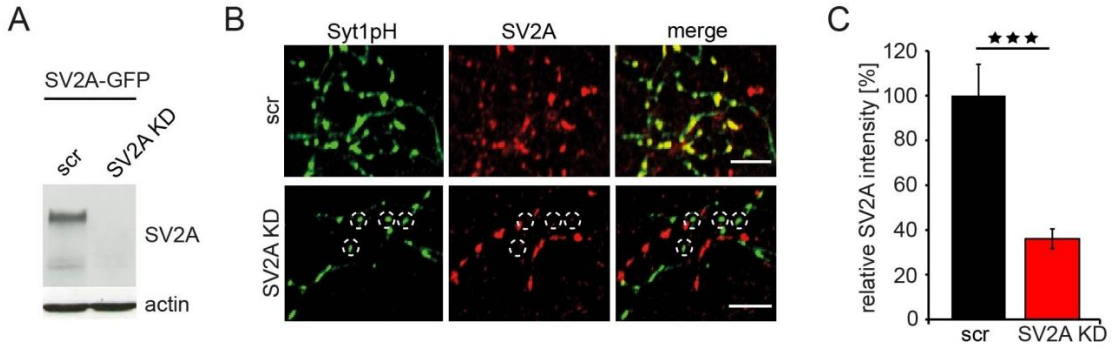


**Figure 16: Efficacy of SV2A knockdown in hippocampal neuronal cultures. (A)** Immunoblot of lysates from HEK 293T cells overexpressing eGFP-SV2A and treated with scr or SV2A siRNA probed with SV2A antibody. **(B)** Representative confocal images of hippocampal neurons coexpressing Syt1-pHluorin with scrambled (scr) siRNA (upper panel) or SV2A siRNA (lower panel) and immunostained with GFP (green) and SV2A (red) specific antibodies. (Scale bar, 10 µm.) **(C)** SV2A levels are significantly decreased in neurons treated with SV2A siRNA (KD), compared with the neurons treated with scr siRNA (scr, 100 ± 14.1 %; SV2AKD, 36.1 ± 4.4 %; n = 4; ***P < 0.0001). Data represent mean ± SEM.

The depletion of SV2A in neuronal cultures was accompanied by a reduction in Syt1 (Figure 17 and Figure 19) levels consistent with our previous observations in DKO mice. However, Syt1 protein levels were only reduced by 21 % likely due to the incomplete depletion of SV2A compared to the full knockout in the mouse. Re-expression of siRNA

resistant SV2A was able to rescue the partial Syt1 loss in SV2A depleted neurons. Hence, Syt1 maintenance is specifically mediated by SV2A in neuronal cultures.

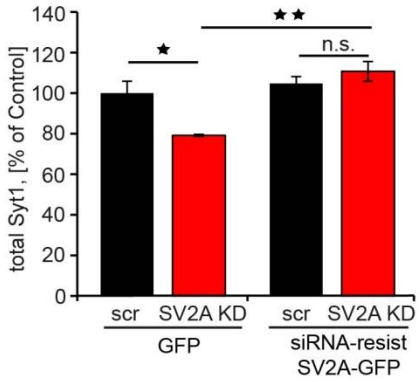


**Figure 17: SV2 KD causes partial loss of Syt1 in neuronal cultures.** SV2A KD significantly reduced Syt1 total levels compared with control (scr, 100 ± 5.8 %; SV2AKD, 79.1 ± 0.6 %; *P < 0.05; quantification of Figure 19A) and was rescued by overexpression of siRNA-resistant SV2A-GFP (scr, 104.7 ± 3.4 %; SV2AKD, 110.7 ± 4.8 %; **P < 0.01; n = 3 independent experiments; >3,000 boutons per condition).

### 4.1.4. Impaired Syt1 sorting in the absence of Stn2 and SV2A show additive defects

Next we addressed the question whether Stn2 and SV2A are both required for correct sorting of Syt1. To this end we overexpressed Syt1-pHluorin in cultured neurons and investigated its partitioning between the internal vesicle pool and the surface-stranded pool in the absence of SV2A, Stn2 or combined deletion of SV2A and Stn2. We performed an acid quenching-dequenching experiment, which can reveal the surface pool of Syt1-pHluorin upon perfusing the neurons with an acidic buffer, whereas the total Syt1-pHluorin pool within the synapse can be detected with an ammoniumcloride pulse (Figure 11). Depletion of SV2A on its own significantly increased the surface-stranded pool of Syt1-pHluorin as quantified by an increased surface/total ratio of Syt1-pHluorin. As published before (Kononenko et al., 2013) Stn2 deletion resulted in elevated surface accumulation of Syt1-pHluorin as well. Interestingly, the level of Syt1-pHluorin missorting to the surface was comparable in SV2A knockdown or Stn2 knockout neurons. The combined absence of SV2A and Stn2 increased the ratio of surface-stranded over total Syt1-pHluorin even further, revealing an additive defect in Syt1-pHluorin sorting (Figure 18). Thus, Stn2 and SV2A have overlapping functions in maintaining and sorting Syt1.

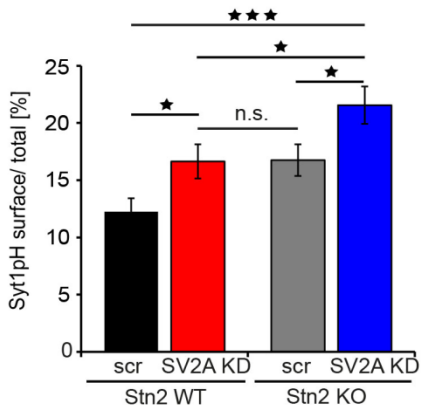


**Figure 18: Surface accumulation of Syt1pHluorin.** Surface/total ratios of Syt1-pHluorin expressed in hippocampal wildtype (WT) or Stn2 KO neurons cotransfected with scr or SV2A siRNA (KD). The surface/total Syt1pHluorin ratio was significantly increased in the absence of either SV2A or Stn2 (Stn2 WT, scr, 12.2 ± 0.1 %; Stn2 WT, SV2A KD, 16.6 ± 0.1 %; Stn2 KO, scr, 16.8 ± 0.1 %) and further aggravated by depletion of both proteins (Stn2 KO, SV2A KD, 21.6 ± 0.1 %; n = 5; >510 boutons per condition;*P < 0.05, ***P < 0.0001). Data represent mean ± SEM.

To avoid misinterpretations that may result from exogeneous overexpression of Syt1, we also stained for endogenous Syt1 in SV2A depleted neurons. We applied an antibody that specifically recognizes the luminal domain (LD) of Syt1 prior to membrane permeabilization to detect the surface pool of Syt1 (Syt1 LD). A second Syt1 antibody targeting the cytoplasmic part of Syt1 was subsequently applied under permeabilizing conditions to assess the total pool of Syt1 (Figure 19A). As expected, SV2A knockdown also increased the surface-stranded pool of endogenous Syt1. This phenotype was rescued by re-expression of siRNA-resistant SV2A fused to GFP (Figure 19B), which suggests a specific role of SV2A in Syt1 sorting. In addition, we probed the sorting of another SV protein, Syp, that does not associate with SV2 or Stn2. Indeed, the Syp surface levels were unaltered in SV2A depleted neurons compared to the scrambled control (Figure 19B).

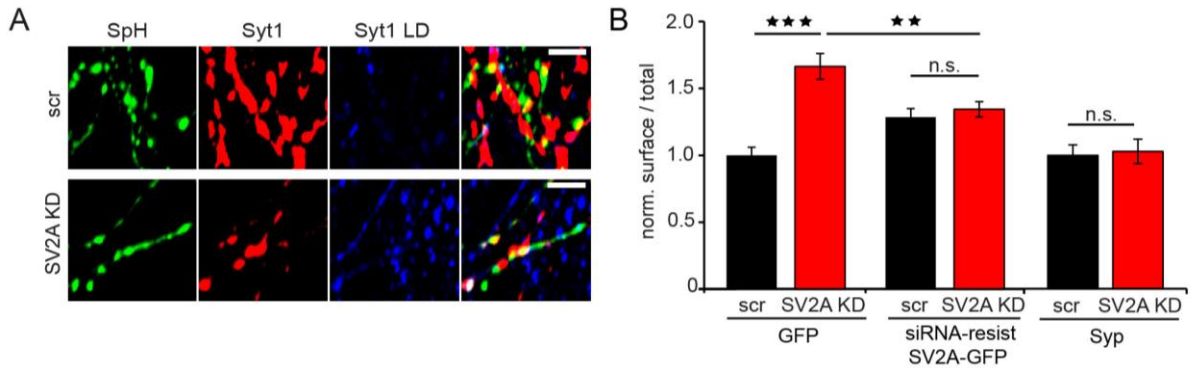


**Figure 19: Selective increase of endogenous surface-stranded Syt1 in SV2A deficient neurons. (A)** Representative confocal images of mouse hippocampal neurons coexpressing Syp-pHluorin (SpH, green) with scr or SV2A siRNA (SV2A KD) and immunostained for total Syt1 (red) and surface Syt1 (Syt1 LD, blue). (Scale bar, 5 µm.) **(B)** Elevated normalized ratio of surface/total Syt1 in SV2A KD neurons compared with scr siRNA-treated controls (scr, 1.0 ± 0.14; SV2A KD, 1.65 ± 0.13; ***P < 0.001) is rescued by overexpression of siRNA-resistant SV2A-GFP (scr, 1.28 ± 0.06; SV2A KD, 1.34 ± 0.06; **P < 0.01; n = 3; >3,000 boutons per condition). Syp surface/total ratio is unaffected (scr, 1.0 ± 0.08; SV2A KD, 1.03 ± 0.09; n = 3; >1,700 boutons per condition). All data represent mean ± SEM.

Next, we performed similar experiments in Stn2 deficient neurons that were either treated with scrambled or SV2A siRNA. Consistent with the results regarding Syt1-pHluorin the additional SV2A loss in Stn2 knockout neurons further increased the surface accumulation of Syt1 (Figure 20A, B). As observed before in the wildtype background (Figure 17), SV2A depletion in Stn2 deficient neurons also led to a reduction in total Syt1 levels (Figure 20C).

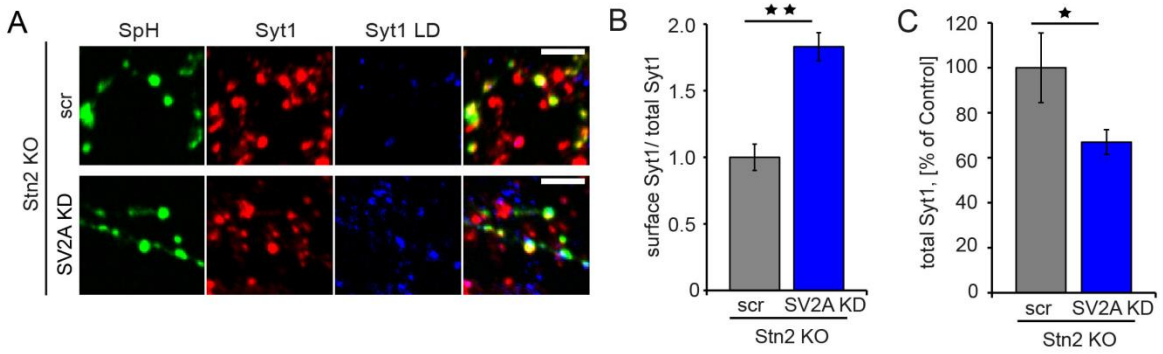


**Figure 20: Surface accumulation of Syt1 in SV2A deficient Stn2 KO neurons. (A)** Representative confocal images of Stn2 KO neurons coexpressing Syp-pHluorin (SpH, green) and either scr or SV2A siRNA (KD) and immunostained for total Syt1 (red) and surface Syt1 (Syt1 LD, blue). (Scale bar, 5 µm.) **(B)** Elevated ratio of surface/total Syt1 in Stn2 KO neurons depleted of SV2A (scr, 1.0 ± 0.1; SV2A KD, 1.8 ± 0.1; >1,000 boutons per condition; **P < 0.001). **(C)** Total Syt1 levels are reduced in SV2A deficient Stn2 KO neurons (SV2A KD, 67 ± 5.6 %), compared with control Stn2 KO neurons (scr, 100 ± 15.5 %; *P < 0.05). All data represent mean ± SEM.

The results so far suggest that despite their distinct molecular architectures Stn2 and SV2A share overlapping functions in Syt1 sorting. To corroborate our hypothesis we analysed the endogenous Syt1 surface and total levels in vivo in hippocampal brain slices of SV2A/B DKO animals as well as of TKO mice. As in neuronal culture experiments, we stained for surface Syt1 levels under non-permeabilizing conditions (Syt1 LD) and subsequently permeabilized to detect total Syt1 levels using the same antibodies as in Figure 19A. The ratio of endogenous surface/total Syt1 was significantly increased in hippocampal slices of SV2A/B DKO mice compared to control mice. In TKO brain slices this defect was further aggravated (Figure 21A, B). This is in line with the repartitioning of overexpressed Syt1-pHluorin and endogenous Syt1 in SV2A and Stn2 deficient neuronal cultures. Taken together these data indicate that SV2A and Stn2 execute overlapping functions with respect to selective Syt1 sorting from the neuronal surface to SVs.

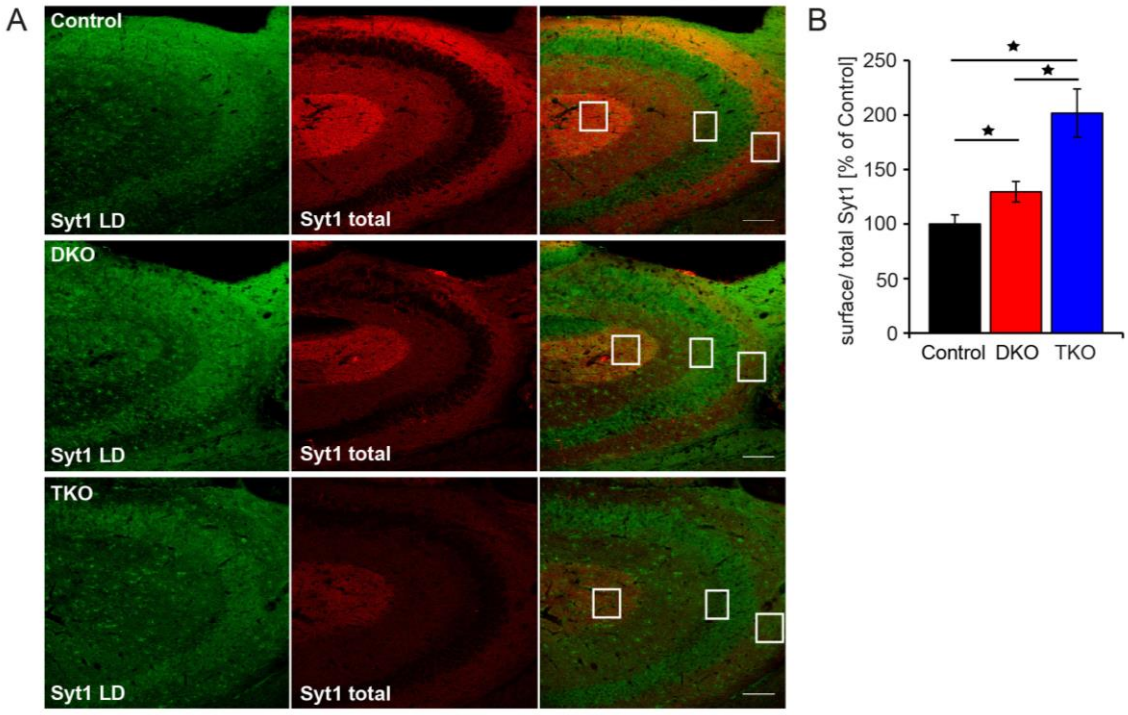


**Figure 21: Aggravated surface/total ratio of Syt1 in mice with combined deletion of SV2A/B and Stn2. (A)** Representative confocal images of sagittal brain sections from 12-days-old mice. Sections were stained for total (red) and surface levels (green) of Syt1 in the hippocampus of control, SV2A/B DKO, and SV2A/B/Stn2 TKO mice. (Scale bar, 100 μm). ROIs in A indicate areas taken for quantification. **(B)** Syt1 surface levels are elevated in SV2A/B DKO and more pronouncedly in SV2A/B/Stn2 TKO mice (DKO, 129.6 ± 9.4 %; TKO, 201.8 ± 22.2 %) compared with controls (control, 100 ± 8.4 %; n control/DKO = 4; n control/TKO = 3; *P < 0.05). Data represent mean ± SEM.

### 4.1.5. SV2A regulates Syt1 sorting to SVs during neuronal activity

The surface accumulation of Syt1 in the absence of SV2A and Stn2 at steady state conditions is probably due to defective endocytic sorting after multiple rounds of SV fusion. In order to test whether the observed Syt1 missorting in SV2A depleted neurons is dependent on neuronal activity we silenced control and SV2A deficient neurons for 5 days with the sodium channel blocker tetrodotoxin (TTX) and analysed the levels of surface-stranded Syt1 levels in comparison to endogenously active neuronal cultures. In the absence of TTX SV2A deficient neurons showed increased surface/total ratios compared to control neurons as observed before. However, silencing of network activity abolished the missorting of endogenous Syt1 in SV2A deficient neurons: in fact, the ratio of surface to total Syt1 levels were comparable to control neurons (Figure 22).

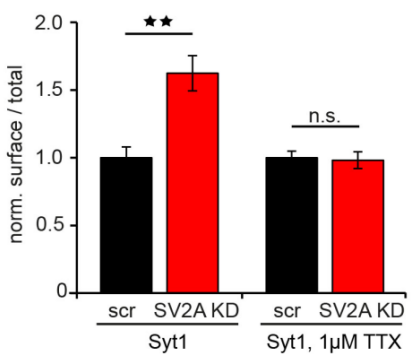


**Figure 22: SV2 regulates Syt1 sorting to SVs during neuronal activity.** Normalized ratio of surface/total Syt1 in neurons treated with SV2A siRNA are elevated compared with scr siRNA-treated controls (set to 1; scr, 1.0 ± 0.08; SV2A KD, 1.62 ± 0.13; n = 3; >1,800 boutons per condition; **P < 0.001). Surface accumulation of Syt1 is rescued in TTX-silenced neurons (scr, 1.0 ± 0.5; SV2AKD, 0.98 ± 0.06; n = 2; > 4,500 boutons per condition).

Hence, the absence of SV2A selectively impairs the endocytic retrieval of Syt1 from the surface to SVs during neuronal activity. Consequently, this surface accumulation of Syt1 should be accompanied by a loss of Syt1 from recycled SVs. To probe the copy numbers of Syt1 on SVs that actively undergo recycling we expressed Syt1-pHluorin and stimulated control and SV2A deficient neurons with a train of 200 APs at 10 Hz. This sustained stimulation was shown to trigger the rapid reuse of SVs (Ertunc et al., 2007). In addition, this stimulation paradigm is known to enhance release probability due to accumulation of residual calcium in the synaptic bouton (Regehr, 2012). Therefore, it should bypass defects in SV release that were observed in previous studies in the absence of SV2A/B (Chang and Sudhof, 2009; Custer et al., 2006; Janz et al., 1999). In order to detect all exocytosed Syt1-pHluorin molecules we treated the neuronal cultures shortly with the vesicular ATPase blocker folimycin inhibiting the reacidification of internalized membranes. Thus, all exocytosed pHluorin molecules will remain fluorescent even after their subsequent endocytosis (Figure 23A, B). We first imaged control and SV2A deficient Syt1-pHluorin expressing neurons in the absence of folimycin to ensure their responsiveness to stimulation and subsequently in the presence of folimycin. By quantifying the change in fluorescence (ΔF) after stimulation we were able to determine the relative number of exocytosed Syt1 molecules. The loss of SV2A significantly reduced ΔF of Syt1-pHluorin compared to control neurons, reflecting a partial loss of Syt1-pHluorin molecules from recycling SVs (Figure 23C, D, G). To exclude any effects due to differences in overexpression levels we applied an ammoniumchloride pulse to reveal all overexpressed Syt1-pHluorin molecules. Thereby, we confirmed that we imaged boutons from control and SV2A deficient neurons with near identical Syt1-pHluorin expression (Figure 23I).

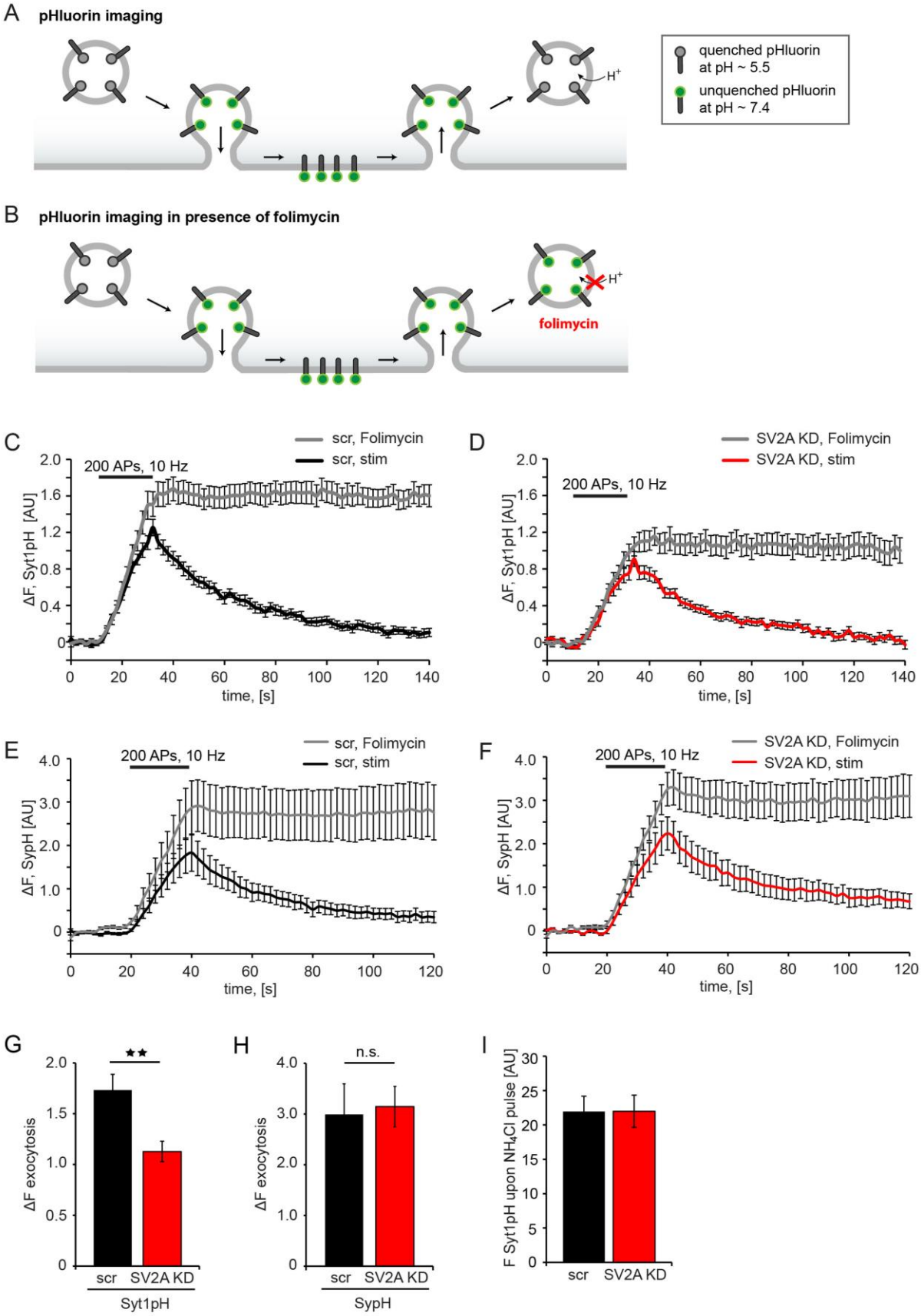


**Figure 23: Loss of SV2A selectively impairs Syt1-pHluorin (Syt1pH) sorting to SVs during repetitive rounds of exo-/endocytosis. (A)** and **(B)** Schematic of pHluorin imaging to monitor exo-

and endocytosis of SVs in absence or presence of folimycin. pHluorin fused to the luminal domain of SV proteins is quenched at pH 5.5 within the SV. Upon stimulation SVs fuse with the plasma membrane and pHluorin will be unquenched at the neutral pH (7.4) of the extracellular medium. This increase of fluorescence will decline after endocytic retrieval and re-acidification of internalized membranes. In the presence of folimycin the vATPase and thus vesicular re-acidification are inhibited, which leaves all exocytosed pHluorin molecules in an unquenched state. **(C)** and **(D)** Average traces in response to 200 APs (10 Hz) in the absence or presence of folimycin. Neurons were cotransfected with Syt1-pH and scr **(C)** or SV2A siRNA (KD, **D**). **(E)** and **(F)** Depletion of SV2A does not affect Syp-pHluorin (SypH) sorting fidelity during stimulation. Average traces of hippocampal neurons cotransfected with SypH and scr **(E)** or SV2A siRNA **(F)** in response to 200 APs (10 Hz) in the absence or presence of folimycin. **(G)** Reduced apparent number of exocytosed Syt1-pHluorin molecules in SV2A deficient neurons (SV2AKD, 1.13 ± 0.10) compared with control (scr, 1.73 ± 0.15; **P < 0.001; n = 13; >630 boutons per genotype). The apparent number of exocytosed SypH molecules **(H)** is unaffected (scr, 3.0 ± 0.6; SV2AKD, 3.1 ± 0.4; n = 8; >300 boutons per genotype). **(I)** Ammoniumchloride ($NH_4Cl$) pulse in SV2A-deficient neurons overexpressing Syt1-pHluorin reveals similar Syt1-pHluorin expression levels compared with scr siRNA-transfected neurons (scr, 21.9 ± 2.2 AU; SV2AKD, 22.0 ± 2.3 AU; n = 5; >510 boutons per condition). All data represent mean ± SEM.

Repeating the same experiment with overexpressed Syp-pHluorin showed that the depletion of SV2A affected only the copy number of Syt1-pHluorin on SVs as the relative number of exocytosed Syp-pHluorin molecules remained unchanged (Figure 23E, F, H). These data indicate that loss of SV2A leads to a defective endocytic retrieval of Syt1 from the surface during neuronal activity resulting in Syt1 surface accumulation and partial loss of Syt1 from recycling SVs.

### 4.1.6. Combined deficiency of Stn2 and SV2A/B aggravates impaired evoked release

The drastic loss of Syt1 from SVs and its missorting to the plasma membrane in synapses from SV2A/B DKO, and more pronouncedly in TKO synapses, might impact the efficacy of neurotransmitter release. To address this hypothesis, Dr. Gaga Kochlamazashvili (FMP, Berlin) measured synaptic responses of hippocampal CA1 pyramidal neurons in acute brain slices derived from p12 SV2A/B DKO or SV2A/B/Stn2 TKO mice. First, we analyzed evoked neurotransmission (field excitatory postsynaptic potential (fEPSP) amplitudes, gray arrow) in response to increasing stimulus intensities measured as presynaptic fiber volleys (black arrow, Figure 24A) and plotted the data as input-output curves (Figure 24C, D). For comparison we measured evoked neurotransmission and paired-pulse responses from SV2A WT/ SV2B KO/ Stn2 WT (WT/KO/WT) or SV2A WT/ SV2B KO/ Stn2 heterozygous

(WT/KO/HET) littermates. They showed similar responses and were therefore used as controls (Figure S1 in Appendix B).

In slices from SV2A/B DKO mice the size of maximal fEPSPs was decreased about twofold compared to controls (Figure 24C). This effect was exacerbated in slices from TKOs where maximal fEPSP sizes were reduced additionally by 20 % compared to the DKO amplitude (Figure 24D). These reduced postsynaptic responses in DKO and TKO mice were not a result of decreased presynaptic input, as evident in measurements of fiber volley amplitudes plotted as a function of increasing stimulus intensity (Figure 24B). Moreover, CA1 synapses from DKO or TKO mice also displayed a normal overall morphology with unaltered numbers of SVs or length of the active zone (Figure 13B and Table 24).

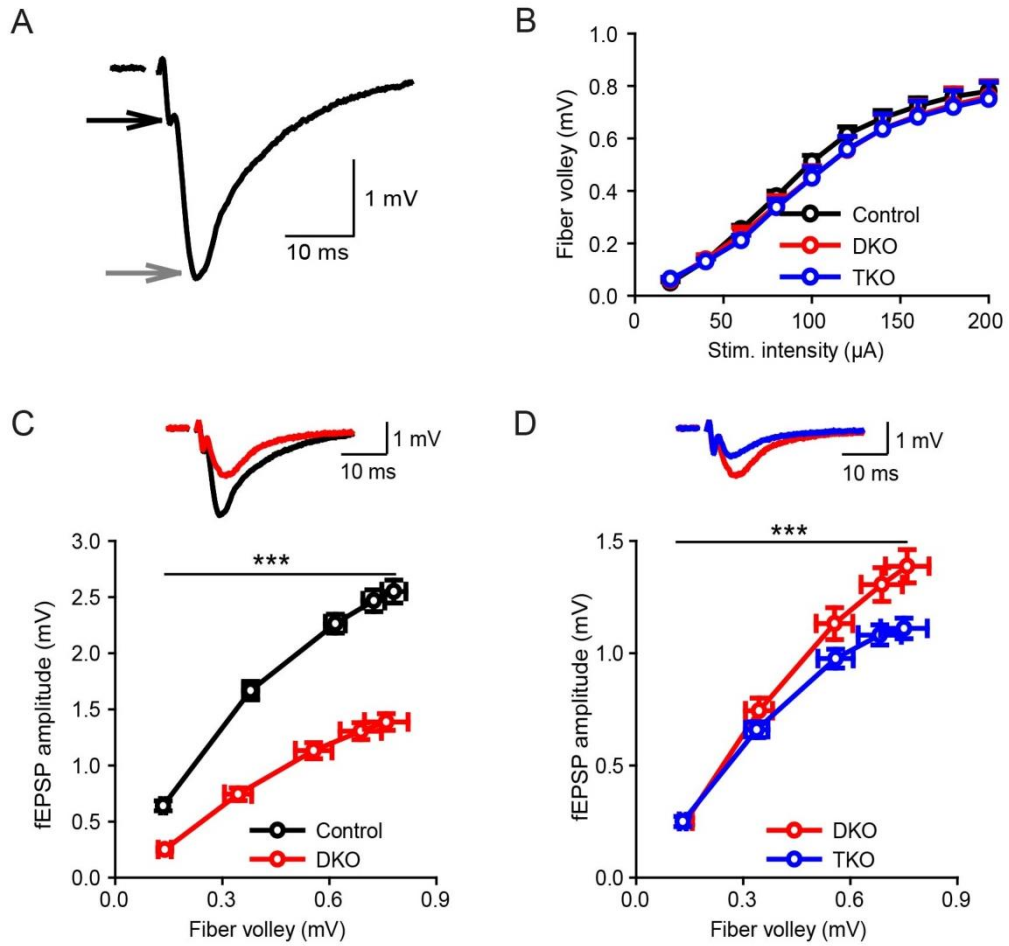


**Figure 24: Combined deficiency of SV2 and Stn2 aggravates impairments in synaptic strength caused by deletion of SV2. (A)** A representative trace of a maximal field excitatory postsynaptic potentials (fEPSP) recorded in CA1 stratum radiatum of a p12 mouse, illustrating the time points taken for measurements of presynaptic fiber volleys (black arrow) and fEPSP amplitudes (gray arrow). **(B)** Presynaptic excitability of controls, DKO, and TKO, measured as a relationship between the fiber volley amplitudes and stimulation intensities. Synapses of DKO (P = 0.7) and TKO (P = 0.6) mice show no significant differences in presynaptic excitability, compared with the control. **(C and D)** Basal transmission is reduced at excitatory Schaffer collateral to CA1 pyramidal cell synapses in

SV2A/B DKO (red trace) and SV2A/B/Stn2 TKO (blue trace) mice in response to increasing stimulus intensities. **(C)** fEPSP amplitudes are significantly reduced in DKO mice compared with control (***P < 0.001). Inset illustrates sample traces of maximal fEPSPs in DKO animals (red) and controls (black). **(D)** fEPSP amplitudes in TKO are significantly lower compared with DKO mice (***P < 0.001). Inset illustrates sample traces of maximal fEPSPs in TKO (blue) and in DKO mice (red). Courtesy: Dr. Gaga Kochlamazashvili (FMP, Berlin).

The reduced basal transmission in DKO and TKO slices is consistent with a partial loss of Syt1. Syt1 null mice have been shown to suffer from highly reduced synchronous release in excitatory neurons, which is accompanied by increased miniature excitatory postsynaptic currents (mEPSCs) (Kerr et al., 2008). However, neither the frequency (Figure 25A, B) nor the amplitude of mEPSCs (Figure 25A, C) was altered in slices from TKO mice, akin to what has been observed at hippocampal synapses from SV2A single or SV2A/B DKOs (Venkatesan et al., 2012).

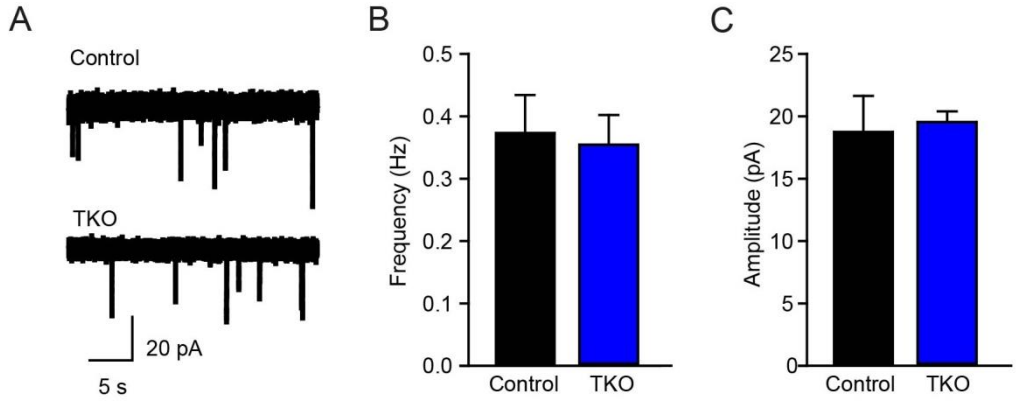


**Figure 25: Unaltered action potential-independent neurotransmission in TKO mice. (A)** Representative traces of miniature excitatory postsynaptic currents (mEPSCs) recorded from CA1 neurons of control and TKO mice. **(B)** Frequency of miniature excitatory postsynaptic events is not changed in TKO compared with controls (P = 0.8). **(C)** Average amplitudes of mEPSCs are not affected in TKO mice (P = 0.7) compared with controls (control n = 4, n = 3; TKO n = 5, n = 3). Courtesy: Dr. Gaga Kochlamazashvili (FMP, Berlin).

### 4.1.7. Exacerbated reduction of release probability by additional depletion of Stn2 in SV2A/B DKO

Next, we analyzed short-term plasticity at the excitatory Schaffer collateral to CA1 pyramidal cell synapse in acute brain slices from control, DKO and TKO mice. To this end Dr. Gaga Kochlamazashvili (FMP, Berlin) measured synaptic responses to paired stimuli given at various interstimulus intervals (ISIs). This revealed increased facilitation in slices from DKO mice, which was further aggravated in slices from TKO mice when compared to controls (Figure 26A-C). As the analysis of short-term plasticity is often taken as a surrogate measure

for release probability (Dobrunz and Stevens, 1997), these data are most likely explained by a reduction of release probability in SV2A/B DKO, which is even more pronounced in SV2A/B/Stn2 TKO synapses. This is consistent with published data showing initial facilitation in DKO mice (Custer et al., 2006) and correlates with the depletion of Syt1 from SVs.

To exclude that the altered short-term plasticity in DKO and TKO synapses is caused by alterations in the refilling of the releasable SV pool, we analyzed responses of DKO and TKO synapses during a train of APs applied at high stimulation frequency (20 Hz, 500 APs). This stimulation paradigm elevates release probability and depletes the readily releasable pool of vesicles, thereby unmasking possible defects in its refilling once exocytosis reaches a steady state. During the initial phase of the train, responses of DKO and, more pronouncedly, those of TKO mice were reduced followed by strong hyperfacilitation to eventually reach amplitudes that were similar to those elicited from controls (~2 mV). Following this initial facilitation phase, amplitudes declined to eventually reach a baseline steady-state level neurotransmission that was similar between genotypes (Figure 26D). Analyses of cumulative amplitudes revealed an unaltered SV pool challenged by repeated stimulation (Figure 26E). The facilitation in DKO and TKO synapses we observed is, thus, unlikely to be caused by alterations in the refilling of the releasable SV pool and may rather be a consequence of the reduced ability of SVs from DKO or TKO to fuse in response to calcium (Chang and Sudhof, 2009; Custer et al., 2006).

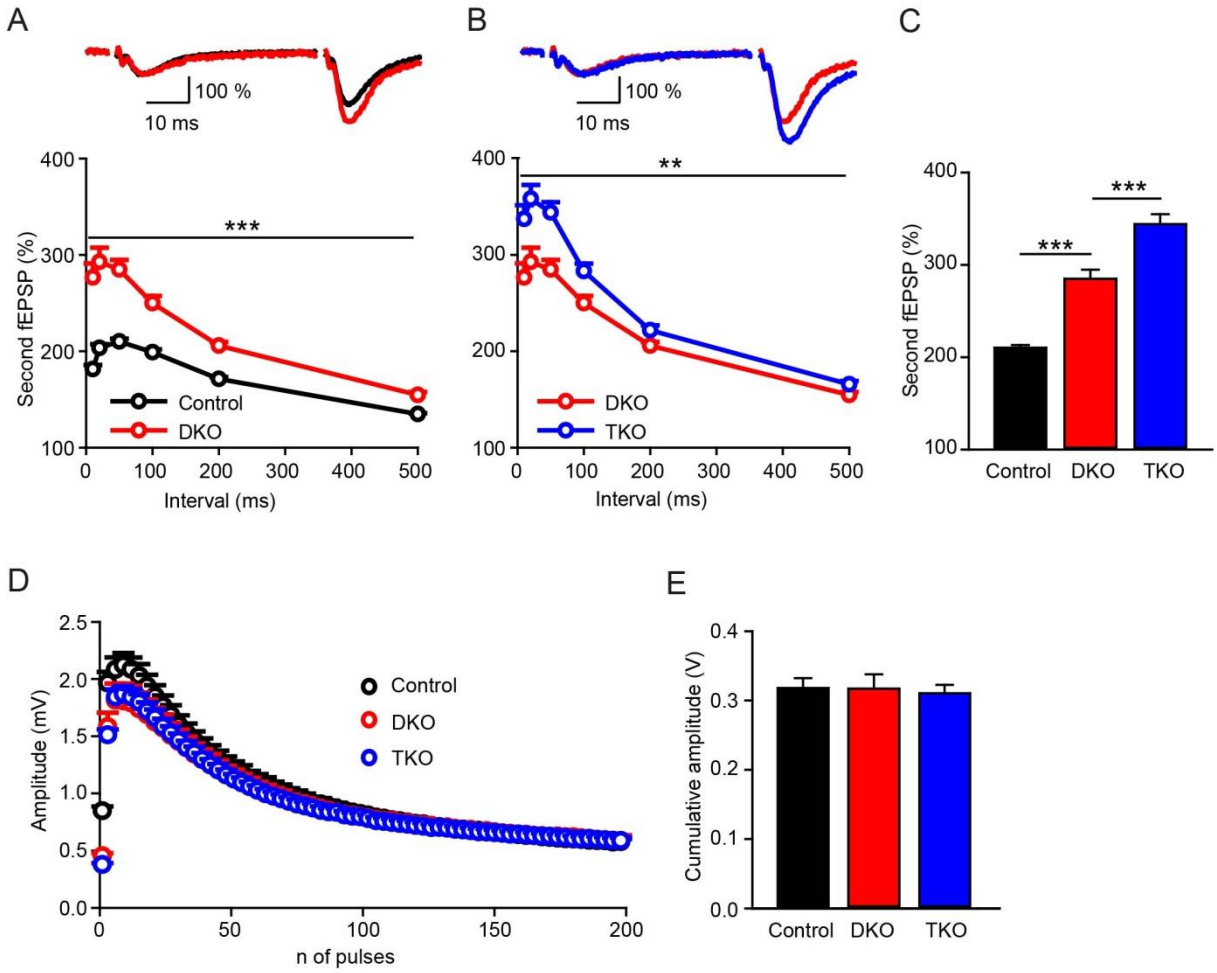


**Figure 26: Altered paired-pulse facilitation (PPF) at excitatory Schaffer collateral to CA1 pyramidal cell synapses in DKO and TKO mice. (A)** PPF measured at 10, 20, 50, 100, 200, and 500 ms interpulse intervals (ISIs) reveals increased facilitation in DKO mice compared with control (***P < 0.001). Inset depicts sample traces of fEPSPs at 50 ms ISI normalized to the first response of DKO (red) and control (black) synapses. **(B)** Significantly elevated PPF (fEPSP2/fEPSP1) at 10, 20, 50, 100, 200, and 500 ms ISI at synapses of TKO, compared with DKO (**P = 0.004). Inset illustrates sample traces of fEPSPs at 50 ms ISI normalized to the first response at DKO (red) and TKO (blue) synapses. **(C)** PPF at 50 ms ISI is significantly increased in DKO mice compared with controls (***P < 0.001) and is further increased in TKO animals (***P < 0.001). Note that maximal facilitation of the second response is detected at 50 ms in control slices (control n = 20, n = 8; DKO n = 9, n = 4; TKO n = 14, n = 5). **(D)** Normal steady-state level of neurotransmission in DKO and TKO mice probed by high-frequency stimulation (20 Hz). Each value is an average of three consecutive responses except for n = 1. Only the first 200 out of 500 pulses are presented. **(E)** Cumulative amplitudes in response to 500 pulses at 20 Hz show no differences in DKO (P = 0.96) and TKO (P = 0.50) compared with control synapses (control n = 19, n = 8; DKO n = 9, n = 4; TKO n = 14, n = 5). Courtesy: Dr. Gaga Kochlamazashvili (FMP, Berlin).

Collectively, these data show that loss of SV2A/B and, more pronouncedly, of SV2A/B/Stn2, impairs basal neurotransmission and reduces release probability, most likely as a consequence of impaired Syt1 sorting to SVs, though additional functions of SV2A/B (e.g.

in SV priming to acquire competence for calcium-induced exocytosis (Chang and Sudhof, 2009; Custer et al., 2006)) and/or Stn2 may contribute to the phenotype.

## 4.2. The molecular function of Syt1 sorting at the synapse

Our data unravel a crucial overlapping function of the endocytic adaptor Stn2 and the SV protein SV2A/B in Syt1 sorting and maintenance at mammalian synapses. The absence of Syt1 sorting proteins severely affects basal neurotransmission and short-term plasticity correlating with the partial loss of Syt1. However, the question remains, which functional consequences the surface-stranding of Syt1 in the absence of Syt1 sorting proteins has for synaptic exo- and endocytosis. Surprisingly, previous data have shown that the deletion of Stn2 *in vivo* specifically facilitates endocytic retrieval kinetics in hippocampal cultures measured by pHluorin reporters. Moreover, the overexpression of a Stn2 binding-defective mutant Syt1 phenocopies the accelerated pHluorin retrieval kinetics (Kononenko et al., 2013). In contrast, the deletion of the specific sorting adaptor AP180 responsible for Syb endocytic retrieval delays Syb-pHluorin retrieval, but does not affect the endocytic retrieval of SV proteins in general (Koo et al., 2015). Thus, the facilitated pHluorin retrieval appears to be specific for Stn2 deletion and correlates with Syt1 missorting. To understand this phenomenon we investigated the functional role of Syt1 sorting in the synapse and examined the underlying mechanism and possible effectors of SV exo- and endocytosis in more detail by using Stn2 and SV2 deficient neurons.

### 4.2.1. Accelerated endocytic retrieval in the absence of Syt1 sorting adaptors

The repartitioning of Syt1 to the neuronal surface in Stn2 KO neurons is accompanied by an increased rate of SV membrane retrieval during high-frequency stimulation (Kononenko et al., 2013). Since combined depletion of SV2A and Stn2 led to aggravated surface accumulation of Syt1, we tested the hypothesis whether SV protein retrieval would be further accelerated in the absence of both proteins.

We analyzed the kinetics of Syt1 exo-/ endocytosis at room temperature using Syt1-pHluorin in response to high-frequency stimulation with 200 APs at 40 Hz (Figure 27A, B). As expected, retrieval of Syt1-pHluorin was significantly facilitated in neurons derived from Stn2 KO mice ($\tau$ KO = 35.1 ± 1.2 s) compared to controls ($\tau$ scr = 43.1 ± 3.6 s). Interestingly, the depletion of SV2A by siRNA accelerated the endocytic retrieval of Syt1-pHluorin as well

(τ KD = 34.5 ± 1.8 s), and this phenotype was further augmented by combined deficiency of both SV2A and Stn2 (τ KO, SV2A KD = 25.3 ± 1.0 s) (Figure 27B). Similar results were obtained in SV2A KD neurons expressing Syp-pHluorin (Figure 27C) indicating that the increased rate of SV protein retrieval is independent of the pHluorin sensor. Moreover, the depletion of SV2A and Stn2, which both result in surface-stranded Syt1, accelerated endocytic retrieval to the same degree. This suggests a correlation of Syt1 repartitioning and faster endocytic retrieval kinetics.

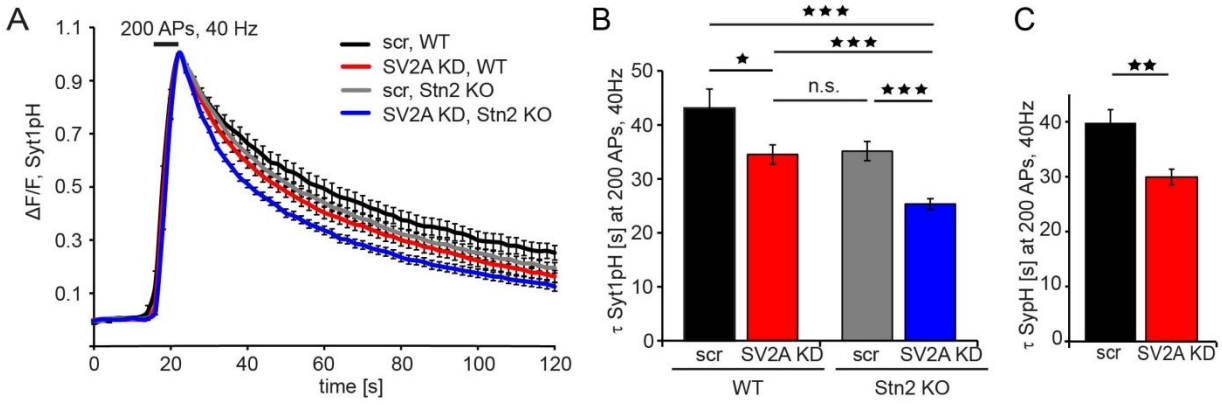


**Figure 27: Accelerated pHluorin retrieval in Stn2 and SV2A depleted neurons at room temperature.** Time course **(A)** and endocytic time constants (τ) **(B)** of Syt1-pHluorin endocytosis/reacidification in WT and Stn2 KO neurons coexpressing Syt1-pHluorin and scr or SV2A siRNA (KD) in response to 200 APs (40 Hz, 5s). Endocytosis is facilitated in the absence of either SV2A (τ WT, scr = 43.1 ± 3.6 s; τ WT, SV2A KD = 34.5 ± 1.8 s) or Stn2 (τ KO, scr = 35.1 ± 1.2 s), an effect further elevated by depletion of both proteins (τ KO, SV2A KD = 25.3 ± 1.0 s; *P < 0.05, ***P < 0.0001; n = 3; >950 boutons per condition). **(C)** Accelerated retrieval of Syp-pHluorin in SV2A-deficient neurons stimulated with 200 APs at 40 Hz (τ WT scr = 39.8 ± 2.4 s; τ WT SV2A KD = 29.9 ± 1.4 s; **P < 0.001; mean ± SEM of n = 4 independent experiments; >1,900 boutons per genotype). Data represent mean ± SEM.

Recent data have shown that endocytic retrieval kinetics are highly temperature sensitive (Delvendahl et al., 2016; Soykan et al., 2017). Therefore we monitored SV exo- and endocytosis during high-frequency stimulation at 37 °C in Stn2 depleted neurons using Syp-pHluorin as a sensor (Figure 28A). As expected pHluorin retrieval kinetics were accelerated at 37 °C in both Stn2 WT and KO. Similar to experiments carried out at room temperature we observed faster retrieval kinetics in the absence of Stn2 (Figure 28B) albeit less prominent than observed at room temperature. In response to a mild stimulation of 50 APs at 10 Hz we did not observe significant differences in endocytic retrieval kinetics in Stn2 depleted neurons compared to the control (Figure 28C). Thus, the facilitation appears to be temperature and stimulus dependent.

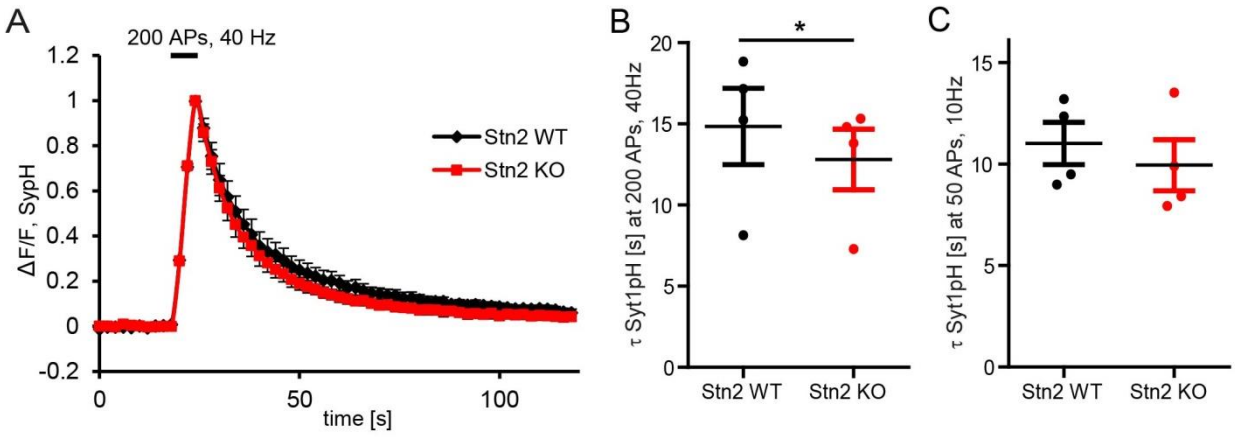


**Figure 28: Temperature and frequency dependent facilitation of endocytic kinetics in Stn2 depleted neurons. (A)** Normalized time course and **(B)** decay constants τ of Syp-pHluorin retrieval at 37 °C upon high-frequency stimulation with 200 APs at 40 Hz in Stn2 WT (τ WT = 14.9 ± 2.4 s) and Stn2 KO (τ WT = 12.8 ± 1.9 s) neurons. (*P < 0.05, n = 4 independent experiments). (C) Decay constants τ of Syp-pHluorin retrieval show no significant facilitation in Stn2 KO neurons at 50 APs with 10 Hz field stimulation at 37 °C (τ WT = 11.0 ± 1.0 s and τ KO = 9.9 ± 1.3 s; P = 0.5 of n = 4 independent experiments). Data represent mean ± SEM.

One possible explanation for accelerated SV protein retrieval could be reduced SV exocytosis, which would reduce the retrieval load of the endocytic machinery and would therefore allow faster kinetics. To compare the apparent SV release of Stn2 WT and KO neurons we normalized pHluorin time courses to their initial fluorescence prior to stimulation. Interestingly, Stn2 depleted neurons display increased apparent exocytosis at high frequency field stimulation compared to WT neurons (Figure 29A). The fluorescence amplitude ΔF of the Stn2 KO neurons is significantly higher (ΔF Stn2 KO = 126.7 ± 11.3 %) than the WT (Figure 29B). The increased apparent release is even more prominent at prolonged and mild stimulation at 10 Hz for 300 APs and 2 mM calcium concentration in the imaging buffer (Figure 29C, D). Therefore, faster SV retrieval in absence of Stn2 does not appear to be due to reduced SV release.

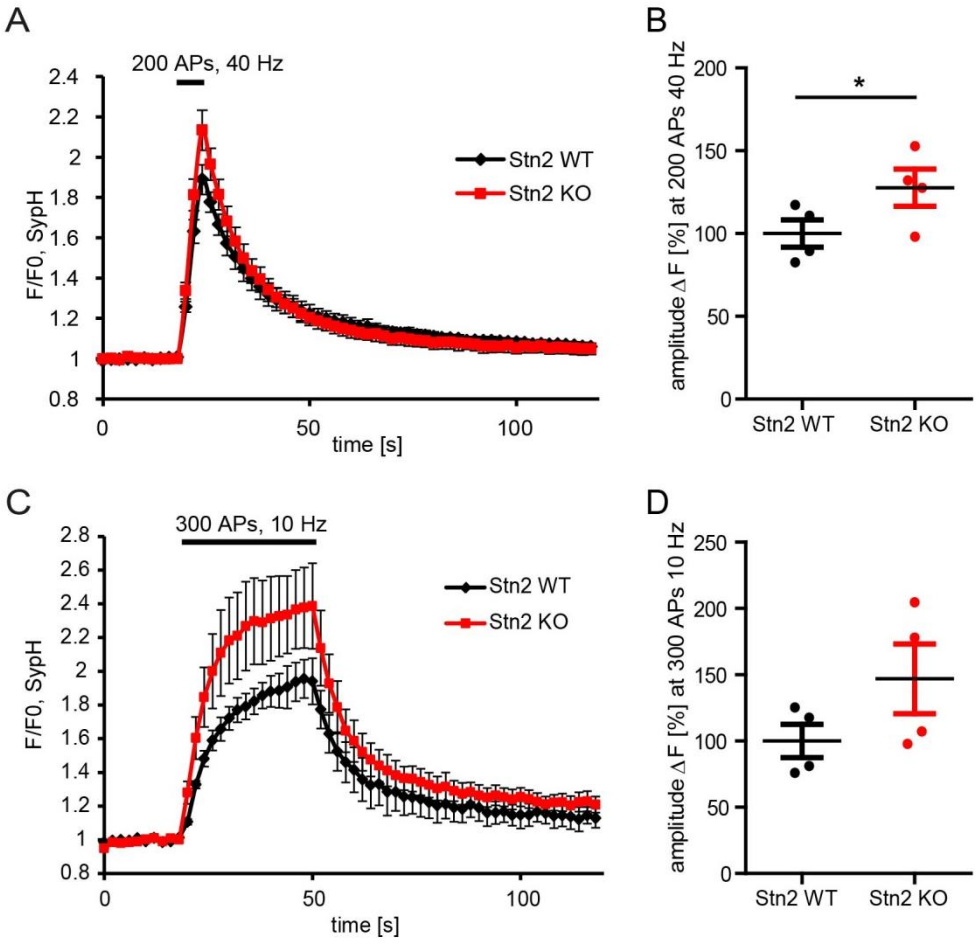


**Figure 29: Stn2 depletion results in increased apparent SV release. (A)** Syp-pHluorin time courses of Stn2 WT and KO neurons normalized to pre-stimulus fluorescence show increased peak fluorescence amplitudes in response to 200 APs at 40 Hz. **(B)** Quantification of relative peak fluorescence in Stn2 WT (ΔF Stn2 WT = 100 ± 8.3 %) and Stn2 KO (ΔF Stn2 KO = 126.7 ± 11.3 %). (*P < 0.05, n = 4 independent experiments). **(C)** Prolonged and mild field stimulation of 300 APs (10 Hz, 30 s) display a prominent increase in peak fluorescence amplitudes of Syp-pHluorin traces normalized to pre-stimulus fluorescence in Stn2 WT and KO neurons with 2 mM $CaCl_2$ in imaging buffer. **(D)** Relative peak amplitudes of Syp-pHluorin are elevated to ΔF Stn2 KO = 146.9 ± 26.3 % compared to ΔF Stn2 WT = 100 ± 12.6 % (n = 1 independent experiment, data points represent individual neurons). Data represent mean ± SEM.

The accelerated endocytic retrieval in Stn2 depleted neurons is in line with published data (Kononenko et al., 2013) and correlates with Syt1 missorting to the plasma membrane as SV2A depletion displays the same facilitation and combined deletion of Stn2 and SV2A enhances it. However, all data were acquired with pHluorin live cell imaging, which monitors SV endocytosis based on SV protein retrieval. To corroborate our data we capitalized on a protein independent technique, membrane capacitance measurements allowing us to directly measure membrane retrieval. Membrane capacitance is proportional to the cell surface area. Therefore, the release of SVs is reflected in a capacitance jump followed by a decay of this capacitance increase due to the subsequent endocytic membrane retrieval. Capacitance was

measured by our collaboration partner Takeshi Sakaba (Doshisha University, Japan) using patch clamp in the calyx of Held terminals. The calyx of Held is a giant synapse located in the auditory brain stem and can respond to high frequency firing rates. Therefore this technique enabled us at the same time to test the facilitated retrieval in the absence of Stn2 in a different kind of synapse. The terminals of Stn2 WT and KO mice were challenged with increasing stimulation (depolarized from -80 mV to 0 mV for varied duration or depolarized to +40 mV for 1 ms repetitively) at room temperature resulting in capacitance jumps. The endocytic membrane retrieval was analyzed as the half decay of the resulting traces and plotted against the capacitance jump. While the membrane retrieval slowed down with increasing exocytosis of SVs in Stn2 WT terminals, the Stn2 depleted terminals were invariant to the amount of exocytosis. The membrane retrieval in Stn2 KO terminals was equally fast after a capacitance jump of 0.2 pF (corresponding to the ready releasable pool) and 0.7 pF eliciting a much stronger release. Thus, the membrane capacitance measurements supported faster endocytic retrieval monitored by pHluorin imaging. Furthermore, the capacitance measurements are in line with the observed frequency dependence of facilitated pHluorin retrieval in Stn2 KO neurons. The accelerated membrane retrieval becomes more apparent upon strong depolarization at the calyx of Held terminal of Stn2 KO mice similar to high frequency stimulation of hippocampal cultures.

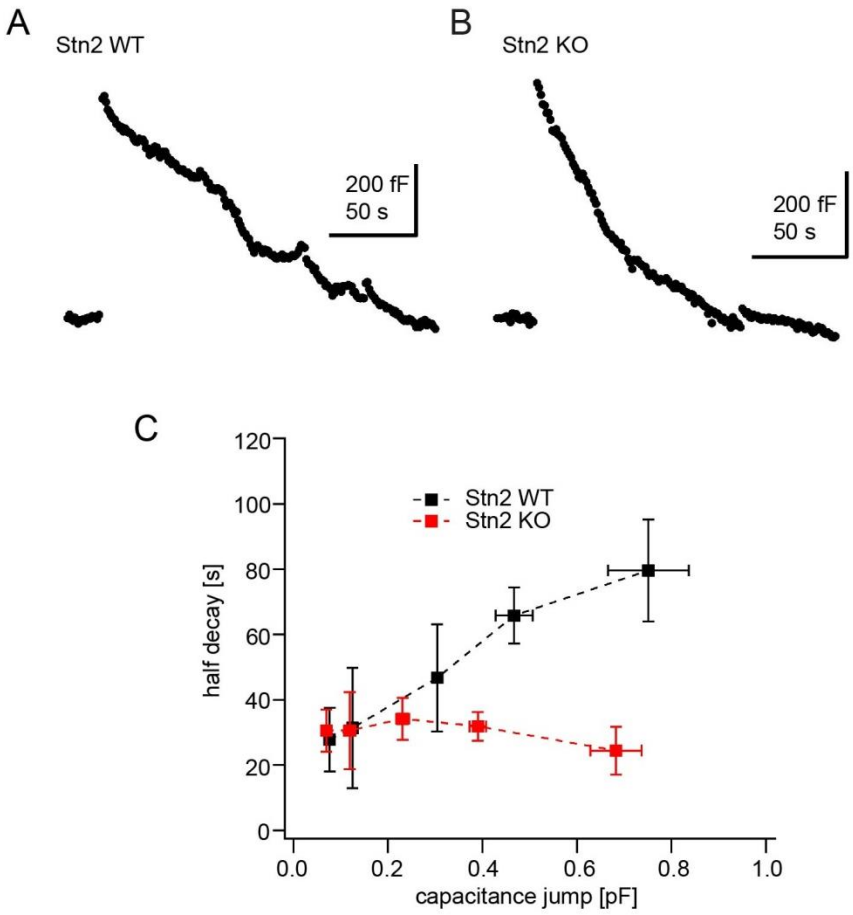


**Figure 30: Stn2 KO synapses are invariant to the amount of exocytosis. (A)** and **(B)** show representative capacitance measurements of patch clamped calyx of Held terminals from Stn2 WT **(A)** and Stn2 KO **(B)** mice at room temperature. Terminals were depolarized from -80 mV to 0 mV for varied duration or repetitively depolarized to +40 mV for 1 ms. **(C)** The half decay of capacitance in response to depolarization was plotted against the capacitance jump. While WT terminals displayed increasing endocytic time constants with stronger depolarization, endocytic retrieval in Stn2 KO terminals remained constantly fast independent of the amount of exocytosis. Courtesy of Takeshi Sakaba (Doshisha University, Japan)

### 4.2.2. Calcium influx during stimulation is not affected in Stn2 depleted neurons

To dissect the mechanism of increased SV release and facilitated endocytic retrieval in the absence of Stn2 we investigated possible effector molecules, which regulate both processes. Calcium ions are a likely candidate as calcium influx during neurotransmission triggers the fusion of SVs with the plasma membrane (Katz and Miledi, 1967a; Sabatini and Regehr, 1996) and also regulates SV endocytosis via calcium effectors like calmodulin (Wu et al., 2009). Therefore, we monitored calcium influx during neurotransmission with Fluo-5F-AM in Stn2 WT and KO neurons. However, the calcium influx during high frequency stimulation in

Stn2 depleted neurons was unaltered compared to Stn2 WT neurons. Thus, differences in calcium level during stimulation cannot account for the observed phenotypes.

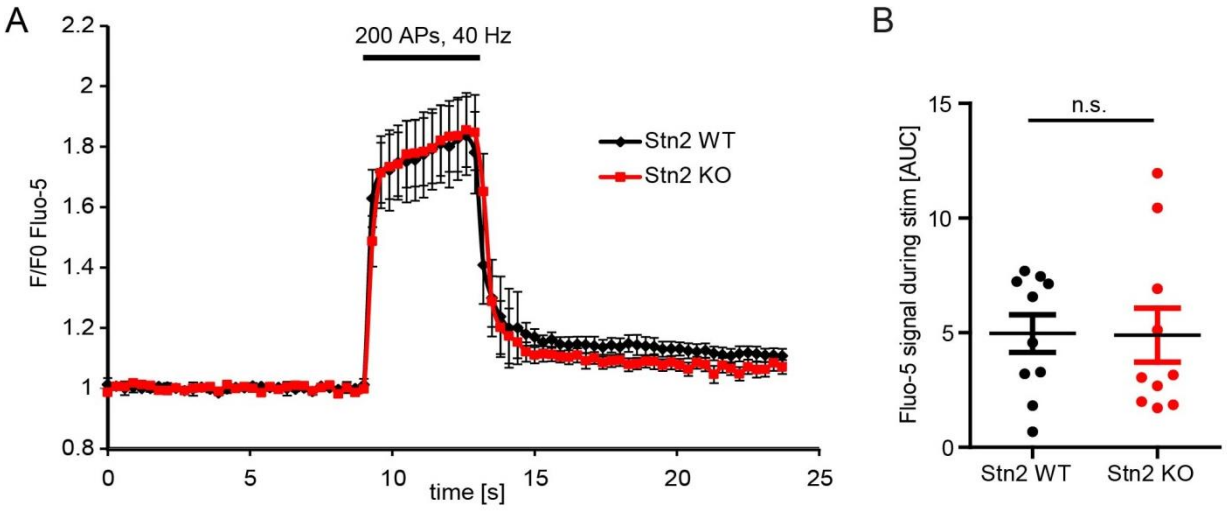


**Figure 31: Unaltered calcium influx during stimulation in Stn2 depleted neurons. (A)** Fluo-5F-AM signal of Stn2 WT and KO neurons normalized to pre-stimulus fluorescence displays no differences in calcium influx during 200 APs at 40 Hz stimulation. **(B)** Quantification of Fluo-5F signal during stimulation as the area-under-the-curve (AUC) in Stn2 WT (Fluo-5 signal Stn2 WT = 5 ± 0.8 AUC) and Stn2 KO (Fluo-5 signal Stn2 KO = 4.9 ± 1.2 AUC). ($P < 0.95$, statistical analysis was done on individual neurons of n = 3 independent experiments due to highly variable signals within an independent experiment). Data represent mean ± SEM.

### 4.2.3. $PI(4,5)P_2$ levels are specifically increased in Stn2 deficient neurons

Another crucial second messenger molecule involved in SV exocytosis and endocytosis is the phosphoinositide $PI(4,5)P_2$. Exocytosis is specifically triggered by $PI(4,5)P_2$ (Walter et al., 2017). $PI(4,5)P_2$ marks endocytic sites by recruiting endocytic proteins and manipulation of $PI(4,5)P_2$ levels has severe consequences for neurotransmission (Cremona et al., 1999; Di Paolo et al., 2004).

To test whether $PI(4,5)P_2$ levels are changed in Stn2 depleted neurons we labeled $PI(4,5)P_2$ in neuronal cultures of Stn2 WT and KO mice with the GFP-fused PH domain of the PLCδ1 (PH-PLCδ1-GFP) (Figure 32A), which specifically interacts with $PI(4,5)P_2$ (Milosevic et al., 2005). Interestingly, $PI(4,5)P_2$ levels were increased in Syp-positive presynaptic boutons upon potassium chloride stimulation of WT neurons. Stn2 depleted neurons displayed elevated $PI(4,5)P_2$ levels in unstimulated conditions and stimulation further elevated $PI(4,5)P_2$ well above the levels seen in WT neurons (Figure 32B). To confirm the labelling specificity we made use of a $PI(4,5)P_2$ specific antibody. Stn2 depleted and control neurons were stained either in unstimulated or stimulated conditions (Figure S2 in Appendix

B). The relative PI(4,5)$P_2$ levels detected by the antibody qualitatively resembled the results obtained with the PH-domain labelling (Figure 32C).

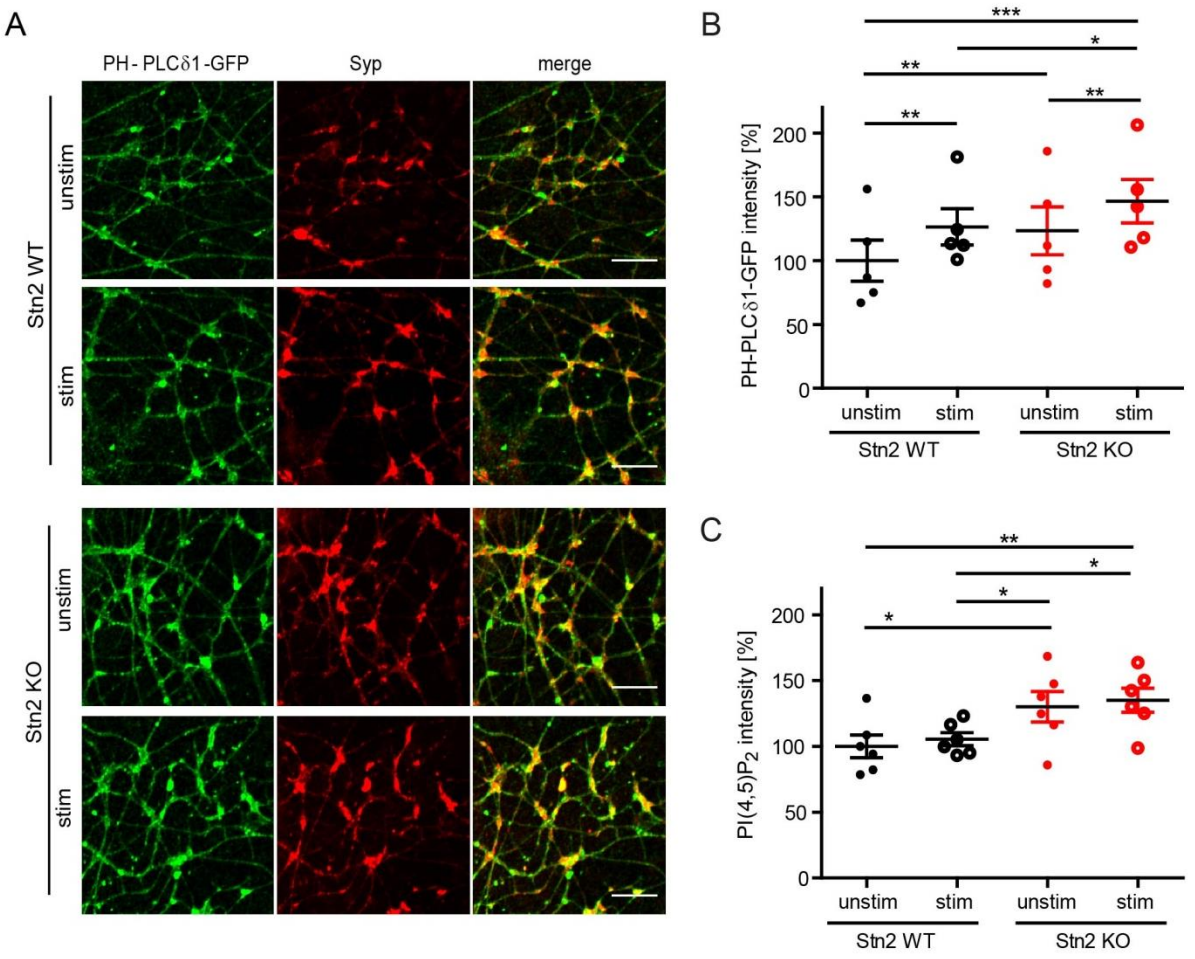


**Figure 32: Elevated PI(4,5)$P_2$ levels in Stn2 deficient neurons. (A)** Representative confocal images of PI(4,5)$P_2$ immunostaining with PH-PLCδ1-GFP (green) in Syp positive boutons (red) of Stn2 WT and KO neuronal cultures left unstimulated or stimulated with 80 mM KCl. Scale bar, 10 µm. **(B)** PH-PLCδ1-GFP intensity levels rise in boutons of stimulated WT cultures (126.4 ± 14.2 %) compared to unstimulated neurons (100 ± 16.2 %), while Stn2 KO neurons display already increased PH-PLCδ1-GFP labelling (123.4 ± 18.8 %), which is potentiated upon stimulation (146.6 ± 17.0 %); (*P < 0.05, **P < 0.01, ***P < 0.001, n = 5 independent experiments). **(C)** Quantification of PI(4,5)$P_2$ in Syb2 positive boutons immunostained with PI(4,5)$P_2$ specific antibody reveals increased PI(4,5)$P_2$ levels in Stn2 KO neurons (WT, unstim 100 ± 8.6 %; WT stim 105.5 ± 4.9 %; KO unstim 130.1 ± 11.5 %; KO stim 135.0 ± 9.2 %; *P < 0.05, **P < 0.01, n = 5 independent experiments). Data represent mean ± SEM.

To analyze whether the increase of PI(4,5)$P_2$ levels is phosphoinositide specific we stained for PI(4)P. PI(4)P is one of the precursors of PI(4,5)$P_2$ and abundant at the plasma membrane and Golgi (Dickson et al., 2014). Labeling with a PI(4)P specific antibody revealed no genotype specific differences between PI(4)P intensities in WT and Stn2 KO neurons. PI(4)P levels increased in WT neurons upon stimulation to the same levels as in the Stn2 KO neurons (Figure 33A, B). These data suggest that the second messenger molecule PI(4,5)$P_2$

specifically increases in the absence of Stn2 and, thus, can explain the increase of SV exocytosis and facilitation of SV retrieval. They further indicate that genomic differences may arise from a different ratio of PI(4)P to PI(4,5)$P_2$ synthesis or altered PI(4,5)$P_2$ turnover in Stn2 KO neurons.

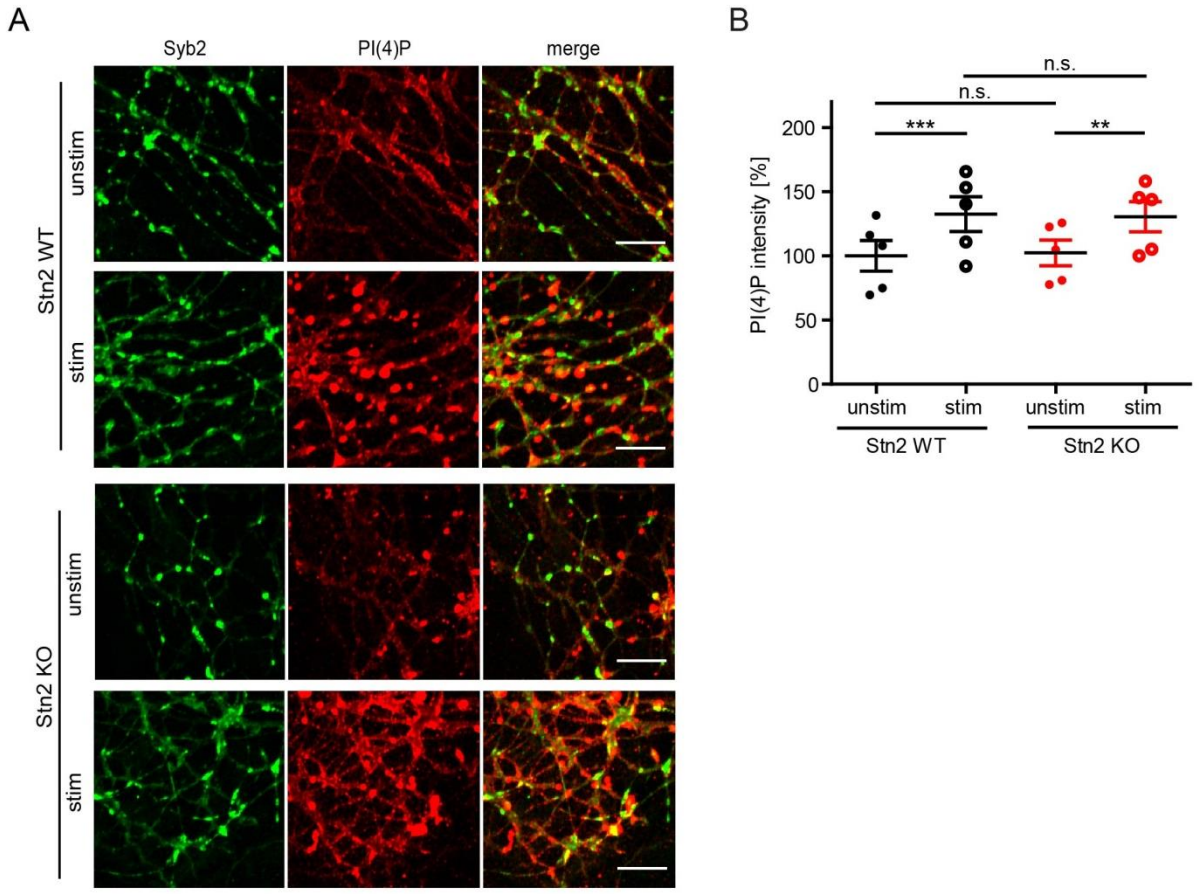


**Figure 33: PI(4)P levels are not changed in Stn2 depleted neurons. (A)** Representative confocal images of PI(4)P staining (red) in Syb positive boutons (green) of WT and Stn2 KO neuronal cultures either unstimulated or stimulated with 80 mM KCl. Scale bar, 10 µm. **(B)** Quantification of PI(4)P immunostained with PI(4)P specific antibody in Syb2 positive boutons shows no significant differences between Stn2 WT and KO neurons (WT, unstim 100.0 ± 12.0 %; WT stim 132.4 ± 13.6 %; KO unstim 102.3 ± 10.1 %; KO stim 130.4 ± 11.7 %; **P < 0.01, ***P < 0.001, n = 5 independent experiments). Data represent mean ± SEM.

## 4.2.4. Syt1 redistribution correlates with elevated PI(4,5)$P_2$ levels

Stn2 and SV2 deficient neurons both show facilitated endocytic retrieval. If increased PI(4,5)$P_2$ levels mediate the faster retrieval, SV2 depleted neurons should display similarly elevated PI(4,5)$P_2$ levels. To test our hypothesis we stained SV2A/B DKO and control neurons with PI(4,5)$P_2$ specific antibody either after stimulation or in resting conditions.

Indeed, immunostaining of $PI(4,5)P_2$ revealed increased $PI(4,5)P_2$ intensities in Syb2-positive boutons of SV2A/B deficient neurons, which were further aggravated upon stimulation (Figure S3 in Appendix B and Figure 34A). SV2A/B deficient neurons not only phenocopy Stn2 depleted neurons with respect to their increased $PI(4,5)P_2$ levels, but also display a similar Syt1 redistribution to the plasma membrane as previously discussed. Thus, Syt1 missorting could be a causative link that directly or indirectly causes $PI(4,5)P_2$ elevation. To assess this relationship in more detail, we analyzed whether silencing of neuronal network activity with TTX that rescues Syt1 surface accumulation also reduces elevated $PI(4,5)P_2$ levels in Stn2 KO neurons. Therefore, Stn2 depleted and WT neurons were cultured for 5 days in the presence or absence of TTX and stained subsequently with the PH-PLCδ1-GFP domain to specifically label $PI(4,5)P_2$ (Figure 34B). Quantitative analysis revealed that neuronal silencing of Stn2 deficient neurons indeed rescued elevated $PI(4,5)P_2$ levels efficiently back to those measured in WT neurons (Figure 34C). All in all, these data substantiate the correlation of surface-stranded Syt1 and elevated $PI(4,5)P_2$ levels in the absence of Stn2 and SV2, that might mediate increased SV release and accelerated retrieval.

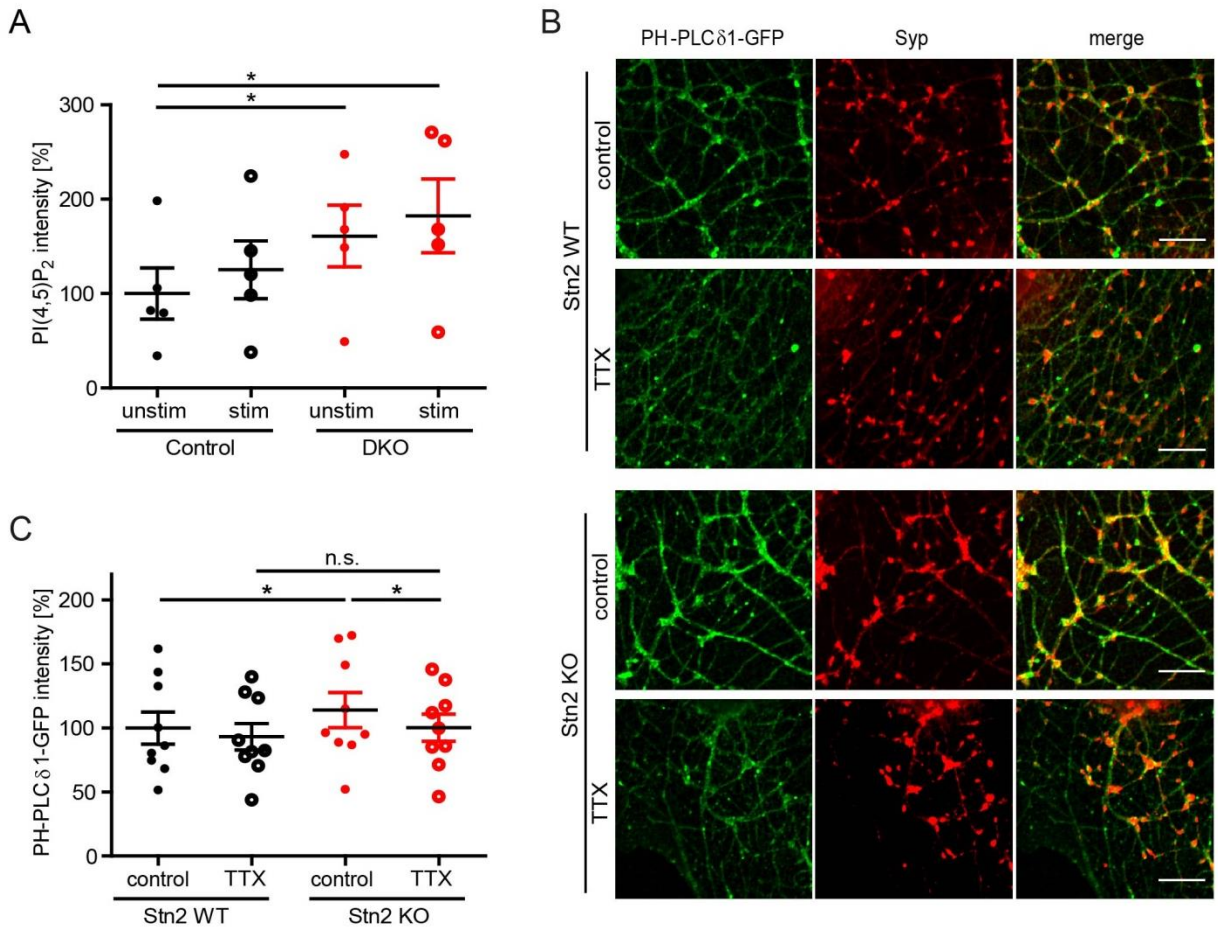


**Figure 34: Elevated PI(4,5)$P_2$ levels correlate with surface-stranded Syt1 in SV2A/B neurons and are activity dependent. (A)** Quantitative analysis of PI(4,5)$P_2$ intensities in SV2A/B depleted and control neurons stained with PI(4,5)$P_2$ specific antibody in Syb2 positive boutons shows significant elevation of PI(4,5)$P_2$ levels in DKO (WT, unstim 100.0 ± 27.2 %; WT stim 125.3 ± 30.5 %; KO unstim 161.0 ± 32.5 %; KO stim 182.3 ± 39.1 %; *P < 0.05, n = 5 independent experiments). **(B)** Representative confocal images of control (treated with sodium acetate used for dissolving TTX) and TTX silenced Stn2 WT and KO neuronal cultures stained with PH-PLCδ1-GFP (green) to label PI(4,5)$P_2$ and with a Syp specific antibody (red). Scale bar, 10 µm. **(C)** Quantification of PH-PLCδ1-GFP intensities reveals a significant reduction of PI(4,5)$P_2$ in Stn2 KO neurons to 100.2 ± 10.6 % after silencing neuronal network activity (Stn2 KO control 113.9 ± 13.8 %) comparable to WT control (100.0 ± 12.6 %) and TTX silenced WT neurons (93.2 ± 10.4 %). (*P < 0.05, n.s. – not significant, n = 9 independent experiments). Data represent mean ± SEM.

## 4.2.5. Syt1 interacts with PIPK1γ

The prominent and consistent increase of PI(4,5)$P_2$ in the absence of Stn2 or SV2A/B correlates with Syt1 missorting to the plasma membrane. These data raised the question of how surface-stranded Syt1 can mechanistically affect PI(4,5)$P_2$ levels. The observed increase of PI(4,5)$P_2$ can either be the result of increased synthesis or reduced degradation of PI(4,5)$P_2$. To dissect the cause for the PI(4,5)$P_2$ increase, we analyzed a possible role of Syt1

in PI(4,5)$P_2$ synthesis by investigating a potential interaction of Syt1 with PIPK1γ, the major PI(4,5)$P_2$ synthesizing kinase in the brain (Di Paolo et al., 2004). Interestingly, Dr. Michael Krauss (FMP, Berlin) was able to identify an interaction between PIPK1γ and Syt1 using purified synaptosomes from rat brain lysates. This interaction was regulated by the presence of calcium. While the depletion of calcium during the immunoprecipitation with EDTA reduced the interaction of PIPK1γ with Syt1, the presence of 200 µM $CaCl_2$ enhanced complex formation (Figure 35A). This is compatible with the calcium influx at the synapse during neurotransmission suggesting that PIPK1γ and Syt1 interact during neuronal activity. Moreover, this calcium dependence was not shown for the known PIPK1γ binding partner AP-2 and is therefore specific for the Syt1 - PIPK1γ interaction. Affinity purification using single GST-fused C2 domains of Syt1, C2A and C2B, and rat brain extracts supported the specific interaction of PIPK1γ and Syt1. In addition, these experiments identified the C2B domain as the interaction site within Syt1 that mediates its association with PIPK1γ (Figure 35B). Complex formation between Syt1 and PIPK1γ provides an attractive explanation for the correlation of elevated PI(4,5)$P_2$ levels and surface-stranded Syt1 in Stn2 and SV2 deficient neurons. It appears plausible to assume that surface-stranded Syt1 via this interaction can recruit PIPK1γ to the plasma membrane where the kinase in turn can synthesize PI(4,5)$P_2$.

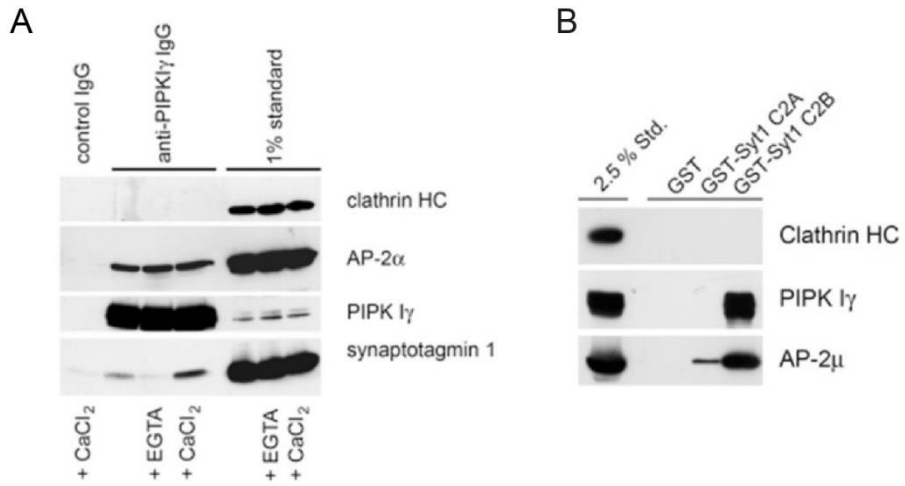


**Figure 35: Syt1 interacts with PIPK1γ in the presence of calcium. (A)** Co-immunoprecipitation of PIPKIγ with Syt1 from synaptosomes isolated from rat brain lysates in absence (5 mM EGTA) or presence of 200 µM $CaCl_2$. **(B)** Affinity purifications using GST-tagged C2 domains of Syt1 reveal the association of PIPKIγ from rat brain extracts with Syt1-C2B domain. Courtesy of Dr. Michael Krauss (FMP, Berlin).

### 4.2.6. Overexpression of Syt1 and PIPK1γ in HEK cells mimic elevated $PI(4,5)P_2$ levels

If surface-stranded Syt1 recruits PIPK1γ and thereby can regulate $PI(4,5)P_2$ levels at the plasma membrane, overexpression of Syt1 should suffice to elevate $PI(4,5)P_2$ levels in transfected HEK 293T cells. Previous data have shown that overexpression of Syt1 in fibroblasts results in its surface accumulation as neuronal specific sorting adaptors needed for its internalization from the plasma membrane are missing (Feany and Buckley, 1993; Jarousse and Kelly, 2001). Interestingly, ectopic expression of Syt1 led to morphological changes of HEK cells such as increased filopodia formation (Figure 36A) as reported before (Feany and Buckley, 1993). Using the PH-PLCδ1-GFP domain to specifically detect $PI(4,5)P_2$ we found significantly elevated $PI(4,5)P_2$ levels in HEK 293T cells stably overexpressing Flag-tagged Syt1 compared to control cells (Figure 36B, C). These data suggests that surface Syt1 can induce $PI(4,5)P_2$ synthesis in HEK cells, likely by interacting with the endogenous PIPK1 (Schill and Anderson, 2009).

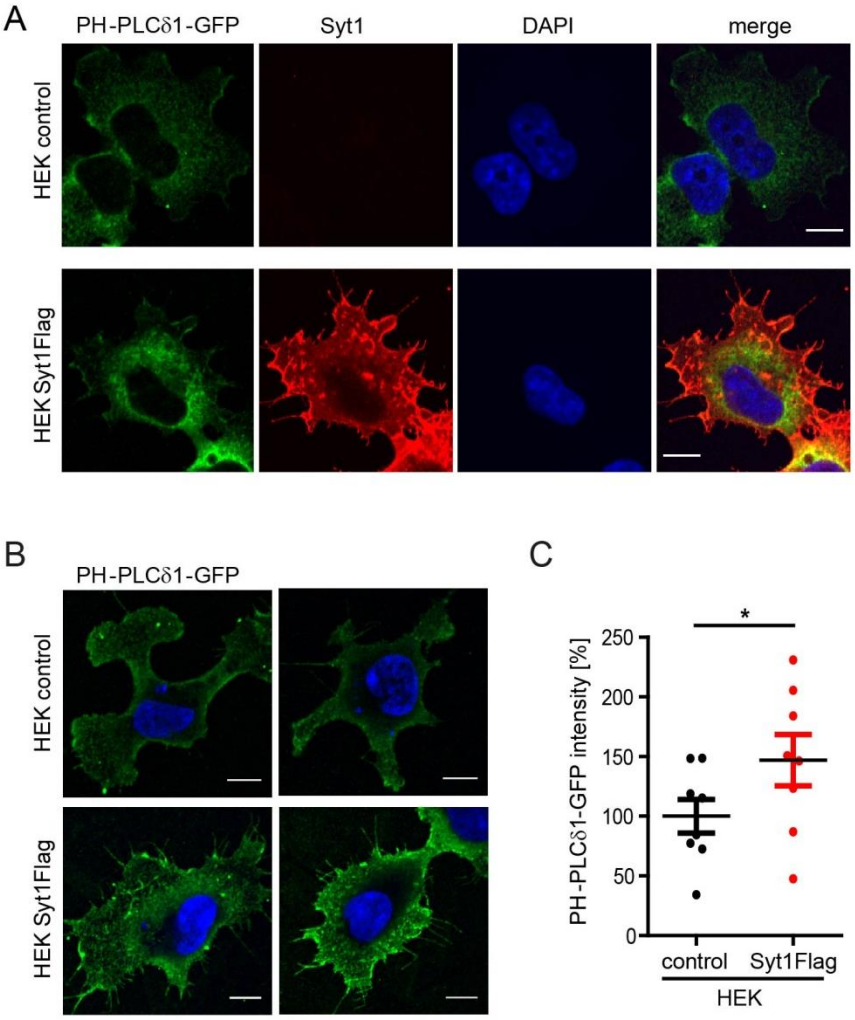


**Figure 36: Elevated PI(4,5)$P_2$ levels are mimicked by Syt1 overexpression in HEK cells. (A)** Representative confocal images of control and Syt1-Flag overexpressing HEK cells stained for PI(4,5)$P_2$ with the PH-PLCδ1-GFP domain (green), for Syt1 with a Syt1 specific antibody (red) and with DAPI to label nuclei (blue). Scale bar, 10 µm. **(B)** HEK cells stained with PH-PLCδ1-GFP after glutaraldehyde fixation reveal increased PI(4,5)$P_2$ levels specifically upon Syt1-Flag overexpression (scale bar, 10 µm). **(C)** Quantification of PH-PLCδ1-GFP intensities normalized to controls (Syt1-Flag expressing HEK cells: 146.9 ± 21.5 %; controls: 100.0 ± 14.1 %; *P < 0.05, n = 8 independent experiments). All data represent mean ± SEM.

To challenge the system even further, we used HEK cells with doxycyclin inducible PIPK1γ expression (Krauss et al., 2006) and transiently overexpressed mCherry (mCh)-tagged Syt1. As expected, Syt1mCh or WT PIPK1γ expression increased PI(4,5)$P_2$ levels compared to mCh transfected control cells (Figure S4 in Appendix B and **Figure 37**). The combined overexpression of PIPK1γ and Syt1mCh even further elevated PI(4,5)$P_2$ levels. This additional increase was dependent on kinase activity of PIPK1γ as the induced expression of kinase-inactive (KI) mutant of PIPK1γ unable to synthesize PI(4,5)$P_2$ resulted in reduced PI(4,5)$P_2$ levels compared to WT PIPK1γ. Interestingly, Syt1mCh expression in

HEK cells that harbor an inactive PIPK1γ still increased PI(4,5)$P_2$ to the same amount as in control HEK cells suggesting that Syt1 can induce PI(4,5)$P_2$ synthesis also via other isoforms of PIPK1γ, which are endogenously present in HEK cells like PIPK1α and PIPK1β.

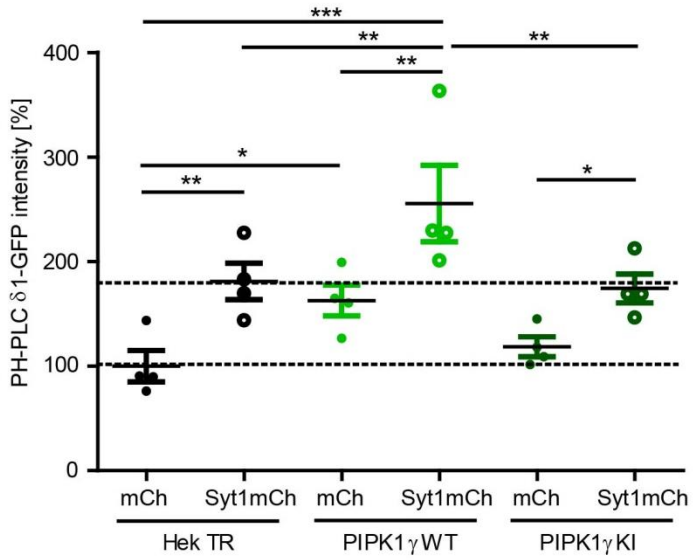


**Figure 37: Overexpression of PIPK1γ together with Syt1 further elevates PI(4,5)$P_2$ levels.** FlpIN HEK 293T cells with inducible expression of HA-tagged PIPK1γ p90 WT and kinase inactive (KI) mutant as well as control cells only harboring the tetracycline repressor (TR) were either transfected with mCherry (mCh) or Syt1mCherry (Syt1mCh) and all were treated with 1 µg/ml doxycycline for 7 h. Doxycyclin induced expression of WT PIPK1γ in HEK cells transfected with mCh elevates PH-PLCδ1-GFP intensities (PIPK1γWT, mCh 162.8 ± 14.8 %) compared to control HEK TR cells (control HEK TR cells and mCh 100 ± 15.0 %). Transient Syt1mCh expression increases PI(4,5)$P_2$ level to a similar degree (HEK TR + Syt1mCh 181.1 ± 17.5 %), while Syt1mCh expression together with PIPK1γ WT increases PI(4,5)$P_2$ levels further to 225.5 ± 36.6 %. HEK cells with induced expression of PIPK1γ KI and mCh expression only show mildly increased PH-PLCδ1-GFP intensities (118.5 ± 9.5 %) while Syt1mCh in the same background increases PH-PLCδ1-GFP intensities significantly to 174.3 ± 13.8 %. (*P < 0.05, **P < 0.01; ***P < 0.001, n = 4 independent experiments). All data represent mean ± SEM.

### 4.2.7. Facilitated recruitment of PIPK1γ to the plasma membrane in Stn2 deficient neurons

To elucidate the mechanism of elevated PI(4,5)$P_2$ levels and surface-stranded Syt1 in Stn2 depleted neurons in detail, we examined the nanoscale localization of endogenous PIPK1γ in hippocampal neurons. Because of the interaction of PIPK1γ and Syt1 we hypothesized that more PIPK1γ is recruited to the plasma membrane in the absence of Stn2. This, in turn, would allow increased synthesis of PI(4,5)$P_2$ in Stn2 KO neurons. To address this question we first validated the specificity of our PIPK1γ antibody (a kind gift from Pietro De Camili) by siRNA mediated knockdown in wildtype neurons. Two different siRNAs (si11 and si12)

against endogenous PIPK1γ efficiently reduced PIPK1γ level in immunostainings to about 25 % of that observed in control neurons treated with scrambled siRNA (Figure S5 in Appendix B and Figure 38A, B). This complies with a specific knockdown and a specific antibody staining. Furthermore, we confirmed that the expression levels of PIPK1γ are not changed in neuronal cultures of Stn2 KO mice compared to WT mice, which would impede interpretation of localization changes. We immunofluorescently stained PIPK1γ in neuronal cultures of both genotypes and quantified the total intensity of PIPK1γ in cell bodies and in pre- and postsynapses based on confocal images (Figure 38C). No significant differences of PIPK1γ intensity were detected in Stn2 depleted neuronal cultures compared to WT cultures. This is in line with previous data showing no significant changes of PIPK1γ protein levels in brain homogenates of Stn2 KO mice compared to WT animals (Kononenko et al., 2013).

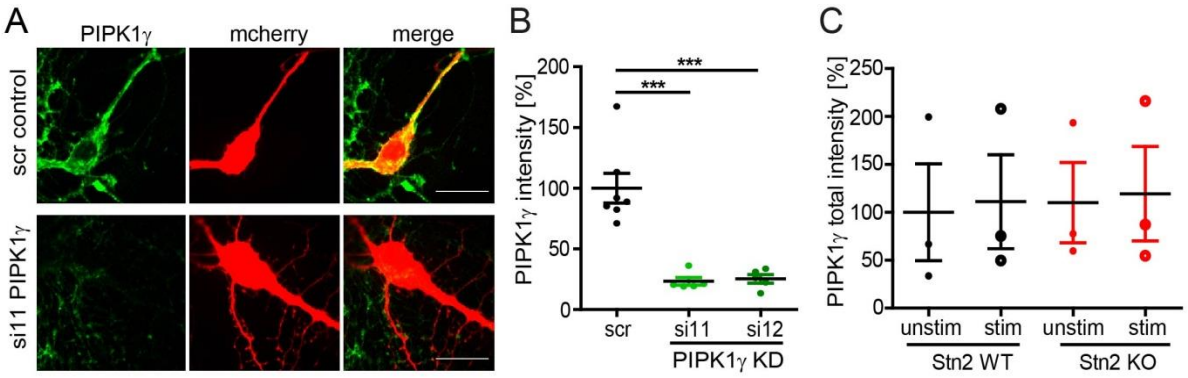


**Figure 38: Validation of PIPK1γ antibody specificity and unaltered PIPK1γ levels in Stn2 depleted neuronal cultures. (A)** Representative confocal images of neurons coexpressing mcherry and scrambled (scr) control siRNA or PIPK1γ siRNA (si11; see Appendix for example images of PIPK1γ si12) and immunostained for PIPK1γ (green) (scale bar, 20 µm). **(B)** Both siRNAs significantly decrease PIPK1γ staining intensity (scr, 100.0 ± 12.2 %; si11, 23.3 ± 3.2 % and si12, 25.3 ± 3.5 %; ***P < 0.001, n = 5 independent experiments). **(C)** Quantification of PIPK1γ total intensity in Stn2 WT and KO neuronal cultures either stimulated (stim) with 80 mM KCl or left unstimulated (unstim) shows no differences in PIPK1γ protein levels (Stn2 WT, unstim 100.0 ± 50.6 %; Stn2 WT, stim 111.0 ± 49.1 %; Stn2 KO, unstim 110.2 ± 41.9 %; Stn2 KO, stim 119.3 ± 49.3 %; n = 3 independent experiments). All data represent mean ± SEM.

As the PIPK1γ antibody showed high specificity and the overall PIPK1γ protein levels were unchanged in Stn2 deficient neurons, we next addressed the question of the nanoscale distribution of PIPK1γ by multicolor 3D-gSTED-based superresolution microscopy analysis of fixed WT and Stn2 KO neurons. In addition to PIPK1γ we stained for the C-terminus of bassoon as an active zone marker and for homer1 to label the postsynaptic density. While bassoon and homer1 appeared as defined opposing clusters, PIPK1γ localized as small puncta within the pre- and postsynapse (Figure 39A). To analyze the localization of all three proteins relative to each other we projected the acquired z-stacks, selected synapses with distinct

bassoon and homer1 clusters and performed a line plot analysis perpendicular to these co-clusters (s. section 3.4.3 and Figure 9). The fluorescence intensities of all three proteins were plotted as line profiles, in which all positions were normalized to the maximum intensity of the bassoon profile. Strikingly, PIPK1γ was enriched within the bassoon positive area in unstimulated Stn2 deficient neurons, while the kinase was widely distributed all over the bassoon and homer1 clusters in unstimulated control neurons (Figure 39A, B). Upon KCl stimulation PIPK1γ distribution displayed also in WT control neurons an increased localization within the bassoon positive active zone, which was further elevated in the absence of Stn2 (Figure 39A, C). This change of PIPK1γ localization is reflected in a trend towards increased maximum peak intensity of PIPK1γ in the presynapse of Stn2 KO neurons (Figure 39D) and in a closer distance of PIPK1γ to bassoon (Figure 39E). Interestingly, the PIPK1γ peak is located 130 nm away from bassoon in WT unstimulated neurons and is recruited closer to bassoon after stimulation (115 nm). In Stn2 depleted neurons the PIPK1γ peak displayed a marked shift towards bassoon already in the unstimulated condition with a mean distance of about 90 nm, which decreased to about 70 nm after stimulation. Of note, the mean distance of bassoon to homer1 clusters was consistently around 150 nm independent of the genotype and stimulation condition (Figure 39F). This distance of pre- and postsynaptic clusters is in agreement with previous studies using stochastic optical reconstruction microscopy (STORM) (Dani et al., 2010) and from our laboratory using gSTED microscopy (Gerth et al., 2017).

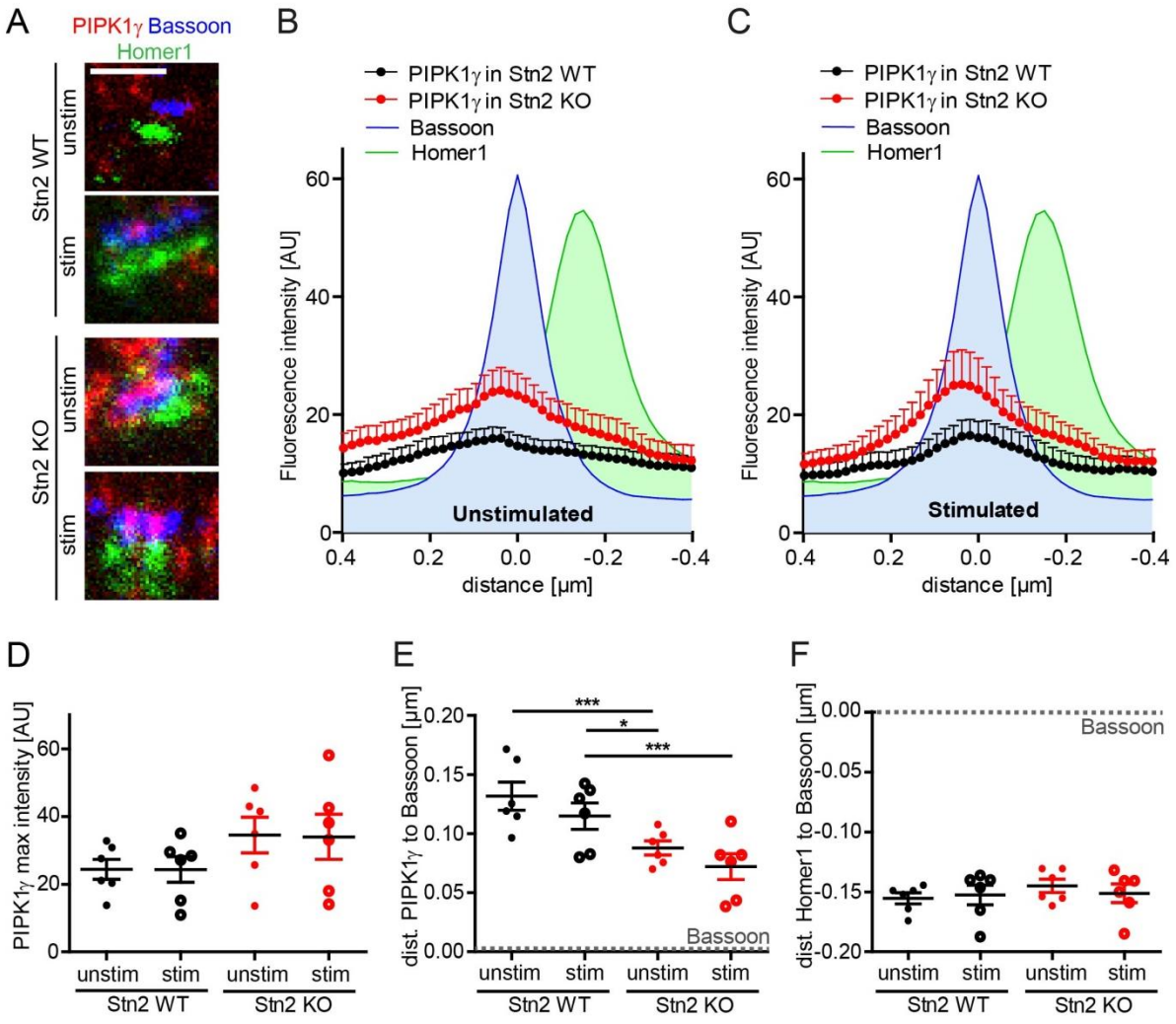


**Figure 39: Nanoscale distribution of PIPK1γ in Stn2 deficient neurons. (A)** Representative sum intensity projected gSTED images of WT and Stn2 KO synapses in resting (unstim) or KCl stimulated (stim) conditions stained for PIPK1γ (red), bassoon (blue) or homer1 (green). Scale bar, 0.5 µm. Mean line profiles of all three markers aligned to the bassoon maximum display the distribution of PIPK1γ with respect to bassoon and homer1 localization in WT and Stn2 depleted neurons in unstimulated **(B)** or stimulated **(C)** conditions. **(D)** The maximum intensity of PIPK1γ within the presynapse is increased in Stn2 depleted neurons. (Stn2 WT, unstim 24.4 ± 3.0 AU; Stn2 WT, stim 24.4 ± 3.8 AU; Stn2 KO, unstim 34.5 ± 5.3 AU; Stn2 KO, stim 34.0 ± 6.6 AU). **(E)** Mean distance (dist.) of PIPK1γ to bassoon (dashed line) shows significant recruitment of PIPK1γ towards bassoon in the absence of Stn2 and upon stimulation (Stn2 WT, unstim 0.132 ± 0.012 µm; Stn2 WT, stim 0.115 ± 0.011 µm; Stn2 KO, unstim 0.088 ± 0.006 µm; Stn2 KO, stim 0.072 ± 0.011 µm). **(F)** The average distance (dist.) of homer1 to bassoon (dashed line) is unaltered in Stn2 KO synapses compared to the WT in unstimulated and stimulated conditions (Stn2 WT, unstim 0.155 ± 0.005 µm; Stn2 WT, stim 0.153 ± 0.008 µm; Stn2 KO, unstim 0.145 ± 0.006 µm; Stn2 KO, stim 0.152 ± 0.008 µm). All data represent mean ± SEM from n = 6 independent experiments with 180 synapses per condition. *P < 0.05, ***P < 0.001.

These data show that the nanoscale localization of PIPK1γ is significantly altered in the absence of Stn2. This agrees with our hypothesis that PIPK1γ is recruited closer to the

presynaptic plasma membrane via the surface-stranded Syt1 in Stn2 deficient neurons to potentiate PI(4,5)$P_2$ synthesis. Previous data suggested that PIPK1γ activity is positively regulated by the endocytic adaptor AP-2, and both proteins interact at endocytic sites (Krauss et al., 2006; Nakano-Kobayashi et al., 2007). We therefore also investigated the nanoscale distribution of AP-2 in Stn2 depleted neurons in stimulated and unstimulated conditions compared to WT neurons. AP-2 displayed a punctate localization pattern (Figure 40A). The localization and fluorescence intensity of AP-2 remained unaltered after KCl stimulation of WT neurons compared to resting conditions and did not show any significant changes in the absence of Stn2 (Figure 40B-E). The average distance of AP-2 within the presynapse to the active zone center was constantly around 110 nm for Stn2 WT and KO neurons (Figure 40E). Thus, PIPK1γ recruitment towards the plasma membrane is independent of AP-2 localization. AP-2 does not mediate PIPK1γ recruitment and in turn is not affected by PIPK1γ localization and the elevated PI(4,5)$P_2$ levels in the absence of Stn2. Moreover the distance of AP-2 to bassoon is in line with AP-2's primary role in SV reformation from endosomal-like vacuoles (Kononenko et al., 2014; Soykan et al., 2017).

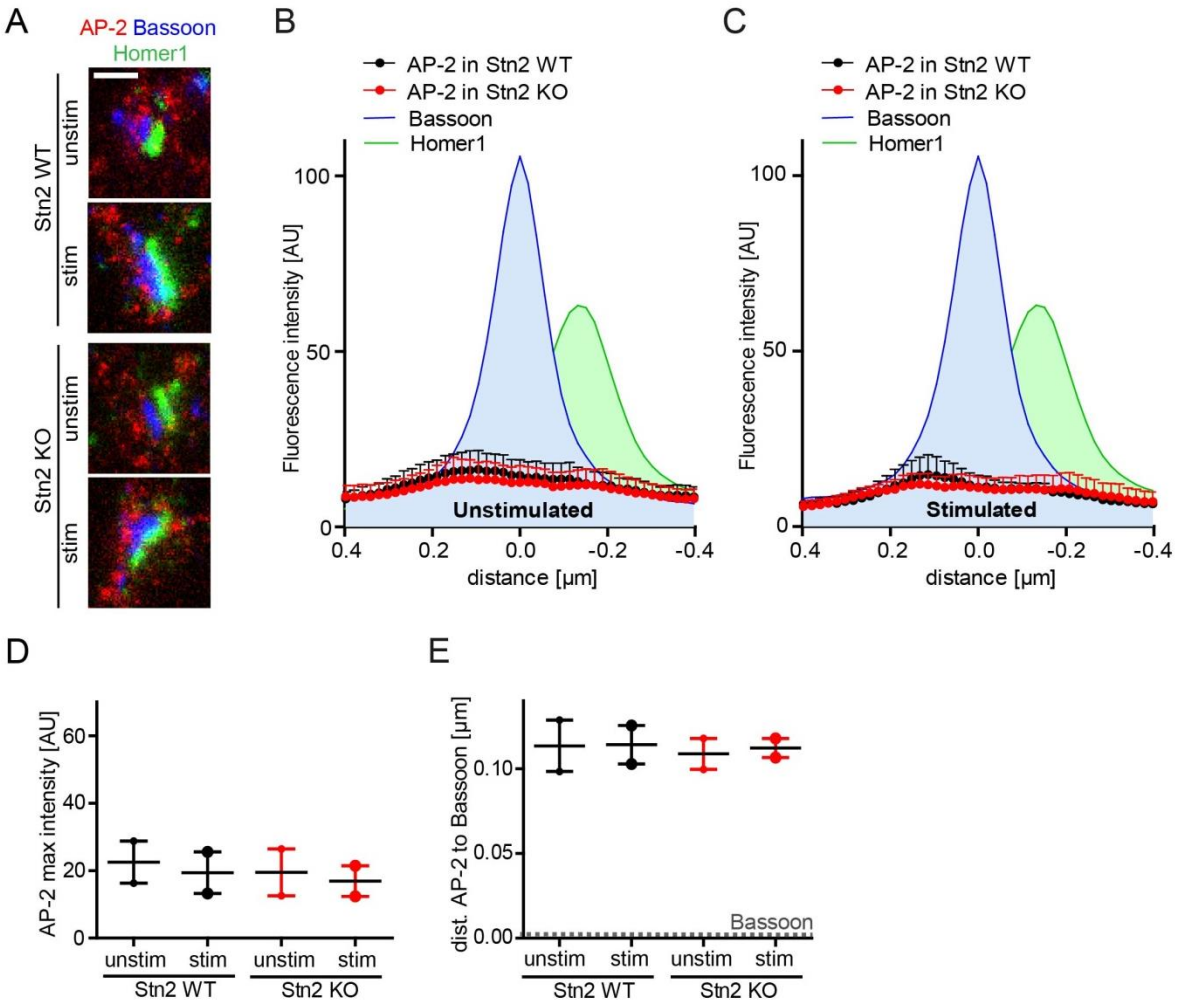


**Figure 40: Nanoscale distribution of AP-2 in Stn2 deficient neurons is unaltered. (A)** Representative sum intensity projected gSTED images of Stn2 WT and Stn2 KO synapses in unstimulated (unstim) or KCl stimulated (stim) conditions triple stained for AP2 (red), bassoon (blue) and homer1 (green). Scale bar, 0.5 µm. **(B, C)** Average multicolor line profiles aligned to bassoon maximum intensity display the distribution of AP-2 with respect to bassoon and homer1 in WT and Stn2 KO neurons in unstimulated **(B)** or stimulated **(C)** conditions. **(D)** The maximum intensity of AP-2 within the presynapse is unchanged in Stn2 depleted neurons. (Stn2 WT, unstim 22.5 ± 6.2 AU; Stn2 WT, stim 19.4 ± 6.2 AU; Stn2 KO, unstim 19.5 ± 6.9 AU; Stn2 KO, stim 16.9 ± 4.5 AU). **(E)** The mean distance (dist.) of AP-2 to bassoon (dashed line) remains unaltered in the absence of Stn2 and upon stimulation (Stn2 WT, unstim 0.114 ± 0.015 µm; Stn2 WT, stim 0.114 ± 0.011 µm; Stn2 KO, unstim 0.109 ± 0.009 µm; Stn2 KO, stim 0.112 ± 0.006 µm). All data represent mean ± SEM from n = 2 independent experiments with 60 synapses per condition.

Collectively, these data indicate that missorted Syt1 at the presynaptic plasma membrane correlates with augmented SV exo- and endocytosis as well as elevated $PI(4,5)P_2$ levels. Complex formation between Syt1 and PIPK1γ likely causes recruitment of PIPK1γ to the plasma membrane and facilitation of $PI(4,5)P_2$ synthesis at or near release sites potentiating both $PI(4,5)P_2$-dependent SV release and endocytosis.

# 5. Discussion

This work unravels two parallel mechanisms that accomplish the endocytic sorting of Syt1 in mammalian central synapses. The SV protein SV2 and the cargo specific adaptor protein Stn2 share crucial overlapping functions in Syt1 sorting. Both proteins ensure the maintenance and the correct retrieval of Syt1 during neurotransmission in the presynaptic terminal. Moreover, we identified that surface-stranded Syt1 is not only the target of endocytic sorting to reform functional SVs, but also triggers PIPK1γ mediated synthesis of presynaptic $PI(4,5)P_2$ promoting SV release as well as their retrieval. Thus, we propose a new SV protein- and membrane lipid-based mechanism to couple SV exo- and endocytosis.

## 5.1. Integrating cargo specific SV protein sorting in SV reformation

The calcium triggered exocytic SV fusion requires subsequent compensatory endocytosis to sustain neurotransmission. The fused SVs have to be replenished by local reformation of SVs within the presynaptic terminal as *de novo* synthesis in the soma is unable to acutely resupply distantly located synapses. These SVs comprise numerous proteins mediating important synaptic functions and display very little intervesicle variability regarding copy numbers of some SV proteins (Mutch et al., 2011). Consequently, mechanisms have to exist that ensure the compositional identity of SVs after full collapse fusion (Chen et al., 2008; Gimber et al., 2015; Li and Murthy, 2001). How high-fidelity sorting of SV proteins into new SVs is accomplished and integrated in endocytic retrieval remains enigmatic.

Several models for SV protein incorporation have been proposed including adaptor-based sorting of SV proteins. Whether only one major endocytic adaptor is sufficient or dedicated adaptors sort SV proteins individually is under debate (Willox and Royle, 2012). Moreover, the formation of detergent-resistant SV proteins complexes (Bennett et al., 1992) have fueled the idea that SV proteins stay clustered by specific or unspecific interactions after SV fusion. Such a scenario would alleviate the need to orchestrate SV protein sorting by individual and specific adaptors. To address these unresolved questions we investigated the sorting of the SV calcium sensor Syt1. Because Syt1 mediates calcium triggered SV fusion (Jahn and Fasshauer, 2012), it is crucial to maintain Syt1 copy numbers on SVs after multiple rounds of exo-/endocytosis. Biochemical analysis as well as genetic inactivation in *D. melanogaster* identified Stn2 and its homologs as dedicated endocytic adaptors for Syt1 sorting (Diril et al., 2006; Fergestad and Broadie, 2001; Phillips et al., 2000; Walther et al.,

2001). While the loss of stoned B results in severe neurotransmission defects due to Syt1 missorting and degradation in *D. melanogaster* (Andrews et al., 1996; Estes et al., 2003; Fergestad et al., 1999; Grigliatti et al., 1973), Stn2 KO mice exhibit a comparably mild phenotype, albeit with reduced fidelity of Syt1 sorting (Kononenko et al., 2013). This led us to the hypothesis that Syt1 high-fidelity sorting is governed by additional mechanisms in mammals. The SV protein SV2 exceled as an alternative candidate to chaperone Syt1 retrieval via SV protein complex formation as a SV2 derived peptide can facilitate Syt1 internalization (Haucke and De Camilli, 1999) and SV2 has been associated with Syt1 trafficking (Yao et al., 2010).

### 5.1.1. Overlapping activities of SV2 and Stn2 in Syt1 sorting

In this study combined deletion of Stn2 and SV2 *in vivo* has revealed their overlapping function in Syt1 maintenance and sorting from the neuronal surface to SVs. Compared to the single deletion we observed aggravated missorting of Syt1 to the plasma membrane (Figure 18, Figure 19, Figure 21), exacerbated Syt1 loss (Figure 14, Figure 15) and impaired neurotransmission in animals lacking both Stn2 and SV2A/B (Figure 24, Figure 26). Moreover, Stn2 levels were elevated in SV2A/B depleted mice (Figure 14) arguing for a compensatory role of Stn2 in the absence of SV2. The additive phenotypes further suggest that Stn2 and SV2 cooperate in Syt1 sorting via parallel mechanisms. Therefore, in the mammalian synapse high-fidelity retrieval of Syt1 is ensured by two retrieval pathways: cargo selective sorting via the endocytic adaptor protein Stn2 and complex formation of the SV protein SV2 with Syt1. The latter, thus, provides an explanation for the comparably mild phenotype of Stn2 KO mice compared to the severe neurotransmission defects in invertebrates with depleted stonin expression.

The overlapping activities of SV2 and Stn2 are supported by their distinct molecular properties and their binding to different C2 domains of Syt1. The cytosolic Stn2 can facilitate the sorting of Syt1 by binding simultaneously the C2A domain of Syt1 and AP-2 (Jung et al., 2007). In contrast, the large SV protein SV2 contacts the C2B domain of Syt1 (Schivell et al., 1996). Together with the tyrosine-based motif within the N-terminal domain SV2 promotes Syt1 retrieval (Yao et al., 2010). Thereby, SV2 and Stn2 likely do not compete for Syt1 binding. This further supports our observation that both proteins operate via parallel and distinct mechanisms in Syt1 sorting (Figure 41). Furthermore, the interaction of Stn2 and SV2 with Syt1 is differently regulated. While Stn2 binding to Syt1 is calcium-independent (Walther et al., 2004; Walther et al., 2001), SV2A has been shown to only interact with Syt1

under low calcium concentration (Schivell et al., 1996). This implies a segregation of Syt1 and SV2A during calcium triggered exocytosis and complex formation when calcium transients have declined. Moreover, phosphorylation of SV2A by CK1 family kinases positively controls the interaction of Syt1 and SV2A (Zhang et al., 2015).

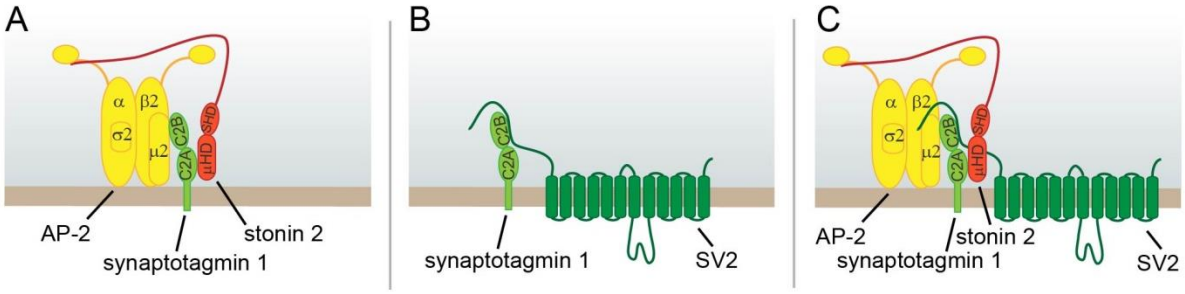


**Figure 41: Sorting of Syt1 by Stn2 and SV2. (A)** Syt1 associates with AP-2μ2 via its C2B domain. However, this interaction does not suffice for efficient Syt1 retrieval. The specific adaptor protein Stn2 is needed to strengthen the link between AP-2 and Syt1 by interacting simultaneously with Syt1's C2A domain and the AP-2α ear. **(B)** Syt1 can also be sorted by association with SV2, another SV protein. The N-terminus of SV2 binds to the C2B domain of Syt1 and thereby facilitates correct Syt1 sorting. **(C)** As Stn2 and SV2 interact with distinct C2 domains of Syt1, both proteins might bind at the same time to the calcium ion sensor and link it to AP-2 to enable its precise retrieval (Kaempf and Maritzen, 2017).

The selective sorting of Syt1 by SV2 and Stn2 contradicts a model of one major endocytic adaptor that accomplishes sorting of all SV proteins. Such a role had been suggested for AP-2 given its crucial role in binding cargo proteins and recruiting clathrin triskelia during CME in non-neuronal cells. Most SV proteins do not display any overt canonical AP-2 recognition motifs. Instead cargo specific adaptors have been identified to mediate SV protein sorting such as Stn2. Stn2 had also been considered as a major sorting adaptor based on the severe neurotransmission defects in *D. melanogaster* in the absence of stoned B (Estes et al., 2003; Fergestad et al., 1999) and siRNA mediated knockdown of Stn2 in neuronal cultures (Willox and Royle, 2012). However, the mild phenotype of Stn2 KO mice demonstrated that Stn2 cannot serve as a crucial player during endocytic retrieval, but is a dedicated sorting adaptor for Syt1 (Kononenko et al., 2013). Our data support the idea that multiple mechanisms bind and direct SV proteins for endocytic retrieval. The interaction of SV proteins with each other has been described previously (Edelmann et al., 1995; Schivell et al., 1996; Siddiqui et al., 2007), but its relevance for SV protein sorting was unclear. We show that SV protein complex formation contributes to the efficient retrieval of Syt1. This is in line with the proposed sorting of Syb2 by the endocytic adaptors AP180/CALM and the SV protein Syp (Gordon et al., 2016; Gordon et al., 2011; Koo et al., 2015; Koo et al., 2011). The

combination of adaptor-based sorting and complex formation of SV proteins simplifies the complex task to sort all SV proteins individually with the help of dedicated adaptors. It reduces the amount of required selective adaptors and the time that the sorting of single SV proteins would demand.

The nature of these SV protein complexes is an unknown variable in the process of SV protein retrieval: How many SV proteins cluster in such a complex and do they form specific clusters? Our data show that SV2 depletion selectively impairs the endocytic sorting of Syt1 while Syp sorting is not affected (Figure 19, Figure 23). This excludes that SV2 and Syt1 are part of one SV protein cluster that is retrieved as one package with the help of various adaptors. Consistently, the absence of Syp impairs Syb2 sorting, while the endocytic retrieval kinetics of other SV proteins such as Syt1 and VGLUT1 are only mildly slowed down (Gordon et al., 2011). Thus, the self-assembly of SV proteins is restricted to defined interaction partners and confers specificity for SV protein sorting.

### 5.1.2. Spatio-temporal regulation of Syt1 sorting

The identification of SV2 and Stn2 as mediators of Syt1 sorting ultimately leads to the question when and where sorting occurs after SV fusion. Do SV2 and Stn2 follow a sequence of events? Do they bind stochastically to Syt1 or simultaneously and link it to the endocytic machinery via AP-2 (Figure 41)?

Monitoring pHluorin-tagged SV proteins has shown that SV proteins do not stay in one large cluster after exocytosis, but are mobile on the presynaptic membrane (Fernandez-Alfonso et al., 2006) and rapidly diffuse out of the active zone. Interestingly, the diffusion coefficient of the SV proteins Syp, Syt1 and Syb2 were not significantly different (Gimber et al., 2015) even though they differ in their number of transmembrane domains. With four transmembrane domains Syp has an increased radius and should have slower diffusion compared to single-pass transmembrane proteins such as Syt1 and Syb2 (Saffman and Delbruck, 1975). Moreover, Syb2 alone diffuses more than 10 times faster in reconstituted giant unilamellar vesicles (Ramadurai et al., 2009). Thus, the slow and uniform diffusion coefficient of the tested SV proteins suggests that SV proteins likely diffuse as clusters. In case of SV2 and Syt1, they could in principle first cluster after exocytosis due to their close localization within a SV. This defined complex formation could be beneficial for the diffusional spread. SV2 with 12-transmembrane domains slows down the diffusion of Syt1 and thereby increases the chances of their capture at the periactive zone. A similar complex

formation of a single- and multi-pass transmembrane protein can be observed for Syb2 and Syp (Gordon et al., 2011; Rajappa et al., 2016). These defined complexes might be small and fast enough to move through the dense cytomatrix of the active zone. In contrast, if SVs stay as one cluster the SV protein package would presumably be too slow and immobile to efficiently clear the release site for new rounds of exocytosis.

The adaptor proteins AP180 and CALM have been shown to slow down the diffusional spread of Syb2 as well (Gimber et al., 2015). Thus, these adaptors have to bind Syb2 shortly after SV exocytosis. If Stn2 binds Syt1 upstream of release site clearance and thereby affects Syt1 spreading to the periactive zone, is unknown and has to be further investigated. However, the increased surface-stranding of Syt1 in the absence of Stn2 or SV2A/B ((Kononenko et al., 2013) and Figure 18, Figure 19) suggests, that Stn2 as well as SV2 mediate Syt1 sorting in concert at the neuronal surface. Therefore, it is likely that mixed clusters of Stn2, Syt1 and SV2 are formed at the plasma membrane to confine the dispersion of Syt1 after SV fusion.

The formation of defined complexes might be relevant to incorporate SV proteins with the correct stoichiometry. The similar copy numbers of SV2 and Syt1 (Wilhelm et al., 2014) as well as their self-assembly would suggest that SV2 is better suited to regulate the quantitative Syt1 incorporation than the cytosolic Stn2. The substantial redistribution and loss of Syt1 in the absence of SV2A/B compared to the mild phenotype of Stn2 KO mice (Figure 42) favors this hypothesis. Likewise, Syp has been suggested to bind Syb2 in a 1:2 ratio and thereby controls their stoichiometry (Gordon et al., 2016). In case of Syb2 sorting the deletion of the cytosolic adaptor AP180 has a postnatal lethal phenotype (Koo et al., 2015) in contrast to mild effects observed upon Syp loss in mice (Eshkind and Leube, 1995; McMahon et al., 1996; Schmitt et al., 2009). Thus, the major contribution of SV protein complex formation for orchestrating the correct stoichiometry cannot be generalized without further experimental evidence.

The mixed clusters of Syt1 with Stn2 and SV2 can interact with endocytic proteins and link Syt1 to the CME machinery (Martina et al., 2001; Walther et al., 2004; Yao et al., 2010). Whether this step of sorting SV proteins into newly reformed SVs is occurring at the presynaptic plasma membrane or after membrane retrieval is controversial and intimately linked to the proposed SV endocytosis mechanisms. Interestingly, the quantitative analysis of adaptor molecules within the synapse revealed that only 5-10 % of SV cargo can be retrieved simultaneously via CME (Mori and Takamori, 2018; Wilhelm et al., 2014) and will become limiting upon intense stimulation. This is consistent with recent data challenging the role of

clathrin-dependent endocytosis as the primary endocytic retrieval pathway from the presynaptic plasma membrane. Genetic manipulations of AP-2 and clathrin (Kononenko et al., 2014; Soykan et al., 2017) as well as highly time-resolved electron microscopy (Watanabe et al., 2013a; Watanabe et al., 2013b) suggest that depending on neuronal activity SV endocytosis occurs predominantly via a clathrin-independent invagination of membrane, which subsequently requires CME for SV reformation (Kononenko et al., 2014; Watanabe et al., 2014). This sequence of endocytosis events meets the requirements for sustained neurotransmission: Via clathrin-independent membrane retrieval the presynaptic architecture is restored on a fast time scale (Soykan et al., 2016), while SV reformation is postponed and gains more time for "proofreading" the protein composition of newly endocytosed SVs (Figure 3). The huge pool of SVs in the central mammalian synapse also alleviates the need for immediate replenishment, as it allows to respond to multiple rounds of depolarization without entire depletion (Neher, 2010).

This model further implies that membrane retrieval and SV reformation are two separable events. Consistently, we observe unperturbed retrieval kinetics of pHluorin-tagged SV proteins in neurons depleted of Stn2 and SV2 (Figure 27, Figure 28). Thus, both proteins are required for correct Syt1 sorting, but have no essential role in the membrane retrieval itself. Moreover, the surface accumulation of SV proteins in absence of sorting proteins (Kononenko et al., 2013; Koo et al., 2015) excludes an exclusive role of UFE in SV retrieval that had been proposed by Watanabe and colleagues (Watanabe et al., 2014) and would only result in an accumulation of SV proteins on ELVs. It rather suggests that various retrieval mechanisms govern SV endocytosis including clathrin/AP-2 dependent sorting at the neuronal surface.

To assess the temporal and spatial coordination of Syt1 sorting in detail, highly time-resolved superresolution imaging would be required. Single molecules of Syt1 and SV2 could be tracked during SV exo- and endocytosis to determine when and where they form clusters and hot spots as previously proposed for Syt1 by Willig and colleagues (Willig et al., 2006). Furthermore, complex formation of SV2A with Syt1 can be regulated via phosphorylation of SV2A by CK1 family kinases (Zhang et al., 2015). Thus, examining the exact signaling cascade of these kinases during neurotransmission would help to investigate when the SV2A-Syt1 interaction is potentiated and therefore is likely to facilitate Syt1 sorting.

## 5.2. Functional implications of Syt1 sorting in central synapses

Both SV proteins SV2 and Syp are involved in SV protein sorting, but appear relatively late in evolution and do not have any close homologs in invertebrates (Janz et al., 1998; Leube et al., 1987). Therefore it is tempting to speculate that the mechanism of SV protein sorting by SV protein self-assembly may be a unique feature of mammalian synapses. The question remains, why SV protein sorting has to be safeguarded so well in mammalian synapses and which functional consequences arise from Syt1 missorting.

Syt1 deletion revealed its important presynaptic function causing severely impaired neurotransmission with reduced SV release as well as slower SV retrieval. Thus, we hypothesized that not only the presence of Syt1 but also its correct sorting is crucial for its presynaptic roles.

### 5.2.1. Regulation of Syt1 levels and turnover by SV2/Stn2

Our data reveal that the missorting of Syt1 in the absence of sorting proteins SV2 and Stn2 is accompanied by a reduction of Syt1 total levels. The pronounced loss of Syt1 in the absence of SV2A/B is further aggravated in the combined deletion of Stn2 and SV2A/B (Figure 14, Figure 15 and Figure 42). Interestingly, the synaptic SV number is not reduced and cannot explain the reduction in Syt1 total level (Figure 13B). Moreover, only the protein levels of Syt1 are significantly reduced as levels of Syp and Syb2 remain unchanged in SV2A/B and Stn2 KO mice (Figure 14, Figure 15). Thus, it appears that Syt1 loss is specifically related to the absence of SV2 and Stn2. Yao and colleagues proposed a reduced expression or instability of Syt1 in the absence of SV2, that may account for the loss of Syt1 (Yao et al., 2010). However, levels of overexpressed Syt1-pHluorin in SV2A depleted neuronal cultures are comparable to control neurons (Figure 23I), which argues against a general instability of Syt1 in the absence of SV2. As we observe an additional loss of Syt1 in TKO mice, it is plausible to speculate that the missorted Syt1 is directed for degradation to compensate for a failed clearance of release sites or periactive zones or to consume ELVs with accumulated Syt1. If protein turnover of Syt1 is specifically increased in SV2 deficient neurons due to SV2's role in chaperoning Syt1 retrieval, overexpression of WT SV2 but not of Syt1 binding-defective SV2 should rescue facilitated Syt1 turnover in SV2 KO neurons.

Nevertheless, how Syt1 turnover in SV2 deficient neurons would be mediated, is unknown and difficult to answer as the mechanisms of SV protein degradation in the synapse are so far incompletely understood. Recent evidence suggests that the majority of SV proteins

are degraded independently of the proteasomal degradation system (Hakim et al., 2016). On the contrary "left over" Syt1 molecules residing on ELVs are more likely to be targeted to the endolysosomal pathway or to autophagic degradation. Work in *D. melanogaster* identified a Rab35-dependent endolysosomal trafficking pathway involved in the degradation of aged or damaged SVs (Fernandes et al., 2014; Uytterhoeven et al., 2011). Based on recent publications autophagy seems to be implicated in synaptic protein turnover and could also account for the Syt1 loss in SV2A/B and Stn2 depleted mice. The endocytic protein endophilin as well as bassoon have been shown to regulate autophagosome formation (Okerlund et al., 2017; Soukup et al., 2016). Whether and how Syt1 degradation is facilitated in the absence of Stn2 and SV2 needs to be addressed in the future.

### 5.2.2. Functional consequences of Syt1 redistribution and loss for neurotransmission

Comparing the phenotypes of Stn2, SV2A/B depletion and their combined deletion highlights a correlation of redistribution and loss of total Syt1 levels with reduced basal neurotransmission (Figure 42, Table 25). Stn2 deletion causes only slightly reduced release probability in mossy fiber synapses and only a mild Syt1 loss paired with strong Syt1 surface accumulation (Kononenko et al., 2013). In agreement with earlier studies we find that loss of SV2A/B impairs basal neurotransmission and SV release probability (Figure 24, Figure 26) that are accompanied by a profound Syt1 loss from SVs. The additional deletion of Stn2 in SV2A/B knockout mice reduced the efficacy of stimulus evoked neurotransmission even more (Figure 24, Figure 26), which correlates with an exacerbated surface accumulation and loss of Syt1. Even though the exact role of SV2 during neurotransmission is still under debate, many functions of SV2 have been suggested based on its deletion phenotype. SV2 has been implicated in regulating residual calcium (Janz et al., 1999) and in converting SVs into a calcium-responsive state during SV priming (Chang and Sudhof, 2009). Other studies propose a role of SV2 in release probability (Custer et al., 2006) and SV priming modulating the size of the readily-releasable pool (Xu and Bajjalieh, 2001). These described neurotransmission defects in the absence of SV2 as well as our data correlate with the loss of Syt1 from SVs. The reduced calcium responsiveness of evoked release could be explained by the significantly reduced vesicular Syt1. Thus, our data suggest, that SV2 at least partially regulates neurotransmission efficiency via its role in Syt1 sorting during activity-dependent SV recycling.

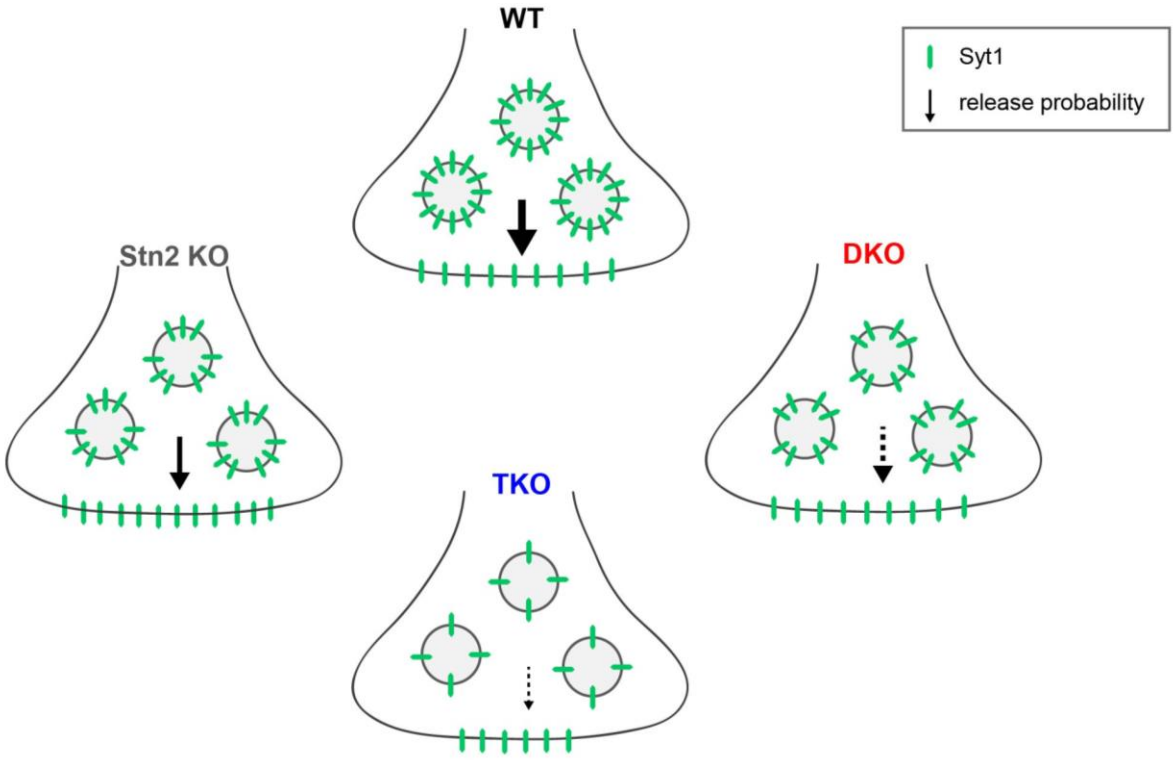


**Figure 42: Schematic depicting Syt1 loss and missorting in the absence of Stn2, SV2, or both proteins.** Stn2 KO mice have slightly reduced levels and partial missorting of Syt1 to the neuronal surface (Kononenko et al., 2013), while SV2A/B DKO synapses show strongly reduced Syt1 levels and Syt1 missorting to the neuronal surface resulting in its partial depletion from SVs. Loss of total Syt1 and depletion from SVs are further aggravated by deletion of both SV2A/B and Stn2 in TKO synapses.

**Table 25: Summary of observed phenotypes in KO mice lacking Stn2 (Stn2 KO), SV2A/B (DKO), SV2A/B + Stn2 (TKO) and Syt1 (Syt1 KO).**

| | WT | Stn2 KO | DKO | TKO | Syt1 KO |
|---|---|---|---|---|---|
| **Total Syt1** | 100% | 90%[1] | 70% | 40% | 0% |
| **Surface/total Syt1** | 100% | 160%[1] | 130% | 200% | 0% |
| **EPSP amplitude** | 100% | not analyzed | 50% | 30% | failure[3]/ 15%[4] |
| **mEPSP frequency** | 100% | not analyzed | unchanged[2] | unchanged | 300 %[3] |
| **Release probability** | 100% | slightly reduced[1] | reduced | severely reduced | severely reduced[3] |

[1](Kononenko et al., 2013); [2](Venkatesan et al., 2012); [3](Kerr et al., 2008); [4](Nishiki and Augustine, 2004)

Besides its important role in evoked release, Syt1 has been suggested to act as a calcium-dependent clamp of SV fusion in the absence of neuronal activity (Giraudo et al., 2006). The conformational change of Syt1 upon calcium binding allows the rapid and synchronous SNARE mediated exocytosis of SVs. Consequently, the spontaneous fusion of

SVs is greatly increased when Syt1 is deleted or mutated (Kerr et al., 2008; Littleton et al., 1994). Interestingly, the significant reduction of vesicular Syt1 in the absence of Stn2 and SV2A/B does not affect the spontaneous fusion of SVs in silenced TKO neurons (Figure 25, Table 25). Thus, the remaining Syt1 molecules on the SV appear to be sufficient to inhibit spontaneous SV fusion, while evoked neurotransmission potentially requires higher vesicular Syt1 copy numbers. Quantitative analysis and manipulation of vesicular Syt1 levels directly e.g. by varying the re-expression of Syt1 in Syt1 KO neurons could help to estimate how many Syt1 molecules are required to restrain spontaneous SV fusion but still impair evoked release. Thereby, it would be possible to determine how many Syt1 molecules are needed to mediate its respective functions during SV exocytosis e.g. in the observed calcium cooperativity triggering SV fusion (Schneggenburger and Neher, 2000).

### 5.2.3. Speed of SV retrieval independent of Syt1 sorting

So far we can conclude that maintenance of Syt1 levels is dependent on its correct sorting by SV2 and Stn2. Moreover, Syt1 missorting and accompanied Syt1 loss correlate with impaired neurotransmission in the absence of SV2 and Stn2. To prevent the loss of crucial SV proteins and defective neurotransmission mammalian synapses appear to safeguard the retrieval of SV proteins by multiple mechanisms. This endows mammals with a much more efficient and precise SV reformation compared to a system based on one sorting adaptor. Any disturbances of synaptic transmission can be compensated more readily. Especially in the complex mammalian nervous system many signals have to be integrated by balanced inhibitory and excitatory neurons. As inhibitory neurons are characterized by tonic activity (Hausser and Clark, 1997), the SV reformation in these neurons is particularly essential to balance excitatory inputs avoiding severe consequences at the organism level such as epileptic seizures.

In contrast, Syt1 sorting is dispensable for the speed of endocytosis. Syt1 is incorporated incorrectly during SV reformation in the absence of Stn2 and SV2 (Figure 23), but we do not observe decelerated endocytic retrieval (Figure 27, Figure 28). Also the impaired Syb2 sorting in the absence of AP180 did not dramatically compromise endocytic retrieval (Koo et al., 2015). Loss of AP180 only mildly slowed Syb2 internalization, while Syt1 retrieval remained completely unperturbed. These data support a SV endocytosis mechanism with predominantly separated membrane retrieval and SV reformation as discussed above (s. section 5.1.2) and implies that SV protein sorting is not required for rapid

SV retrieval. Moreover, it contradicts the idea that SV proteins such as Syt1 and Syb2 serve as sole cargo molecules facilitating endocytic retrieval by recruitment of endocytic proteins, when CME is predominantly acting on ELVs to reform SVs. Alternatively, SV proteins could regulate SV retrieval by clustering SV proteins functioning as "endocytosis hubs". Such roles have been proposed for VGLUT1 and Syt1 (Koch and Holt, 2012; Pan et al., 2015): The knockdown of VGLUT1 selectively delayed the retrieval kinetics of SV2 and Syp endocytosis, while Syt1 retrieval remained unaltered (Pan et al., 2015). These data together with the severe endocytic defect of Syt1 KO neurons (Nicholson-Tomishima and Ryan, 2004), led to the hypothesis that VGLUT1 and Syt1 might function in parallel to orchestrate SV retrieval by SV protein clustering. If this hypothesis was true, redistributed Syt1 would be less efficient in SV protein clustering and consequently would slow down endocytic kinetics. On the contrary our data show, that endocytic kinetics are accelerated when Syt1 is missorted. Thus, the role of Syt1 during endocytosis goes beyond its function as a cargo molecule or its possible contribution to SV protein clustering.

## 5.3. Coupling of SV exo- and endocytosis by SV proteins

Equally important as the question how functional SVs are reformed with the correct protein composition is the question how exo- and endocytosis are coupled to initiate endocytic retrieval. Various functional and physical links between SV exocytosis at the active zone and compensatory SV endocytosis at the periactive zone have been proposed. Among the potential coupling factors are the exocytosed SV proteins themselves that could trigger endocytosis once they appear on the surface of the presynapse as SV fusion is required to initiate SV endocytosis (Wu et al., 2005; Yamashita et al., 2005). Based on our data SV proteins do not regulate endocytic retrieval only by orchestrating SV protein sorting as a cargo molecule, but may trigger other mechanisms to initiate endocytosis.

Similarly important is the enrichment of the phosphoinositide $PI(4,5)P_2$ at the plasma membrane to activate SV exocytosis and to facilitate endocytosis (Di Paolo et al., 2004). Whether exocytosed SV proteins and $PI(4,5)P_2$ enriched sites are functionally connected has remained unclear. Since we observe accelerated endocytosis in the absence of Syt1 sorting proteins and the presence of surface-stranded Syt1 we hypothesized that Syt1 serves as a signal indicating SV fusion and initiates endocytic retrieval. Moreover, we provide a model according to which Syt1 at the axonal surface facilitates the local $PI(4,5)P_2$ synthesis at the presynapse by recruiting the $PI(4,5)P_2$ synthesizing kinase PIPK1γ to the plasma membrane.

### 5.3.1. Surface-localized Syt1 as an exo-endocytic coupling factor

Syt1 is one of the SV proteins associated with a role in coupling exo- and endocytosis. The manipulation of Syt1 levels affected SV endocytosis in all model systems tested suggesting an evolutionary conserved role of Syt1 in SV recycling. Sustained or acute loss of Syt1 during endocytosis in *C. elegans*, *D. melanogaster* or *M. musculus* led to defects in SV endocytosis characterized by slow retrieval kinetics (Jorgensen et al., 1995; Nicholson-Tomishima and Ryan, 2004; Poskanzer et al., 2006; Poskanzer et al., 2003). In contrast, overexpression of Syt1 in *D. melanogaster* significantly increased the internalization of the membrane dye FM1-43 during SV retrieval (Fergestad and Broadie, 2001). Interestingly, the deletion of Stn2 results in surface accumulation of Syt1, which correlates with an increased rate of SV retrieval in mouse primary hippocampal cultures. Surface-stranded Syt1 mutants that either are unable to bind Stn2 or are primarily targeted to the plasma membrane, can phenocopy these fast SV retrieval kinetics (Kononenko et al., 2013). The results described in this study agree with these published data and further emphasize Syt1's role in SV exo- and endocytosis. The depletion of SV2A/B mimics the increased surface-stranding of Syt1 observed in the Stn2 KO neurons and more importantly also accelerates the endocytic retrieval of Syt1- and Syp-pHluorin reporters. The combined loss of Stn2 and SV2A/B facilitates SV endocytosis even further correlating with an even stronger Syt1 surface accumulation (Figure 27). While results of SV2A/B depleted neurons are more difficult to interpret due to the concomitant profound loss of total Syt1 levels, we examined the functional role of Syt1 more in detail in Stn2 deficient neurons. Interestingly, the endocytic facilitation in Stn2 KO neurons represents a use-dependent phenotype: It is more pronounced during repetitive high frequency stimulation when more components such as Syt1 molecules are released from SVs into the presynaptic membrane. In contrast, low frequency stimulation at 10 Hz only mildly accelerates endocytic retrieval (Figure 28). Capacitance measurements independently confirmed our pHluorin data and revealed facilitated membrane retrieval in Stn2 KO mice, which was most striking at repetitive and strong depolarization of presynaptic terminals (Figure 30). Thus, endocytic SV protein as well as membrane retrieval are both facilitated in the absence of Stn2.

The compromised high-fidelity sorting of Syt1 in Stn2 and SV2A/B deficient neurons during repetitive rounds of stimulation will consequently reduce the number of vesicular Syt1 (Figure 23). At the same time surface-stranded Syt1 could block release sites. Thus, efficient SV exocytosis could be reduced and less fused SV material would need to be retrieved accounting for faster endocytic kinetics. However, pHluorin experiments show that not only

endocytosis is significantly facilitated in Stn2 depleted neurons, but also exocytosis of SVs is substantially increased, particularly during prolonged neuronal stimulation (Figure 29). Therefore, SV exocytosis and endocytosis are augmented in neurons with surface-stranded Syt1 in the absence of Stn2.

### 5.3.2. PI(4,5)$P_2$ as an effector molecule of surface-stranded Syt1

Our data suggest that the surface accumulation of Syt1 facilitates the coupling of SV exo- and endocytosis. The question remains how redistributed Syt1 exerts its role as a coupling signal. An effector molecule that has roles in SV release and retrieval and has altered levels in Stn2 KO neurons, is the phospholipid PI(4,5)$P_2$. The levels of PI(4,5)$P_2$ are significantly elevated in the presynaptic terminals of Stn2 deficient neurons (Figure 32). In contrast, the influx of calcium, another potential second messenger for SV exo- and endocytic coupling, remained unchanged during neuronal stimulation of Stn2 KO neurons (Figure 31). Moreover, the increased PI(4,5)$P_2$ levels correlate with the surface-stranding of Syt1. SV2A/B depleted neurons display a similar elevation of PI(4,5)$P_2$ levels (Figure 34A), while neuronal silencing reduced the activity-dependent Syt1 surface accumulation as well as the PI(4,5)$P_2$ levels (Figure 22 and Figure 34B, C). The elevated PI(4,5)$P_2$ levels provide an explanation for augmented SV exo- and endocytosis based on earlier work. Several studies have shown that increased PI(4,5)$P_2$ levels promote the fusion of secretory vesicles (Milosevic et al., 2005; Walter et al., 2017) and are required for endocytic retrieval in neuronal and non-neuronal cells (Antonescu et al., 2011; Di Paolo et al., 2004; Puchkov and Haucke, 2013). PI(4,5)$P_2$ enrichment at the plasma membrane serves as a platform to recruit and bind proteins, which are essential for the various trafficking processes. During exocytosis PI(4,5)$P_2$ clusters syntaxin 1A and binds the C2B domain of Syt1 facilitating SV release (Honigmann et al., 2013; Schiavo et al., 1996; van den Bogaart et al., 2011). Similarly, PI(4,5)$P_2$ is required for endocytic retrieval and allows the assembly of endocytic proteins, membrane shaping proteins and proteins involved in membrane scission like dynamin. Moreover, its turnover has been reported to be an essential aspect during the maturation of CME in non-neuronal cells (Posor et al., 2015) and is crucial for SV recycling in the synaptic terminal. The deletion of synaptojanin inhibits the hydrolysis of PI(4,5)$P_2$ and consequently arrests SV reformation at the stage of clathrin-coated vesicles resulting in synaptic depression (Cremona et al., 1999). The calcium-dependent activation of PLC during exocytosis provides an alternative degradation pathway for PI(4,5)$P_2$ producing DAG and $IP_3$. DAG in turn can regulate SV

release by activating Munc13 (Rosenmund et al., 2002). The extent of PI(4,5)$P_2$ metabolism at release sites has not been quantified extensively. So far a reduction of PI(4,5)$P_2$ levels at the plasma membrane after neuronal activity has been shown in synaptic boutons (Micheva et al., 2001). In addition, the activity-dependent compound release in mast cells is accompanied by substantial PLC-mediated depletion of PI(4,5)$P_2$ at the plasma membrane that is restored subsequently (Hammond et al., 2006). Given its crucial role in SV exocytosis, replenishment of the PI(4,5)$P_2$ pool at the active zone seems to be important during SV recycling to allow sustained neurotransmission.

The interaction of the PI(4,5)$P_2$ synthesizing PIPK1γ and Syt1 (Figure 35) corroborated the functional correlation of Syt1 redistribution and increased PI(4,5)$P_2$ levels. Moreover, the superresolution nanoscopy revealed a selective relocalization of PIPK1γ towards the plasma membrane in Stn2 deficient neurons (Figure 39). Interestingly, the ectopic overexpression of Syt1 in HEK cells mimics the surface-stranding of Syt1 due to the absence of Stn2 and SV2 in these cells and yields an elevation of PI(4,5)$P_2$ levels (Figure 36) akin to effects observed in Stn2 and/or SV2 depleted neurons. Thus, we hypothesize that Syt1 on the axonal surface regulates local PI(4,5)$P_2$ synthesis by recruitment of PIPK1γ to the plasma membrane. On the one hand, it facilitates PI(4,5)$P_2$ dependent endocytosis and on the other hand provides a local PI(4,5)$P_2$ pool to activate the release machinery for SV exocytosis. Replenishment of PI(4,5)$P_2$ levels by PIPK1γ allows for sustained SV release after PLC-mediated PI(4,5)$P_2$ turnover. In the absence of Stn2, this coupling becomes even more overt as PIPK1γ is recruited closer to or near release sites by significantly elevated Syt1 surface accumulation. The increased PI(4,5)$P_2$ synthesis in turn allows the substantial increase of SV exocytosis and the acceleration of endocytic retrieval in Stn2 deficient neurons (Figure 43).

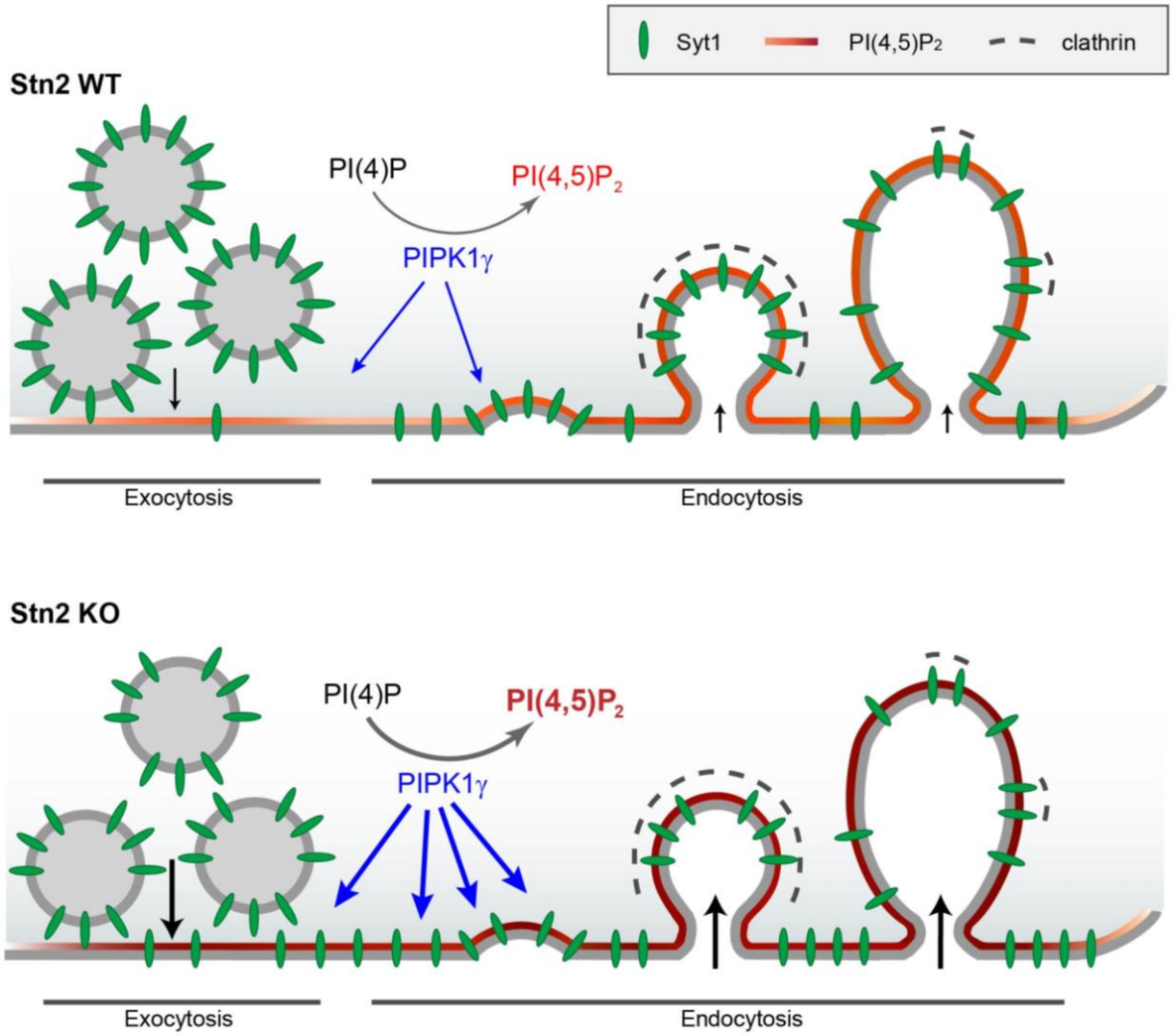


**Figure 43: Hypothetical model for Syt1-mediated coupling of SV exo- and endocytosis by facilitating PI(4,5)$P_2$ synthesis.** In the WT exocytosed surface-stranded Syt1 (green) interacts and recruits PIPK1γ to or near release sites to locally synthesize PI(4,5)$P_2$ (red cytoplasmic membrane layer) at the plasma membrane. At the active zone the PI(4,5)$P_2$ pool allows efficient SV release, while PI(4,5)$P_2$ at the periactive zone is required to initiate clathrin- (grey) dependent and independent endocytic retrieval. In the absence of Stn2, Syt1 is redistributed to the neuronal surface, directing PIPK1γ closer to the plasma membrane. Thus, PI(4,5)$P_2$ is even more enriched at the plasma membrane (dark red) facilitating SV exocytosis as well as endocytic retrieval (bold arrows).

To test our model additional experiments are required. First of all, the overexpression of a mutant Syt1 in WT neurons that is predominantly targeted to the plasma membrane and facilitates SV endocytosis, should be accompanied by an elevation of PI(4,5)$P_2$. Likewise, we hypothesize that the impaired SV retrieval in the absence of Syt1 (Nicholson-Tomishima and Ryan, 2004) can be explained by reduced PIPK1γ recruitment to the plasma membrane and subsequently results in lower PI(4,5)$P_2$ levels, especially during stimulation. Specific labeling of PI(4,5)$P_2$ in resting and stimulation conditions of either WT, Syt1 overexpressing or Syt1 depleted neurons should reveal, if PI(4,5)$P_2$ levels are changed substantially when Syt1 levels

are manipulated. Given the moderate reduction of $PI(4,5)P_2$ levels in PIPK1γ KO mice (Di Paolo et al., 2004), we do not expect a dramatic loss of total $PI(4,5)P_2$ levels in Syt1 depleted neurons. Besides, PIPK1γ can be recruited by alternative pathways including Arf6, talin and AP-2 (Di Paolo et al., 2002; Krauss et al., 2003; Krauss et al., 2006; Nakano-Kobayashi et al., 2007). In contrast, the Syt1-PIPK1γ interaction, especially during neuronal activity, could provide a temporally and spatially controlled $PI(4,5)P_2$ pool that may be crucial for neurotransmission. Manipulating this pool either by external application of membrane-permeant $PI(4,5)P_2$ derivatives (Walter et al., 2017) or by regulating $PI(4,5)P_2$ metabolism during SV exo- and endocytosis e.g. with optogenetic systems should further elucidate $PI(4,5)P_2$ importance to couple SV release and endocytic retrieval.

The synthesis of $PI(4,5)P_2$ and the origin of its precursor PI(4)P remain an open questions. So far $PI(4,5)P_2$ labelings suggested that $PI(4,5)P_2$ is absent from secretory vesicles and predominantly localized on the plasma membrane (Hammond et al., 2006; Holz et al., 2000; Micheva et al., 2001). These observations are consistent with the subcellular fractionation of PIPK1γ in synaptosomes: PIPK1γ is present, but not enriched in the crude SV fraction, similar to other cytosolic proteins involved in SV recycling such as dynamin and synaptojanin (Wenk et al., 2001). Moreover, $PI(4,5)P_2$ is degraded during SV reformation by synaptojanin. Due to the dual phosphatase activity of synaptojanin (Mani et al., 2007), $PI(4,5)P_2$ is either hydrolyzed to PI(4)P or PI on SVs, which can potentially be used as a substrate by other kinases. Early studies associated a 4-kinase activity with SVs (Wiedemann et al., 1998), suggesting SVs as a potential source for PI(4)P. Later, the PI 4-kinase type IIα was proposed to be localized on SVs (Guo et al., 2003). However, the recruitment of PI4KIIα to SVs and the regulation of its activity on SVs during SV recycling are still enigmatic. In general, the family of PI 4-kinases is implicated in cellular trafficking and Golgi function. Specifically the PI 4-kinases PI4KIIα and IIIα have been shown to mediate PI(4)P synthesis on the plasma membrane in non-neuronal cells (Balla and Balla, 2006; Tan and Brill, 2014). Interestingly, deletion of PI4KIIIα in mouse embryonic fibroblasts (MEF) selectively depleted the plasma membrane pool of PI(4)P and reduced $PI(4,5)P_2$ levels as well (Nakatsu et al., 2012) suggesting a tight link between PI(4)P at the plasma membrane and $PI(4,5)P_2$ synthesis. In contrast, acute depletion of PI(4)P at the plasma membrane by rapamycin recruitment of Sac1 phosphatase did not affect $PI(4,5)P_2$ replenishment after PLC-mediated degradation in COS-7 cells (Hammond et al., 2012). Therefore, the PI(4)P supply for $PI(4,5)P_2$ synthesis on the neuronal surface could either originate from exocytosed SVs or from a PI(4)P pool on the plasma membrane. Whether the latter is a resting pool or is spatio-temporally controlled

during neurotransmission by PI 4-kinases remains to be examined. Interestingly, we observe an activity-dependent increase of free PI(4)P with comparable levels in WT and Stn2 deficient neurons (Figure 33), suggesting that the elevated $PI(4,5)P_2$ synthesis during stimulation does not deplete the PI(4)P pool in the presynaptic terminal.

### 5.3.3. Syt1 interacts and recruits PIPK1γ

We identify a novel interaction of $PI(4,5)P_2$ synthesizing kinase PIPK1γ and Syt1 (Figure 35A). The C2B domain of Syt1 is essential and sufficient to mediate binding (Figure 35B). Moreover, superresolution gSTED microscopy revealed a tendency for elevated PIPK1γ levels in the presynapse of Stn2 KO neurons compared to WT neurons (Figure 39D), while total PIPK1γ levels assessed with confocal microscopy (Figure 38C) and western blot analysis were not changed in Stn2 WT and KO mice (Kononenko et al., 2013). Strikingly, Stn2 deficient neurons display a significant relocalization of PIPK1γ towards the active zone (Figure 39E), which lead us to propose a model according to which surface-stranded Syt1 mediates PIPK1γ recruitment to the plasma membrane to facilitate local $PI(4,5)P_2$ synthesis.

Immunoprecipitation from rat synaptosome extracts demonstrated the interaction of PIPK1γ and Syt1, which is potentiated in the presence of elevated calcium concentrations (Figure 35A). These results may suggest a facilitated interaction during neuronal activity, correlating with the regulation of the kinase activity itself during neurotransmission (Nakano-Kobayashi et al., 2007). This interaction of Syt1 and PIPK1γ provides a potential mechanism how the $PI(4,5)P_2$ pool can be replenished at the release site after PLC-mediated degradation (Hammond et al., 2006; Micheva et al., 2001; Rosenmund et al., 2002). At the same time $PI(4,5)P_2$ can be generated for recruiting endocytic proteins during $PI(4,5)P_2$-dependent endocytosis. This endocytic $PI(4,5)P_2$ pool can be amplified locally by AP-2 binding to $PI(4,5)P_2$, which in a positive feedback loop further recruits PIPK1γ (Nakano-Kobayashi et al., 2007). Interestingly, Syt1 is not completely retrieved from the neuronal surface during endocytosis unlike other SV proteins such as SV2 and VGLUT1. 10-20 % of the total Syt1 molecules are present at the plasma membrane (Figure 18) (Kononenko et al., 2013; Koo et al., 2015). These surface-resident Syt1 molecules could assist in maintaining the $PI(4,5)P_2$ levels at the plasma membrane due to the moderate binding of Syt1 and PIPK1γ already during resting conditions.

Future experiments need to address the direct interaction of the C2B domain and the kinase to test our hypothetical model. The identification of the putative binding interface

would be required for crucial rescue experiments e.g. in Syt1 deficient neurons with described exo- and endocytosis defects. Whether the interaction of Syt1 and PIPK1γ is conserved among Syt isoforms will be interesting in order to learn more about the functional roles of various Syts. We would expect that the isoforms, Syt1 and Syt2, are similar with respect to their PIPK1γ binding site, as the calyx of Held terminals express Syt2 and display accelerated membrane retrieval in the absence of Stn2 (Figure 30).

In addition, the specificity of PIPK1 isoforms in regards to their interaction with Syt1 needs to be addressed. The overexpression of Syt1 in HEK cells was able to elevate $PI(4,5)P_2$ levels even in the presence of co-expressed inactive PIPK1γ (Figure 36, Figure 37). Thus, either Syt1 can also interact with other endogenous PIPK1 isoforms in HEK cells or the inactive PIPK1γ dimerizes with endogenous PIPK1γ and, thus, is not fully abrogating PIPK1γ activity. Even though PIPK1γ is the major isoform in the synapse (Wenk et al., 2001), the α and β isoforms could conceivably contribute to Syt1 regulated $PI(4,5)P_2$ synthesis.

Apart from the structural analysis of the Syt1 and PIPK1γ interaction *in vitro*, it will be important to show an increased complex formation of Syt1 and PIPK1γ in Stn2 deficient neurons at the neuronal surface. According to our hypothesis a surface biotinylation of Syt1 in cultured neurons of WT and Stn2 KO mice and a subsequent analysis of bound interaction partners should reveal elevated PIPK1γ levels in Stn2 depleted neurons akin to the redistribution of PIPK1γ shown in gSTED superresolution. Likewise, we would expect a reduction of PIPK1γ recruitment in Syt1 KO neurons, which can be visualized with superresolution nanoscopy. Accordingly, knockdown of Syt1 in Stn2 depleted neurons should reverse the observed relocalization of PIPK1γ towards the plasma membrane in Stn2 KO neurons. In addition, the manipulation of PIPK1γ in neurons by siRNA-mediated depletion or pharmacological inactivation (Wright et al., 2014) would help to corroborate the specificity of PIPK1γ in our model.

The interaction and recruitment of PIPK1γ by Syt1 to the neuronal surface provides a potential mechanism of how PIPK1γ function can be regulated. However, also other mechanisms can contribute to the recruitment of the cytosolic PIPK1γ to the plasma membrane apart from Syt1. Thus, to elucidate how Arf6 and talin together with surface Syt1 mediate PIPK1γ recruitment during neurotransmission is crucial to understand the regulation of $PI(4,5)P_2$ turnover during SV recycling. Moreover, a retrograde signaling cascade mediated by NO after NMDA receptor activation at the postsynapse has been suggested to activate PIPK1γ as well (Micheva et al., 2001). At mature calyces of Held NO stimulates the cGMP-

dependent protein kinase (PKG), which regulates RhoA and RhoA kinase activity and in turn elevates PI(4,5)$P_2$ levels by PIPK1γ activation (Eguchi et al., 2012; Taoufiq et al., 2013).

Even though calcium influx alone is insufficient to couple SV exo- and endocytosis, it does have a major role in regulating various aspects of SV recycling. The PI(4,5)$P_2$ turnover in the synapse is governed by the activity-dependent dephosphorylation of PIPK1γ and synaptojanin mediated by calcineurin (Lee et al., 2004; Nakano-Kobayashi et al., 2007). As calcineurin is a downstream target of the calcium binding protein calmodulin, both PIPK1γ and synaptojanin are activated by calcium influx during neurotransmission. Furthermore, calcium binding to Syt1 is proposed to trigger the conformational change, which allows the tight SNARE complex assembly and SV exocytosis (Zhou et al., 2017). During endocytosis Syt1 is thought to act as a calcium sensor as well (Yao et al., 2011). The interaction of PIPK1γ and Syt1 is also potentiated in the presence of calcium ions reflecting either that the complex formation is facilitated in the dephosphorylated state of PIPK1γ or that the calcium bound C2B domain of Syt1 has an enhanced affinity for PIPK1γ. Therefore, Syt1, PIPK1γ activity and PI(4,5)$P_2$ synthesis seem to be regulated on multiple levels to couple SV exocytosis and endocytic retrieval.

### 5.3.4. Other potential effectors regulated by PI(4,5)$P_2$ in SV exo- and endocytosis

A plethora of PI(4,5)$P_2$ interacting proteins have been identified, which are associated with SV exocytosis and endocytic retrieval (see 1.7.1 and 1.7.2). The question remains: Which are the key proteins that are recruited by elevated PI(4,5)$P_2$ levels during SV recycling? The surface accumulation of Syt1 in the absence of Stn2 allows us to investigate these effector proteins that drive the augmented SV fusion and endocytosis.

The elevated SV fusion observed in Stn2 KO neurons (Figure 29) is most likely explained by a faster replenishment and increased PI(4,5)$P_2$ levels at the release sites (Figure 43) that may allow a more efficient SV release. At the molecular level elevated PI(4,5)$P_2$ levels can facilitate membrane insertion of the remaining vesicular Syt1. This would help to destabilize the membrane promoting fast SV fusion (Hui et al., 2009; Martens et al., 2007). Moreover, the calcium binding affinity of Syt1 is elevated upon PI(4,5)$P_2$ binding (van den Bogaart et al., 2012), which will increase the calcium responsiveness of SV exocytosis (Figure 42). Whether syntaxin 1A clusters are facilitated at the active zone by elevated PI(4,5)$P_2$ levels remains to be analyzed. However, increased docking of SVs and a larger

readily releaseable pool can be excluded as a reason for augmented SV exocytosis as electron microscopy of Stn2 KO mossy fiber synapses has not revealed significant changes in SV numbers within 100 nm from the active zone (Kononenko et al., 2013).

Among the endocytic proteins recruited by $PI(4,5)P_2$, AP-2 does not seem to redistribute in response to elevated $PI(4,5)P_2$ during stimulation or in the absence of Stn2 (Figure 40). This observation is consistent with AP-2's function in SV reformation from ELVs (Kononenko et al., 2014; Soykan et al., 2017). Other candidates that may mediate accelerated SV retrieval upon elevation of $PI(4,5)P_2$ are dynamin and endophilin. Endophilin does not specifically bind $PI(4,5)P_2$, but can be recruited by the increase of negative charges at the plasma membrane (Rao and Haucke, 2011). Functionally endophilin A2 is involved both in clathrin-independent endocytosis of bacterial Shiga and cholera toxins in non-neuronal cells (Renard et al., 2015) as well as in SV recycling (Kononenko et al., 2014). Endophilin A2 could therefore contribute to the accelerated endocytic retrieval in Stn2 KO neurons. In addition to endophilin, dynamin represents an even better effector candidate as it binds via its PH domain to $PI(4,5)P_2$, $PI(3,4)P_2$ and $PI(3,4,5)P_3$ (Salim et al., 1996; Zheng et al., 1996). The interaction with $PI(4,5)P_2$ allows oligomerization of dynamin and the dynamin-mediated fission reaction (Reubold et al., 2015), which is required for all modes of SV membrane retrieval. An increased recruitment or activation of dynamin by elevated $PI(4,5)P_2$ levels would provide a plausible explanation for the accelerated SV endocytosis in Stn2 deficient neurons and needs to be further examined.

$PI(4,5)P_2$ enriched membranes can modulate actin dynamics in many cellular processes by regulating actin binding proteins or by Rho GTPases (Saarikangas et al., 2010). In the synapse actin is highly enriched (Cingolani and Goda, 2008) and has recently gained attention for being functionally important in SV endocytosis. Indeed, depletion of actin as well as of actin binding proteins or pharmacological inhibition of actin dynamics affect endocytic retrieval (Soykan et al., 2017; Watanabe et al., 2013b; Wu et al., 2016). Components of the actin cytoskeleton are potential effectors of elevated $PI(4,5)P_2$ levels that might mediate accelerated SV retrieval. Interestingly, the ectopic expression of Syt1 in non-neuronal cells has been associated with alterations of the actin cytoskeleton and of neurite outgrowth, as it enhances filopodia formation (Figure 36 and (Feany and Buckley, 1993)). Increased filopodia outgrowth in Syt1 overexpressing fibroblasts was associated with $PI(4,5)P_2$ on the plasma membrane (Johnsson and Karlsson, 2012). However, the relevance of Syt1 induced actin remodeling for SV recycling and exo-/ endocytic coupling in the presynaptic terminal has not been addressed so far. Monitoring actin cytoskeleton dynamics

in the presence of elevated PI(4,5)$P_2$ levels and Syt1 surface accumulation would allow us to unravel whether a change in actin dynamics is implicated in faster SV retrieval kinetics (Ganguly et al., 2015; Lemieux et al., 2014). The exact mechanism and the molecular factors that are required for the actomyosin cytoskeleton function during SV endocytosis are not completely understood. Actin binding proteins have emerged as relevant molecules from recent studies and can be potential candidates. Formins can bind to negatively charged membranes including PI(4,5)$P_2$ to facilitate linear actin filament formation and are required for SV endocytosis (Ganguly et al., 2015; Soykan et al., 2017). On the contrary, N-WASP promotes branched actin filaments via the Arp2/3 complex, is regulated by PI(4,5)$P_2$ (Derivery and Gautreau, 2010; Tomasevic et al., 2007) and appears not to be essential for SV endocytosis (Soykan et al., 2017). Therefore, we would not expect a functional redistribution of N-WASP to the plasma membrane in Stn2 depleted neurons to facilitate endocytic retrieval kinetics, whereas proteins of the formin family are more likely to be functionally involved.

# 6. Outlook

Despite decades of research the mechanism of SV recycling remain incompletely understood. This study contributes to a more detailed understanding of SV exo- and endocytosis with respect to the high-fidelity sorting of SV proteins after full collapse fusion and the coupling of SV release and retrieval.

Unraveling the molecular details of SV recycling within central synapses is of pivotal importance to understand and treat several neurological disorders. Indeed, many presynaptic proteins, including SV2 and Stn2, are associated with neurological and neurodegenerative diseases. While mutations in Stn2 are implicated in schizophrenia and autism spectrum disorders (Breedveld et al., 2010; Luan et al., 2011), SV2 is involved in late onset Alzheimer's disease and epilepsy since it is an important antiepileptic drug target (Lynch et al., 2004; Nowack et al., 2011; Rhinn et al., 2013). Our study demonstrates that SV2 modulates efficient neurotransmission at least partially by chaperoning Syt1 retrieval. The loss of SV2A accompanied by a dramatic depletion of Syt1 might especially affect the balance of inhibitory and excitatory inputs. This imbalance is believed to be the major cause for epilepsy and could be an explanation for the observed seizures in DKO and TKO mice. The topology of SV2 fosters the idea of other so far unknown SV2 functions during neurotransmission apart from Syt1 sorting and has to be addressed in the future. Moreover, human mutations in Syt1 have been associated with neurological impairments affecting SV recycling dynamics (Baker et al., 2015). Still, future research has to elucidate the underlying molecular mechanisms of these disorders to develop new therapeutic approaches for efficient treatment.

Furthermore, we identify a new role of Syt1 in coupling exo- and endocytosis and suggest a novel model, which combines a SV protein- and lipid-based mechanism to initiate SV endocytosis after exocytic release. We show that exocytosed Syt1 serves as a signal and triggers the synthesis of $PI(4,5)P_2$ at the plasma membrane by recruiting PIPK1γ to or near release sites. This emphasizes $PI(4,5)P_2$'s crucial role in SV recycling by facilitating $PI(4,5)P_2$ dependent endocytosis as well as by replenishing $PI(4,5)P_2$ levels at the release site for sustained neurotransmission.

$PI(4,5)P_2$ is the best characterized PI species due to its high abundance and still many aspects of its functional relevance and dynamic turnover are enigmatic especially in the presynaptic terminal. First attempts to visualize $PI(4,5)P_2$ during neuronal activity using GFP-tagged PH domain were made by Micheva and colleagues (Micheva et al., 2001). New

advances regarding superresolution live-cell imaging as well as protein labeling with bright fluorescent chemical probes and small polypeptide tags will provide a deeper insight into the precise localization of $PI(4,5)P_2$ pools during SV recycling within the presynapse. The localization together with functional manipulation of $PI(4,5)P_2$ will help to gain a better understanding of this crucial phosphoinositide.

Apart from plasma membrane localized $PI(4,5)P_2$, PIs are not well understood as landmarks in the presynaptic terminal. However, the importance of efficient PI conversion at the presynapse for preventing neurodegenerative diseases has been highlighted recently. A mutation in the phosphatase synaptojanin has been associated with early-onset Parkinson's disease and has unraveled the relevance of a so far underrated phosphatase activity (Cao et al., 2017; Vanhauwaert et al., 2017). PI conversion has been extensively studied in CME in non-neuronal cells (Posor et al., 2015). In contrast, the dominant role of CME for SV retrieval from the plasma membrane has been questioned. Multiple studies support a clathrin-independent membrane retrieval, which requires the subsequent SV reformation from ELVs. This ultimately raises the question of the lipid identity of these ELVs. As AP-2 specifically binds to $PI(4,5)P_2$ and mediates SV reformation from these ELVs, they probably do not represent bona fide endosomes characterized by PI(3)P, but are likely to still maintain the plasma membrane identity. How these ELVs communicate with other endosomal compartments to ensure quality control of SVs and the degradation of old SV proteins has to be addressed in the future as well. New superresolution imaging approaches with specific lipid probes or correlative light electron microscopy will provide great possibilities to analyze the membrane identity of ELVs and the dynamic conversion of PI species at presynaptic sites.

# 7. Bibliography


Albillos, A., Dernick, G., Horstmann, H., Almers, W., Alvarez de Toledo, G., and Lindau, M. (1997). The exocytotic event in chromaffin cells revealed by patch amperometry. Nature *389*, 509-512.

Ales, E., Tabares, L., Poyato, J.M., Valero, V., Lindau, M., and Alvarez de Toledo, G. (1999). High calcium concentrations shift the mode of exocytosis to the kiss-and-run mechanism. Nature cell biology *1*, 40-44.

Andrews, J., Smith, M., Merakovsky, J., Coulson, M., Hannan, F., and Kelly, L.E. (1996). The stoned locus of Drosophila melanogaster produces a dicistronic transcript and encodes two distinct polypeptides. Genetics *143*, 1699-1711.

Antonescu, C.N., Aguet, F., Danuser, G., and Schmid, S.L. (2011). Phosphatidylinositol-(4,5)-bisphosphate regulates clathrin-coated pit initiation, stabilization, and size. Mol Biol Cell *22*, 2588-2600.

Arioka, M., Nakashima, S., Shibasaki, Y., and Kitamoto, K. (2004). Dibasic amino acid residues at the carboxy-terminal end of kinase homology domain participate in the plasma membrane localization and function of phosphatidylinositol 5-kinase gamma. Biochemical and biophysical research communications *319*, 456-463.

Atluri, P.P., and Ryan, T.A. (2006). The kinetics of synaptic vesicle reacidification at hippocampal nerve terminals. The Journal of neuroscience : the official journal of the Society for Neuroscience *26*, 2313-2320.

Bai, J., Hu, Z., Dittman, J.S., Pym, E.C., and Kaplan, J.M. (2010). Endophilin functions as a membrane-bending molecule and is delivered to endocytic zones by exocytosis. Cell *143*, 430-441.

Bai, J., Tucker, W.C., and Chapman, E.R. (2004). PIP2 increases the speed of response of synaptotagmin and steers its membrane-penetration activity toward the plasma membrane. Nature structural & molecular biology *11*, 36-44.

Bai, J., Wang, P., and Chapman, E.R. (2002). C2A activates a cryptic Ca(2+)-triggered membrane penetration activity within the C2B domain of synaptotagmin I. Proceedings of the National Academy of Sciences of the United States of America *99*, 1665-1670.

Bajjalieh, S.M., Frantz, G.D., Weimann, J.M., McConnell, S.K., and Scheller, R.H. (1994). Differential expression of synaptic vesicle protein 2 (SV2) isoforms. The Journal of neuroscience : the official journal of the Society for Neuroscience *14*, 5223-5235.

Baker, K., Gordon, S.L., Grozeva, D., van Kogelenberg, M., Roberts, N.Y., Pike, M., Blair, E., Hurles, M.E., Chong, W.K., Baldeweg, T., *et al.* (2015). Identification of a human synaptotagmin-1 mutation that perturbs synaptic vesicle cycling. The Journal of clinical investigation *125*, 1670-1678.

Balla, A., and Balla, T. (2006). Phosphatidylinositol 4-kinases: old enzymes with emerging functions. Trends in cell biology *16*, 351-361.

Balla, T. (2013). Phosphoinositides: tiny lipids with giant impact on cell regulation. Physiological reviews *93*, 1019-1137.

Bartholome, O., Van den Ackerveken, P., Sanchez Gil, J., de la Brassinne Bonardeaux, O., Leprince, P., Franzen, R., and Rogister, B. (2017). Puzzling Out Synaptic Vesicle 2 Family Members Functions. Frontiers in molecular neuroscience *10*, 148.

Behnia, R., and Munro, S. (2005). Organelle identity and the signposts for membrane traffic. Nature *438*, 597-604.

Bennett, M.K., Calakos, N., Kreiner, T., and Scheller, R.H. (1992). Synaptic vesicle membrane proteins interact to form a multimeric complex. The Journal of cell biology *116*, 761-775.

Betz, A., Ashery, U., Rickmann, M., Augustin, I., Neher, E., Sudhof, T.C., Rettig, J., and Brose, N. (1998). Munc13-1 is a presynaptic phorbol ester receptor that enhances neurotransmitter release. Neuron *21*, 123-136.

Breedveld, G.J., Fabbrini, G., Oostra, B.A., Berardelli, A., and Bonifati, V. (2010). Tourette disorder spectrum maps to chromosome 14q31.1 in an Italian kindred. Neurogenetics *11*, 417-423.

Brewer, K.D., Bacaj, T., Cavalli, A., Camilloni, C., Swarbrick, J.D., Liu, J., Zhou, A., Zhou, P., Barlow, N., Xu, J., *et al.* (2015). Dynamic binding mode of a Synaptotagmin-1-SNARE complex in solution. Nature structural & molecular biology *22*, 555-564.

Brose, N., Petrenko, A.G., Sudhof, T.C., and Jahn, R. (1992). Synaptotagmin: a calcium sensor on the synaptic vesicle surface. Science *256*, 1021-1025.

Buckley, K., and Kelly, R.B. (1985). Identification of a transmembrane glycoprotein specific for secretory vesicles of neural and endocrine cells. The Journal of cell biology *100*, 1284-1294.

Calakos, N., and Scheller, R.H. (1994). Vesicle-associated membrane protein and synaptophysin are associated on the synaptic vesicle. The Journal of biological chemistry *269*, 24534-24537.

Calderwood, D.A., Zent, R., Grant, R., Rees, D.J., Hynes, R.O., and Ginsberg, M.H. (1999). The Talin head domain binds to integrin beta subunit cytoplasmic tails and regulates integrin activation. The Journal of biological chemistry *274*, 28071-28074.

Cao, M., Wu, Y., Ashrafi, G., McCartney, A.J., Wheeler, H., Bushong, E.A., Boassa, D., Ellisman, M.H., Ryan, T.A., and De Camilli, P. (2017). Parkinson Sac Domain Mutation in Synaptojanin 1 Impairs Clathrin Uncoating at Synapses and Triggers Dystrophic Changes in Dopaminergic Axons. Neuron *93*, 882-896 e885.

Ceccarelli, B., Hurlbut, W.P., and Mauro, A. (1972). Depletion of vesicles from frog neuromuscular junctions by prolonged tetanic stimulation. The Journal of cell biology *54*, 30-38.

Ceccarelli, B., Hurlbut, W.P., and Mauro, A. (1973). Turnover of transmitter and synaptic vesicles at the frog neuromuscular junction. The Journal of cell biology *57*, 499-524.

Chang-Ileto, B., Frere, S.G., Chan, R.B., Voronov, S.V., Roux, A., and Di Paolo, G. (2011). Synaptojanin 1-mediated PI(4,5)P2 hydrolysis is modulated by membrane curvature and facilitates membrane fission. Dev Cell *20*, 206-218.

Chang, W.P., and Sudhof, T.C. (2009). SV2 renders primed synaptic vesicles competent for Ca2+ -induced exocytosis. The Journal of neuroscience : the official journal of the Society for Neuroscience *29*, 883-897.

Chappie, J.S., Mears, J.A., Fang, S., Leonard, M., Schmid, S.L., Milligan, R.A., Hinshaw, J.E., and Dyda, F. (2011). A pseudoatomic model of the dynamin polymer identifies a hydrolysis-dependent powerstroke. Cell *147*, 209-222.

Chen, X., Barg, S., and Almers, W. (2008). Release of the styryl dyes from single synaptic vesicles in hippocampal neurons. The Journal of neuroscience : the official journal of the Society for Neuroscience *28*, 1894-1903.

Cheung, G., and Cousin, M.A. (2012). Adaptor protein complexes 1 and 3 are essential for generation of synaptic vesicles from activity-dependent bulk endosomes. The Journal of neuroscience : the official journal of the Society for Neuroscience *32*, 6014-6023.

Chiang, H.C., Shin, W., Zhao, W.D., Hamid, E., Sheng, J., Baydyuk, M., Wen, P.J., Jin, A., Momboisse, F., and Wu, L.G. (2014). Post-fusion structural changes and their roles in exocytosis and endocytosis of dense-core vesicles. Nature communications *5*, 3356.

Chicka, M.C., Hui, E., Liu, H., and Chapman, E.R. (2008). Synaptotagmin arrests the SNARE complex before triggering fast, efficient membrane fusion in response to Ca2+. Nature structural & molecular biology *15*, 827-835.

Cingolani, L.A., and Goda, Y. (2008). Actin in action: the interplay between the actin cytoskeleton and synaptic efficacy. Nature reviews. Neuroscience *9*, 344-356.

Clayton, E.L., and Cousin, M.A. (2009). The molecular physiology of activity-dependent bulk endocytosis of synaptic vesicles. Journal of neurochemistry *111*, 901-914.

Collins, B.M., McCoy, A.J., Kent, H.M., Evans, P.R., and Owen, D.J. (2002). Molecular architecture and functional model of the endocytic AP2 complex. Cell *109*, 523-535.

Cousin, M.A., and Robinson, P.J. (2001). The dephosphins: dephosphorylation by calcineurin triggers synaptic vesicle endocytosis. Trends in neurosciences *24*, 659-665.

Craxton, M. (2010). A manual collection of Syt, Esyt, Rph3a, Rph3al, Doc2, and Dblc2 genes from 46 metazoan genomes--an open access resource for neuroscience and evolutionary biology. BMC genomics *11*, 37.

Cremona, O., Di Paolo, G., Wenk, M.R., Luthi, A., Kim, W.T., Takei, K., Daniell, L., Nemoto, Y., Shears, S.B., Flavell, R.A., *et al.* (1999). Essential role of phosphoinositide metabolism in synaptic vesicle recycling. Cell *99*, 179-188.

Crowder, K.M., Gunther, J.M., Jones, T.A., Hale, B.D., Zhang, H.Z., Peterson, M.R., Scheller, R.H., Chavkin, C., and Bajjalieh, S.M. (1999). Abnormal neurotransmission in mice lacking synaptic vesicle protein 2A (SV2A). Proceedings of the National Academy of Sciences of the United States of America *96*, 15268-15273.

Custer, K.L., Austin, N.S., Sullivan, J.M., and Bajjalieh, S.M. (2006). Synaptic vesicle protein 2 enhances release probability at quiescent synapses. The Journal of neuroscience : the official journal of the Society for Neuroscience *26*, 1303-1313.

Dani, A., Huang, B., Bergan, J., Dulac, C., and Zhuang, X. (2010). Superresolution imaging of chemical synapses in the brain. Neuron *68*, 843-856.

Dardou, D., Dassesse, D., Cuvelier, L., Deprez, T., De Ryck, M., and Schiffmann, S.N. (2011). Distribution of SV2C mRNA and protein expression in the mouse brain with a particular emphasis on the basal ganglia system. Brain research *1367*, 130-145.

De Matteis, M.A., and Godi, A. (2004). PI-loting membrane traffic. Nature cell biology *6*, 487-492.

Delvendahl, I., Vyleta, N.P., von Gersdorff, H., and Hallermann, S. (2016). Fast, Temperature-Sensitive and Clathrin-Independent Endocytosis at Central Synapses. Neuron *90*, 492-498.

Derivery, E., and Gautreau, A. (2010). Generation of branched actin networks: assembly and regulation of the N-WASP and WAVE molecular machines. BioEssays : news and reviews in molecular, cellular and developmental biology *32*, 119-131.

Di Paolo, G., and De Camilli, P. (2006). Phosphoinositides in cell regulation and membrane dynamics. Nature *443*, 651-657.

Di Paolo, G., Moskowitz, H.S., Gipson, K., Wenk, M.R., Voronov, S., Obayashi, M., Flavell, R., Fitzsimonds, R.M., Ryan, T.A., and De Camilli, P. (2004). Impaired PtdIns(4,5)P2 synthesis in nerve terminals produces defects in synaptic vesicle trafficking. Nature *431*, 415-422.

Di Paolo, G., Pellegrini, L., Letinic, K., Cestra, G., Zoncu, R., Voronov, S., Chang, S., Guo, J., Wenk, M.R., and De Camilli, P. (2002). Recruitment and regulation of phosphatidylinositol phosphate kinase type 1 gamma by the FERM domain of talin. Nature *420*, 85-89.

Dickson, E.J., Jensen, J.B., and Hille, B. (2014). Golgi and plasma membrane pools of PI(4)P contribute to plasma membrane PI(4,5)P2 and maintenance of KCNQ2/3 ion channel current. Proceedings of the National Academy of Sciences of the United States of America *111*, E2281-2290.

Diril, M.K., Wienisch, M., Jung, N., Klingauf, J., and Haucke, V. (2006). Stonin 2 is an AP-2-dependent endocytic sorting adaptor for synaptotagmin internalization and recycling. Dev Cell *10*, 233-244.

Dobrunz, L.E., and Stevens, C.F. (1997). Heterogeneity of release probability, facilitation, and depletion at central synapses. Neuron *18*, 995-1008.

Doray, B., Lee, I., Knisely, J., Bu, G., and Kornfeld, S. (2007). The gamma/sigma1 and alpha/sigma2 hemicomplexes of clathrin adaptors AP-1 and AP-2 harbor the dileucine recognition site. Mol Biol Cell *18*, 1887-1896.

Eberhard, D.A., Cooper, C.L., Low, M.G., and Holz, R.W. (1990). Evidence that the inositol phospholipids are necessary for exocytosis. Loss of inositol phospholipids and inhibition of secretion in permeabilized cells caused by a bacterial phospholipase C and removal of ATP. The Biochemical journal *268*, 15-25.

Edelmann, L., Hanson, P.I., Chapman, E.R., and Jahn, R. (1995). Synaptobrevin binding to synaptophysin: a potential mechanism for controlling the exocytotic fusion machine. EMBO J *14*, 224-231.

Eguchi, K., Nakanishi, S., Takagi, H., Taoufiq, Z., and Takahashi, T. (2012). Maturation of a PKG-dependent retrograde mechanism for exoendocytic coupling of synaptic vesicles. Neuron *74*, 517-529.

Ertunc, M., Sara, Y., Chung, C., Atasoy, D., Virmani, T., and Kavalali, E.T. (2007). Fast synaptic vesicle reuse slows the rate of synaptic depression in the CA1 region of hippocampus. The Journal of neuroscience : the official journal of the Society for Neuroscience *27*, 341-354.

Eshkind, L.G., and Leube, R.E. (1995). Mice Lacking Synaptophysin Reproduce and Form Typical Synaptic Vesicles. Cell Tissue Res *282*, 423-433.

Estes, P.S., Jackson, T.C., Stimson, D.T., Sanyal, S., Kelly, L.E., and Ramaswami, M. (2003). Functional dissection of a eukaryotic dicistronic gene: transgenic stonedB, but not stonedA, restores normal synaptic properties to Drosophila stoned mutants. Genetics *165*, 185-196.

Feany, M.B., and Buckley, K.M. (1993). The synaptic vesicle protein synaptotagmin promotes formation of filopodia in fibroblasts. Nature *364*, 537-540.

Feany, M.B., Lee, S., Edwards, R.H., and Buckley, K.M. (1992). The synaptic vesicle protein SV2 is a novel type of transmembrane transporter. Cell *70*, 861-867.

Feany, M.B., Yee, A.G., Delvy, M.L., and Buckley, K.M. (1993). The synaptic vesicle proteins SV2, synaptotagmin and synaptophysin are sorted to separate cellular compartments in CHO fibroblasts. The Journal of cell biology *123*, 575-584.

Fenster, S.D., Kessels, M.M., Qualmann, B., Chung, W.J., Nash, J., Gundelfinger, E.D., and Garner, C.C. (2003). Interactions between Piccolo and the actin/dynamin-binding protein Abp1 link vesicle endocytosis to presynaptic active zones. The Journal of biological chemistry *278*, 20268-20277.

Fergestad, T., and Broadie, K. (2001). Interaction of stoned and synaptotagmin in synaptic vesicle endocytosis. The Journal of neuroscience : the official journal of the Society for Neuroscience *21*, 1218-1227.

Fergestad, T., Davis, W.S., and Broadie, K. (1999). The stoned proteins regulate synaptic vesicle recycling in the presynaptic terminal. The Journal of neuroscience : the official journal of the Society for Neuroscience *19*, 5847-5860.

Ferguson, S.M., Raimondi, A., Paradise, S., Shen, H., Mesaki, K., Ferguson, A., Destaing, O., Ko, G., Takasaki, J., Cremona, O., *et al.* (2009). Coordinated actions of actin and BAR proteins upstream of dynamin at endocytic clathrin-coated pits. Dev Cell *17*, 811-822.

Fernandes, A.C., Uytterhoeven, V., Kuenen, S., Wang, Y.C., Slabbaert, J.R., Swerts, J., Kasprowicz, J., Aerts, S., and Verstreken, P. (2014). Reduced synaptic vesicle protein degradation at lysosomes curbs TBC1D24/sky-induced neurodegeneration. The Journal of cell biology *207*, 453-462.

Fernandez-Alfonso, T., Kwan, R., and Ryan, T.A. (2006). Synaptic vesicles interchange their membrane proteins with a large surface reservoir during recycling. Neuron *51*, 179-186.

Fernandez-Chacon, R., Konigstorfer, A., Gerber, S.H., Garcia, J., Matos, M.F., Stevens, C.F., Brose, N., Rizo, J., Rosenmund, C., and Sudhof, T.C. (2001). Synaptotagmin I functions as a calcium regulator of release probability. Nature *410*, 41-49.

Fernandez, I., Arac, D., Ubach, J., Gerber, S.H., Shin, O., Gao, Y., Anderson, R.G., Sudhof, T.C., and Rizo, J. (2001). Three-dimensional structure of the synaptotagmin 1 C2B-domain: synaptotagmin 1 as a phospholipid binding machine. Neuron *32*, 1057-1069.

Feutlinske, F., Browarski, M., Ku, M.C., Trnka, P., Waiczies, S., Niendorf, T., Stallcup, W.B., Glass, R., Krause, E., and Maritzen, T. (2015). Stonin1 mediates endocytosis of the proteoglycan NG2 and regulates focal adhesion dynamics and cell motility. Nature communications *6*, 8535.

Gad, H., Ringstad, N., Low, P., Kjaerulff, O., Gustafsson, J., Wenk, M., Di Paolo, G., Nemoto, Y., Crun, J., Ellisman, M.H., *et al.* (2000). Fission and uncoating of synaptic clathrin-coated vesicles are perturbed by disruption of interactions with the SH3 domain of endophilin. Neuron *27*, 301-312.

Gamper, N., Reznikov, V., Yamada, Y., Yang, J., and Shapiro, M.S. (2004). Phosphatidylinositol [correction] 4,5-bisphosphate signals underlie receptor-specific Gq/11-mediated modulation of N-type Ca2+ channels. The Journal of neuroscience : the official journal of the Society for Neuroscience *24*, 10980-10992.

Ganguly, A., Tang, Y., Wang, L., Ladt, K., Loi, J., Dargent, B., Leterrier, C., and Roy, S. (2015). A dynamic formin-dependent deep F-actin network in axons. The Journal of cell biology *210*, 401-417.

Genc, O., Kochubey, O., Toonen, R.F., Verhage, M., and Schneggenburger, R. (2014). Munc18-1 is a dynamically regulated PKC target during short-term enhancement of transmitter release. eLife *3*, e01715.

Geppert, M., Goda, Y., Hammer, R.E., Li, C., Rosahl, T.W., Stevens, C.F., and Sudhof, T.C. (1994). Synaptotagmin I: a major Ca2+ sensor for transmitter release at a central synapse. Cell *79*, 717-727.

Gerth, F., Japel, M., Pechstein, A., Kochlamazashvili, G., Lehmann, M., Puchkov, D., Onofri, F., Benfenati, F., Nikonenko, A.G., Fredrich, K., *et al.* (2017). Intersectin associates with synapsin and regulates its nanoscale localization and function. Proceedings of the National Academy of Sciences of the United States of America *114*, 12057-12062.

Gimber, N., Tadeus, G., Maritzen, T., Schmoranzer, J., and Haucke, V. (2015). Diffusional spread and confinement of newly exocytosed synaptic vesicle proteins. Nature communications *6*, 8392.

Giraudo, C.G., Eng, W.S., Melia, T.J., and Rothman, J.E. (2006). A clamping mechanism involved in SNARE-dependent exocytosis. Science *313*, 676-680.

Giudici, M.L., Emson, P.C., and Irvine, R.F. (2004). A novel neuronal-specific splice variant of Type I phosphatidylinositol 4-phosphate 5-kinase isoform gamma. The Biochemical journal *379*, 489-496.

Gordon, S.L., Harper, C.B., Smillie, K.J., and Cousin, M.A. (2016). A Fine Balance of Synaptophysin Levels Underlies Efficient Retrieval of Synaptobrevin II to Synaptic Vesicles. PLoS One *11*, e0149457.

Gordon, S.L., Leube, R.E., and Cousin, M.A. (2011). Synaptophysin is required for synaptobrevin retrieval during synaptic vesicle endocytosis. The Journal of neuroscience : the official journal of the Society for Neuroscience *31*, 14032-14036.

Gorelik, R., Yang, C., Kameswaran, V., Dominguez, R., and Svitkina, T. (2011). Mechanisms of plasma membrane targeting of formin mDia2 through its amino terminal domains. Mol Biol Cell *22*, 189-201.

Gormal, R.S., Nguyen, T.H., Martin, S., Papadopulos, A., and Meunier, F.A. (2015). An acto-myosin II constricting ring initiates the fission of activity-dependent bulk endosomes in neurosecretory cells. The Journal of neuroscience : the official journal of the Society for Neuroscience *35*, 1380-1389.

Granseth, B., Odermatt, B., Royle, S.J., and Lagnado, L. (2006). Clathrin-mediated endocytosis is the dominant mechanism of vesicle retrieval at hippocampal synapses. Neuron *51*, 773-786.

Grass, I., Thiel, S., Honing, S., and Haucke, V. (2004). Recognition of a basic AP-2 binding motif within the C2B domain of synaptotagmin is dependent on multimerization. The Journal of biological chemistry *279*, 54872-54880.

Grienberger, C., and Konnerth, A. (2012). Imaging calcium in neurons. Neuron *73*, 862-885.

Grigliatti, T.A., Hall, L., Rosenbluth, R., and Suzuki, D.T. (1973). Temperature-sensitive mutations in Drosophila melanogaster. XIV. A selection of immobile adults. Mol Gen Genet *120*, 107-114.

Guan, Z., Bykhovskaia, M., Jorquera, R.A., Sutton, R.B., Akbergenova, Y., and Littleton, J.T. (2017). A synaptotagmin suppressor screen indicates SNARE binding controls the timing and Ca(2+) cooperativity of vesicle fusion. eLife *6*.

Guo, J., Wenk, M.R., Pellegrini, L., Onofri, F., Benfenati, F., and De Camilli, P. (2003). Phosphatidylinositol 4-kinase type IIalpha is responsible for the phosphatidylinositol 4-kinase activity associated with synaptic vesicles. Proceedings of the National Academy of Sciences of the United States of America *100*, 3995-4000.

Hakim, V., Cohen, L.D., Zuchman, R., Ziv, T., and Ziv, N.E. (2016). The effects of proteasomal inhibition on synaptic proteostasis. EMBO J *35*, 2238-2262.

Hammond, G.R., Dove, S.K., Nicol, A., Pinxteren, J.A., Zicha, D., and Schiavo, G. (2006). Elimination of plasma membrane phosphatidylinositol (4,5)-bisphosphate is required for exocytosis from mast cells. Journal of cell science *119*, 2084-2094.

Hammond, G.R., Fischer, M.J., Anderson, K.E., Holdich, J., Koteci, A., Balla, T., and Irvine, R.F. (2012). PI4P and PI(4,5)P2 are essential but independent lipid determinants of membrane identity. Science *337*, 727-730.

Hammond, G.R., and Schiavo, G. (2007). Polyphosphoinositol lipids: under-PPInning synaptic function in health and disease. Developmental neurobiology *67*, 1232-1247.

Harata, N.C., Choi, S., Pyle, J.L., Aravanis, A.M., and Tsien, R.W. (2006). Frequency-dependent kinetics and prevalence of kiss-and-run and reuse at hippocampal synapses studied with novel quenching methods. Neuron *49*, 243-256.

Haucke, V., and De Camilli, P. (1999). AP-2 recruitment to synaptotagmin stimulated by tyrosine-based endocytic motifs. Science *285*, 1268-1271.

Haucke, V., Neher, E., and Sigrist, S.J. (2011). Protein scaffolds in the coupling of synaptic exocytosis and endocytosis. Nature reviews. Neuroscience *12*, 127-138.

Haucke, V., Wenk, M.R., Chapman, E.R., Farsad, K., and De Camilli, P. (2000). Dual interaction of synaptotagmin with mu2- and alpha-adaptin facilitates clathrin-coated pit nucleation. EMBO J *19*, 6011-6019.

Hausser, M., and Clark, B.A. (1997). Tonic synaptic inhibition modulates neuronal output pattern and spatiotemporal synaptic integration. Neuron *19*, 665-678.

Hay, J.C., Fisette, P.L., Jenkins, G.H., Fukami, K., Takenawa, T., Anderson, R.A., and Martin, T.F. (1995). ATP-dependent inositide phosphorylation required for Ca(2+)-activated secretion. Nature *374*, 173-177.

He, L., Wu, X.S., Mohan, R., and Wu, L.G. (2006). Two modes of fusion pore opening revealed by cell-attached recordings at a synapse. Nature *444*, 102-105.

Henne, W.M., Boucrot, E., Meinecke, M., Evergren, E., Vallis, Y., Mittal, R., and McMahon, H.T. (2010). FCHo proteins are nucleators of clathrin-mediated endocytosis. Science *328*, 1281-1284.

Heuser, J.E. (1989). Review of electron microscopic evidence favouring vesicle exocytosis as the structural basis for quantal release during synaptic transmission. Quarterly journal of experimental physiology *74*, 1051-1069.

Heuser, J.E., and Reese, T.S. (1973). Evidence for recycling of synaptic vesicle membrane during transmitter release at the frog neuromuscular junction. The Journal of cell biology *57*, 315-344.

Holz, R.W., Hlubek, M.D., Sorensen, S.D., Fisher, S.K., Balla, T., Ozaki, S., Prestwich, G.D., Stuenkel, E.L., and Bittner, M.A. (2000). A pleckstrin homology domain specific for phosphatidylinositol 4, 5-bisphosphate (PtdIns-4,5-P2) and fused to green fluorescent protein identifies plasma membrane PtdIns-4,5-P2 as being important in exocytosis. The Journal of biological chemistry *275*, 17878-17885.

Honigmann, A., van den Bogaart, G., Iraheta, E., Risselada, H.J., Milovanovic, D., Mueller, V., Mullar, S., Diederichsen, U., Fasshauer, D., Grubmuller, H., *et al.* (2013). Phosphatidylinositol 4,5-bisphosphate clusters act as molecular beacons for vesicle recruitment. Nature structural & molecular biology *20*, 679-686.

Hui, E., Johnson, C.P., Yao, J., Dunning, F.M., and Chapman, E.R. (2009). Synaptotagmin-mediated bending of the target membrane is a critical step in Ca(2+)-regulated fusion. Cell *138*, 709-721.

Imig, C., Min, S.W., Krinner, S., Arancillo, M., Rosenmund, C., Sudhof, T.C., Rhee, J., Brose, N., and Cooper, B.H. (2014). The morphological and molecular nature of synaptic vesicle priming at presynaptic active zones. Neuron *84*, 416-431.

Itoh, T., Koshiba, S., Kigawa, T., Kikuchi, A., Yokoyama, S., and Takenawa, T. (2001). Role of the ENTH domain in phosphatidylinositol-4,5-bisphosphate binding and endocytosis. Science *291*, 1047-1051.

Jackson, L.P., Kelly, B.T., McCoy, A.J., Gaffry, T., James, L.C., Collins, B.M., Honing, S., Evans, P.R., and Owen, D.J. (2010). A large-scale conformational change couples membrane recruitment to cargo binding in the AP2 clathrin adaptor complex. Cell *141*, 1220-1229.

Jahn, R., and Fasshauer, D. (2012). Molecular machines governing exocytosis of synaptic vesicles. Nature *490*, 201-207.

Janz, R., Goda, Y., Geppert, M., Missler, M., and Sudhof, T.C. (1999). SV2A and SV2B function as redundant Ca2+ regulators in neurotransmitter release. Neuron *24*, 1003-1016.

Janz, R., Hofmann, K., and Sudhof, T.C. (1998). SVOP, an evolutionarily conserved synaptic vesicle protein, suggests novel transport functions of synaptic vesicles. The Journal of neuroscience : the official journal of the Society for Neuroscience *18*, 9269-9281.

Jarousse, N., and Kelly, R.B. (2001). The AP2 binding site of synaptotagmin 1 is not an internalization signal but a regulator of endocytosis. The Journal of cell biology *154*, 857-866.

Johnsson, A.K., and Karlsson, R. (2012). Synaptotagmin 1 causes phosphatidyl inositol lipid-dependent actin remodeling in cultured non-neuronal and neuronal cells. Exp Cell Res *318*, 114-126.

Jorgensen, E.M., Hartwieg, E., Schuske, K., Nonet, M.L., Jin, Y., and Horvitz, H.R. (1995). Defective recycling of synaptic vesicles in synaptotagmin mutants of Caenorhabditis elegans. Nature *378*, 196-199.

Jung, N., Wienisch, M., Gu, M., Rand, J.B., Muller, S.L., Krause, G., Jorgensen, E.M., Klingauf, J., and Haucke, V. (2007). Molecular basis of synaptic vesicle cargo recognition by the endocytic sorting adaptor stonin 2. The Journal of cell biology *179*, 1497-1510.

Kaempf, N., and Maritzen, T. (2017). Safeguards of Neurotransmission: Endocytic Adaptors as Regulators of Synaptic Vesicle Composition and Function. Frontiers in cellular neuroscience *11*, 320.

Kahlfeldt, N., Vahedi-Faridi, A., Koo, S.J., Schafer, J.G., Krainer, G., Keller, S., Saenger, W., Krauss, M., and Haucke, V. (2010). Molecular basis for association of PIPKI gamma-p90 with clathrin adaptor AP-2. The Journal of biological chemistry *285*, 2734-2749.

Kaksonen, M., Toret, C.P., and Drubin, D.G. (2005). A modular design for the clathrin- and actin-mediated endocytosis machinery. Cell *123*, 305-320.

Katz, B., and Miledi, R. (1967a). Ionic requirements of synaptic transmitter release. Nature *215*, 651.

Katz, B., and Miledi, R. (1967b). The timing of calcium action during neuromuscular transmission. The Journal of physiology *189*, 535-544.

Kerr, A.M., Reisinger, E., and Jonas, P. (2008). Differential dependence of phasic transmitter release on synaptotagmin 1 at GABAergic and glutamatergic hippocampal synapses. Proceedings of the National Academy of Sciences of the United States of America *105*, 15581-15586.

Khuong, T.M., Habets, R.L., Kuenen, S., Witkowska, A., Kasprowicz, J., Swerts, J., Jahn, R., van den Bogaart, G., and Verstreken, P. (2013). Synaptic PI(3,4,5)P3 is required for Syntaxin1A clustering and neurotransmitter release. Neuron *77*, 1097-1108.

Kim, S.H., and Ryan, T.A. (2009). A distributed set of interactions controls mu2 functionality in the role of AP-2 as a sorting adaptor in synaptic vesicle endocytosis. The Journal of biological chemistry *284*, 32803-32812.

Kim, W.T., Chang, S., Daniell, L., Cremona, O., Di Paolo, G., and De Camilli, P. (2002). Delayed reentry of recycling vesicles into the fusion-competent synaptic vesicle pool in synaptojanin 1 knockout mice. Proceedings of the National Academy of Sciences of the United States of America *99*, 17143-17148.

Kittel, R.J., Hallermann, S., Thomsen, S., Wichmann, C., Sigrist, S.J., and Heckmann, M. (2006). Active zone assembly and synaptic release. Biochemical Society transactions *34*, 939-941.

Koch, M., and Holt, M. (2012). Coupling exo- and endocytosis: an essential role for PIP(2) at the synapse. Biochimica et biophysica acta *1821*, 1114-1132.

Koh, T.W., and Bellen, H.J. (2003). Synaptotagmin I, a Ca2+ sensor for neurotransmitter release. Trends in neurosciences *26*, 413-422.

Kononenko, N.L., Diril, M.K., Puchkov, D., Kintscher, M., Koo, S.J., Pfuhl, G., Winter, Y., Wienisch, M., Klingauf, J., Breustedt, J., *et al.* (2013). Compromised fidelity of endocytic synaptic vesicle protein sorting in the absence of stonin 2. Proceedings of the National Academy of Sciences of the United States of America *110*, E526-535.

Kononenko, N.L., Puchkov, D., Classen, G.A., Walter, A.M., Pechstein, A., Sawade, L., Kaempf, N., Trimbuch, T., Lorenz, D., Rosenmund, C., *et al.* (2014). Clathrin/AP-2 mediate synaptic vesicle reformation from endosome-like vacuoles but are not essential for membrane retrieval at central synapses. Neuron *82*, 981-988.

Koo, S.J., Kochlamazashvili, G., Rost, B., Puchkov, D., Gimber, N., Lehmann, M., Tadeus, G., Schmoranzer, J., Rosenmund, C., Haucke, V., and Maritzen, T. (2015). Vesicular Synaptobrevin/VAMP2 Levels Guarded by AP180 Control Efficient Neurotransmission. Neuron *88*, 330-344.

Koo, S.J., Markovic, S., Puchkov, D., Mahrenholz, C.C., Beceren-Braun, F., Maritzen, T., Dernedde, J., Volkmer, R., Oschkinat, H., and Haucke, V. (2011). SNARE motif-mediated sorting of synaptobrevin by the endocytic adaptors clathrin assembly lymphoid myeloid leukemia (CALM) and AP180 at synapses. Proceedings of the National Academy of Sciences of the United States of America *108*, 13540-13545.

Krauss, M., and Haucke, V. (2007). Phosphoinositide-metabolizing enzymes at the interface between membrane traffic and cell signalling. EMBO reports *8*, 241-246.

Krauss, M., Kinuta, M., Wenk, M.R., De Camilli, P., Takei, K., and Haucke, V. (2003). ARF6 stimulates clathrin/AP-2 recruitment to synaptic membranes by activating phosphatidylinositol phosphate kinase type Igamma. The Journal of cell biology *162*, 113-124.

Krauss, M., Kukhtina, V., Pechstein, A., and Haucke, V. (2006). Stimulation of phosphatidylinositol kinase type I-mediated phosphatidylinositol (4,5)-bisphosphate synthesis by AP-2mu-cargo complexes. Proceedings of the National Academy of Sciences of the United States of America *103*, 11934-11939.

Kunz, J., Wilson, M.P., Kisseleva, M., Hurley, J.H., Majerus, P.W., and Anderson, R.A. (2000). The activation loop of phosphatidylinositol phosphate kinases determines signaling specificity. Molecular cell *5*, 1-11.

Lazzell, D.R., Belizaire, R., Thakur, P., Sherry, D.M., and Janz, R. (2004). SV2B regulates synaptotagmin 1 by direct interaction. The Journal of biological chemistry *279*, 52124-52131.

Lee, S.Y., Voronov, S., Letinic, K., Nairn, A.C., Di Paolo, G., and De Camilli, P. (2005). Regulation of the interaction between PIPKI gamma and talin by proline-directed protein kinases. The Journal of cell biology *168*, 789-799.

Lee, S.Y., Wenk, M.R., Kim, Y., Nairn, A.C., and De Camilli, P. (2004). Regulation of synaptojanin 1 by cyclin-dependent kinase 5 at synapses. Proceedings of the National Academy of Sciences of the United States of America *101*, 546-551.

Lemieux, M.G., Janzen, D., Hwang, R., Roldan, J., Jarchum, I., and Knecht, D.A. (2014). Visualization of the actin cytoskeleton: different F-actin-binding probes tell different stories. Cytoskeleton *71*, 157-169.

Leube, R.E., Kaiser, P., Seiter, A., Zimbelmann, R., Franke, W.W., Rehm, H., Knaus, P., Prior, P., Betz, H., Reinke, H., and et al. (1987). Synaptophysin: molecular organization and mRNA expression as determined from cloned cDNA. EMBO J *6*, 3261-3268.

Li, C., Ullrich, B., Zhang, J.Z., Anderson, R.G., Brose, N., and Sudhof, T.C. (1995). Ca(2+)-dependent and -independent activities of neural and non-neural synaptotagmins. Nature *375*, 594-599.

Li, L., Shin, O.H., Rhee, J.S., Arac, D., Rah, J.C., Rizo, J., Sudhof, T., and Rosenmund, C. (2006). Phosphatidylinositol phosphates as co-activators of Ca2+ binding to C2 domains of synaptotagmin 1. The Journal of biological chemistry *281*, 15845-15852.

Li, Z., and Murthy, V.N. (2001). Visualizing postendocytic traffic of synaptic vesicles at hippocampal synapses. Neuron *31*, 593-605.

Lin, C.C., Seikowski, J., Perez-Lara, A., Jahn, R., Hobartner, C., and Walla, P.J. (2014). Control of membrane gaps by synaptotagmin-Ca2+ measured with a novel membrane distance ruler. Nature communications *5*, 5859.

Littleton, J.T., Bai, J., Vyas, B., Desai, R., Baltus, A.E., Garment, M.B., Carlson, S.D., Ganetzky, B., and Chapman, E.R. (2001). synaptotagmin mutants reveal essential functions for the C2B domain in Ca2+-triggered fusion and recycling of synaptic vesicles in vivo. The Journal of neuroscience : the official journal of the Society for Neuroscience *21*, 1421-1433.

Littleton, J.T., Stern, M., Perin, M., and Bellen, H.J. (1994). Calcium dependence of neurotransmitter release and rate of spontaneous vesicle fusions are altered in Drosophila synaptotagmin mutants. Proceedings of the National Academy of Sciences of the United States of America *91*, 10888-10892.

Lois, C., Hong, E.J., Pease, S., Brown, E.J., and Baltimore, D. (2002). Germline transmission and tissue-specific expression of transgenes delivered by lentiviral vectors. Science *295*, 868-872.

Lou, X., Paradise, S., Ferguson, S.M., and De Camilli, P. (2008). Selective saturation of slow endocytosis at a giant glutamatergic central synapse lacking dynamin 1. Proceedings of the National Academy of Sciences of the United States of America *105*, 17555-17560.

Luan, Z., Zhang, Y., Lu, T., Ruan, Y., Zhang, H., Yan, J., Li, L., Sun, W., Wang, L., Yue, W., and Zhang, D. (2011). Positive association of the human STON2 gene with schizophrenia. Neuroreport *22*, 288-293.

Lynch, B.A., Lambeng, N., Nocka, K., Kensel-Hammes, P., Bajjalieh, S.M., Matagne, A., and Fuks, B. (2004). The synaptic vesicle protein SV2A is the binding site for the antiepileptic drug levetiracetam. Proceedings of the National Academy of Sciences of the United States of America *101*, 9861-9866.

Mani, M., Lee, S.Y., Lucast, L., Cremona, O., Di Paolo, G., De Camilli, P., and Ryan, T.A. (2007). The dual phosphatase activity of synaptojanin1 is required for both efficient synaptic vesicle endocytosis and reavailability at nerve terminals. Neuron *56*, 1004-1018.

Maritzen, T., and Haucke, V. (2017). Coupling of exocytosis and endocytosis at the presynaptic active zone. Neuroscience research.

Maritzen, T., Koo, S.J., and Haucke, V. (2012). Turning CALM into excitement: AP180 and CALM in endocytosis and disease. Biology of the cell / under the auspices of the European Cell Biology Organization *104*, 588-602.

Maritzen, T., Podufall, J., and Haucke, V. (2010). Stonins--specialized adaptors for synaptic vesicle recycling and beyond? Traffic *11*, 8-15.

Martens, S., Kozlov, M.M., and McMahon, H.T. (2007). How synaptotagmin promotes membrane fusion. Science *316*, 1205-1208.

Martina, J.A., Bonangelino, C.J., Aguilar, R.C., and Bonifacino, J.S. (2001). Stonin 2: an adaptor-like protein that interacts with components of the endocytic machinery. The Journal of cell biology *153*, 1111-1120.

Marx, V. (2014). A deep look at synaptic dynamics. Nature *515*, 293-297.

McMahon, H.T., Bolshakov, V.Y., Janz, R., Hammer, R.E., Siegelbaum, S.A., and Sudhof, T.C. (1996). Synaptophysin, a major synaptic vesicle protein, is not essential for neurotransmitter release. Proceedings of the National Academy of Sciences of the United States of America *93*, 4760-4764.

McMahon, H.T., and Boucrot, E. (2011). Molecular mechanism and physiological functions of clathrin-mediated endocytosis. Nat Rev Mol Cell Biol *12*, 517-533.

McPherson, P.S., and Ritter, B. (2005). Peptide motifs: building the clathrin machinery. Molecular neurobiology *32*, 73-87.

Mettlen, M., Pucadyil, T., Ramachandran, R., and Schmid, S.L. (2009). Dissecting dynamin's role in clathrin-mediated endocytosis. Biochemical Society transactions *37*, 1022-1026.

Micheva, K.D., Holz, R.W., and Smith, S.J. (2001). Regulation of presynaptic phosphatidylinositol 4,5-biphosphate by neuronal activity. The Journal of cell biology *154*, 355-368.

Miesenbock, G. (2012). Synapto-pHluorins: genetically encoded reporters of synaptic transmission. Cold Spring Harbor protocols *2012*, 213-217.

Miesenbock, G., De Angelis, D.A., and Rothman, J.E. (1998). Visualizing secretion and synaptic transmission with pH-sensitive green fluorescent proteins. Nature *394*, 192-195.

Milosevic, I., Sorensen, J.B., Lang, T., Krauss, M., Nagy, G., Haucke, V., Jahn, R., and Neher, E. (2005). Plasmalemmal phosphatidylinositol-4,5-bisphosphate level regulates the releasable vesicle pool size in chromaffin cells. The Journal of neuroscience : the official journal of the Society for Neuroscience *25*, 2557-2565.

Minta, A., Kao, J.P., and Tsien, R.Y. (1989). Fluorescent indicators for cytosolic calcium based on rhodamine and fluorescein chromophores. The Journal of biological chemistry *264*, 8171-8178.

Mitsunari, T., Nakatsu, F., Shioda, N., Love, P.E., Grinberg, A., Bonifacino, J.S., and Ohno, H. (2005). Clathrin adaptor AP-2 is essential for early embryonal development. Mol Cell Biol *25*, 9318-9323.

Morgan, J.R., Di Paolo, G., Werner, H., Shchedrina, V.A., Pypaert, M., Pieribone, V.A., and De Camilli, P. (2004). A role for talin in presynaptic function. The Journal of cell biology *167*, 43-50.

Morgans, C.W., Kensel-Hammes, P., Hurley, J.B., Burton, K., Idzerda, R., McKnight, G.S., and Bajjalieh, S.M. (2009). Loss of the Synaptic Vesicle Protein SV2B results in reduced

neurotransmission and altered synaptic vesicle protein expression in the retina. PLoS One *4*, e5230.

Mori, Y., and Takamori, S. (2018). Molecular Signatures Underlying Synaptic Vesicle Cargo Retrieval. Frontiers in cellular neuroscience *11*.

Mullen, G.P., Grundahl, K.M., Gu, M., Watanabe, S., Hobson, R.J., Crowell, J.A., McManus, J.R., Mathews, E.A., Jorgensen, E.M., and Rand, J.B. (2012). UNC-41/stonin functions with AP2 to recycle synaptic vesicles in Caenorhabditis elegans. PLoS One *7*, e40095.

Mutch, S.A., Kensel-Hammes, P., Gadd, J.C., Fujimoto, B.S., Allen, R.W., Schiro, P.G., Lorenz, R.M., Kuyper, C.L., Kuo, J.S., Bajjalieh, S.M., and Chiu, D.T. (2011). Protein quantification at the single vesicle level reveals that a subset of synaptic vesicle proteins are trafficked with high precision. The Journal of neuroscience : the official journal of the Society for Neuroscience *31*, 1461-1470.

Nakano-Kobayashi, A., Yamazaki, M., Unoki, T., Hongu, T., Murata, C., Taguchi, R., Katada, T., Frohman, M.A., Yokozeki, T., and Kanaho, Y. (2007). Role of activation of PIP5Kgamma661 by AP-2 complex in synaptic vesicle endocytosis. EMBO J *26*, 1105-1116.

Nakatsu, F., Baskin, J.M., Chung, J., Tanner, L.B., Shui, G., Lee, S.Y., Pirruccello, M., Hao, M., Ingolia, N.T., Wenk, M.R., and De Camilli, P. (2012). PtdIns4P synthesis by PI4KIIIalpha at the plasma membrane and its impact on plasma membrane identity. The Journal of cell biology *199*, 1003-1016.

Neher, E. (2010). What is Rate-Limiting during Sustained Synaptic Activity: Vesicle Supply or the Availability of Release Sites. Frontiers in synaptic neuroscience *2*, 144.

Neher, E., and Sakaba, T. (2008). Multiple roles of calcium ions in the regulation of neurotransmitter release. Neuron *59*, 861-872.

Nicholson-Fish, J.C., Kokotos, A.C., Gillingwater, T.H., Smillie, K.J., and Cousin, M.A. (2015). VAMP4 Is an Essential Cargo Molecule for Activity-Dependent Bulk Endocytosis. Neuron *88*, 973-984.

Nicholson-Tomishima, K., and Ryan, T.A. (2004). Kinetic efficiency of endocytosis at mammalian CNS synapses requires synaptotagmin I. Proceedings of the National Academy of Sciences of the United States of America *101*, 16648-16652.

Nili, U., de Wit, H., Gulyas-Kovacs, A., Toonen, R.F., Sorensen, J.B., Verhage, M., and Ashery, U. (2006). Munc18-1 phosphorylation by protein kinase C potentiates vesicle pool replenishment in bovine chromaffin cells. Neuroscience *143*, 487-500.

Nishiki, T., and Augustine, G.J. (2004). Synaptotagmin I synchronizes transmitter release in mouse hippocampal neurons. The Journal of neuroscience : the official journal of the Society for Neuroscience *24*, 6127-6132.

Nowack, A., Malarkey, E.B., Yao, J., Bleckert, A., Hill, J., and Bajjalieh, S.M. (2011). Levetiracetam reverses synaptic deficits produced by overexpression of SV2A. PLoS One *6*, e29560.

Ohno, H., Stewart, J., Fournier, M.C., Bosshart, H., Rhee, I., Miyatake, S., Saito, T., Gallusser, A., Kirchhausen, T., and Bonifacino, J.S. (1995). Interaction of tyrosine-based sorting signals with clathrin-associated proteins. Science *269*, 1872-1875.

Okerlund, N.D., Schneider, K., Leal-Ortiz, S., Montenegro-Venegas, C., Kim, S.A., Garner, L.C., Waites, C.L., Gundelfinger, E.D., Reimer, R.J., and Garner, C.C. (2017). Bassoon Controls Presynaptic Autophagy through Atg5. Neuron *93*, 897-913 e897.

Pan, P.Y., Marrs, J., and Ryan, T.A. (2015). Vesicular Glutamate Transporter 1 Orchestrates Recruitment of Other Synaptic Vesicle Cargo Proteins during Synaptic Vesicle Recycling. The Journal of biological chemistry *290*, 22593-22601.

Park, Y., Seo, J.B., Fraind, A., Perez-Lara, A., Yavuz, H., Han, K., Jung, S.R., Kattan, I., Walla, P.J., Choi, M., *et al.* (2015). Synaptotagmin-1 binds to PIP(2)-containing membrane but not to SNAREs at physiological ionic strength. Nature structural & molecular biology *22*, 815-823.

Paul, A.S., and Pollard, T.D. (2009). Review of the mechanism of processive actin filament elongation by formins. Cell motility and the cytoskeleton *66*, 606-617.

Pechstein, A., Shupliakov, O., and Haucke, V. (2010). Intersectin 1: a versatile actor in the synaptic vesicle cycle. Biochemical Society transactions *38*, 181-186.

Perera, R.M., Zoncu, R., Lucast, L., De Camilli, P., and Toomre, D. (2006). Two synaptojanin 1 isoforms are recruited to clathrin-coated pits at different stages. Proceedings of the National Academy of Sciences of the United States of America *103*, 19332-19337.

Perin, M.S., Fried, V.A., Mignery, G.A., Jahn, R., and Sudhof, T.C. (1990). Phospholipid binding by a synaptic vesicle protein homologous to the regulatory region of protein kinase C. Nature *345*, 260-263.

Phillips, A.M., Smith, M., Ramaswami, M., and Kelly, L.E. (2000). The products of the Drosophila stoned locus interact with synaptic vesicles via synaptotagmin. The Journal of neuroscience : the official journal of the Society for Neuroscience *20*, 8254-8261.

Podufall, J., Tian, R., Knoche, E., Puchkov, D., Walter, A.M., Rosa, S., Quentin, C., Vukoja, A., Jung, N., Lampe, A., *et al.* (2014). A presynaptic role for the cytomatrix protein GIT in synaptic vesicle recycling. Cell reports *7*, 1417-1425.

Poskanzer, K.E., Fetter, R.D., and Davis, G.W. (2006). Discrete residues in the c(2)b domain of synaptotagmin I independently specify endocytic rate and synaptic vesicle size. Neuron *50*, 49-62.

Poskanzer, K.E., Marek, K.W., Sweeney, S.T., and Davis, G.W. (2003). Synaptotagmin I is necessary for compensatory synaptic vesicle endocytosis in vivo. Nature *426*, 559-563.

Posor, Y., Eichhorn-Grunig, M., and Haucke, V. (2015). Phosphoinositides in endocytosis. Biochimica et biophysica acta *1851*, 794-804.

Puchkov, D., and Haucke, V. (2013). Greasing the synaptic vesicle cycle by membrane lipids. Trends in cell biology *23*, 493-503.

Pyle, R.A., Schivell, A.E., Hidaka, H., and Bajjalieh, S.M. (2000). Phosphorylation of synaptic vesicle protein 2 modulates binding to synaptotagmin. The Journal of biological chemistry *275*, 17195-17200.

Rajappa, R., Gauthier-Kemper, A., Boning, D., Huve, J., and Klingauf, J. (2016). Synaptophysin 1 Clears Synaptobrevin 2 from the Presynaptic Active Zone to Prevent Short-Term Depression. Cell reports *14*, 1369-1381.

Ramadurai, S., Holt, A., Krasnikov, V., van den Bogaart, G., Killian, J.A., and Poolman, B. (2009). Lateral Diffusion of Membrane Proteins. J Am Chem Soc *131*, 12650-12656.

Rao, Y., and Haucke, V. (2011). Membrane shaping by the Bin/amphiphysin/Rvs (BAR) domain protein superfamily. Cellular and molecular life sciences : CMLS *68*, 3983-3993.

Regehr, W.G. (2012). Short-term presynaptic plasticity. Cold Spring Harb Perspect Biol *4*, a005702.

Renard, H.F., Simunovic, M., Lemiere, J., Boucrot, E., Garcia-Castillo, M.D., Arumugam, S., Chambon, V., Lamaze, C., Wunder, C., Kenworthy, A.K., *et al.* (2015). Endophilin-A2 functions in membrane scission in clathrin-independent endocytosis. Nature *517*, 493-496.

Reubold, T.F., Faelber, K., Plattner, N., Posor, Y., Ketel, K., Curth, U., Schlegel, J., Anand, R., Manstein, D.J., Noe, F., *et al.* (2015). Crystal structure of the dynamin tetramer. Nature *525*, 404-408.

Rhee, J.S., Betz, A., Pyott, S., Reim, K., Varoqueaux, F., Augustin, I., Hesse, D., Sudhof, T.C., Takahashi, M., Rosenmund, C., and Brose, N. (2002). Beta phorbol ester- and diacylglycerol-induced augmentation of transmitter release is mediated by Munc13s and not by PKCs. Cell *108*, 121-133.

Rhee, J.S., Li, L.Y., Shin, O.H., Rah, J.C., Rizo, J., Sudhof, T.C., and Rosenmund, C. (2005). Augmenting neurotransmitter release by enhancing the apparent Ca2+ affinity of synaptotagmin 1. Proceedings of the National Academy of Sciences of the United States of America *102*, 18664-18669.

Rhinn, H., Fujita, R., Qiang, L., Cheng, R., Lee, J.H., and Abeliovich, A. (2013). Integrative genomics identifies APOE epsilon4 effectors in Alzheimer's disease. Nature *500*, 45-50.

Richards, D.A., Bai, J., and Chapman, E.R. (2005). Two modes of exocytosis at hippocampal synapses revealed by rate of FM1-43 efflux from individual vesicles. The Journal of cell biology *168*, 929-939.

Rodriguez-Menchaca, A.A., Adney, S.K., Zhou, L., and Logothetis, D.E. (2012). Dual Regulation of Voltage-Sensitive Ion Channels by PIP(2). Frontiers in pharmacology *3*, 170.

Rohde, G., Wenzel, D., and Haucke, V. (2002). A phosphatidylinositol (4,5)-bisphosphate binding site within mu2-adaptin regulates clathrin-mediated endocytosis. The Journal of cell biology *158*, 209-214.

Rosenmund, C., Sigler, A., Augustin, I., Reim, K., Brose, N., and Rhee, J.S. (2002). Differential control of vesicle priming and short-term plasticity by Munc13 isoforms. Neuron *33*, 411-424.

Saarikangas, J., Zhao, H., and Lappalainen, P. (2010). Regulation of the actin cytoskeleton-plasma membrane interplay by phosphoinositides. Physiological reviews *90*, 259-289.

Sabatini, B.L., and Regehr, W.G. (1996). Timing of neurotransmission at fast synapses in the mammalian brain. Nature *384*, 170-172.

Saffman, P.G., and Delbruck, M. (1975). Brownian-Motion in Biological-Membranes. Proceedings of the National Academy of Sciences of the United States of America *72*, 3111-3113.

Sakaba, T., Kononenko, N.L., Bacetic, J., Pechstein, A., Schmoranzer, J., Yao, L., Barth, H., Shupliakov, O., Kobler, O., Aktories, K., and Haucke, V. (2013). Fast neurotransmitter release regulated by the endocytic scaffold intersectin. Proceedings of the National Academy of Sciences of the United States of America *110*, 8266-8271.

Salim, K., Bottomley, M.J., Querfurth, E., Zvelebil, M.J., Gout, I., Scaife, R., Margolis, R.L., Gigg, R., Smith, C.I., Driscoll, P.C., *et al.* (1996). Distinct specificity in the recognition of phosphoinositides by the pleckstrin homology domains of dynamin and Bruton's tyrosine kinase. EMBO J *15*, 6241-6250.

Sanger, F., and Coulson, A.R. (1975). A rapid method for determining sequences in DNA by primed synthesis with DNA polymerase. Journal of molecular biology *94*, 441-448.

Sankaranarayanan, S., and Ryan, T.A. (2000). Real-time measurements of vesicle-SNARE recycling in synapses of the central nervous system. Nature cell biology *2*, 197-204.

Sankaranarayanan, S., and Ryan, T.A. (2001). Calcium accelerates endocytosis of vSNAREs at hippocampal synapses. Nature neuroscience *4*, 129-136.

Schauer, C., and Leinders-Zufall, T. (2012). Imaging calcium responses in GFP-tagged neurons of hypothalamic mouse brain slices. Journal of visualized experiments : JoVE, e4213.

Schiavo, G., Gu, Q.M., Prestwich, G.D., Sollner, T.H., and Rothman, J.E. (1996). Calcium-dependent switching of the specificity of phosphoinositide binding to synaptotagmin. Proceedings of the National Academy of Sciences of the United States of America *93*, 13327-13332.

Schill, N.J., and Anderson, R.A. (2009). Two novel phosphatidylinositol-4-phosphate 5-kinase type Igamma splice variants expressed in human cells display distinctive cellular targeting. The Biochemical journal *422*, 473-482.

Schivell, A.E., Batchelor, R.H., and Bajjalieh, S.M. (1996). Isoform-specific, calcium-regulated interaction of the synaptic vesicle proteins SV2 and synaptotagmin. The Journal of biological chemistry *271*, 27770-27775.

Schivell, A.E., Mochida, S., Kensel-Hammes, P., Custer, K.L., and Bajjalieh, S.M. (2005). SV2A and SV2C contain a unique synaptotagmin-binding site. Molecular and cellular neurosciences *29*, 56-64.

Schmitt, U., Tanimoto, N., Seeliger, M., Schaeffel, F., and Leube, R.E. (2009). Detection of Behavioral Alterations and Learning Deficits in Mice Lacking Synaptophysin. Neuroscience *162*, 234-243.

Schneggenburger, R., and Neher, E. (2000). Intracellular calcium dependence of transmitter release rates at a fast central synapse. Nature *406*, 889-893.

Schoch, S., Deak, F., Konigstorfer, A., Mozhayeva, M., Sara, Y., Sudhof, T.C., and Kavalali, E.T. (2001). SNARE function analyzed in synaptobrevin/VAMP knockout mice. Science *294*, 1117-1122.

Schuske, K.R., Richmond, J.E., Matthies, D.S., Davis, W.S., Runz, S., Rube, D.A., van der Bliek, A.M., and Jorgensen, E.M. (2003). Endophilin is required for synaptic vesicle endocytosis by localizing synaptojanin. Neuron *40*, 749-762.

Senju, Y., Kalimeri, M., Koskela, E.V., Somerharju, P., Zhao, H., Vattulainen, I., and Lappalainen, P. (2017). Mechanistic principles underlying regulation of the actin cytoskeleton by phosphoinositides. Proceedings of the National Academy of Sciences of the United States of America *114*, E8977-E8986.

Siddiqui, T.J., Vites, O., Stein, A., Heintzmann, R., Jahn, R., and Fasshauer, D. (2007). Determinants of synaptobrevin regulation in membranes. Mol Biol Cell *18*, 2037-2046.

Soukup, S.F., Kuenen, S., Vanhauwaert, R., Manetsberger, J., Hernandez-Diaz, S., Swerts, J., Schoovaerts, N., Vilain, S., Gounko, N.V., Vints, K., *et al.* (2016). A LRRK2-Dependent EndophilinA Phosphoswitch Is Critical for Macroautophagy at Presynaptic Terminals. Neuron *92*, 829-844.

Soykan, T., Kaempf, N., Sakaba, T., Vollweiter, D., Goerdeler, F., Puchkov, D., Kononenko, N.L., and Haucke, V. (2017). Synaptic Vesicle Endocytosis Occurs on Multiple Timescales and Is Mediated by Formin-Dependent Actin Assembly. Neuron *93*, 854-866 e854.

Soykan, T., Maritzen, T., and Haucke, V. (2016). Modes and mechanisms of synaptic vesicle recycling. Current opinion in neurobiology *39*, 17-23.

Suh, B.C., Leal, K., and Hille, B. (2010). Modulation of high-voltage activated Ca(2+) channels by membrane phosphatidylinositol 4,5-bisphosphate. Neuron *67*, 224-238.

Takamori, S., Holt, M., Stenius, K., Lemke, E.A., Gronborg, M., Riedel, D., Urlaub, H., Schenck, S., Brugger, B., Ringler, P., *et al.* (2006). Molecular anatomy of a trafficking organelle. Cell *127*, 831-846.

Takei, K., McPherson, P.S., Schmid, S.L., and De Camilli, P. (1995). Tubular membrane invaginations coated by dynamin rings are induced by GTP-gamma S in nerve terminals. Nature *374*, 186-190.

Tan, J., and Brill, J.A. (2014). Cinderella story: PI4P goes from precursor to key signaling molecule. Critical reviews in biochemistry and molecular biology *49*, 33-58.

Tan, P.K., Waites, C., Liu, Y., Krantz, D.E., and Edwards, R.H. (1998). A leucine-based motif mediates the endocytosis of vesicular monoamine and acetylcholine transporters. The Journal of biological chemistry *273*, 17351-17360.

Taoufiq, Z., Eguchi, K., and Takahashi, T. (2013). Rho-kinase accelerates synaptic vesicle endocytosis by linking cyclic GMP-dependent protein kinase activity to phosphatidylinositol-

4,5-bisphosphate synthesis. The Journal of neuroscience : the official journal of the Society for Neuroscience *33*, 12099-12104.

Thieman, J.R., Mishra, S.K., Ling, K., Doray, B., Anderson, R.A., and Traub, L.M. (2009). Clathrin regulates the association of PIPKIgamma661 with the AP-2 adaptor beta2 appendage. The Journal of biological chemistry *284*, 13924-13939.

Tomasevic, N., Jia, Z., Russell, A., Fujii, T., Hartman, J.J., Clancy, S., Wang, M., Beraud, C., Wood, K.W., and Sakowicz, R. (2007). Differential regulation of WASP and N-WASP by Cdc42, Rac1, Nck, and PI(4,5)P2. Biochemistry *46*, 3494-3502.

Traub, L.M., and Bonifacino, J.S. (2013). Cargo recognition in clathrin-mediated endocytosis. Cold Spring Harb Perspect Biol *5*, a016790.

Uytterhoeven, V., Kuenen, S., Kasprowicz, J., Miskiewicz, K., and Verstreken, P. (2011). Loss of skywalker reveals synaptic endosomes as sorting stations for synaptic vesicle proteins. Cell *145*, 117-132.

van den Bogaart, G., Meyenberg, K., Diederichsen, U., and Jahn, R. (2012). Phosphatidylinositol 4,5-bisphosphate increases Ca2+ affinity of synaptotagmin-1 by 40-fold. The Journal of biological chemistry *287*, 16447-16453.

van den Bogaart, G., Meyenberg, K., Risselada, H.J., Amin, H., Willig, K.I., Hubrich, B.E., Dier, M., Hell, S.W., Grubmuller, H., Diederichsen, U., and Jahn, R. (2011). Membrane protein sequestering by ionic protein-lipid interactions. Nature *479*, 552-555.

Vanhauwaert, R., Kuenen, S., Masius, R., Bademosi, A., Manetsberger, J., Schoovaerts, N., Bounti, L., Gontcharenko, S., Swerts, J., Vilain, S., *et al.* (2017). The SAC1 domain in synaptojanin is required for autophagosome maturation at presynaptic terminals. EMBO J *36*, 1392-1411.

Venkatesan, K., Alix, P., Marquet, A., Doupagne, M., Niespodziany, I., Rogister, B., and Seutin, V. (2012). Altered balance between excitatory and inhibitory inputs onto CA1 pyramidal neurons from SV2A-deficient but not SV2B-deficient mice. Journal of neuroscience research *90*, 2317-2327.

Verstreken, P., Koh, T.W., Schulze, K.L., Zhai, R.G., Hiesinger, P.R., Zhou, Y., Mehta, S.Q., Cao, Y., Roos, J., and Bellen, H.J. (2003). Synaptojanin is recruited by endophilin to promote synaptic vesicle uncoating. Neuron *40*, 733-748.

Voglmaier, S.M., Kam, K., Yang, H., Fortin, D.L., Hua, Z., Nicoll, R.A., and Edwards, R.H. (2006). Distinct endocytic pathways control the rate and extent of synaptic vesicle protein recycling. Neuron *51*, 71-84.

Walter, A.M., Muller, R., Tawfik, B., Wierda, K.D., Pinheiro, P.S., Nadler, A., McCarthy, A.W., Ziomkiewicz, I., Kruse, M., Reither, G., *et al.* (2017). Phosphatidylinositol 4,5-bisphosphate optical uncaging potentiates exocytosis. eLife *6*.

Walter, A.M., Wiederhold, K., Bruns, D., Fasshauer, D., and Sorensen, J.B. (2010). Synaptobrevin N-terminally bound to syntaxin-SNAP-25 defines the primed vesicle state in regulated exocytosis. The Journal of cell biology *188*, 401-413.

Walther, K., Diril, M.K., Jung, N., and Haucke, V. (2004). Functional dissection of the interactions of stonin 2 with the adaptor complex AP-2 and synaptotagmin. Proceedings of the National Academy of Sciences of the United States of America *101*, 964-969.

Walther, K., Krauss, M., Diril, M.K., Lemke, S., Ricotta, D., Honing, S., Kaiser, S., and Haucke, V. (2001). Human stoned B interacts with AP-2 and synaptotagmin and facilitates clathrin-coated vesicle uncoating. EMBO reports *2*, 634-640.

Wan, Q.F., Zhou, Z.Y., Thakur, P., Vila, A., Sherry, D.M., Janz, R., and Heidelberger, R. (2010). SV2 acts via presynaptic calcium to regulate neurotransmitter release. Neuron *66*, 884-895.

Watanabe, S., Liu, Q., Davis, M.W., Hollopeter, G., Thomas, N., Jorgensen, N.B., and Jorgensen, E.M. (2013a). Ultrafast endocytosis at Caenorhabditis elegans neuromuscular junctions. eLife *2*, e00723.

Watanabe, S., Rost, B.R., Camacho-Perez, M., Davis, M.W., Sohl-Kielczynski, B., Rosenmund, C., and Jorgensen, E.M. (2013b). Ultrafast endocytosis at mouse hippocampal synapses. Nature *504*, 242-247.

Watanabe, S., Trimbuch, T., Camacho-Perez, M., Rost, B.R., Brokowski, B., Sohl-Kielczynski, B., Felies, A., Davis, M.W., Rosenmund, C., and Jorgensen, E.M. (2014). Clathrin regenerates synaptic vesicles from endosomes. Nature *515*, 228-233.

Weber, J.P., Reim, K., and Sorensen, J.B. (2010). Opposing functions of two sub-domains of the SNARE-complex in neurotransmission. EMBO J *29*, 2477-2490.

Wenk, M.R., Lucast, L., Di Paolo, G., Romanelli, A.J., Suchy, S.F., Nussbaum, R.L., Cline, G.W., Shulman, G.I., McMurray, W., and De Camilli, P. (2003). Phosphoinositide profiling in complex lipid mixtures using electrospray ionization mass spectrometry. Nature biotechnology *21*, 813-817.

Wenk, M.R., Pellegrini, L., Klenchin, V.A., Di Paolo, G., Chang, S., Daniell, L., Arioka, M., Martin, T.F., and De Camilli, P. (2001). PIP kinase Igamma is the major PI(4,5)P(2) synthesizing enzyme at the synapse. Neuron *32*, 79-88.

Wiedemann, C., Schafer, T., Burger, M.M., and Sihra, T.S. (1998). An essential role for a small synaptic vesicle-associated phosphatidylinositol 4-kinase in neurotransmitter release. The Journal of neuroscience : the official journal of the Society for Neuroscience *18*, 5594-5602.

Wieffer, M., Maritzen, T., and Haucke, V. (2009). SnapShot: endocytic trafficking. Cell *137*, 382 e381-383.

Wienisch, M., and Klingauf, J. (2006). Vesicular proteins exocytosed and subsequently retrieved by compensatory endocytosis are nonidentical. Nature neuroscience *9*, 1019-1027.

Wilhelm, B.G., Mandad, S., Truckenbrodt, S., Krohnert, K., Schafer, C., Rammner, B., Koo, S.J., Classen, G.A., Krauss, M., Haucke, V., *et al.* (2014). Composition of isolated synaptic boutons reveals the amounts of vesicle trafficking proteins. Science *344*, 1023-1028.

Willig, K.I., Rizzoli, S.O., Westphal, V., Jahn, R., and Hell, S.W. (2006). STED microscopy reveals that synaptotagmin remains clustered after synaptic vesicle exocytosis. Nature *440*, 935-939.

Willox, A.K., and Royle, S.J. (2012). Stonin 2 is a major adaptor protein for clathrin-mediated synaptic vesicle retrieval. Current biology : CB *22*, 1435-1439.

Wright, B.D., Loo, L., Street, S.E., Ma, A., Taylor-Blake, B., Stashko, M.A., Jin, J., Janzen, W.P., Frye, S.V., and Zylka, M.J. (2014). The lipid kinase PIP5K1C regulates pain signaling and sensitization. Neuron *82*, 836-847.

Wu, L., Bauer, C.S., Zhen, X.G., Xie, C., and Yang, J. (2002). Dual regulation of voltage-gated calcium channels by PtdIns(4,5)P2. Nature *419*, 947-952.

Wu, L.G., Hamid, E., Shin, W., and Chiang, H.C. (2014a). Exocytosis and endocytosis: modes, functions, and coupling mechanisms. Annual review of physiology *76*, 301-331.

Wu, L.G., Ryan, T.A., and Lagnado, L. (2007). Modes of vesicle retrieval at ribbon synapses, calyx-type synapses, and small central synapses. The Journal of neuroscience : the official journal of the Society for Neuroscience *27*, 11793-11802.

Wu, W., Xu, J., Wu, X.S., and Wu, L.G. (2005). Activity-dependent acceleration of endocytosis at a central synapse. The Journal of neuroscience : the official journal of the Society for Neuroscience *25*, 11676-11683.

Wu, X.S., Lee, S.H., Sheng, J., Zhang, Z., Zhao, W.D., Wang, D., Jin, Y., Charnay, P., Ervasti, J.M., and Wu, L.G. (2016). Actin Is Crucial for All Kinetically Distinguishable Forms of Endocytosis at Synapses. Neuron *92*, 1020-1035.

Wu, X.S., McNeil, B.D., Xu, J., Fan, J., Xue, L., Melicoff, E., Adachi, R., Bai, L., and Wu, L.G. (2009). Ca(2+) and calmodulin initiate all forms of endocytosis during depolarization at a nerve terminal. Nature neuroscience *12*, 1003-1010.

Wu, Y., O'Toole, E.T., Girard, M., Ritter, B., Messa, M., Liu, X., McPherson, P.S., Ferguson, S.M., and De Camilli, P. (2014b). A dynamin 1-, dynamin 3- and clathrin-independent pathway of synaptic vesicle recycling mediated by bulk endocytosis. eLife *3*, e01621.

Xu, T., and Bajjalieh, S.M. (2001). SV2 modulates the size of the readily releasable pool of secretory vesicles. Nature cell biology *3*, 691-698.

Yamashita, T., Eguchi, K., Saitoh, N., von Gersdorff, H., and Takahashi, T. (2010). Developmental shift to a mechanism of synaptic vesicle endocytosis requiring nanodomain Ca2+. Nature neuroscience *13*, 838-844.

Yamashita, T., Hige, T., and Takahashi, T. (2005). Vesicle endocytosis requires dynamin-dependent GTP hydrolysis at a fast CNS synapse. Science *307*, 124-127.

Yao, J., de la Iglesia, H.O., and Bajjalieh, S.M. (2013). Loss of the SV2-like protein SVOP produces no apparent deficits in laboratory mice. PLoS One *8*, e68215.

Yao, J., Kwon, S.E., Gaffaney, J.D., Dunning, F.M., and Chapman, E.R. (2011). Uncoupling the roles of synaptotagmin I during endo- and exocytosis of synaptic vesicles. Nature neuroscience *15*, 243-249.

Yao, J., Nowack, A., Kensel-Hammes, P., Gardner, R.G., and Bajjalieh, S.M. (2010). Cotrafficking of SV2 and synaptotagmin at the synapse. The Journal of neuroscience : the official journal of the Society for Neuroscience *30*, 5569-5578.

Yao, L.H., Rao, Y., Varga, K., Wang, C.Y., Xiao, P., Lindau, M., and Gong, L.W. (2012). Synaptotagmin 1 is necessary for the Ca2+ dependence of clathrin-mediated endocytosis. The Journal of neuroscience : the official journal of the Society for Neuroscience *32*, 3778-3785.

Zhang, N., Gordon, S.L., Fritsch, M.J., Esoof, N., Campbell, D.G., Gourlay, R., Velupillai, S., Macartney, T., Peggie, M., van Aalten, D.M., *et al.* (2015). Phosphorylation of synaptic vesicle protein 2A at Thr84 by casein kinase 1 family kinases controls the specific retrieval of synaptotagmin-1. The Journal of neuroscience : the official journal of the Society for Neuroscience *35*, 2492-2507.

Zheng, J., Cahill, S.M., Lemmon, M.A., Fushman, D., Schlessinger, J., and Cowburn, D. (1996). Identification of the binding site for acidic phospholipids on the pH domain of dynamin: implications for stimulation of GTPase activity. Journal of molecular biology *255*, 14-21.

Zheng, Q., McFadden, S.C., and Bobich, J.A. (2004). Phosphatidylinositol 4,5-bisphosphate promotes both [3H]-noradrenaline and [14C]-glutamate exocytosis from nerve endings. Neurochemistry international *44*, 243-250.

Zhou, Q., Zhou, P., Wang, A.L., Wu, D., Zhao, M., Sudhof, T.C., and Brunger, A.T. (2017). The primed SNARE-complexin-synaptotagmin complex for neuronal exocytosis. Nature *548*, 420-425.

# 8. Appendix

## 8.1. Appendix A: Abbreviations

| | | | |
|---|---|---|---|
| A | ampere | DIV | days *in vitro* |
| A/A | acrylamide | DKO | double knockout |
| AA | amino acid | DMEM | dulbecco's modified Eagle's mediem |
| ACSF | artificial cerebrospinal fluid | DMSO | dimethylsulfoxid |
| ADBE | activity-dependent bulk endocytosis | DNA | deoxyribonucleic acid |
| AM | acetoxymethylester | DNase | deoxyribonuclease |
| ANTH | AP180 N-terminal homology | dNTP | deoxynucleosidtriphosphate |
| AP | action potential | Dyn | dynamin |
| AP180 | monomeric adaptor protein with 180 kDa | *E. coli* | *Escherichia coli* |
| AP-2 | adaptor protein 2 | ECL | enhanced chemiluminescence |
| APS | ammonium persulfate | EF | endotoxin free |
| APV | (2R)-amino-5-phosphonovaleric acid | EGTA | ethylene glycol-bis(β-aminoethyl ether)-N,N,N',N'-tetraacetic acid |
| AraC | Cytosine β-D-arabinofuranoside | ELV | endosomal-like vacuole |
| Arf | ADP-ribosylation factor | ENTH | epsin N-terminal homology |
| Arp2/3 | actin-related protein 2/3 | et al. | and others (et alii) |
| ATG | Autophagy related | F | fluoresence intensity |
| AUC | area-under-the-curve | $F_0$ | initial fluorescence intensity |
| BA | N, N'-methylenebisacrylamide | FCHo | Fer/Cip4 homology domain-only proteins |
| BAR | Bin1 / amphiphysin / Rvs | FCS | fetal calf serum |
| bp | base pairs | fEPSP | field excitatory postsynaptic potential |
| BSA | bovine serum albumin | FERM | band4.1 / Ezrin / Radixin / Moesin |
| *C. elegans* | *Caenorhabditis elegans* | fl | full length |
| CALM | clathrin assembly lymphoid myeloid leukemia | fw | forward |
| CAPS | calcium activated protein for secretion | GA | glutaraldehyd |
| CdK5 | cyclin dependent kinase 5 | g | acceleration of gravity |
| CHC | clathrin heavy chain | g | gram |
| CIE | clathrin-independent endocytosis | GFP | green fluorescent protein |
| CIP | calf intestinal phosphatase | GST | glutathione-S-transferase |
| CME | clathrin-mediated endocytosis | gSTED | time-gated stimulated emission depletion |
| CMV | cytomegalovirus | GTP | guanosine triphosphate |
| CNQS | 6-cyano-7-nitroquinoxaline-2,3-dione | h | hour |
| CNS | central nervous system | HA | hemagglutinin |
| C-terminal | carboxy-terminal | HBSS | Hanks's Balanced Salt Solution |
| *D. melanogaster* | *Drosophila melanogaster* | HD | homology domain |
| DAG | diacylglycerol | HEK | human embryonic kidney |
| DAPI | 4',6-Diamidino-2-phenylindole | Hepes | 4-(2-hydroxyethyl)piperazine-1-ethanesulfonic acid |

| | |
|---|---|
| HET | heterozygous |
| $HIS_6$ | 6x Histidine tag |
| HRP | horseradish peroxidase |
| Hsc70 | heat shock cognate 70 |
| Hz | Herz |
| ICC | immunocytochemistry |
| IgG | Immunoglobulin G |
| IgM | Immunoglobulin M |
| IHC | immunohistochemistry |
| $IP_3$ | inositol-1,4,5-trisphosphate |
| IPTG | Isopropyl-β-D-thiogalactopyranoside |
| ISI | Interstimulus interval |
| KD | knockdown |
| kDa | kilo dalton |
| KI | kinase inactive |
| KO | knockout |
| LAGeSo | Landesamt für Gesundheit und Soziales |
| LB | Luria-Bertani Broth |
| LD | luminal domain |
| µl | micro liters |
| M | molar |
| *M. musculus* | *Mus musculus* |
| mch | mcherry |
| MEF | mouse embryonic fibroblast |
| mEPSC | miniature excitatory postsynaptic current |
| MES | 2-(N-morpholino)ethansulfonic acid |
| MFS | major facilitator superfamily |
| m | milli |
| min | minutes |
| n.s. | not significant |
| NSF | N-ethylmaleimide-sensitive factor |
| NGS | normal goat serum |
| N-terminal | amino-terminal |
| N-WASP | neuronal Wiskott-Aldrich syndrome protein |
| p | postnatal |
| P/S | penicillin/ streptomycin |
| PB | phosphate buffer |
| PBS | phosphate buffered saline |
| PCR | polymerase chain reaction |
| PDL | poly-D-Lysin hydromide |
| PFA | paraformaldehyde |
| PH | pleckstrin-homology |
| pH | preponderance of hydrogen ions |
| PI | phosphoinositide |
| PI(3)P | phosphatidylinositol-3-phosphate |
| $PI(3,4,5)P_3$ | phosphatidylinositol-(3,4,5)-trisphosphate |
| PI(4)P | phosphatidylinositol-4-phosphate |
| $PI(4,5)P_2$ | phosphatidylinositol-4,5-bisphosphate |
| PI(5)P | phosphatidylinositol-5-phosphate |
| PI4K | PI 4-kinase |
| PIPK1γ | phosphatidylinositol 4-phosphate 5-kinase type Iγ |
| PKG | cGMP-dependent protein kinase |
| PLC | phospholipase C |
| PLL | poly-L-Lysin |
| PMSF | phenylmethylsulfonyl fluoride |
| PPF | paired-pulse facilitation |
| rev | reverse |
| RNA | ribonucleic acid |
| ROI | region of interest |
| s | seconds |
| scr | scrambled |
| SDS | sodium dodecylphosphate |
| SDS-PAGE | sodium dodecylsulfate polyacrylamide gel electrophoresis |
| SEM | standard error of the mean |
| SHD | stonin homology domain |
| siRNA | small interfering RNA |
| SNARE | soluble NSF attachment protein receptor |
| stim | stimulated |
| Stn | stonin |
| STORM | stochastic optical reconstruction microscopy |
| SV | synaptic vesicle |
| SV2 | synaptic vesicle protein 2 |
| SVOP | SVtwO related protein |
| Syb2 | synatobrevin 2 |
| Syp | synaptophysin |
| Syt1 | synaptotagmin 1 |
| τ | endocytic time constant |
| TAE | Tris-Acetate-EDTA |
| TBE | Tris-Borate-EDTA |
| TBS | Tris buffered saline |

| | | | |
|---|---|---|---|
| TEMED | N,N,N',N'-tetramethylenediamin | UV | ultraviolet |
| TES | N-tris[hydroxy-methyl]-methyl-2-aminoethane-sulphonic acid | V | voltage |
| TMD | transmembrane domain | v/v | volume per volume |
| TKO | triple knockout | v/w | weight per volume |
| TR | tetracycline repressor | VGLUT1 | vesicular glutamate transporter |
| TTX | tetrodotoxin | WB | western blot |
| UFE | ultra fast endocytosis | WT | wild type |
| unstim | unstimulated | | |

## 8.2. Appendix B: Supplementary Figures

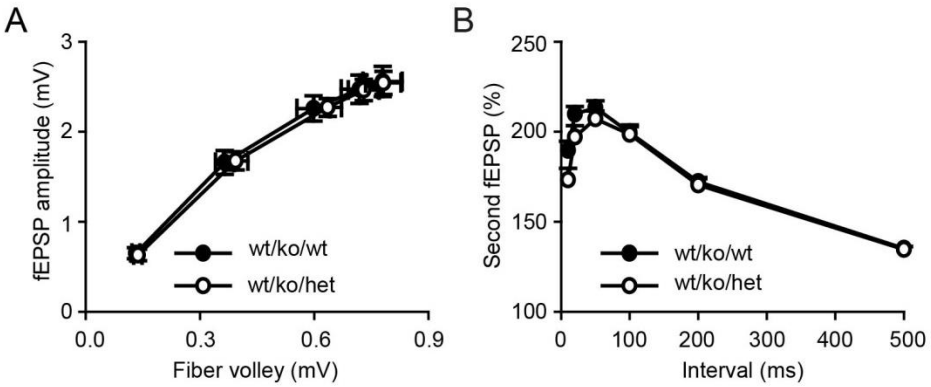


**Figure S1: WT/KO/WT and WT/KO/HET littermates show similar responses in electrophysiological recordings.** Graphs illustrating comparable basal neurotransmission **(A)** and short-term plasticity **(B)** at the synapses of two controls used in this study (SV2A WT/SV2B KO/Stn2 WT: WT/KO/WT and SV2A WT/SV2B KO/Stn2 Het: WT/KO/HET). Relationships between fEPSPs and fiber volley amplitudes **(A)** or interpulse interval and PPF are plotted **(B)**.

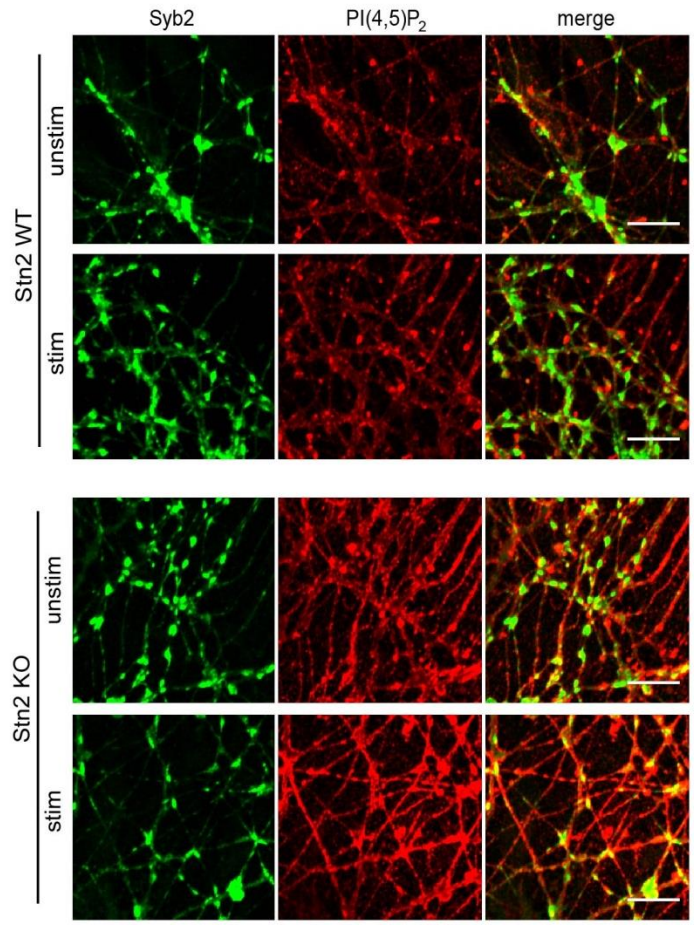


**Figure S2: Elevated PI(4,5)$P_2$ level in Stn2 deficient neurons.** Representative confocal images of PI(4,5)$P_2$ immunostaining with specific antibodies (red) and Syb2 positive boutons (green) of Stn2 WT and KO neuronal cultures left unstimulated or stimulated with 80 mM KCl. Scale bar, 10 µm.

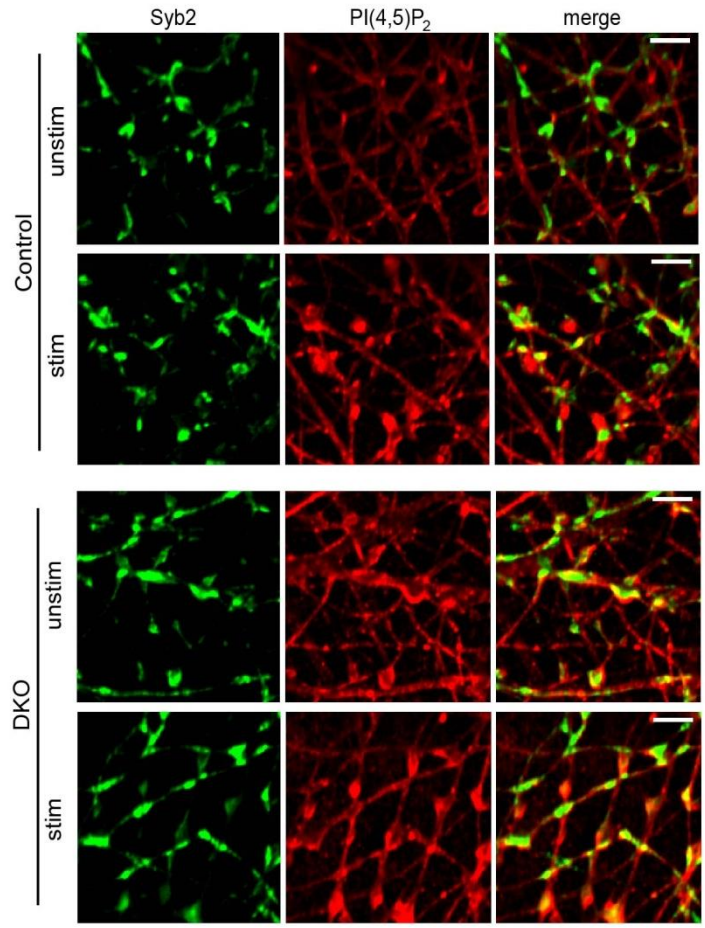


**Figure S3: Elevated $PI(4,5)P_2$ level in SV2A/B DKO neurons.** Representative confocal images of Syb2 (green) and $PI(4,5)P_2$ (red) staining with specific antibodies in control and SV2A/B DKO neuronal cultures left unstimulated or stimulated with 80 mM KCl. Scale bar, 5 µm.

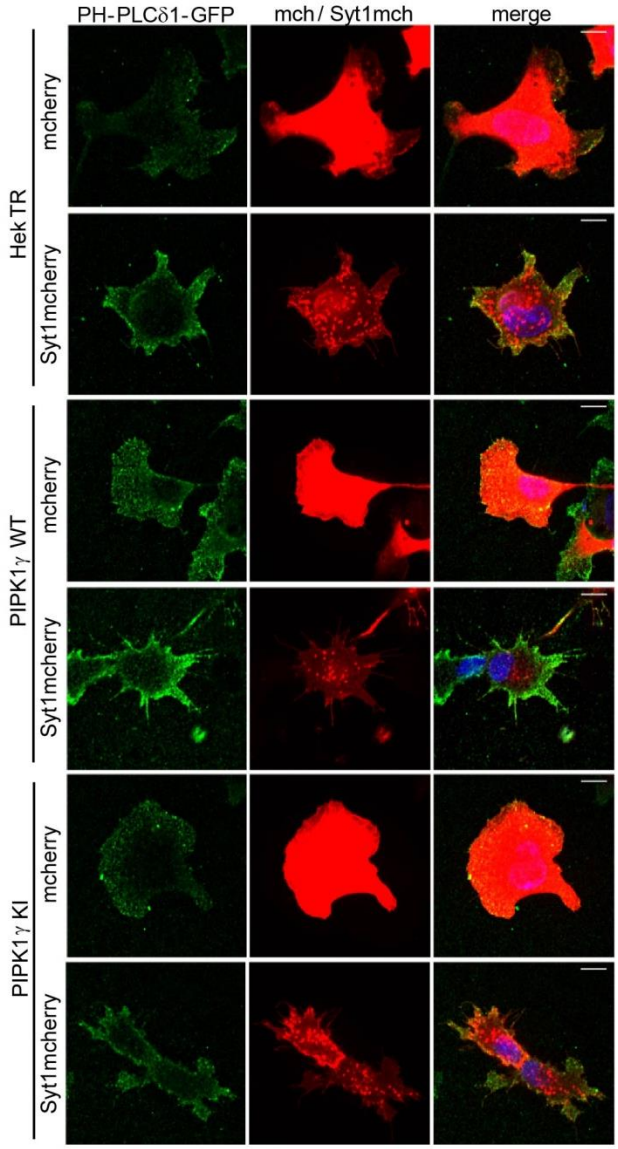


**Figure S4: Overexpression of PIPK1γ together with Syt1 further elevates PI(4,5)$P_2$ levels**. Representative confocal images of FlpIN HEK 293T cells with inducible expression of HA-tagged PIPK1γ p90 WT and kinase inactive (KI) mutant as well as control cells only harboring the tetracycline repressor (TR) were either transfected with mCherry (mch, red) or Syt1mCherry (Syt1mch, red). All cells were treated with 1µg/ml doxycycline for 7 h and after glutaraldehyde fixation were stained with PH-PLCδ1-GFP (green) and with DAPI to label nuclei (blue) (scale bar, 10 µm).

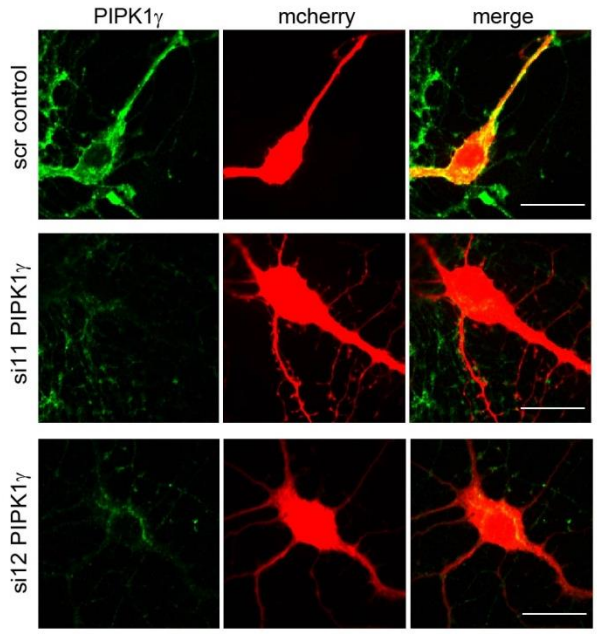


**Figure S5: Validation of PIPK1γ antibody specificity.** Representative confocal images of neurons coexpressing mcherry and scrambled (scr) control siRNA, PIPK1γ si11 and PIPK1γ si12 and immunostained for PIPK1γ (green) (scale bar, 20 µm).

## 8.3. Appendix C: List of Tables and Figures

### 8.3.1. List of Tables



### 8.3.2. List of Figures

## 8.4. Appendix D: Publications

**Kaempf N**, Krauss M, Sakaba T, Maritzen T, Haucke V. *Synaptotagmin1 couples synaptic vesicle exo- and endocytosis by facilitating phosphatidylinositol 4,5-bisphosphate synthesis*. (in preparation).

**Kaempf N** and Maritzen T. *Safeguards of Neurotransmission: Endocytic Adaptors as Regulators of Synaptic Vesicle Composition and Function*. Front. Cell Neurosci. **2017** Oct 11; 11:320.

Soykan T, **Kaempf N**, Sakaba T, Vollweiter D, Goerdeler F, Puchkov D, Kononenko NL, Haucke V. *Synaptic Vesicle Endocytosis Occurs on Multiple Timescales and Is Mediated by Formin-Dependent Actin Assembly. Neuron* **2017** Feb 22; 93(4):854-866.e4.

**Kaempf N**, Kochlamazashvili G, Puchkov D, Maritzen T, Bajjalieh SM, Kononenko NL and Haucke V. *Overlapping functions of stonin 2 and SV2 in sorting of the calcium sensor synaptotagmin 1 to synaptic vesicles*. *Proc. Natl. Acad. Sci* **2015** Jun 9;112(23):7297-302.

Kononenko NL, Puchkov D, Classen GA, Walter AM, Pechstein A, Sawade L, **Kaempf N**, Trimbuch T, Lorenz D, Rosenmund C, Maritzen T, Haucke V. *Clathrin/AP-2 mediate synaptic vesicle reformation from endosome-like vacuoles but are not essential for membrane retrieval at central synapses*. Neuron. **2014** Jun 4;82(5):981-8.

## 8.5. Appendix E: Curriculum Vita

For reasons of data protection, the curriculum vitae is not included in the online version.

For reasons of data protection, the curriculum vitae is not included in the online version.